Forcings of Indo-Pacific Warm Pool Climate During the Past One Million Years

By

Meredith C. Parish

BA Colorado College, Colorado Springs, CO, 2016

MSc, University of Wyoming, Laramie, WY, 2019

MSc, Brown University, Providence, RI, 2021

A dissertation submitted in partial fulfillment of the requirements for the degree of Doctor of Philosophy in the Department of Earth, Environmental and Planetary Sciences at Brown University

Providence, Rhode Island, USA

October 2024

This dissertation by Meredith Parish is accepted in its present form by the Department of Earth, Environmental and Planetary Sciences as satisfying the dissertation requirement for the degree of Doctor of Philosophy.

Date 7/16/24 ______________________
James Russell, PhD, Advisor

Recommended to the Graduate Council

Date 7/16/24 ______________________
Timothy Herbert, PhD, Reader

Date 7/16/24 ______________________
Colleen Dalton, PhD, Reader

Date 7/16/24 ______________________
Steven Clemens, PhD, Reader

Date 7/16/24 ______________________
Bronwen Konecky, PhD, External Reader

Approved by the Graduate Council

Date______________ ______________________
Thomas Lewis, Dean of the Graduate School

CURRICULUM VITAE

Meredith C. Parish

Education

PhD in Earth, Environmental, and Planetary Science, Brown University, 2024
Advisor: James Russell
MSc in Earth, Environmental, and Planetary Science, Brown University, 2021
Advisor: James Russell
MSc in Geology, University of Wyoming, 2019
Advisor: Bryan Shuman
BA in Environmental Science, Colorado College, 2016
Advisor: Miroslav Kummel

Publications

1 **Parish, M.C.**, Russell, J., Konecky, B., Du, X., He, C., Bijaksana, S. and Vogel, H., 2024. Changes in Indo-Pacific Warm Pool hydroclimate and vegetation during the last deglaciation. *Quaternary Science Reviews*, 336, p.108755.
2 Clark-Wolf, K.D., Higuera, P.E., McLauchlan, K.K., Shuman, B.N. and **Parish, M.C.**, 2023. Fire-regime variability and ecosystem resilience over four millennia in a Rocky Mountain subalpine watershed. *Journal of Ecology*.
3 Zhao, B., Russell, J.M., Tsai, V.C., Blaus, A., **Parish, M.C.**, Liang, J., Wilk, A., Du, X. and Bush, M.B., 2023. Evaluating global temperature calibrations for lacustrine branched GDGTs: Seasonal variability, paleoclimate implications, and future directions. *Quaternary Science Reviews*, 310, p.108124.
4 **Parish, M.C.**, Du, X., Bijaksana, S. and Russell, J.M., 2023. A brGDGT-based reconstruction of terrestrial temperature from the Maritime Continent spanning the Last Glacial Maximum. *Paleoceanography and Paleoclimatology*, p.e2022PA004501.
5 **Parish, M.C.**, Wolf, K.D., Higuera, P.E. and Shuman, B.N., 2022. Holocene water levels of Silver Lake, Montana, and the hydroclimate history of the Inland Northwest. *Quaternary Research*, pp.1-13.
6 Chileen, B.V., McLauchlan, K.K., Higuera, P.E., **Parish, M.C.** and Shuman, B.N., 2020. Vegetation response to wildfire and climate forcing in a Rocky Mountain lodgepole pine forest over the past 2500 years. *The Holocene*, *30*(11), pp.1493-1503.
7 **Parish, M.C.**, Calder, W.J., and Shuman, B.N. A millennial-scale increase in winter precipitation in the southern Rocky Mountains during the Common Era.. *Quaternary Research* 2020 94, 1.
8 Galik, C.S.; Murray, B.C.; **Parish, M.C.** Near-Term Pathways for Achieving Forest and Agricultural Greenhouse Gas Mitigation in the U.S.. *Climate* 2017, 5, 69.

Manuscripts in preparation

1 **M. C. Parish,** J. M. Russell, J. W. King, A. L. Deino, C. J. Harpel, H. Vogel, S. Bijaksana, A. Wilk, and G. Traietti. A 1-million year record of terrestrial temperature from the Indo-Pacific Warm Pool. In preparation, *Geophysical Research Letters*.

2 **M. C. Parish,** J. M. Russell, H. Vogel, S. Bijaksana, A. Wilk, and G. Traietti. A 1-Myr record of Maritime Continent hydroclimate. In preparation, *Nature Geoscience.*

Conference abstracts (* denotes presenting author)

1 **Parish, M.C.***, Russell, J.M., Vogel, H., Bijaksana, S. and Wilk, A., 2023, December. The response of Indo-Pacific Warm Pool climate to global forcings over the past 1 Myr. AGU 2023, oral presentation.
2 **Parish, M.C.**, Russell, J.M.*, Vogel, H., Bijaksana, S. and Wilk, A., 2023, July. Dramatic Shifts in Vegetation and Hydroclimate in the Indo-Pacific Warm Pool During the Last Two Glacial Cycles, INQUA 2023, oral presentation.
3 Wolf, K.D.C.*, McLauchlan, K., **Parish, M.C.**, Shuman, B.N. and Higuera, P.E., 2022, December. Paleo-pyro-diversity and Ecosystem Resilience to Wildfires over the Late Holocene in a Northern Rocky Mountain Forested Watershed. AGU 2022, oral presentation.
4 Wilk, A.*, Russell, J.M., **Parish, M.C.**, Bijaksana, S. and Vogel, H., 2022, December. Pleistocene" Super-interglacials" and Hydroclimates of the Tropical Indo-Pacific Warm Pool. AGU 2022, poster presentation.
5 **Parish, M.C.***, Russell, J.M., Vogel, H. and Bijaksana, S., 2022, December. Synchronous Changes in Vegetation and Hydroclimate Across Broad Spatial Scales in the Indo-Pacific Warm Pool During the Past 450,000 Years. AGU 2022, poster presentation.
6 Zhao, B.*, Russell, J.M., Tsai, V.C., **Parish, M.**, Blaus, A. and Bush, M.B., 2022, December. Revisiting Global Temperature Calibrations for Lacustrine Branched GDGTs, AGU 2022, oral presentation.
7 **Parish, M.C.***, Russell, J.M., Vogel, H., Bijaksana, S., 2022, June. Dramatic Shifts in Vegetation and Hydroclimate in the Indo-Pacific Warm Pool During the Last Two Glacial Cycles, AMQUA 2022, oral presentation.
8 **Parish, M.C.*** and Russell, J.M., 2021, December. Leaf wax δD indicates sensitivity to shelf inundation in the Indo-Pacific Warm Pool as sea levels rise during the last deglaciation. AGU 2021, oral presentation.
9 **Parish, M.C.*** and Russell, J.M., 2020, December. A Terrestrial Indo-Pacific Warm Pool Temperature Reconstruction Enables a Mechanistic Understanding of Climate Changes in the Tropics. AGU 2020, oral presentation.
10 **Parish, M.C.*,** Shuman, B.S., and Calder, W.J., 2018, December. Applying the Modern Analog Technique to high elevation fossil-pollen records from the Colorado Rocky Mountains over the past 2000 years. AGU 2018, oral presentation.

Teaching experience

Teaching assistant, The Evolution of a Habitable Earth, Spring 2023
Instructor, Sheridan Teaching Seminar - Reflective Teaching (Certificate I), Fall 2022
Teaching assistant, Sedimentology and Stratigraphy, Fall 2021

Teaching Certificates

Sheridan Teaching Seminar - Course Design (Certificate II), Spring 2023
Sheridan Teaching Seminar - Reflective Teaching (Certificate I), Fall 2019

Honors, Awards, and Grants

2024 Graduate Student Council Conference Funding Grant

2023 AGU Outstanding Student Presentation Award

2023 USNC INQUA Fellowship Grant

2023 INQUA Travel Grant

2023 IBES Graduate Research, Training, and Travel Award

2022 AMQUA Student Travel Grant

2021 GSA Continental Scientific Drilling Division Student Research Grant

2021 IBES Graduate Research, Training, and Travel Award

2020 Graduate Student Council Conference Funding Grant

2018 J. H. Hanley Memorial Scholarship

2018 Geology & Geophysics Meritorious Graduate Research Grant

2018 Colorado Scientific Society Memorial Research Funds Grant

2016 The Keller Family Venture Grant for Student Research

2016 Colorado College Dean's List Spring

2015 Colorado College Dean's List Fall

2015 Faculty-Student Collaborative Research Grant

Academic Activities

Panel convener, AGU 2022, Organic compounds as environmental proxies: calibrations and applications.
Panel convener, AGU 2022, Inclusivity in Geosciences: A Conversation between Scientists and Educators.
Panel convener, AGU 2021, Inclusivity in Geosciences: A Conversation between Scientists and Educators.
Geoclub co-president, 2020-2021.
Graduate Women in Science and Engineering (GWISE) coordinator, 2020-2023.
Unlearning Racism in the Geoscience (URGE) participant, Spring 2021.
Graduate Student Representative in Faculty Meetings, 2018-2019.
Master's Student Representative on the Candidate Search Committee, 2018.

Other Professional Experience

Research Assistant, North Carolina State University, 2017
Field Organizer, NextGen Climate, 2016
Summer Research Intern, Colorado College, 2015
Summer Intern, The Trust for Public, San Francisco, 2014
Backpacking Trip Leader, Colorado College, 2013-2016
Science Camp Counselor, Crissy Field Center, San Francisco, 2008 and 2011

ACKNOWLEDGEMENTS

The work presented in this dissertation would not have been possible without significant support from many people around me. First and foremost, I would like to thank Jim Russell for being an incredible advisor over the past five years. He has been a superb scientific mentor. His quick response time to emails and insanely fast turnaround time with comments on manuscript drafts has made my life as a graduate student exponentially easier. I am extremely grateful to have had Jim as an advisor. I also want to thank the members of my Advisory and Preliminary Exam committees: Colleen Dalton, Tim Herbert, Steve Clemens, and Jung-Eun Lee, who always had open doors (or Zoom rooms) for research and career advice; and Bronwen Konecky for serving on my dissertation committee.

The undergraduate researchers who have assisted me in the lab have been fantastic, and I have enjoyed watching them develop from student assistants to research colleagues. A huge thank you goes to Alex and Gabriel who spent countless hours processing samples for my research. This dissertation would not have been possible without their careful lab work.

I am grateful for my fellow members of the Russell Lab: Andrea, Sloane, Lina, Boyang, Ellen, Bryce, Xiaojing, and Desmond. With kindness, each of you have helped me develop my ideas on many of the scientific topics within this dissertation. A special thank you to Sloane for hosting me when I first visited and being so welcoming when I arrived, and to Andrea for being the best trekking and ‘Pomodoro Technique’ accomplice.

To the DEEPS community, I am so thankful for incredible graduate student colleagues who were supportive of me throughout my PhD. Kristin has been the best officemate I could have ever asked for and a wonderful caretaker of our office plants (most of which survived). Ewerton and Marcelo made my research significantly easier by maintaining all of the finnicky instruments. The office staff, especially Pat, Richard, and Dina, allowed me to fully focus on my research by dealing with so many bureaucratic tasks for me.

I am deeply appreciative of my family and my community of lifelong friends within and outside the department, all of whom have been incredibly encouraging through this process. I am very thankful to have the most supportive parents on the planet, Anne and Michael. I am so grateful to my sister Chelsea, who is always my first call in a crisis. I also want to thank my friend Emily who kept me sane with nightly phone calls when I was living alone during deep COVID lockdown, and Anna for being an incredible roommate and friend that could handle me through the highs and lows of graduate school. Finally, I'd like to thank my partner Ian and our dog Tava, whose love and support I've felt from across the country.

TABLE OF CONTENTS

LIST OF TABLES

LIST OF FIGURES

CHAPTER 1

Introduction

Meredith Parish

1. Future climate change in Indonesia and the Indo-Pacific Warm Pool

Human-generated emissions of greenhouse gases (GHGs) into Earth's atmosphere have caused the planet to warm. The average global surface temperature from 2011 to 2020 was ~1.1°C above the 1850–1900 average, with a larger increase of ~1.6°C over land (Lee et al., 2023). This warming is largely the result of increased emissions of carbon dioxide (CO_2) and methane (CH_4) from human activity (Lee et al., 2023). Atmospheric CO_2 concentrations have increased over 47% since 1750 (Lee et al., 2023), reaching 426 ppm in June 2024 (Lan and Keeling, 2024). According to the IPCC, scientists are 'very highly confident' that climate change has already led to adverse impacts related to water availability, food production, health, wellbeing, and infrastructure (Lee et al., 2023). Crop production, fisheries yields, infectious diseases, mental health, displacement, malnutrition, wildfires, and coastal and inland flooding have all been adversely impacted by anthropogenic climate change in at least one region on Earth (Lee et al., 2023). The most vulnerable people and systems have already been disproportionally impacted by anthropogenic climate change (Lee et al., 2023).

One of the most vulnerable countries to climate change is Indonesia, which is the world's 4^{th} most populated country (Djalante et al., 2021). Understanding how climate will change in Indonesia is critically important for the 278 million people who live on its over 17,000 islands (Indonesia BPS, 2023). Sea level rise and extreme precipitation events are the major climatic concerns for the country, with the potential to cause inland flooding, coastal flooding, outbreaks of crop pests, and decreased fisheries yields (Djalante et al., 2021). In 2016, floods caused $275 million USD in infrastructure damage (Djalante et al., 2021), and climate change is expected to increase the frequency of flooding (Kelley and Prabowo, 2019). Climate change also threatens ecosystems in Indonesia, which is one of the most biodiverse regions on Earth (Djalante et al., 2021; Lee et al., 2023).

Indonesia is located within the Indo-Pacific Warm Pool (IPWP), which spans from the Indian Ocean into the Pacific Ocean and has sea surface temperatures (SSTs) over 28°C year-round. The high SSTs cause some of the most intense atmospheric convection on Earth, which exports heat to higher latitudes (Zhou et al., 2019). The IPWP, therefore, plays an important role in regulating Earth's climate. Understanding how climate will change in the IPWP is not only important for the people who live in the region, but for the region's influence on global climate.

Current global GHG reduction efforts have not proven sufficient to avoid raising global temperatures by 1.5°C (Lee et al., 2023). Governments are planning and implementing adaptations to lessen the impacts of this warming (Lee et al., 2023), but require accurate projections of future climate to adequately prepare. Simulations of future climate change from global climate models are powerful tools scientists use to predict how temperature and precipitation will change in response to rising greenhouse gas concentrations. All land area in the Maritime Continent (MC) is projected to warm by 3°C from the 1986–2005 baseline by the end of the century if we continue 'business-as-usual' without major emissions reductions (Iturbide et al., 2020). ~80% of climate models agree on the projected temperature change in the IPWP (Lee et al., 2023). However, current atmospheric concentrations of CO_2 are unprecedented for at least the past 2 million years (Lee et al., 2023), leaving questions about how climate sensitivity could change across different climate states (Tierney et al., 2020). Temperature changes could potentially be greater than models predict. Moreover, changes in precipitation over the IPWP are much more uncertain than temperature change, with less than 80% of climate model projections agreeing on precipitation increases (Iturbide et al., 2020). Even though these models are an incredibly useful tool for helping us to prepare for future climate changes, they are not a perfect representation of the climate system under boundary conditions that are different than today.

2. Paleoclimate of the Indo-Pacific Warm Pool

Reconstructing past climate change across major transitions in Earth's history is an another method used to diagnose the controls of climate under boundary conditions that are unlike the present. During the past one million years, glacial-interglacial cycles transitioned from 41-kyr cycles to 100-kyr cycles during the Mid-Pleistocene Transition (MPT; ~950 ka; Herbert, 2023), and the amplitude of glacial-interglacial cycles increased during the Mid-Brunhes Transition (MBT; ~430 ka; Barth et al., 2018). These transitions were reorganizations of Earth's carbon cycle, which enable tests of the impact of CO_2 on climate in the IPWP. Understanding the impact of CO_2 on climate in the IPWP helps constrain future climate change the region.

Our current understanding of the controls on tropical climate across the MPT and MBT is informed largely by SST records, as long, highly-resolved records of terrestrial climate are extraordinarily rare. Tropical SST stacks indicate a cooling across the MPT and an increasing amplitude of glacial-interglacial changes, which suggest a strong control of CO_2 on tropical SSTs (Clark et al., 2024; Herbert et al., 2010). In contrast to most regions, SST records from the IPWP do not exhibit a cooling during the MPT nor a significant increase in interglacial temperatures (Clark et al., 2024). However, the alkenone-based SST records included in the stack suffer from issues unique to waters as warm as the IPWP; in particular, the chemistry of SST proxies may limit their fidelity at very high temperatures (Gray and Evans, 2019). A new terrestrial temperature record from the IPWP would add to the currently-limited slate of terrestrial records, help reconcile the differences between the IPWP SST stack and global SST, and be used to estimate the relationships between land and ocean temperatures. The only pre-existing terrestrial temperature reconstruction from the IPWP, a speleothem-based cave temperature record, only spans the last deglaciation (Løland et al., 2022) and although this record points to CO_2 as a dominant forcing of IPWP temperature (Løland et al., 2022), the record does not span the MPT and MBT.

Records of hydroclimate in the IPWP largely come from water isotope records from speleothems and from leaf waxes preserved in marine sediment. A 450-kyr leaf wax record from offshore Sumatra (Windler et al., 2019) and a 570-kyr speleothem record from northern Borneo (Carolin et al., 2016, 2013; Meckler et al., 2012; Partin et al., 2007) indicate hydroclimate in the IPWP is dominated by 100-kyr glacial-interglacial cycles (Windler et al., 2021). Strong 100-kyr cycles suggest that the dominant control on IPWP hydroclimate is atmospheric CO_2, global ice volume and/or temperature, and/or sea level change, as observed during the last deglaciation (Windler et al., 2021). An IPWP proxy-model comparison from the Last Glacial Maximum (LGM; 21 ka) and Pre-Industrial (PI) identified the dominant climate forcing of IPWP climate as sea level, and in particular the exposure/inundation of the shallow continental shelves of the MC caused by sea level change (DiNezio et al., 2018). However, carbon isotope records suggest that the continental shelves were permanently exposed prior to ~250 ka (McGrath et al., 2023; Sarr et al., 2019), and to the best of our knowledge, the regional climate prior to 250 ka does not resemble the climate of recent glacial periods when these shelves were exposed. Thus, a forcing mechanism other than shelf exposure likely causes the 100-kyr cycle in the Sumatra and Borneo records prior to ~250 ka.

We reconstructed temperature and hydroclimate in Indonesia over the past 1-Myr to diagnose the dominant controls on IPWP climate, presented in Chapter 4 and Chapter 5. The reconstructions in this dissertation are the only terrestrial temperature and hydroclimate records that span both the MPT and MBT in the IPWP. These records allow us to disentangle the effect of shelf exposure from other forcing mechanisms, such as CO_2, ice volume, and insolation.

3. Controls on Indo-Pacific Warm Pool climate during the past 1 Myr

During the past one million years there have been ~11 glacial-interglacial cycles that we can use to test the controls of climate in the IPWP. The study site featured in this dissertation is Lake Towuti, which is located on the island of Sulawesi in Indonesia (Figure 1). Lake Towuti is the ideal location for producing regionally representative records because monthly precipitation is highly correlated with monthly precipitation in the majority of the MC (Figure 1). Tectonically-driven subsidence created the Towuti lake basin about one million years ago and sediment has been steadily accumulating in Lake Towuti since its formation (Russell et al., 2020), preserving organic biomarkers and locking in a history of past climate. The Towuti Drilling Project developed a ~1 million year composite sediment stratigraphy from drill cores recovered from Towuti's central basin (Russell et al., 2020), allowing us to develop the region's first, long, continuous terrestrial climate records.

Before we could reconstruct how climate changed over the past one million years, we first needed to test the performance of existing organic geochemical proxies for temperature and precipitation on orbital timescales at our study site. We first tested our proxies by producing records only spanning the last deglaciation, using samples from a piston core (IDLE-TOW10-9B) extracted from the center of Lake Towuti's northern basin (Russell et al., 2014, 2020).

3.1 The last deglaciation at Lake Towuti

To reconstruct temperature during the last deglaciation we used glycerol dialkyl glycerol tetraethers (brGDGTs), which are membrane-spanning lipids. The degree of methylation of these microbial membrane lipids varies with temperature, enabling paleotemperature calibrations and reconstructions (Russell et al., 2018; Schouten et al., 2013; Zhao et al., 2023). Even though global calibrations using modern sediment show a strong correlation between methylation and mean annual air temperature, we were unsure whether this proxy would work in Lake Towuti, which has an uncommon, ferruginous chemistry that produces an unusual microbial biosphere (Russell et al., 2020).

Chapter 2 of this dissertation presents a 60-kyr brGDGT record from Lake Towuti (Parish et al., 2023). We found that the cyclization of brGDGTs, a proxy for pH, is the dominant mode of variation in the Lake Towuti brGDGT record. The cyclization of brGDGTs reflects important changes in the lacustrine biogeochemical environment. However, we were able to separate the influence of lake chemistry changes from temperature changes on the brGDGT records, and developed a temperature record spanning the last 60 kyr. We used the temperature reconstruction to narrow the possible forcing mechanisms of temperature on the MC during the deglaciation. We compared the timing of the onset of warming in the Towuti record to climate forcings, finding that the timing of the deglacial warming in our record occurs shortly after the onset of the deglacial increase in CO_2 concentrations. The timing of the warming suggests rising GHG concentrations and the associated radiative forcing may have forced deglacial warming in the IPWP. The record may also reflect an influence of Northern Hemisphere insolation on land surface temperature, exhibiting peaks in temperature around 55 ka and 34 ka. We determined that brGDGTs can be used to reconstruct temperature at Lake Towuti on orbital timescales, giving us more confidence brGDGTs could be used to reconstruct a 1-Myr record of temperature from the entire composite record.

To reconstruct hydroclimate during the last deglaciation, we produced hydrogen and carbon isotope records measured from leaf waxes preserved in Lake Towuti's sediment. Leaf wax δ^2H (δ^2H_{wax}) in the tropics is usually used as a proxy for precipitation amount vis-à-vis the 'amount effect' (Dansgaard, 1964), but questions remain regarding the interpretation of water isotope records in the IPWP. In addition to reflecting precipitation amount (Krause et al., 2019), studies from the IPWP suggest water isotope records reflect the strength of large-scale circulation of the Australian-Indonesian monsoon (Konecky et al., 2016) and atmospheric convergence/divergence (Du et al., 2021; Konecky et al., 2019). Leaf wax $\delta^{13}C$ ($\delta^{13}C_{wax}$) reflects the ratio of C_3 to C_4 plants and leaf-gas exchange efficiency, which are both influenced by moisture, temperature, and CO_2 concentrations (Chikaraishi and Naraoka, 2007; Diefendorf et al., 2010).

In Chapter 3, we evaluate the controls on δ^2H_{wax} and $\delta^{13}C_{wax}$ in the IPWP on orbital timescales, using new hydrogen and carbon isotope records from Lake Towuti and nearby Lake Matano using long-chain n-alkanes spanning the last deglaciation (Parish et al., 2024). We compared these new records to marine runoff and salinity records in the IPWP. The runoff and salinity records indicate that precipitation amount began to increase at ~12.3 ka. A compilation of all water isotope records in the IPWP that span the last delegation indicates a shift from more ^2H-enriched to ^2H-depleted waxes at ~12.3 ka, consistent with predictions of the 'amount effect' and coincident with runoff and salinity proxies, suggesting precipitation isotopes respond strongly to rainfall amount in this region. The majority of IPWP $\delta^{13}C_{wax}$ records show increasing C_3 plants beginning at about 19.9 ka, prior to the reconstructed increases in precipitation. We suggest that vegetation shifted in response to the changing seasonality of precipitation, though this remains challenging to test. This work suggests that δ^2H_{wax} will reflect precipitation amount on orbital timescales, likely in addition to influence from moisture source and convergence/divergence.

3.2 1-Myr temperature and hydroclimate records from Lake Towuti

The high-resolution temperature and hydroclimate records from Lake Towuti spanning the last deglaciation provide the backbone for our interpretations of new million-year records. These million-year records are the longest terrestrial temperature and hydroclimate records in the region and are only accompanied by a couple terrestrial temperature (Johnson et al., 2016; Lu et al., 2022) and hydroclimate (Johnson et al., 2016; Lupien et al., 2021) records with the same resolution over the past one million years from other regions on Earth.

In Chapter 4, we present a brGDGT-based record of temperature from Lake Towuti that spans the past one million years to document regional patterns and to constrain the forcings and amplitude of terrestrial temperature in the region. Unlike the IPWP SST stack (Clark et al., 2024), terrestrial temperatures from Lake Towuti cool after the MPT, consistent with a global cooling across the MPT (Clark et al., 2024). The emergence of 100-kyr cycles after the MPT and increasing interglacial temperatures across the MBT strongly and uniquely track atmospheric CO_2 concentrations, suggesting that CO_2 is the dominant forcing of temperature. We are also able to provide estimates on the magnitude of terrestrial amplification in the IPWP region, observing 1.45 times as much warming during deglaciations as SSTs over the past 700 kyr, consistent with existing estimates for tropical terrestrial amplification from the last deglaciation (Seltzer et al., 2023). The consistency between our terrestrial amplification estimate from the past 700 kyr and the estimate only from the last deglaciation points to consistent amplification across climate states. Consistent amplification across climate states suggests that predictions of temperature change made by climate model simulations are likely fairly accurate. Over a 3°C warming in the MC, which is predicted by the end century (Iturbide et al., 2020), could have catastrophic consequences for the 100s of millions of people living on the MC.

Chapter 5 presents orbitally-resolved hydroclimate and vegetation reconstructions that we used to identify the dominant climate forcing mechanisms in the IPWP. The records suggest that the MC experienced relative stability in hydroclimate and vegetation prior to the MBT, and a much more variable climate since. This response suggests strong sensitivity to increased CO_2 concentrations and climate warming, though variations in shelf exposure could also play a role. Significant 41-kyr cycles in δ^2H_{wax} and $\delta^{13}C_{wax}$ suggest a primary role for ice volume and/or GHG concentrations in controlling precipitation in the MC. Increased C_4 plants during the most recent glacial periods reflect the large impact of shelf exposure during the past ~250 ka. Insolation has long been presumed as the dominant forcing of hydroclimate in the tropics, yet our data supports recent studies suggesting glacial-interglacial cycles as the primary forcing of IPWP hydroclimate (Windler et al., 2021). Our findings highlight the sensitivity of the region to global forcings, suggesting the MC will experience increased rainfall with increasing atmospheric CO_2 concentrations.

4. Conclusion

This dissertation provides a strong framework for interpreting brGDGT, δ^2H_{wax} and $\delta^{13}C_{wax}$ records from Lake Towuti on orbital timescales (Chapter 2 and Chapter 3). The framework is then applied to interpreting the 1-Myr records as proxies for temperature, hydroclimate, and vegetation (Chapter 4 and Chapter 5). The 1-Myr temperature record indicates that atmospheric CO_2 is the primary forcing of temperature in the MC. The record also suggests terrestrial amplification in the MC is consistent across climate states, possibly validating climate model projections of temperature change in a higher CO_2 world. The 1-Myr $^{2}H_{wax}$ and $\delta^{13}C_{wax}$ also point to CO_2 as a primary forcing of hydroclimate in the MC. This sensitivity could indicate that increasing future CO_2 will likely cause increased precipitation in the MC. However, studying deglaciations is not a perfect analogy for future warming because atmospheric CO_2 concentrations have not been this high in the past two million years (Lee et al., 2023). The only way to prevent the most catastrophic impacts of climate change is to reduce GHG emissions immediately (Lee et al., 2023).

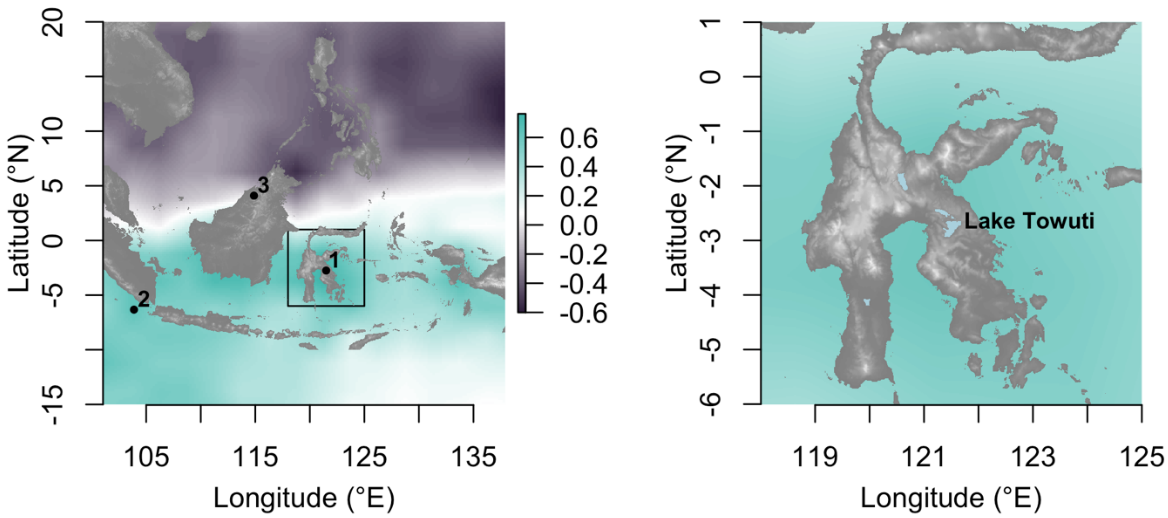

Figure 1 – Location of (1) Lake Towuti in Sulawesi, Indonesia, Lake Towuti, (2) MD98-2152 (Windler et al., 2019), (3) the northern Borneo Cave site (Carolin et al., 2016). Field correlation of the monthly precipitation measured at Lake Towuti from March 2013-August 2016 with monthly precipitation from The Global Precipitation Climatology Project (GPCP) monthly precipitation (Adler et al., 2018). Precipitation and the digital elevation models are plotted using the "raster" package in R (Hijmans et al., 2022).

References

Adler, R.F., Sapiano, M.R.P., Huffman, G.J., Wang, J.-J., Gu, G., Bolvin, D., Chiu, L., Schneider, U., Becker, A., Nelkin, E., Xie, P., Ferraro, R., Shin, D.-B., 2018. The Global Precipitation Climatology Project (GPCP) Monthly Analysis (New Version 2.3) and a Review of 2017 Global Precipitation. Atmosphere 9, 138. https://doi.org/10.3390/atmos9040138

Barth, A.M., Clark, P.U., Bill, N.S., He, F., Pisias, N.G., 2018. Climate evolution across the Mid-Brunhes Transition. Climate of the Past 14, 2071–2087. https://doi.org/10.5194/cp-14-2071-2018

Carolin, S.A., Cobb, K.M., Adkins, J.F., Clark, B., Conroy, J.L., Lejau, S., Malang, J., Tuen, A.A., 2013. Varied Response of Western Pacific Hydrology to Climate Forcings over the Last Glacial Period. Science 340, 1564–1566. https://doi.org/10.1126/science.1233797

Carolin, S.A., Cobb, K.M., Lynch-Stieglitz, J., Moerman, J.W., Partin, J.W., Lejau, S., Malang, J., Clark, B., Tuen, A.A., Adkins, J.F., 2016. Northern Borneo stalagmite records reveal West Pacific hydroclimate across MIS 5 and 6. Earth and Planetary Science Letters 439, 182–193. https://doi.org/10.1016/j.epsl.2016.01.028

Chikaraishi, Y., Naraoka, H., 2007. δ13C and δD relationships among three n-alkyl compound classes (n-alkanoic acid, n-alkane and n-alkanol) of terrestrial higher plants. Organic Geochemistry 38, 198–215. https://doi.org/10.1016/j.orggeochem.2006.10.003

Clark, P.U., Shakun, J.D., Rosenthal, Y., Köhler, P., Bartlein, P.J., 2024. Global and regional temperature change over the past 4.5 million years. Science 383, 884–890. https://doi.org/10.1126/science.adi1908

Dansgaard, W., 1964. Stable isotopes in precipitation. Tellus 16, 436–468. https://doi.org/10.3402/tellusa.v16i4.8993

Diefendorf, A.F., Mueller, K.E., Wing, Scott.L., Koch, P.L., Freeman, K.H., 2010. Global patterns in leaf 13C discrimination and implications for studies of past and future climate. Proceedings of the National Academy of Sciences 107, 5738–5743. https://doi.org/10.1073/pnas.0910513107

DiNezio, P.N., Tierney, J.E., Otto-Bliesner, B.L., Timmermann, A., Bhattacharya, T., Rosenbloom, N., Brady, E., 2018. Glacial changes in tropical climate amplified by the Indian Ocean. Science Advances 4, eaat9658. https://doi.org/10.1126/sciadv.aat9658

Djalante, R., Jupesta, J., Aldrian, E. (Eds.), 2021. Climate Change Research, Policy and Actions in Indonesia: Science, Adaptation and Mitigation, Springer Climate. Springer International Publishing, Cham. https://doi.org/10.1007/978-3-030-55536-8

Du, X., Russell, J.M., Liu, Z., Otto-Bliesner, B.L., Gao, Y., Zhu, C., Oppo, D.W., Mohtadi, M., Yan, Y., Galy, V.V., He, C., 2021. Deglacial trends in Indo-Pacific warm pool hydroclimate in an isotope-enabled Earth system model and implications for isotope-based paleoclimate reconstructions. Quaternary Science Reviews 270, 107188. https://doi.org/10.1016/j.quascirev.2021.107188

Glaser, M. B. "CO_2 ‘greenhouse’ effect." *Exxon Internal Document* (1982).

Gray, W.R., Evans, D., 2019. Nonthermal Influences on Mg/Ca in Planktonic Foraminifera: A Review of Culture Studies and Application to the Last Glacial Maximum. Paleoceanography and Paleoclimatology 34, 306–315. https://doi.org/10.1029/2018PA003517

Herbert, T.D., 2023. The Mid-Pleistocene Climate Transition. Annual Review of Earth and Planetary Sciences 51, 389–418. https://doi.org/10.1146/annurev-earth-032320-104209

Herbert, T.D., Peterson, L.C., Lawrence, K.T., Liu, Z., 2010. Tropical Ocean Temperatures Over the Past 3.5 Million Years. Science 328, 1530–1534. https://doi.org/10.1126/science.1185435

Hijmans, R.J., Etten, J. van, Sumner, M., Cheng, J., Baston, D., Bevan, A., Bivand, R., Busetto, L., Canty, M., Fasoli, B., Forrest, D., Ghosh, A., Golicher, D., Gray, J., Greenberg, J.A., Hiemstra, P., Hingee, K., Ilich, A., Geosciences, I. for M.A., Karney, C., Mattiuzzi, M., Mosher, S., Naimi, B., Nowosad, J., Pebesma, E., Lamigueiro, O.P., Racine, E.B., Rowlingson, B., Shortridge, A., Venables, B., Wueest, R., 2022. raster: Geographic Data Analysis and Modeling.

Indonesia BPS, 2023. Mid Year Population - Statistical Data [WWW Document]. URL https://www.bps.go.id/en/statistics-table/2/MTk3NSMy/mid-year-population--thousand-people-.html (accessed 6.27.24).

Iturbide, M., Gutiérrez, J.M., Alves, L.M., Bedia, J., Cerezo-Mota, R., Cimadevilla, E., Cofiño, A.S., Di Luca, A., Faria, S.H., Gorodetskaya, I.V., Hauser, M., Herrera, S., Hennessy, K., Hewitt, H.T., Jones, R.G., Krakovska, S., Manzanas, R., Martínez-Castro, D., Narisma, G.T., Nurhati, I.S., Pinto, I., Seneviratne, S.I., van den Hurk, B., Vera, C.S., 2020. An update of IPCC climate reference regions for subcontinental analysis of climate model data: definition and aggregated datasets. Earth System Science Data 12, 2959–2970. https://doi.org/10.5194/essd-12-2959-2020

Johnson, T.C., Werne, J.P., Brown, E.T., Abbott, A., Berke, M., Steinman, B.A., Halbur, J., Contreras, S., Grosshuesch, S., Deino, A., Scholz, C.A., Lyons, R.P., Schouten, S., Damsté, J.S.S., 2016. A progressively wetter climate in southern East Africa over the past 1.3 million years. Nature 537, 220–224. https://doi.org/10.1038/nature19065

Kelley, L.C., Prabowo, A., 2019. Flooding and Land Use Change in Southeast Sulawesi, Indonesia. Land 8, 139. https://doi.org/10.3390/land8090139

Konecky, B., Russell, J., Bijaksana, S., 2016. Glacial aridity in central Indonesia coeval with intensified monsoon circulation. Earth and Planetary Science Letters 437, 15–24. https://doi.org/10.1016/j.epsl.2015.12.037

Konecky, B.L., Noone, D.C., Cobb, K.M., 2019. The Influence of Competing Hydroclimate Processes on Stable Isotope Ratios in Tropical Rainfall. Geophysical Research Letters 46, 1622–1633. https://doi.org/10.1029/2018GL080188

Krause, C.E., Gagan, M.K., Dunbar, G.B., Hantoro, W.S., Hellstrom, J.C., Cheng, H., Edwards, R.L., Suwargadi, B.W., Abram, N.J., Rifai, H., 2019. Spatio-temporal evolution of Australasian monsoon hydroclimate over the last 40,000 years. Earth and Planetary Science Letters 513, 103–112. https://doi.org/10.1016/j.epsl.2019.01.045

Lan, X., Keeling, R., 2024. Trends in CO2.

Lee, H., Calvin, K., Dasgupta, D., Krinner, G., Mukherji, A., Thorne, P.W., Trisos, C., Romero, J., Aldunce, P., Barrett, K., Blanco, G., Cheung, W.W.L., Connors, S., Denton, F., Diongue-Niang, A., Dodman, D., Garschagen, M., Geden, O., Hayward, B., Jones, C., Jotzo, F., Krug, T., Lasco, R., Lee, Y.-Y., Masson-Delmotte, V., Meinshausen, M., Mintenbeck, K., Mokssit, A., Otto, F.E.L., Pathak, M., Pirani, A., Poloczanska, E., Pörtner, H.-O., Revi, A., Roberts, D.C., Roy, J., Ruane, A.C., Skea, J., Shukla, P.R., Slade, R., Slangen, A., Sokona, Y., Sörensson, A.A., Tignor, M., Van Vuuren, D., Wei, Y.-M., Winkler, H., Zhai, P., Zommers, Z., Hourcade, J.-C., Johnson, F.X., Pachauri, S., Simpson, N.P., Singh, C., Thomas, A., Totin, E., Arias, P., Bustamante, M., Elgizouli, I., Flato, G., Howden, M., Méndez-Vallejo, C., Pereira, J.J., Pichs-Madruga, R., Rose, S.K., Saheb, Y., Sánchez Rodríguez, R., Ürge-Vorsatz, D., Xiao, C., Yassaa, N., Alegría, A., Armour, K., Bednar-Friedl, B., Blok, K., Cissé, G., Dentener, F., Eriksen, S., Fischer, E., Garner, G., Guivarch, C., Haasnoot, M., Hansen, G., Hauser, M., Hawkins, E., Hermans, T., Kopp, R., Leprince-Ringuet, N., Lewis, J., Ley, D., Ludden, C., Niamir, L., Nicholls, Z., Some, S., Szopa, S., Trewin, B., Van Der Wijst, K.-I., Winter, G., Witting, M., Birt, A., Ha, M., Romero, J., Kim, J., Haites, E.F., Jung, Y., Stavins, R., Birt, A., Ha, M., Orendain, D.J.A., Ignon, L., Park, S., Park, Y., Reisinger, A., Cammaramo, D., Fischlin, A., Fuglestvedt, J.S., Hansen, G., Ludden, C., Masson-Delmotte, V., Matthews, J.B.R., Mintenbeck, K., Pirani, A., Poloczanska, E., Leprince-Ringuet, N., Péan, C., 2023. IPCC, 2023: Climate Change 2023: Synthesis Report. Contribution of Working Groups I, II and III to the Sixth Assessment Report of the Intergovernmental Panel on Climate Change [Core Writing Team, H. Lee and J. Romero (eds.)]. IPCC, Geneva, Switzerland. Intergovernmental Panel on Climate Change (IPCC). https://doi.org/10.59327/IPCC/AR6-9789291691647

Løland, M.H., Krüger, Y., Fernandez, A., Buckingham, F., Carolin, S.A., Sodemann, H., Adkins, J.F., Cobb, K.M., Meckler, A.N., 2022. Evolution of tropical land temperature across the last glacial termination. Nat Commun 13, 5158. https://doi.org/10.1038/s41467-022-32712-3

Lu, H., Liu, W., Yang, H., Leng, Q., Liu, Z., Cao, Y., Hu, J., Sheng, W., Wang, H., Wang, Z., Zhang, Z., Sun, Y., Zhou, W., An, Z., 2022. Decoupled Land and Ocean Temperature

Trends in the Early-Middle Pleistocene. Geophysical Research Letters 49, e2022GL099520. https://doi.org/10.1029/2022GL099520

Lupien, R.L., Russell, J.M., Subramanian, A., Kinyanjui, R., Beverly, E.J., Uno, K.T., de Menocal, P., Dommain, R., Potts, R., 2021. Eastern African environmental variation and its role in the evolution and cultural change of Homo over the last 1 million years. Journal of Human Evolution 157, 103028. https://doi.org/10.1016/j.jhevol.2021.103028

McGrath, S.M., Clemens, S.C., Huang, Y., 2023. Pleistocene Sunda Shelf submersion-exposure cycles initiate vegetation Walker Circulation feedback. Geology. https://doi.org/10.1130/G51412.1

Meckler, A.N., Clarkson, M.O., Cobb, K.M., Sodemann, H., Adkins, J.F., 2012. Interglacial Hydroclimate in the Tropical West Pacific Through the Late Pleistocene. Science 336, 1301–1304. https://doi.org/10.1126/science.1218340

Parish, M., Russell, J., Konecky, B., Du, X., He, C., Bijaksana, S., Vogel, H., 2024. Changes in Indo-Pacific Warm Pool hydroclimate and vegetation during the last deglaciation. Quaternary Science Reviews 336, 108755. https://doi.org/10.1016/j.quascirev.2024.108755

Parish, M.C., Du, X., Bijaksana, S., Russell, J.M., 2023. A brGDGT-Based Reconstruction of Terrestrial Temperature From the Maritime Continent Spanning the Last Glacial Maximum. Paleoceanography and Paleoclimatology 38, e2022PA004501. https://doi.org/10.1029/2022PA004501

Partin, J.W., Cobb, K.M., Adkins, J.F., Clark, B., Fernandez, D.P., 2007. Millennial-scale trends in west Pacific warm pool hydrology since the Last Glacial Maximum. Nature 449, 452–455. https://doi.org/10.1038/nature06164

Russell, J.M., Hopmans, E.C., Loomis, S.E., Liang, J., Sinninghe Damsté, J.S., 2018. Distributions of 5- and 6-methyl branched glycerol dialkyl glycerol tetraethers (brGDGTs) in East African lake sediment: Effects of temperature, pH, and new lacustrine paleotemperature calibrations. Organic Geochemistry 117, 56–69. https://doi.org/10.1016/j.orggeochem.2017.12.003

Russell, J.M., Vogel, H., Bijaksana, S., Melles, M., Deino, A., Hafidz, A., Haffner, D., Hasberg, A.K.M., Morlock, M., von Rintelen, T., Sheppard, R., Stelbrink, B., Stevenson, J., 2020. The late quaternary tectonic, biogeochemical, and environmental evolution of ferruginous Lake Towuti, Indonesia. Palaeogeography, Palaeoclimatology, Palaeoecology 556, 109905. https://doi.org/10.1016/j.palaeo.2020.109905

Sarr, A.-C., Husson, L., Sepulchre, P., Pastier, A.-M., Pedoja, K., Elliot, M., Arias-Ruiz, C., Solihuddin, T., Aribowo, S., Susilohadi, 2019. Subsiding Sundaland. Geology 47, 119–122. https://doi.org/10.1130/G45629.1

Schouten, S., Hopmans, E.C., Sinninghe Damsté, J.S., 2013. The organic geochemistry of glycerol dialkyl glycerol tetraether lipids: A review. Organic Geochemistry 54, 19–61. https://doi.org/10.1016/j.orggeochem.2012.09.006

Seltzer, A.M., Blard, P.-H., Sherwood, S.C., Kageyama, M., 2023. Terrestrial amplification of past, present, and future climate change. Science Advances 9, eadf8119. https://doi.org/10.1126/sciadv.adf8119

Tierney, J.E., Zhu, J., King, J., Malevich, S.B., Hakim, G.J., Poulsen, C.J., 2020. Glacial cooling and climate sensitivity revisited. Nature 584, 569–573. https://doi.org/10.1038/s41586-020-2617-x

Windler, G., Tierney, J.E., Anchukaitis, K.J., 2021. Glacial-Interglacial Shifts Dominate Tropical Indo-Pacific Hydroclimate During the Late Pleistocene. Geophysical Research Letters 48, e2021GL093339. https://doi.org/10.1029/2021GL093339

Windler, G., Tierney, J.E., DiNezio, P.N., Gibson, K., Thunell, R., 2019. Shelf exposure influence on Indo-Pacific Warm Pool climate for the last 450,000 years. Earth and Planetary Science Letters 516, 66–76. https://doi.org/10.1016/j.epsl.2019.03.038

Zhao, B., Russell, J.M., Tsai, V.C., Blaus, A., Parish, M.C., Liang, J., Wilk, A., Du, X., Bush, M.B., 2023. Evaluating global temperature calibrations for lacustrine branched GDGTs: Seasonal variability, paleoclimate implications, and future directions. Quaternary Science Reviews 310, 108124. https://doi.org/10.1016/j.quascirev.2023.108124

Zhou, X., Chen, Q., Xie, F., Li, J., Li, M., Ding, R., Li, Y., Xia, X., Cheng, Z., 2019. Nonlinear response of Northern Hemisphere stratospheric polar vortex to the Indo–Pacific warm pool (IPWP) Niño. Sci Rep 9, 13719. https://doi.org/10.1038/s41598-019-49449-7

CHAPTER 2

A brGDGT-based reconstruction of terrestrial temperature from the Maritime Continent spanning the Last Glacial Maximum

Meredith Parish[1,2], Xiaojing Du[1,2], Satria Bijaksana[3], and James Russell[1,2]

[1]Department of Earth, Environmental, & Planetary Sciences, Brown University, Providence, RI, USA

[2]Institute at Brown for Environment and Society, Brown University, Providence, RI, USA

[3]Global Geophysics Group, Faculty of Mining and Petroleum Engineering, Institut Teknologi Bandung, Bandung, Indonesia

Published in 2023 in *Paleoceanography and Paleoclimatology,* 38, e2022PA004501.

Abstract

The tropics exert enormous influence on global climate. Despite the importance of tropical regions, the terrestrial temperature history in the Indo-Pacific Warm Pool (IPWP) region during the last deglaciation is poorly constrained. Although numerous sea surface temperature (SST) reconstructions provide estimates of SST warming from the Last Glacial Maximum to the Holocene, the timing of the onset of deglacial warming varies between records and inhibits determining the forcings driving deglacial warming in the IPWP. We present a 60,000-year long temperature reconstruction based on branched glycerol dialkyl glycerol tetraethers (brGDGTs) in a sediment core from Lake Towuti, located in Sulawesi, Indonesia. BrGDGTs are bacterial membrane-spanning lipids that, globally, become more methylated with decreasing temperature and more cyclized with decreasing pH. Although changes in temperature are the dominant control on brGDGTs in regional and global calibrations, we find that the cyclization of the brGDGTs is a major mode of variation at Lake Towuti that records important changes in the lacustrine biogeochemical environment. We separate the influence of lake chemistry changes from temperature changes on the brGDGT records, and develop a temperature record spanning the last 60,000 years. The timing of the deglacial warming in our record occurs after the onset of the deglacial increase in CO2 concentrations, which suggests rising greenhouse gas concentrations and the associated radiative forcing may have forced deglacial warming in the IPWP. Peaks in temperature around 55 and 34 ka indicate that Northern Hemisphere summer insolation may also influence land surface temperature in the IPWP region.

Plain Language Summary

The tropics play an important role controlling global climate because they export heat to higher latitudes. Even though the tropics are important, we do not actually know the primary control on tropical temperature. We created a 60,000-year long record of temperature because this length of record spans large changes in the proposed controls on tropical climate (greenhouse gas concentrations and incoming solar radiation). We created a temperature record from a lake sediment core from Lake Towuti in Indonesia. Since sediment gradually accumulated in the bottom of Lake Towuti for over 60,000 years, we took one sample from the lake sediment core every 6 cm to give us one sample every 500 years. We measured different types of molecules that compose the outer protective barrier (membrane) of bacteria cells. The molecules in the membrane are different in cold than hot environments. We measured the abundance of hot-adapted and cold-adapted membrane lipids to determine the temperature in the past. The timing of warming after the last glacial period occurs after the onset of the increase in CO2 concentrations, which suggests rising greenhouse gas concentrations and the associated radiative forcing may be the dominant control on temperature over the past 60,000 years.

1. Introduction

Three major zones of deep atmospheric convection energize the Earth's moisture and energy budgets: tropical Africa, Amazonia, and the Indo-Pacific Warm Pool (IPWP; Figure 1; Chiang, 2009). The IPWP is by far the largest of these, where sea surface temperatures (SSTs) above 28°C extend over an area of more than 30 million km^2, and the region exerts enormous influence on global climate through its interactions with the Walker Circulation, the Austral-Asian monsoons, and the Intertropical Convergence Zone (ITCZ; Chiang, 2009; De Deckker, 2016). Regionally, precipitation is intimately linked to surface temperature over the IPWP with high SSTs generating deep atmospheric convection and some of the highest precipitation rates on Earth (De Deckker, 2016; Figure 1).

Reconstructing a continuous record of terrestrial temperature spanning the past 60 thousand years (kyr) in the IPWP will provide insight into how changing boundary conditions (e.g., insolation and CO_2) from the Last Glacial Maximum (LGM) to modern (Shakun et al., 2012) influenced regional climate, how IPWP climate change will interact with global climate processes in the future, and how increasing anthropogenic CO_2 emissions will impact Indonesia, the fourth most populous country on Earth (Current Population, 2022).

The dominant forcing of deglacial warming in the IPWP is debated, due in large part to a wide range of estimates for the timing of the onset of deglacial warming in the region. The onset of warming indicated in SST records varies from 20.4 to 17.9 ka among existing SST records from the IPWP (Bolliet et al., 2011; Fan et al., 2018; Gibbons et al., 2014; Holbourn et al., 2011; Jian et al., 2020; Levi et al., 2007; Mohtadi et al., 2014; Rosenthal et al., 2003; Schröder et al., 2018; Setiawan et al., 2015; Steinke et al., 2006; Stott et al., 2007; Wang et al., 2018; Xu et al., 2008), spanning the onset of deglacial changes in northern hemisphere insolation and the global onset of increasing CO_2 concentrations after the LGM. The wide range of ages for the onset of deglacial warming has led to a variety of hypotheses for the forcings that control regional temperature, from teleconnections to the northern high latitudes (Stott et al., 2007) to a dominant control by atmospheric CO_2 concentrations (Shakun et al., 2012). Furthermore, to date, temperature reconstructions from this region are almost entirely from marine settings, complicating assessment of terrestrial temperature change. Terrestrial temperature is of particular importance in the tropics because convection there is centered over land masses (Chiang, 2009).

To uncover the forcings of terrestrial temperature in the IPWP, we reconstructed temperatures using sediment cores from Lake Towuti, Indonesia, spanning the past 60 kyr. This interval includes the last deglaciation, the most recent time interval when global warming was accompanied by rising greenhouse gas concentrations. We produced a terrestrial temperature reconstruction based on the fractional abundances of branched glycerol dialkyl glycerol tetraethers (brGDGTs), membrane-spanning lipids whose degree of methylation increases with decreasing temperatures to maintain membrane fluidity (Naafs et al., 2021). The degree of methylation of brGDGTs in lacustrine sediment samples is highly correlated with mean annual air temperature (MAAT) in tropical environments (Russell et al., 2018). Although these global relationships are well-established, Lake Towuti is a relatively unique, ferruginous environment and its microbial communities are likely not well-represented in existing surface sediments used in brGDGT calibrations (Martínez-Sosa et al., 2021; Raberg et al., 2021; Russell et al., 2018). Indeed, the IPWP region is not represented well in existing brGDGT calibrations and regional temperatures can exceed the limits of currently available temperature calibrations. We therefore evaluate brGDGTs in this environment to assess the applicability of existing calibrations and the environmental controls on brGDGT abundances through the 60-kyr record. We then reconstruct terrestrial temperature from Lake Towuti in Indonesia to evaluate the influences of atmospheric CO_2 concentrations and insolation as primary drivers of IPWP terrestrial temperature from the LGM to modern. As the first quantitative terrestrial temperature reconstruction in the IPWP region, our record provides additional constraints on the driving forcing of IPWP climate.

2. Study Site, Materials, and Methods

2.1 Study Site

Lake Towuti is located near the equator (2.75°S, 121.5°E) in central Sulawesi, Indonesia at an elevation of 318 m (Figure 1). Sulawesi is a 174,600 km^2 island in the center of the IPWP. Lake Towuti has a surface area of 560 km^2 and a maximum water depth of 203 m. Modern lake surface temperatures of Lake Towuti range seasonally from 29° to 31°C, with cooler temperatures in austral winter and spring and the warmest temperatures in austral fall (Russell et al., 2020). The water column mixes seasonally to ~100 m depth but a permanent thermocline at 100 m depth separates oxic waters at the surface from hypoxic to anoxic waters below (Costa et al., 2015). The pH is ~7.8 and the lake is ultraoligotrophic. The lake is one of a handful of ferruginous (high iron-low sulfate) systems that exist on Earth today due to its location within the East Sulawesi ophiolite (Crowe et al., 2008; Vuillemin et al., 2016). This setting establishes an uncommon biogeochemical environment within the lake, and the extremely low primary productivity at Lake Towuti has been attributed to low nutrient delivery from surrounding soil and phosphate removal related to high iron concentrations (Crowe et al., 2008; Russell et al., 2020).

The samples analyzed in this study were subsampled from a piston core (IDLE-TOW10-9B) extracted from the center of Lake Towuti's northern basin (Russell et al., 2014, 2020). We analyzed 115 samples, spanning the past 60,000 years for an average sampling resolution of ~500 years, with a minimum sampling resolution of 82 years and maximum sampling resolution of 3575 years. The mean sampling resolution during the last deglaciation (22 to 11.6 ka) is 430 years. There are 23 radiocarbon dates in the top 43-kyr of sediment, which we calibrated to Intcal20 and used to estimate the age of every centimeter of sediment with Bacon in *R* (Blaauw & Christen, 2011).

2.2 Lipid Extraction and Analysis

Lipids were extracted from sediment using a DIONEX Accelerated Solvent Extractor using dichloromethane:methanol (9:1). The lipid extract was divided into neutral and acid fractions using dichloromethane:isopropanol (2:1) and ethyl ether:acetic acid (96:4) over an aminopropyl silica gel column for previous analyses (Konecky et al., 2016). Silica gel columns were used to separate lipids within the neutral fraction, using hexane to isolate n-alkanes, dichloromethane to isolate ketones, and methanol to isolate the remaining hydroxides. We used Al_2O_3 columns to further separate the hydroxide fraction into apolar and polar fractions with the eluents hexane:dichloromethane (9:1) and dichloromethane:methanol (1:1). The polar fraction was filtered through 0.45 μm PTFE filter in hexane: isopropanol (99:1).

We analyzed the polar fractions using atmospheric pressure chemical ionization/high-performance liquid chromatography mass spectrometry (APCI/HPLC-MS) with a bridged ethylsiloxane/silica hybrid (BEH) hydrophilic interaction chromatography (HILIC) 1.7 μm (2.1 mm inner diameter × 150 mm length) column using selective ion monitoring mode, targeting molecules at m/z 1,050, 1,048, 1,046, 1,036, 1,034, 1,032, 1,022, 1,020, 1,018,

1,292, 1,296, 1,298, 1,300, and 1,302 (Hopmans et al., 2016). Ten percent of samples were run in duplicate to assess the precision of the measurements. We manually integrated peak areas of both 5-methyl isomers (Ia, Ib, Ic, IIa, IIb, IIc, IIIa, IIIb, IIIc) and 6-methyl isomers (IIa', IIb', IIc', IIIa', IIIb', IIIc') to quantify the relative abundances of the brGDGTs in each sample.

2.3 Analyses of the Fractional Abundances of GDGTs

Empirical studies, theory, and molecular simulations indicate that the number of methyl branches in brGDGTs increases at decreasing temperatures to maintain cell membrane fluidity

(Loomis et al., 2012, 2014; Martínez-Sosa et al., 2021; Naafs et al., 2021; Raberg et al., 2021; Russell et al., 2018; Tierney & Russell, 2009; Tierney et al., 2010). However, water chemistry, microbial community composition, and other factors may also affect brGDGT relative abundances (Loomis et al., 2014; Martínez-Sosa et al., 2021; Wu et al., 2021). We used principal component analysis (PCA) to evaluate the primary modes of variability in brGDGT abundances in downcore samples from Lake Towuti. We performed a PCA analysis based on the correlation matrix of the fractional abundances of the major brGDGTs in the Lake Towuti record (Ia, Ib, Ic, IIa, IIa', IIb, IIb', IIc', IIIa'), using the princomp() function in the "vegan" package in *R* (Oksanen et al., 2020). The nine major brGDGTs each comprised more than two percent of the total abundance of brGDGTs in at least one sample over the past 60,000 years (Ia, Ib, Ic, IIa, IIa', IIb, IIb', IIc', IIIa').

Many index-based calibrations and multiple linear regression models exist to translate the signals reflected in changing brGDGT assemblages into paleoenvironmental and paleoclimatic parameters (e.g., temperature). Index-based calibrations are based on our theoretical and empirical understanding that brGDGTs with fewer methyl branches increase with increasing temperature, and brGDGTs with fewer cyclopentane rings are more abundant in environments with a higher pH (Weijers et al., 2007). MBT'_{5ME} (Equation 1) is the ratio of brGDGTs with four methyl branches or substituted cyclopentane moieties relative to the total abundance of brGDGTs with 4-6 methyl branches or substituted rings (De Jonge et al., 2013; Russell et al., 2018) and it increases with increasing temperature. To calculate MAAT from MBT'_{5ME}, we used the calibration from Russell et al. (2018) (Equation 2).

$$MBT'_{5ME} = \frac{(Ia + Ib + Ic)}{(Ia + Ib + Ic + IIa + IIb + IIc + IIIa)} \quad (1)$$

$$MAAT = -1.21 + 32.42 \times MBT'_{5ME} \quad (2)$$

In addition to index-based calibrations, there are various multiple linear regression methods based on the best statistical fits of brGDGT fractional abundances to temperature. These methods generally confirm the basic principles inherent to index-based calibrations (i.e., the degree of methylation increases with decreasing temperature), but may include a distinct set of brGDGTs potentially due to influences of multiple correlated environmental parameters on brGDGT abundances (Loomis et al., 2014). Among these calibrations, we calculated the temperature of the months above freezing (MAF) using the stepwise forward selection/backwards elimination (SFS/ SBE) equation published in the supplement of Raberg et al. (2021) (Equation 3). We used the calibration recommended for samples with limited quantities of IIIb and IIIc because these brGDGTs comprised less than 1% of the brGDGTs in all samples from Lake Towuti. The equation is based on the fractional abundances of IIa and IIIa, where fIIa is the fraction of IIa relative to Ia, IIa, and IIIa; and fIIIa is the fraction of IIIa relative to Ia, IIa, and IIIa.

$$MAF = 26.56 - 34.67(\mathrm{fIIa}^2_{meth}) + 29.4(\mathrm{fIIIa}^2_{meth}) - 49.43(\mathrm{fIIIa}_{meth}) \quad (3)$$

We calculated MAAT using the SFS/SBE equation (Equation 4) based on the fractional abundances of the major brGDGTs in 65 lakes from tropical east Africa (Loomis et al., 2012, 2014; Russell et al., 2018). The SFS/SBE equation shows MAAT decreases with increasing penta- and hexamethylated brGDGTs (e.g., IIa, IIb, IIb’, and IIIa), and MAAT increases with increasing tetramethylated brGDGTs (e.g., Ib).

$$MAAT = 23.04 - 30.09\,(IIIa) - 45.31(IIb) - 46.56(IIb') - 22.65(IIa) + 72.85(Ib') \quad (4)$$

We also calculated a new SFS/SBE-based MAAT equation with all global lacustrine samples presented in Martinez-Sosa et al. (2021) and a new SFS/SBE equation based on all samples in the global database that have less than 50% hexamethylated brGDGTs. As hexamethylated brGDGTs are most abundant in cool environments, this restricts the calibration to warmer climates where calibration to MAAT may be more appropriate. We focus on MAAT rather than the mean temperature of MAF (Martínez-Sosa et al., 2021; Raberg et al., 2021) in our choice of calibrations, though MAAT and MAF are equivalent in the tropics due to the lack of seasonality. These SFS/SBE equations are presented in the results section.

The cyclization of branched tetraethers (CBT) indices (Equations 5 and 6) were calculated using brGDGTs with varying degrees of cyclization to evaluate variations in lake pH (De Jonge et al., 2014; Sinninghe Damsté et al., 2012; Tierney et al., 2010; Weijers et al., 2007). We use the CBT_{5ME} index from De Jonge et al. (2014):

$$CBT_{5ME} = -log((Ib + IIb)/(Ia + IIa)) \quad (5)$$

We also use the CBT' from De Jonge et al. (2014):

$$CBT' = -log((Ic + IIa' + IIb' + IIc' + IIIa' + IIIb' + IIIc')/(Ia + IIa + IIIa)) \quad (6)$$

We evaluated the branched and isoprenoidal tretraether (BIT) index (Equation 7; Hopmans et al., 2004; Tierney et al., 2010), which reflects the amount of branched GDGTs (Ia, IIa, IIIa) relative to the amount of branched and isoprenoidal GDGTs (isoGDGTs) as indicated by crenarchaeol (IV).

$$BIT = \frac{([Ia] + [IIa] + [IIIa])}{([Ia] + [IIa] + [IIIa] + [IV])} \quad (7)$$

In addition to analyses of brGDGTs, we analyzed the relative abundances of isoGDGTs, which are produced by Thaumarchaeota. Previous work has shown that the degree of cyclization of isoGDGTs increases with increasing temperature in both marine and lacustrine settings, and developed the TEX_{86} index (Equation 8), the ratio of isoprenoidal GDGTs with 2–3 rings and the regio-isomer of crenarchaeol (IV’) relative to the number of isoGDGTs with 1–3 rings and IV’, to quantify this relationship. The number of rings in isoGDGTs in the TEX_{86} index increases with increasing temperature (Powers et al., 2010; Schouten et al., 2002).

$$TEX_{86} = \frac{([GDGT2] + [GDGT3] + [IV'])}{([GDGT1] + [GDGT2] + [GDGT3] + [IV'])} \quad (8)$$

However, the relative abundances of isoGDGTs may also be influenced by changes in the relative inputs of terrestrial and aquatic isoGDGTs, as well as other microbial community changes. Comparison between the BIT index and the TEX_{86} index allows us to test whether TEX_{86} reflects changes in soil runoff amount (Sinninghe Damsté et al., 2012) or other environmental factors (Baxter et al., 2021).

2.4 Changepoint Analysis

We determined the timing of deglacial warming in our temperature record using the EnvCpt package in *R* to find significant changepoints in the trend (slope) in the data (Killick et al., 2021). The changepoints were determined by calculating a stepwise linear function that minimizes the total residual error. We selected the changepoint detected between 22 and 14 ka as the timing of deglacial warming. Additionally, we calculated the changepoints of atmospheric CO_2 and nearby SST records to compare with the timing of deglacial changes to the Lake Towuti temperature record using identical methods.

3. Results

3.1 Abundances of Tetra-, Penta-, and Hexa-Methylated brGDGTs Relative to Calibration Data Sets

The fractional abundance of brGDGTs from Lake Towuti are dominated by tetramethylated brGDGTs, with greater than 50% brGDGTs with four methyl groups in every sample (Figures 2 and 3). After tetramethylated brGDGTs, pentamethylated brGDGTs are the most abundant brGDGTs in Lake Towuti samples. Hexamethylated brGDGTs make up less than 10% of the total brGDGTs in every sample. Tetramethylated brGDGTs are much more abundant in almost all samples from Lake Towuti than in samples from tropical southeast Africa (Figure 2; Russell et al., 2018) and globally (Figure 2; Martínez-Sosa et al., 2021), and although Lake Towuti samples are in a compositional field that might be expected of a lacustrine setting, they are primarily outside the range of samples in existing calibration datasets (Figure 2). Hexamethylated brGDGTs have more methyl branches than tetra- and pentamethylated brGDGTs, and are found in higher abundance in colder environments. Therefore, the low abundance of hexamethylated brGDGTs and high abundance of tetramethylated brGDGTs is consistent with the high mean annual temperatures observed at Lake Towuti relative to the environments in existing global calibrations.

BrGDGT Ia, containing four methyl groups and zero cyclopentane rings, is the most abundant brGDGT throughout the past 60,000 years (Figure 3). The highest abundances of Ia occur around 45 ka and the lowest abundance between 35 and 10 ka. Ib and Ic are the second and third most abundant brGDGTs, and show the opposite trends as Ia, exhibiting the lowest values of the record at 45 and 10 ka with sustained high abundances from 35 to 10 ka. IIa shows a similar pattern as Ia but is less abundant than each of the tetramethylated brGDGTs. IIb is less variable over the past 60,000 compared to the other brGDGTs due to low abundance. IIb' varies similarly to Ic with the highest abundances at 60 ka and between 30 and 10 ka. IIc' has less than 5% abundance throughout the record with the lowest abundances from 50 to 35 ka and from 15 ka to present. IIc, IIIa, IIIb, IIIb’, IIIc, and IIIc’ have the lowest abundances (less than 2%) in every samples during the past 60,000 years. IIIa’ comprises over 2% of the total abundance of brGDGTs in some samples during the past 60,000 years with the highest abundances between 55 and 40 ka.

3.2 PCA of Fractional Abundances of brGDGTs

A PCA reveals two principal components that explain a total of 80% of the variance in the fractional abundances of brGDGTs. PC1 explains 54% of the variance and PC2 explains 26% of the variance (Figure 4c). All of the brGDGTs without cyclopentane moieties (Ia, IIa, IIa’, and IIIa’) have positive loadings on PC1, all of the brGDGTs with one cyclopentane moiety (Ib, IIb, and IIb’) have negative loadings on PC1, and brGDGTs with two cyclopentane moieties (Ic and IIc’) have even greater magnitude negative loadings on PC1. The distribution of these brGDGTs along PC1 indicates that PC1 reflects the cyclization of brGDGTs (Figure 4c). PC1 has the highest component scores at 45 and 10 ka and lowest scores from 60 to 50 ka and between 35 and 15 ka (Figure 4a).

Tetramethylated brGDGTs (Ia, Ib, and Ic) have a positive or zero loading on PC2 (Figure 4c). Pentamethylated brGDGTs (IIa, IIa’, IIb, IIb’, and IIc’) have negative loadings on PC2. The only hexamethylated brGDGT with greater than 2% abundance in one sample from the record (IIIa’) has the greatest negative loadings on PC2, indicating that PC2 reflects the methylation of brGDGTs throughout the Lake Towuti record. PC2 has the lowest component scores between 50 and 40 ka and at 27 ka, before increasing into the Holocene (Figure 4b).

3.3 Methylation and Temperature

The MBT'$_{5ME}$ -index varies between 0.86 and 0.94 throughout the entire record. These high values reflect the high proportion of tetramethylated brGDGTs in all samples from Lake Towuti and therefore predict high temperatures over the past 60,000 years (Figure S1a in Supporting Information S1). The lowest MBT'$_{5ME}$-values occur between 50 and 40 ka when the proportion of tetramethylated brGDGTs, driven by Ib and Ic, are at their lowest throughout the record. MAAT calculated from the MBT'$_{5ME}$-index is positively correlated with PC2 (Figure 5; *R* = 0.79, all reported correlation coefficients have a *p*-value less than 0.01), presumably reflecting the importance of Ia and Ib to both PC2 and the MBT'$_{5ME}$-index. Using the Russell et al. (2018) MBT'$_{5ME}$ temperature calibration results in the lowest temperature of the record (26.6°C) at 38 ka and the highest temperature of the record (29.7°C) at 13 ka (Figure S1a in Supporting Information S1).

The Raberg et al. (2021) MAF SFS/SBE produces temperatures that vary between 24.2°C and 26.0°C, with the lowest temperatures of the record occurring between 30 and 20 ka (Figure S1c in Supporting Information S1). The MAF reconstruction is moderately correlated with PC2 (Figure 5; *R* = 0.67). The MAF SFS/SBE only includes fIIa and fIIIa. IIIa comprises less than two percent of all samples from Lake Towuti and is therefore not included in the PCA analysis and IIa only has a weak negative loading on PC2. Therefore, it is not surprising that the correlation is lower than the MBT'$_{5ME}$-MAAT and Russell SFS/SBE MAAT correlation with PC2 (Figure 5).

The new global SFS/SBE regression calculated using all global lacustrine samples included in Martinez-Sosa et al. (2021) and identical methods as Russell et al. (2018) is (Equation 9):

$$MAAT = 6.04 + 91.93\,(Ib) + 22.78(Ia) - 27.59(IIa) - 25.16(IIIa') - 72.52(Ic) \quad (9)$$

The global SFS/SBE regression using the same method but only including "warm lake" samples with less than 50% hexamethylated brGDGTs is (Equation 10):

$$MAAT = 10.63 + 84.23\,(Ib) + 18.32(Ia) - 34.71(IIa) - 41.72(IIIa') - 78.76(Ic) \tag{10}$$

Stepwise forward selection regressions thus select the same compounds (Ia, Ib, Ic, IIa, and IIIa') using global or "warm lake" datasets but differ from the brGDGTs used in SFS/SBE regression based on tropical East African samples alone (Ib, IIb, IIb', and IIIa; Equation 4; Russell et al., 2018). Both the global and less than 50% hexamethylated SFS/SBE reconstructions result in similar temperature records over the past 60,000 years (Figures S1e and S1g in Supporting Information S1), and are positively correlated with PC2 (R = 0.69 and R = 0.67, respectively; Figure 5). Ia and Ib, which are included in the SFS/SBE equations (Equations 9 and 10), have strong positive loadings on PC2 and IIa, and IIIa' have negative loadings on PC2. Ic, which is also included in the SFS/ SBE equations, has a near zero loading on PC2, potentially explaining the relatively weak correlations.

The tropical East African SFS/SBE model produces a temperature reconstruction that indicates relatively high temperatures ca. 55 ka, the lowest temperatures in the record between 50 and 37 ka (Figure 6a), a cool LGM that extends from ~27 to 17 ka and warming from the LGM into the Holocene. The temperature reconstruction is highly correlated with PC2 (R = 0.93, shown in Figure 5; $R2$ = 0.84, shown in Figure 6b). The brGDGTs included in the tropical African SFS/SBE (Ib, IIb, IIb', and IIIa) all have strong loadings on PC2 with the exception of IIIa, which comprises less than 2% of all samples from the Lake Towuti record. Assuming that the tropical East African SFS/SBE calibration reflects changing temperature, PC2 reflects changes in temperature and therefore that temperature explains approximately 26% of the total variance in fractional abundances of all major brGDGTs.

The Raberg et al. (2021) calibration is strongly dependent on the fractional abundance of IIIa (Raberg et al., 2021), which has very low abundance in most of the Lake Towuti samples. The magnitude of LGM to modern temperature change in Lake Towuti produced by this calibration is less than two degrees, which is inconsistent with nearby SST reconstructions (Rosenthal et al., 2003; Schröder et al., 2018; Stott et al., 2007). We therefore do not use the Raberg et al. (2021) calibration in further analyses. We also do not use MBT'_{5ME}-based calibration (Russell et al., 2018) to infer temperature. The PCA of the down-core fractional abundances of brGDGTs from

Lake Towuti reveals that Ic, which is included in the MBT'_{5ME}-index, varies with the principal component that may reflect lake pH (PC1) rather than lake temperature (PC2). Ic is also included in the global and "warm lake" SFS/SBE equations. The tropical East African SFS/SBE temperature reconstruction (Russell et al., 2018), in contrast, is based on brGDGTs that principally load on PC2, mitigating these effects. In the following analyses and discussion, we use the tropical African SFS/SBE reconstruction because it has the strongest correlation with PC2 and thus appears to capture the influence of temperature on the brGDGTs at this site.

3.4 Cyclization, pH, and Isoprenoidal GDGTs

The CBT_{5ME} index indicates an interval of abundant cyclized brGDGTs at ~45 ka, a sustained period of low CBT_{5ME} values from 35 to 11 ka, and an abrupt increase to the highest values of the record around ~10 ka (Figure S2g in Supporting Information S1). CBT_{5ME} closely tracks and is highly correlated with PC1 (R = 0.81, Figure 5), confirming that PC1 primarily reflects variations in the cyclization of brGDGTs. Ia and IIa are included in the denominator of the CBT_{5ME} index and have strong loadings on PC1, whereas Ib and IIb are included in the numerator of the CBT_{5ME} index and have negative loadings on PC1. In prior calibration studies CBT_{5ME} has been shown to depend on pH and conductivity (Martínez-Sosa et al., 2021; Raberg et al., 2021). Although this is not always the case in lacustrine sediment calibrations (e.g., Russell et al., 2018), previous studies in Lake Towuti and the surrounding catchment demonstrated that CBT_{5ME} values increased from soils, to river sediments, to lake sediments associated with decreasing pH in these environments (Tierney & Russell, 2009). We infer that the strong correlation of CBT_{5ME} with PC1 indicates the majority of variation in the fractional abundances of the brGDGTs that load on PC1 depend on the pH, and potentially conductivity, of Lake Towuti. Using CBT_{5ME} to reconstruct pH using the soil-based calibration from De Jonge et al. (2014) results in a pH of ~7 from 35 to 11 ka, a sharp drop in pH around 10 ka, before hovering around a pH of ~6.8 during most of the Holocene (Figure S3 in Supporting Information S1). The CBT' index behaves similarly to the CBT_{5ME} index, however the peak in CBT_{5ME} at 45 ka is much less pronounced in the CBT' record (Figure S2 in Supporting Information S1). CBT' is more highly correlated with PC1 (R = 0.83, shown in Figure 5, $R2$ = 0.69, shown in Figure 7b) than CBT_{5ME}. The lake CBT'-base calibration from Russell et al. (2018) indicates lower pH values from 35 to 11 ka than from 10 ka, which indicates that Lake Towuti was more acidic at the LGM. More acidic lake water at the LGM contradicts existing data, which indicate more basic lake water at the LGM (Costa et al., 2015). However, CBT' was weakly correlated with pH in the East African lakes studied by Russell et al. (2018).

Both the BIT index and the TEX_{86} index are significantly correlated with PC1 ($R = -0.65$ and $R = 0.75$, respectively; Figure 5). The correlation of both BIT and TEX_{86} with PC1 indicates that both indices primarily reflect the cyclization of brGDGTs and likely the lake chemistry. BIT and TEX_{86} are also negatively correlated with each other ($R = -0.73$), indicating that TEX_{86} may not reflect temperature and is influenced by the abundance of crenarchaeol (Baxter et al., 2021; Tierney et al., 2010). These correlations imply that BIT is impacted by lake chemistry, terrigenous sediment fluxes, or other environmental parameters that influence GDGT sources to the sediment (Sinninghe Damsté et al., 2012).

3.5 Timing of Temperature Change

Changepoint analysis of the temperature reconstruction from Lake Towuti based on the East African lake SFS/ SBE indicates that deglacial warming begins at 17.5 ka (Figure 8), over 1,000 years after the onset of deglacial increase in CO_2 at 18.7 ka as indicated by identical changepoint detection methods applied to the West Antarctic Ice Sheet (WAIS) Divide CO_2 record (Marcott et al., 2014). Application of the changepoint analysis to nearby SST records indicates deglacial warming starts at a wide range of times. The SST record off the coast of Sumatra has the latest onset of deglacial warming at 16.2 ka (SO189-39KL; Mohtadi et al., 2014), whereas the earliest deglacial warming occurs at 20.6 ka in the Makassar Strait (SO217-18519; Schröder et al., 2018). The timing of deglacial warming indicated in the Lake Towuti records lies exactly on the median timing of warming of all the SST records included in our analysis.

4. Discussion

4.1 Variations in brGDGTs in Sediments From Lake Towuti

Previous work investigating brGDGTs in Lake Towuti, inflowing rivers, and surrounding soils has demonstrated in-situ production of brGDGTs in Lake Towuti (Tierney & Russell, 2009), suggesting changes in the fractional abundances of brGDGTs depend on environmental variables in the lake rather than surrounding soil. Temperature explains the majority of variance in the fractional abundances of brGDGTs in global lacustrine samples (Martínez-Sosa et al., 2021) and in tropical East Africa (Russell et al., 2018). Globally, pH explains only 12% of the variance in the abundances of brGDGTs (Martínez-Sosa et al., 2021) and in tropical East Africa lake water pH does not cause significant variation (Russell et al., 2018). In contrast to brGDGTs in these global datasets, we observe that cyclization, which is most dependent on the pH of the lake water in which the brGDGTs were produced (Martínez-Sosa et al., 2021; Raberg et al., 2021), explains the majority (54%) of the variance in the fractional abundances of brGDGTs in the Lake Towuti record (Figure 4c). Changes in methylation of the brGDGTs is the second mode of variation, explaining 26% of the variance in the brGDGT assemblages (Figure 4c). PC1 is strongly correlated with the CBT_{5ME} index and PC2 correlates with the temperature record reconstructed using the East African SFS/SBE from Russell et al. (2018).

Prior sedimentological studies of Lake Towuti support the inference that changes in PC1 through time reflect changes in lake water chemistry. Lake Towuti experienced very large changes in sediment composition during the LGM that reflect increased mixing, oxygenation, and pH that resulted in substantially higher oxidized metal and carbonate mineral inputs to the sediment, among other shifts (Costa et al., 2015; Russell et al., 2014, 2020). During the LGM, decreased temperatures and increased aridity led to lake surface cooling, increased lake mixing, and thereby oxygenation of the lake water column. This resulted in increased burial of reactive iron (Russell et al., 2020). At the same time, authigenic carbonate in the form of siderite increased during this interval, potentially reflecting increased pH and the burial of reactive iron in the surface sediments (Russell et al., 2020). Reconstructing pH with a soil calibration (De Jonge et al., 2014) indicates higher pH values at the LGM than modern. The pH values were ~7.0 at the LGM, whereas the most modern reconstructed value was 6.6 (Figure S3 in Supporting Information S1). It should be noted that the most modern reconstructed pH value is well below the measured modern pH (7.8); however, the trend in pH values reconstructed from the cyclization index are consistent with previous climatic inferences. These biogeochemical changes were used to infer a more prolonged dry season at the LGM, which could cause increased evaporation and longwave heat loss that increased lake mixing, increase lake water pH, and increased Fe burial (Costa et al., 2015).

Iron measured in Lake Towuti's sediment is negatively correlated with PC1 ($R = -0.73$; Figure 5; Costa et al., 2015), and authigenic carbonate content of the sediment rises during the interval of high Fe. High Fe and carbonate mineral concentrations are consistent with the higher pH values inferred from CBT_{5ME} values (Costa et al., 2015; Russell et al., 2020). Field and experimental studies have shown that brGDGT assemblages depend on dissolved oxygen content and the pH of lake water (Martínez-Sosa & Tierney, 2019; Stefanescu et al., 2021; Tierney et al., 2012; Yao et al., 2020). Although it remains difficult to quantify changes in these variables through time, our results show that they can have substantial impacts on brGDGT abundances in tropical lake settings.

The changes in cyclization of brGDGTs recorded by PC1 and CBT' are consistent with elevated pH values during the LGM (Figure 7a), but it is unclear why these biogeochemical changes in the lake and shifts in cyclization dominate the variation in brGDGTs in Lake Towuti, in contrast to globally distributed lakes. Ferruginous lakes are uncommon on Earth today, and our study could suggest that the microbes that produce brGDGTs in these systems have different sensitivities to pH and temperature than in other tropical lakes.

Principal component analysis reveals the orthogonal behavior of cyclization and methylation of the fractional abundances of the brGDGTs (Figure 4). Changes in methylation of brGDGTs represented by PC2 explain 26% of the variance in the fractional abundances of brGDGTs over the past 60,000 years. PC2 and the East African SFS reconstruction are highly correlated, and PC2 is orthogonal to PC1, giving us confidence in our ability to fully separate the influences of chemical changes in the water of Lake Towuti from the changes in temperature captured by the degree of methylation. Lake Towuti has mostly tetramethylated brGDGTs throughout the past 60,000 years, indicating that the lake experienced higher temperatures than the surface samples included in the tropical African surface sample calibration (Russell et al., 2018). The highest MAAT in the tropical African data set is 26.8°C, which is more than 3°C colder than the modern MAAT at Lake Towuti. Because Lake Towuti's modern MAAT is outside the range of the tropical East African SFS/SBE calibration we apply, we hesitate to make inferences based on the absolute values of the reconstructed temperatures. Indeed, the most modern reconstructed temperature value in the Lake Towuti record is ~34°C at 0.347 ka, which is three degrees warmer than the warm season recorded in measured lake surface temperature at Lake Towuti, again suggesting the absolute reconstructed values are inaccurate. Therefore, we do not interpret the reconstructed values as actual temperature, and instead focus on the timing and structure of the Lake Towuti MAAT record.

We use the East African SFS/SBE equation to reconstruct MAAT; however, the assemblage of brGDGTs is likely more highly correlated with lake water temperature, not air temperature. We are unable to determine whether the reconstructed temperature reflects bottom water temperature or surface water temperature. As in many tropical lakes, there is a weak temperature gradient between the surface and bottom water, with 28.4°–30.5°C surface water and 28.0°C bottom water in modern measurements (Costa et al., 2015).

4.2 Comparison to Regional LGM Temperature Records

The Lake Towuti record indicates a terrestrial temperature change from the LGM to the Holocene of 3.6°C. Although we hesitate to trust the absolute value of the reconstructed temperatures, the record may still capture the amplitude of the changes in temperature with time assuming the brGDGT-MAAT relationship is linear. Indeed, 3.6°C is within the range of deglacial warming inferred from regional palynological records, which estimate the LGM was 2°–4°C cooler than modern. At this time, lowland rainforest decreased, grassland expanded, and high-elevation plant taxa shifted downslope (Reeves et al., 2013). Another nearby pollen record from South Sulawesi was used to infer a 2.5°C temperature change from the LGM to modern (Hope, 2001), though the chronology of this record is highly uncertain. The magnitude of temperature change indicated in our temperature reconstruction is also consistent with SST records from the region. Nearby SST reconstructions from the IPWP indicate 2°–4°C of deglacial warming (Rosenthal et al., 2003; Schröder et al., 2018; Stott et al., 2007). Because of the higher heat capacity of the ocean relative to the continent, the magnitude of terrestrial temperature change is expected to be greater and more variable than changes in SSTs (Clement et al., 2004).

Changepoint analysis of Lake Towuti temperatures indicates deglacial warming began at 17.5 ± 0.33 ka. Atmospheric CO_2 concentrations and their associated radiative forcing began increasing at 18.7 ka (Figure 8; Marcott et al., 2014; Schilt et al., 2010). Warming in Lake Towuti thus began ∼1 kyr after the onset of the deglacial increase in CO_2 concentrations, though this lag could narrow (or widen) given the 0.33 kyr uncertainty of the Lake Towuti age model at 17.5 ka. The timing of the onset of deglacial warming thus considerably lags changes in global forcings, such as CO_2, and occurs well in advance of more regional climate forcings, such as Sunda Shelf inundation. The lag in deglacial warming in the Lake Towuti record behind the deglacial increase in CO_2 points to greenhouse gas forcing as the primary driver of the IPWP temperature as observed in temperature records globally (Shakun et al., 2012).

All but two of the existing SST records from the IPWP show warming coincident with or after the deglacial increase in CO_2, in support of the timing we infer from Lake Towuti (Figure 8). However, the wide range of timing of deglacial warming in IPWP SST records remains difficult to explain and does not exhibit clear patterns that might relate to ocean circulation. SST records from the Makassar Strait (SO217-18519) and the Timor Sea (MD01-2378) show deglacial warming began prior to increasing atmospheric CO_2 concentrations (Schröder et al., 2018; Xu et al., 2008; Figure 8), as does warming in the Sulu Sea record (MD97-2141) as described in the original publication (Rosenthal et al., 2003). Our method does not indicate deglacial warming in the Sulu Sea record until ∼16.5 ka, but may be sensitive to the hiatus in sedimentation from 27.2 to 21.8 ka. Warming was reported to begin at 20 ka by Rosenthal et al. (2003).

Exposure of the Sunda and Sahul Shelves is often invoked to explain deglacial changes in hydroclimate proxies from the LGM to modern in the IPWP (DiNezio et al., 2016, 2018; DiNezio & Tierney, 2013; Griffiths et al., 2013; Windler et al., 2019, 2020), potentially due to changes in surface temperatures marked by cooling over exposed shelf areas. The flooding of the Sunda and Sahul Shelves began at 15.5 ka (Pico et al., 2020), lagging the onset of deglacial warming in the Lake Towuti and marine temperature reconstructions by ~2 kyr. The onset of warming before the inundation of the Maritime Continent shelves indicates that the flooding of the shelves did not cause warming on Sulawesi. These results do not necessarily contradict the hypothesis that shelf exposure affected regional precipitation patterns, as modeling studies suggest the cooling associated with shelf exposure is modest and largely restricted to exposed shelf areas (DiNezio et al., 2018).

The Lake Towuti temperature record shows considerable orbital-scale temperature variations in addition to the last deglaciation. Our MAAT reconstruction indicates peaks in temperature at 55, 34, and 11 ka, similar to the timing of peaks in both Northern Hemisphere summer insolation and local winter insolation (Figure 9b). Both summer insolation from 30°N and local (2.75°S) winter insolation exhibit peaks roughly around 58, 34, and 11 ka, and troughs around 47, 22, and 0 ka (Figure 9c). A temperature reconstruction from Lake Tanganyika in East Africa, located at 6.55°S, also shows peaks in temperature around the same time as summer insolation from 30°N (Tierney et al., 2008) and local winter insolation (Figure 9b). A correlation between temperature and local winter insolation could imply a seasonal bias in our temperature reconstruction likely due to excess winter production of brGDGTs. Excess winter production of brGDGTs is plausible because winter is the mixing season and flux studies suggest increase brGDGT productions after lake mixing seasons (van Bree et al., 2020).

However, due to the lack of seasonality near the equator, we suggest that it is more likely that temperature at Lake Towuti is related to Northern Hemisphere summer insolation due to the influence of Northern Hemisphere insolation on the tropical monsoon (Guo et al., 2012; Ruddiman, 2003; Ruddiman & Raymo, 2003). Feedbacks between temperature and the hydrological cycle have been shown to be important in tropical Africa on orbital timescales (Dee et al., 2021; Gasse, 2000). The covariance between Northern Hemisphere insolation and temperature at Lake Towuti appears to break down during the Holocene, similar to the observation that methane from the Greenland Vostok ice cores diverges from Northern Hemisphere summer insolation at ~5 ka that has been attributed to forest clearance and rice cultivation (Ruddiman, 2003). The breakdown of the covariance between temperature and Northern Hemisphere summer insolation when greenhouse gas concentrations are high further highlights the importance of greenhouse gas concentrations for controlling IPWP climate.

5. Conclusions

The onset of deglacial warming at 17.5 ka indicated in the Lake Towuti temperature reconstruction provides support for CO_2 as the primary mechanism forcing IPWP temperature from the LGM to modern. Northern Hemisphere summer insolation also appears to influence temperature in the IPWP and southeast Africa. The primary control of greenhouse gas concentrations on temperature in the IPWP raises concerns that greenhouse gas-forced climate changes in the IPWP could pose a threat to a region already experiencing frequent floods and landslides that are attributed to anthropogenic climate change.

Acknowledgments

This material is based on work supported by National Science Foundation Grant EAR-2102856. The authors thank Gerald Tamuntuan, Satrio Wicaksono, Nigel Wattrus, and PT Vale Indonesia for field assistance. The authors acknowledge assistance and permission for this work from the Indonesian Ministry of Research and Technology (RISTEK). The authors also thank two anonymous reviewers for their thoughtful comments.

Data Availability Statement

The radiocarbon ages, fractional abundances of brGDGTs, and the temperature reconstruction are available in the PANGEA data repository (Parish, 2022).

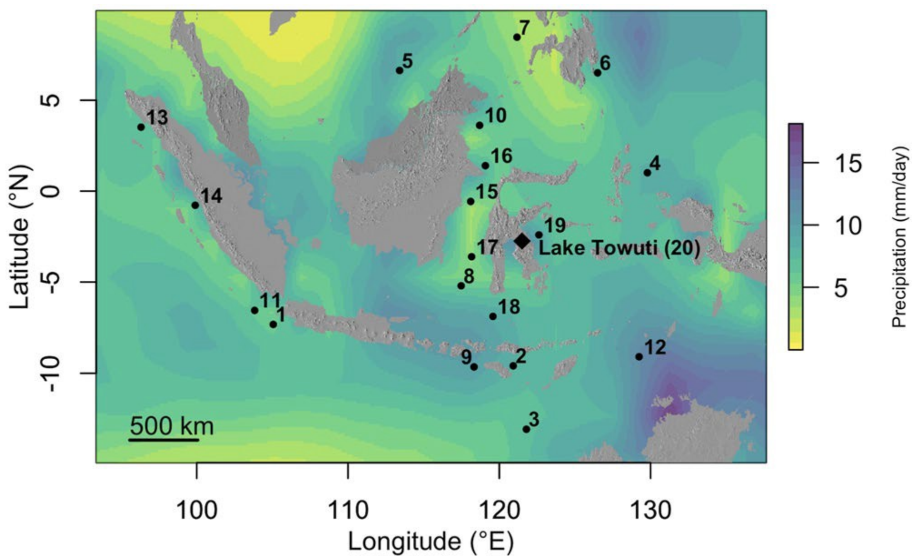

Figure 1. Lake Towuti (2.75°S, 121.5°E) is located in central Sulawesi, Indonesia, at an elevation of 318 m, shown with a diamond. The map also shows nearby SST records that span the last deglaciation, numbered as follows: 1. GeoB10043 (Setiawan et al., 2015), 2. GeoB10069 (Gibbons et al., 2014), 3. MD01-2378 (Xu et al., 2008), 4. MD01-2386 (Jian et al., 2020), 5. MD01-2390 (Steinke et al., 2006), 6. MD06-3067 (Bolliet et al., 2011), 7. MD97-2141 (Rosenthal et al., 2003), 8. MD98-2161 (Fan et al., 2018), 9. MD98-2165 (Levi et al., 2007), 10. MD98-2178 (Fan et al., 2018), 11. SO139-74KL (Wang et al., 2018), 12. SO185-18460 (Holbourn et al., 2011), 13. SO189-119KL (Mohtadi et al., 2014), 14. SO189-39KL (Mohtadi et al., 2014), 15. SO217-18519 (Schröder et al., 2018), 16. SO217-18522 (Schröder et al., 2018), 17. SO217-18526 (Schröder et al., 2018), 18. SO217-18540 (Schröder et al., 2018), 19. TGS-931 (Schröder et al., 2018), and 20. Lake Towuti (this study). Mean annual precipitation per day is shown based on 1991-2021 precipitation reanalysis data (Kalnay et al., 1996). Precipitation and the digital elevation models are plotted using the ‘raster’ package in R (Hijmans et al., 2022).

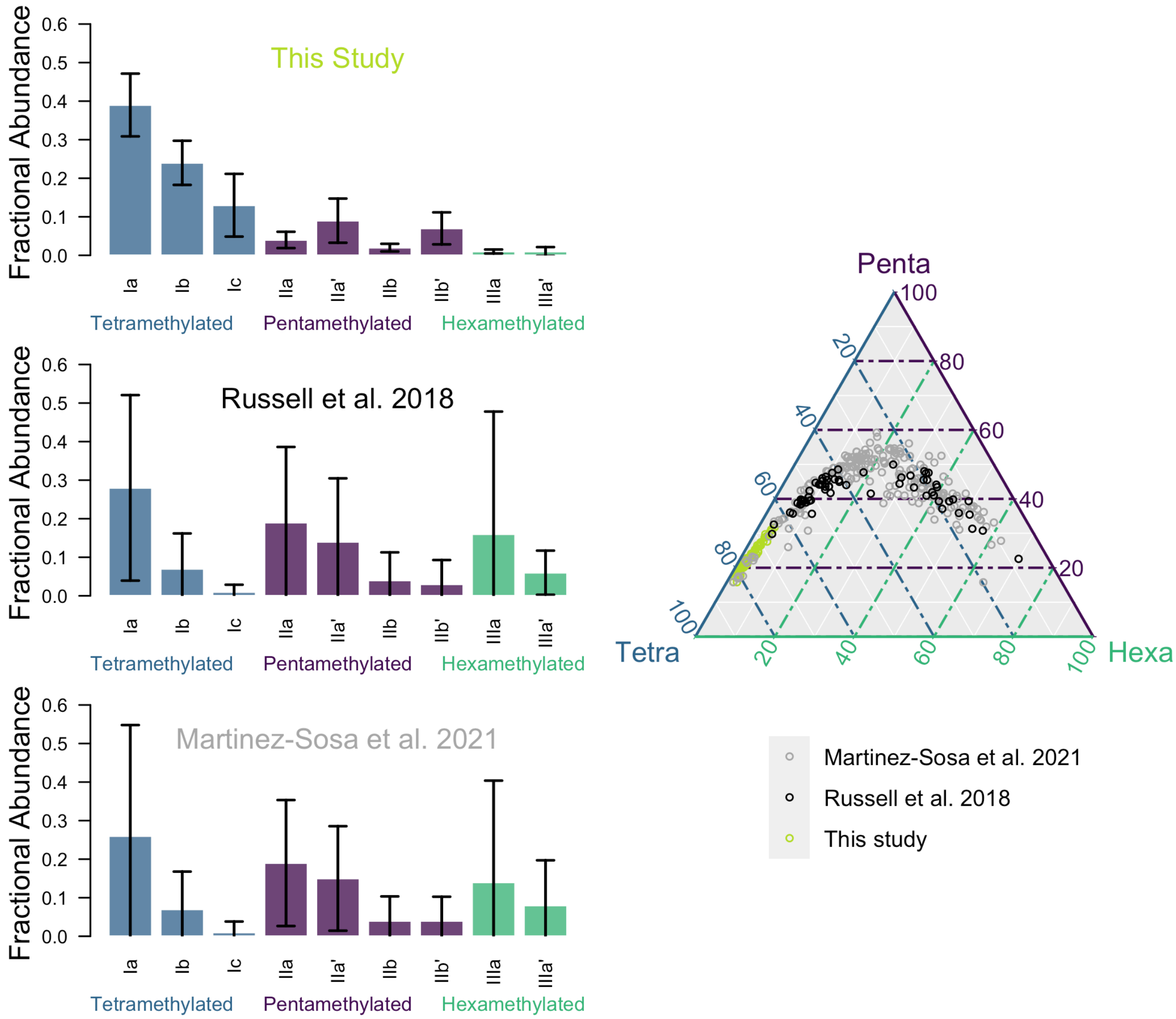

Figure 2. The average fractional abundances of the individual brGDGTs in all samples from the past 60,000 years from Lake Towuti, plotted as the mean ± 2 standard deviations. A ternary diagram of the fractional abundances of summed tetramethylated, pentamethylated, and hexamethylated brGDGTs in all samples from Lake Towuti relative to modern samples from East African lakes (Russell et al., 2018) and global lakes (Martínez-Sosa et al., 2021). The ternary diagram is plotted using the 'ggtern' package in R (Hamilton, 2022).

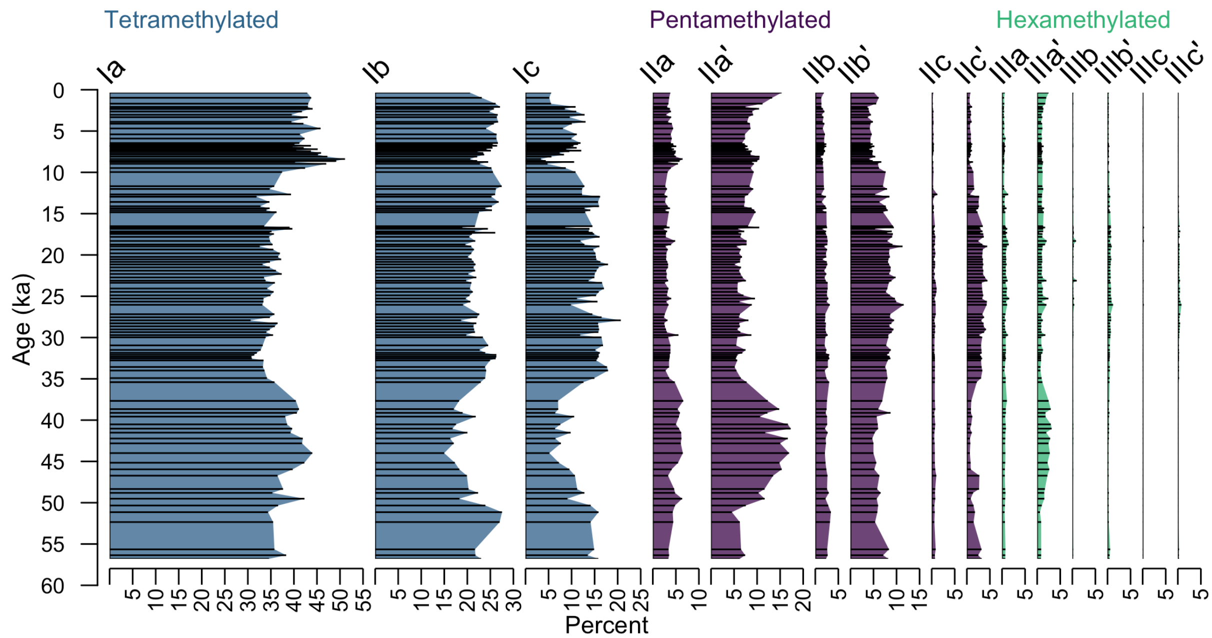

Figure 3. Percent of total tetramethylated (blue), pentamethylated (purple), and hexamethylated (green) brGDGTs in downcore samples from Lake Towuti. The fractional abundance data is plotted using the strat.plot() function in the 'Rioja' package in R (Juggins, 2022).

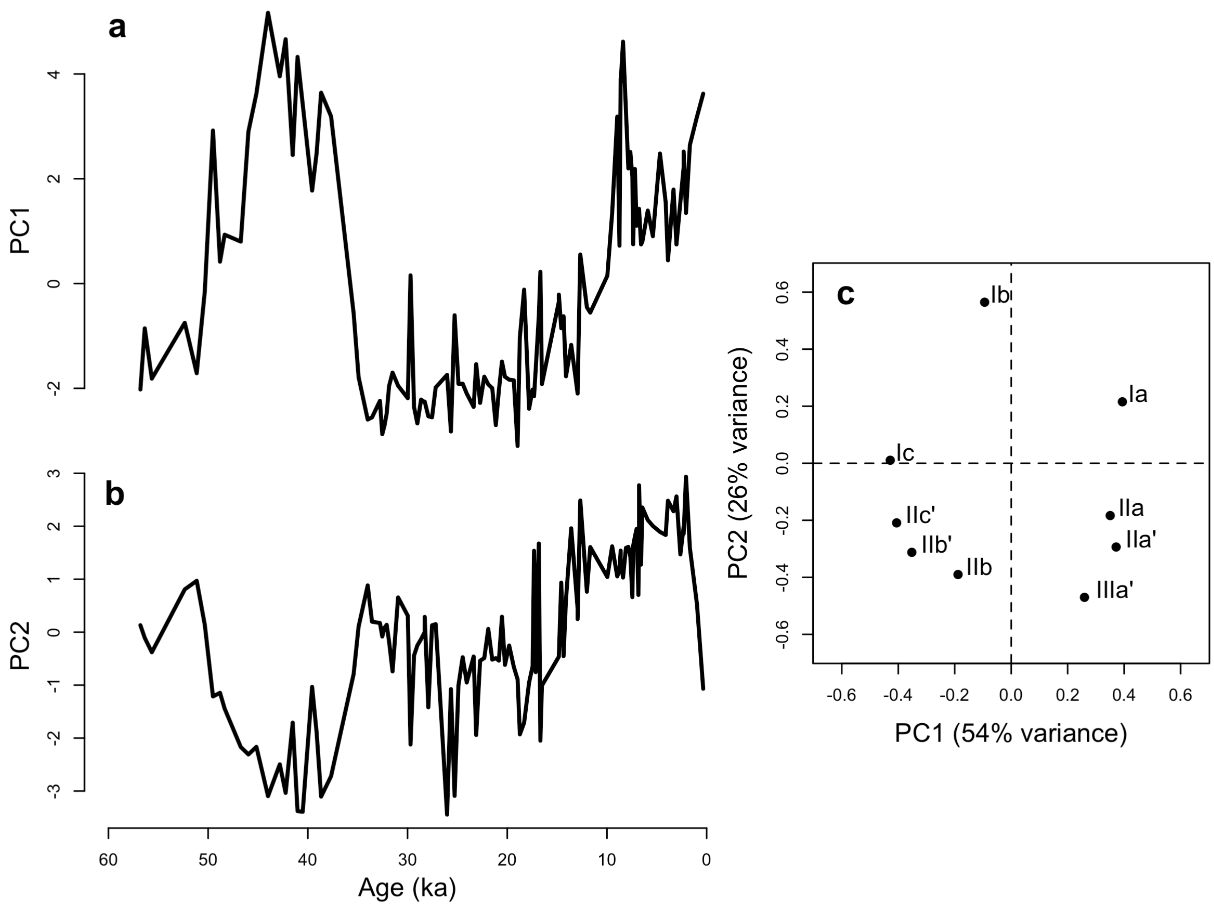

Figure 4. Principal component analysis based on the correlation matrix of the fractional abundances of brGDGTs which comprised more than two percent of the total abundance of brGDGTs in at least one sample over the past 60,000 years (Ia, Ib, Ic, IIa, IIa', IIb, IIb', IIc', IIIa'), made using the princomp() function from the 'vegan' R package to calculate the principal components based on the correlation matrix of the fractional abundances of the major brGDGTs. (a) PC1 scores of every sample, (b) PC2 scores of every sample, and (c) the loadings of the major brGDGTs on PC1 and PC2.

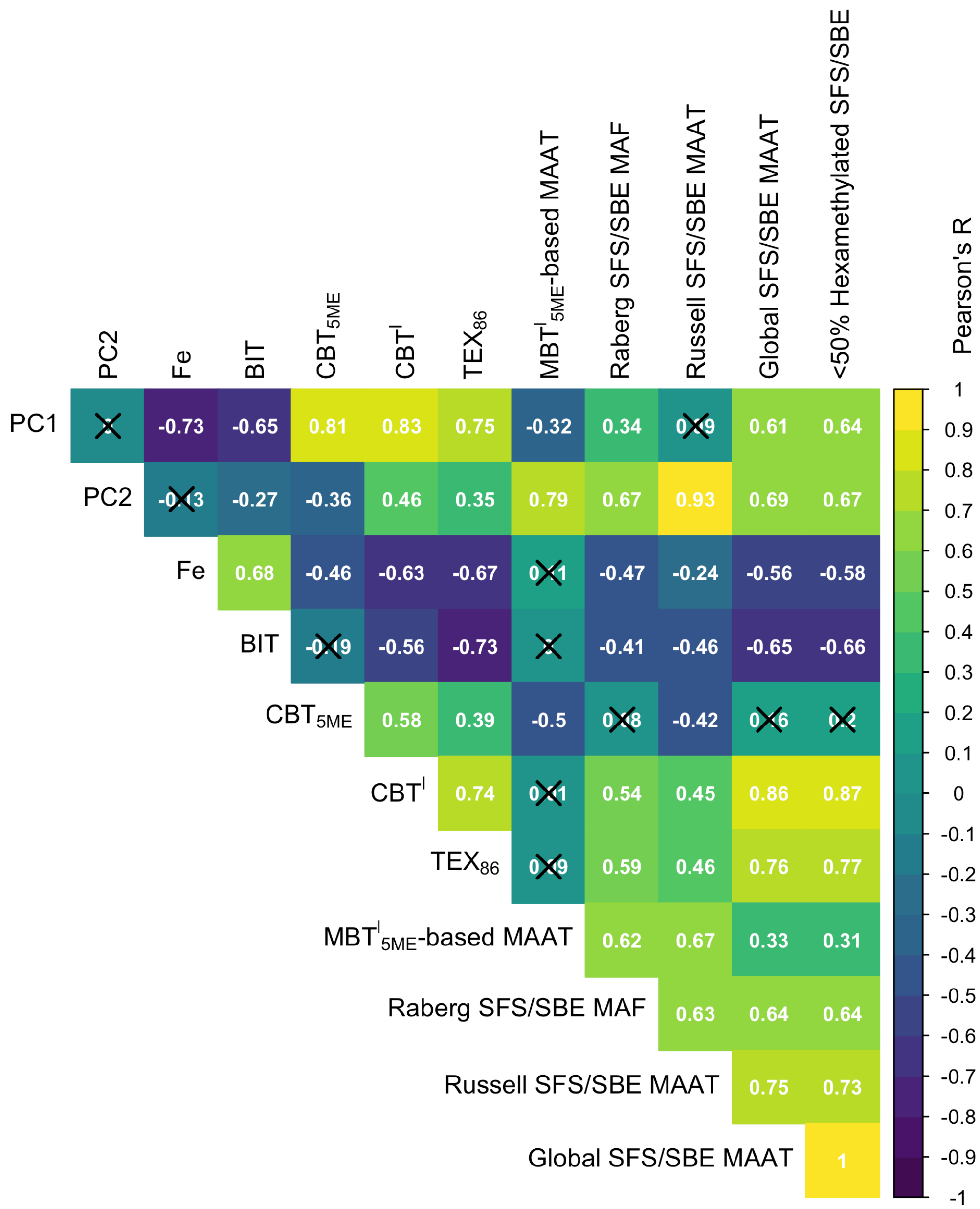

Figure 5. Correlation matrix showing Pearson's R between PC1 and PC2; Iron measured in the Lake Towuti sediment core (Costa et al., 2015); indices based on the fractional abundances of GDGTs in the Lake Towuti record, including: BIT, CBT$_{5ME}$, TEX$_{86}$, and MBT'$_{5ME}$-based MAAT (eq. 2; Russell et al., 2018); SFS/SBE-based reconstructions using published equations from global (eq. 3; Raberg et al., 2021) and East African lake sediment samples (eq. 4; Russell et al., 2018); and new SFS/SBE equations presented in this study from all global lake sediment samples published in Martinez-Sosa et al. (2021) (eq. 9) and samples with less than 50% hexamethylated brGDGTs, representing hotter environments (eq. 10). All reported Pearson correlation coefficients are significant at 99% confidence level ($p<0.01$, $n=115$), except correlation coefficients with a black x that indicates a p-value greater than 0.01. The correlation matrix is plotted using the 'corrplot' package in R (Wei et al., 2021).

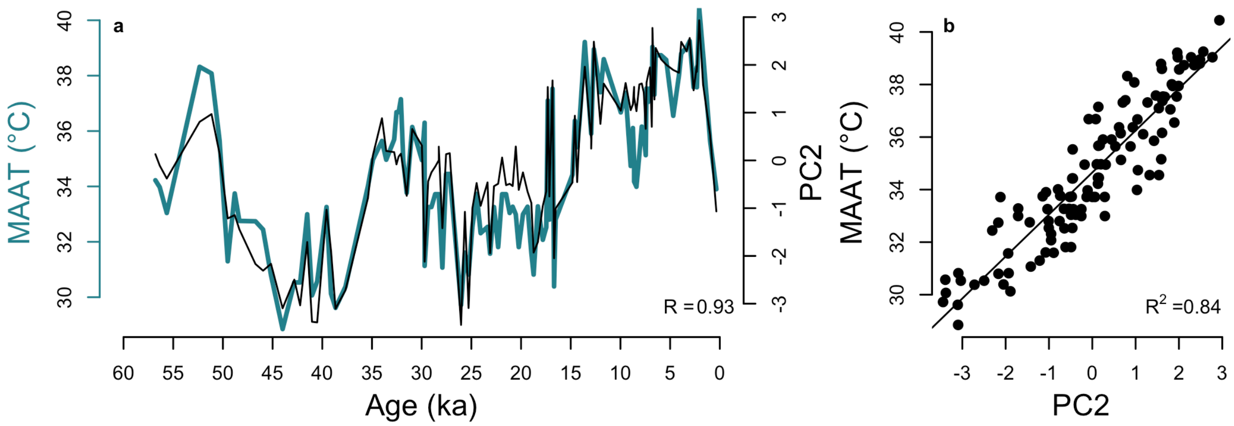

Figure 6. (a) Mean annual air temperature (MAAT) as reconstructed by the SFS/SBE equation published in Russell et al. (2018) (teal). PC2 from the principal component analysis shown in Figure 4 (black). The Pearson correlation coefficient between MAAT and PC2 is 0.93, also shown in Figure 5. (b) Linear regression between MAAT and PC2, and the associated R^2.

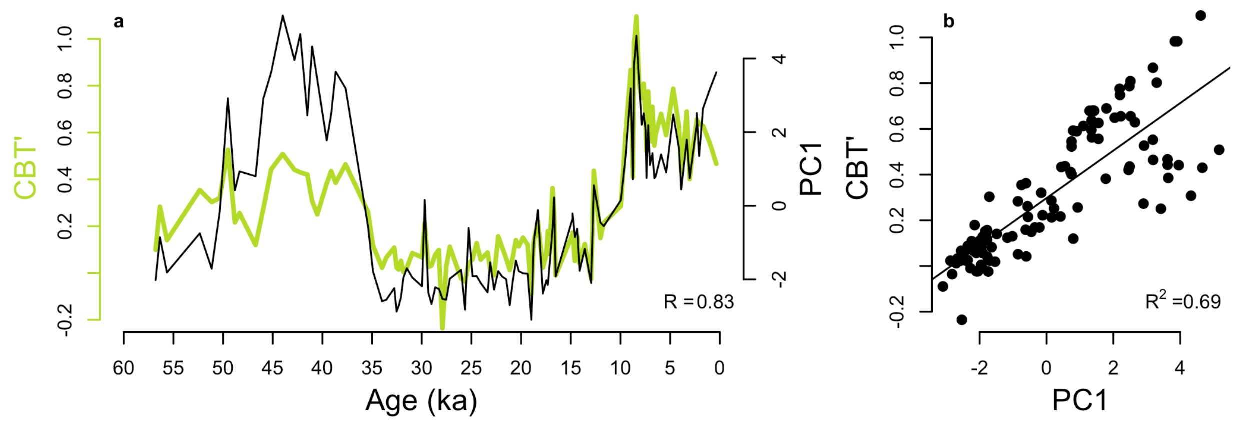

Figure 7. (a) The CBT' index based on the fractional abundances of brGDGTs in the Lake Towuti record (green) and PC1 from the principal component analysis shown in Figure 4 (black). The Pearson correlation coefficient is 0.83, shown in Figure 5. (b) Linear regression between the CBT' and PC1, and the associated R^2.

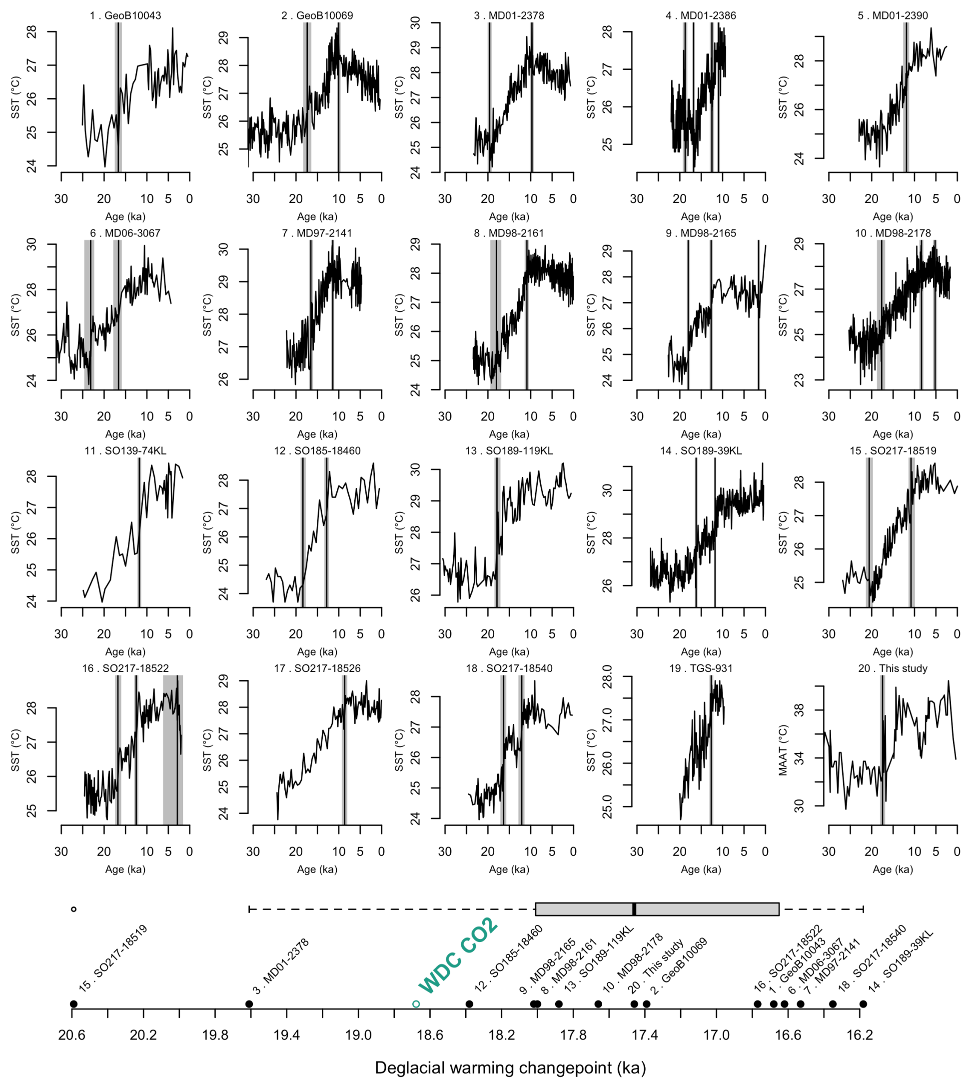

Figure 8. IPWP SST records, numbered as follows: 1. GeoB10043 (Setiawan et al., 2015), 2. GeoB10069 (Gibbons et al., 2014), 3. MD01-2378 (Xu et al., 2008), 4. MD01-2386 (Jian et al., 2020), 5. MD01-2390 (Steinke et al., 2006), 6. MD06-3067 (Bolliet et al., 2011), 7. MD97-2141 (Rosenthal et al., 2003), 8. MD98-2161 (Fan et al., 2018), 9. MD98-2165 (Levi et al., 2007), 10. MD98-2178 (Fan et al., 2018), 11. SO139-74KL (no deglacial changepoint detected; Wang et al., 2018), 12. SO185-18460 (Holbourn et al., 2011), 13. SO189-119KL (Mohtadi et al., 2014), 14. SO189-39KL (Mohtadi et al., 2014), 15. SO217-18519 (Schröder et al., 2018), 16. SO217-18522 (Schröder et al., 2018), 17. SO217-18526 (no deglacial changepoint detected; Schröder et al., 2018), 18. SO217-18540 (Schröder et al., 2018), 19. TGS-931 (no deglacial changepoint detected; Schröder et al., 2018), and our MAAT reconstruction, 20. Lake Towuti (this study). The vertical lines indicate the timing of all the changepoints detected using the 'EnvCpt' package in R (Killick et al., 2021), and the gray shading around the vertical lines shows the age uncertainty from the record. The boxplot shows the median, minimum, maximum, and interquartile range of all the SST deglacial changepoints and the changepoint detected in the Lake Towuti record. The timing of the deglacial changepoint detected using identical methods in the WAIS Divide ice core (WDC) CO_2 record (Marcott et al., 2014) is plotted in teal.

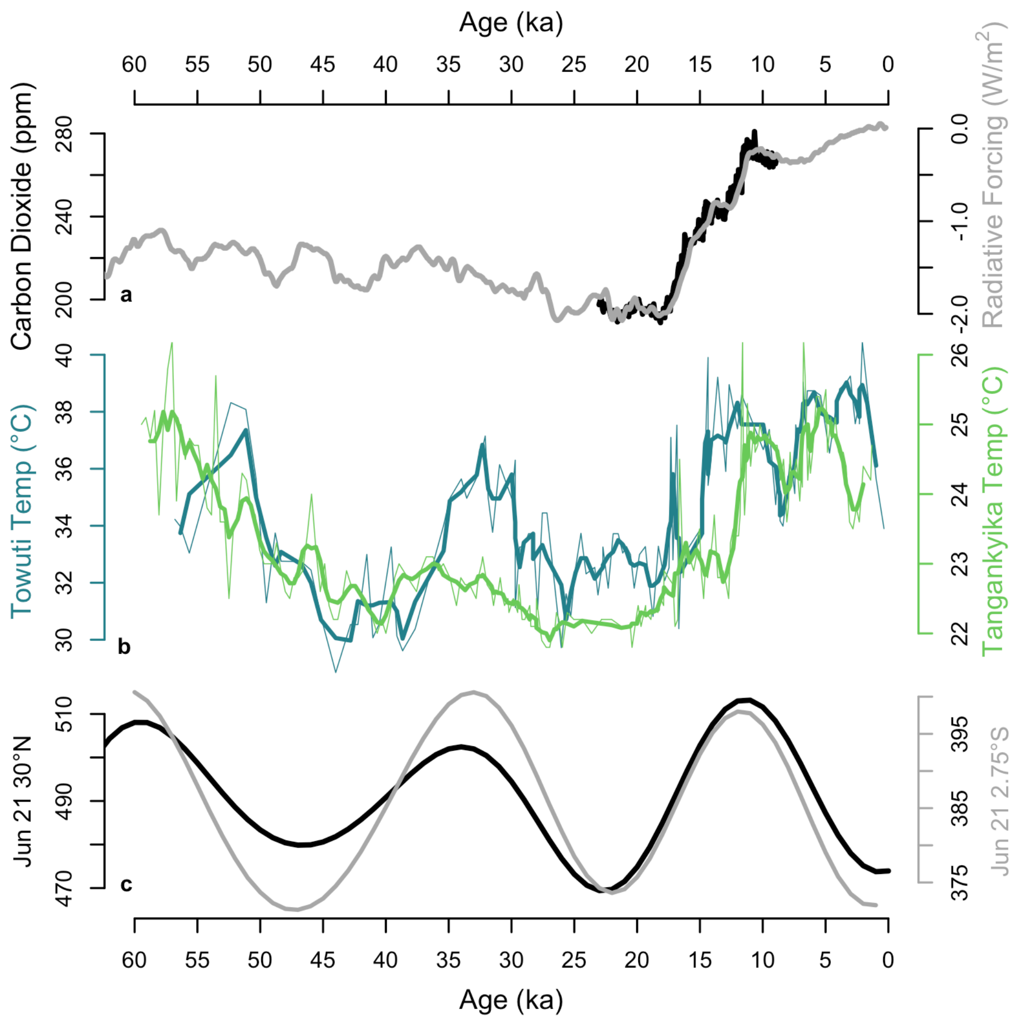

Figure 9. (a) Atmospheric CO_2 concentrations (black; Marcott et al., 2014), and radiative forcing of atmospheric carbon dioxide (gray; Schilt et al., 2010). (b) The reconstructed temperature from Lake Towuti (teal; this study) and the reconstructed lake surface temperature from Lake Tanganyika (green; Tierney et al., 2008), both plotted with a 1,500-yr moving average. (c) June 21 insolation from 30°S (black; Berger & Loutre, 1991) and June 21 insolation from 2.75°S (gray; Laskar et al., 2004).

References

Baxter, A. J., van Bree, L. G. J., Peterse, F., Hopmans, E. C., Villanueva, L., Verschuren, D., & Sinninghe Damsté, J. S. (2021). Seasonal and multi-annual variation in the abundance of isoprenoid GDGT membrane lipids and their producers in the water column of a meromictic equatorial crater lake (Lake Chala, East Africa). *Quaternary Science Reviews*, *273*, 107263. https://doi.org/10.1016/j.quascirev.2021.107263

Berger, A., & Loutre, M. F. (1991). Insolation values for the climate of the last 10 million years. *Quaternary Science Reviews*, *10*(4), 297–317. https://doi.org/10.1016/0277-3791(91)90033-Q

Blaauw, M., & Christen, J. A. (2011). Flexible paleoclimate age-depth models using an autoregressive gamma process. *Bayesian Analysis*, *6*(3), 457–474. https://doi.org/10.1214/11-BA618

Bolliet, T., Holbourn, A., Kuhnt, W., Laj, C., Kissel, C., Beaufort, L., et al. (2011). Mindanao Dome variability over the last 160 kyr: Episodic glacial cooling of the West Pacific warm pool. *Paleoceanography*, *26*(1), PA1208. https://doi.org/10.1029/2010PA001966

Chiang, J. C. H. (2009). The tropics in paleoclimate. *Annual Review of Earth and Planetary Sciences*, *37*(1), 263–297. https://doi.org/10.1146/ annurev.earth.031208.100217

Clement, A. C., Hall, A., & Broccoli, A. J. (2004). The importance of precessional signals in the tropical climate. *Climate Dynamics*, *22*(4), 327–341. https://doi.org/10.1007/s00382-003-0375-8

Costa, K. M., Russell, J. M., Vogel, H., & Bijaksana, S. (2015). Hydrological connectivity and mixing of Lake Towuti, Indonesia in response to paleoclimatic changes over the last

60,000 years. *Palaeogeography, Palaeoclimatology, Palaeoecology*, *417*, 467–475. https://doi.org/ 10.1016/j.palaeo.2014.10.009

Crowe, S. A., O'Neill, A. H., Katsev, S., Hehanussa, P., Haffner, G. D., Sundby, B., et al. (2008). The biogeochemistry of tropical lakes: A case study from Lake Matano, Indonesia. *Limnology & Oceanography*, *53*(1), 319–331. https://doi.org/10.4319/lo.2008.53.1.0319

Current Population. (2022). Current population. Retrieved from https://www.census.gov/popclock/print.php?component=counter

De Deckker, P. (2016). The Indo-Pacific warm pool: Critical to world oceanography and world climate. *Geoscience Letter*s, 3(1), 20. https:// doi.org/10.1186/s40562-016-0054-3

Dee, S. G., Morrill, C., Kim, S. H., & Russell, J. M. (2021). Hot air, hot lakes, or both? Exploring mid-holocene african temperatures using proxy system modeling. *Journal of Geophysical Research: Atmospheres*, *126*(10), e2020JD033269. https://doi.org/10.1029/2020JD033269

De Jonge, C., Hopmans, E. C., Stadnitskaia, A., Rijpstra, W. I. C., Hofland, R., Tegelaar, E., & Sinninghe Damsté, J. S. (2013). Identification of novel penta- and hexamethylated branched glycerol dialkyl glycerol tetraethers in peat using HPLC–MS2, GC–MS and GC–SMB-MS. *Organic Geochemistry*, *54*, 78–82. https://doi.org/10.1016/j.orggeochem.2012.10.004

De Jonge, C., Hopmans, E. C., Zell, C. I., Kim, J.-H., Schouten, S., & Sinninghe Damsté, J. S. (2014). Occurrence and abundance of 6-methyl branched glycerol dialkyl glycerol tetraethers in soils: Implications for palaeoclimate reconstruction. *Geochimica et Cosmochimica Acta*, *141*, 97–112. https://doi.org/10.1016/j.gca.2014.06.013

DiNezio, P. N., & Tierney, J. E. (2013). The effect of sea level on glacial Indo-Pacific climate. *Nature Geoscience*, *6*(6), 485–491. https://doi. org/10.1038/ngeo1823

DiNezio, P. N., Tierney, J. E., Otto-Bliesner, B. L., Timmermann, A., Bhattacharya, T., Rosenbloom, N., & Brady, E. (2018). Glacial changes in tropical climate amplified by the Indian Ocean. *Science Advances*, *4*(12), eaat9658. https://doi.org/10.1126/sciadv.aat9658

DiNezio, P. N., Timmermann, A., Tierney, J. E., Jin, F.-F., Otto-Bliesner, B., Rosenbloom, N., et al. (2016). The climate response of the Indo-Pacific warm pool to glacial sea level. *Paleoceanography*, *31*(6), 866–894. https://doi.org/10.1002/2015PA002890

Fan, W., Jian, Z., Chu, Z., Dang, H., Wang, Y., Bassinot, F., et al. (2018). Variability of the Indonesian throughflow in the Makassar Strait over the last 30 ka. *Scientific Reports*, *8*(1), 5678. https://doi.org/10.1038/s41598-018-24055-1

Gasse, F. (2000). Hydrological changes in the African tropics since the last glacial maximum. *Quaternary Science Reviews*, *19*(1), 189–211. https://doi.org/10.1016/S0277-3791(99)00061-X

Gibbons, F. T., Oppo, D. W., Mohtadi, M., Rosenthal, Y., Cheng, J., Liu, Z., & Linsley, B. K. (2014). Deglacial δ18O and hydrologic variability in the tropical Pacific and Indian Oceans. *Earth and Planetary Science Letters*, *387*, 240–251. https://doi.org/10.1016/j.epsl.2013.11.032

Griffiths, M. L., Drysdale, R. N., Gagan, M. K., Zhao, J., Hellstrom, J. C., Ayliffe, L. K., & Hantoro, W. S. (2013). Abrupt increase in east Indonesian rainfall from flooding of the Sunda Shelf ~9500 years ago. *Quaternary Science Reviews*, *74*, 273–279. https://doi.org/10.1016/j. quascirev.2012.07.006

Guo, Z., Zhou, X., & Wu, H. (2012). Glacial-interglacial water cycle, global monsoon and atmospheric methane changes. *Climate Dynamics*, *39*(5), 1073–1092. https://doi.org/10.1007/s00382-011-1147-5

Hamilton, N. (2022). ggtern: An extension to "ggplot2", for the creation of ternary diagrams (version 3.4.1). Retrieved from https://CRAN.R- project.org/package=ggtern

Hijmans, R. J., Etten, J. V., Sumner, M., Cheng, J., Baston, D., Bevan, A., et al. (2022). raster: Geographic data analysis and modeling (version 3.5-15). Retrieved from https://CRAN.R-project.org/package=raster

Holbourn, A., Kuhnt, W., & Xu, J. (2011). Indonesian Throughflow variability during the last 140 ka: The Timor Sea outflow. *Geological Society, London, Special Publications*, *355*(1), 283–303. https://doi.org/10.1144/SP355.14

Hope, G. (2001). Environmental change in the late Pleistocene and later Holocene at Wanda site, Soroako, South Sulawesi, Indonesia. *Palaeogeography, Palaeoclimatology, Palaeoecology*, *171*(3), 129–145. https://doi.org/10.1016/S0031-0182(01)00243-7

Hopmans, E. C., Schouten, S., & Sinninghe Damsté, J. S. (2016). The effect of improved chromatography on GDGT-based palaeoproxies.

Organic Geochemistry, *93*, 1–6. https://doi.org/10.1016/j.orggeochem.2015.12.006

Hopmans, E. C., Weijers, J. W. H., Schefuß, E., Herfort, L., Sinninghe Damsté, J. S., & Schouten, S. (2004). A novel proxy for terrestrial organic matter in sediments based on branched and isoprenoid tetraether lipids. *Earth and Planetary Science Letters*, *224*(1), 107–116. https://doi. org/10.1016/j.epsl.2004.05.012

Jian, Z., Wang, Y., Dang, H., Lea, D. W., Liu, Z., Jin, H., & Yin, Y. (2020). Half-precessional cycle of thermocline temperature in the Western equatorial Pacific and its bihemispheric dynamics. *Proceedings of the National Academy of Sciences*, *117*(13), 7044–7051. https://doi. org/10.1073/pnas.1915510117

Juggins, S. (2022). rioja: Analysis of quaternary science data (version 1.0-5). Retrieved from https://CRAN.R-project.org/package=rioja Kalnay, E., Kanamitsu, M., Kistler, R., Collins, W., Deaven, D., Gandin, L., et al. (1996). The NCEP/NCAR 40-year reanalysis project. *Bulletin*

of the American Meteorological Society, *77*(3), 437–472. https://doi.org/10.1175/1520-0477(1996)077<0437:TNYRP>2.0.CO;2

Killick, R., Beaulieu, C., Taylor, S., & Hullait, H. (2021). EnvCpt: Detection of structural changes in climate and environment time series (version 1.1.3). Retrieved from https://CRAN.R-project.org/package=EnvCpt

Konecky, B., Russell, J., & Bijaksana, S. (2016). Glacial aridity in central Indonesia coeval with intensified monsoon circulation. *Earth and Planetary Science Letters*, *437*, 15–24. https://doi.org/10.1016/j.epsl.2015.12.037

Laskar, J., Robutel, P., Joutel, F., Gastineau, M., Correia, A. C. M., & Levrard, B. (2004). A long-term numerical solution for the insolation quantities of the Earth. *Astronomy & Astrophysics*, *428*(1), 261–285. https://doi.org/10.1051/0004-6361:20041335

Levi, C., Labeyrie, L., Bassinot, F., Guichard, F., Cortijo, E., Waelbroeck, C., et al. (2007). Low-latitude hydrological cycle and rapid climate changes during the last deglaciation. *Geochemistry, Geophysics, Geosystems*, *8*(5). https://doi.org/10.1029/2006GC001514

Loomis, S. E., Russell, J. M., Eggermont, H., Verschuren, D., & Sinninghe Damsté, J. S. (2014). Effects of temperature, pH and nutrient concentration on branched GDGT distributions in

East African lakes: Implications for paleoenvironmental reconstruction. *Organic Geochemistry*, *66*, 25–37. https://doi.org/10.1016/j.orggeochem.2013.10.012

Loomis, S. E., Russell, J. M., Ladd, B., Street-Perrott, F. A., & Sinninghe Damsté, J. S. (2012). Calibration and application of the branched GDGT temperature proxy on East African lake sediments. *Earth and Planetary Science Letters*, *357*(358), 277–288. https://doi.org/10.1016/j.epsl.2 012.09.031

Marcott, S. A., Bauska, T. K., Buizert, C., Steig, E. J., Rosen, J. L., Cuffey, K. M., et al. (2014). Centennial-scale changes in the global carbon cycle during the last deglaciation. *Nature*, *514*(7524), 616–619. https://doi.org/10.1038/nature13799

Martínez-Sosa, P., & Tierney, J. E. (2019). Lacustrine brGDGT response to microcosm and mesocosm incubations. *Organic Geochemistry*, *127*, 12–22. https://doi.org/10.1016/j.orggeochem.2018.10.011

Martínez-Sosa, P., Tierney, J. E., Stefanescu, I. C., Dearing Crampton-Flood, E., Shuman, B. N., & Routson, C. (2021). A global Bayesian temperature calibration for lacustrine brGDGTs. *Geochimica et Cosmochimica Acta*, *305*, 87–105. https://doi.org/10.1016/j.gca.2021.04.038

Mohtadi, M., Prange, M., Oppo, D. W., De Pol-Holz, R., Merkel, U., Zhang, X., et al. (2014). North Atlantic forcing of tropical Indian Ocean climate. *Nature*, *509*(7498), 76–80. https://doi.org/10.1038/nature13196

Naafs, B. D. A., Oliveira, A. S. F., & Mulholland, A. J. (2021). Molecular dynamics simulations support the hypothesis that the brGDGT paleothermometer is based on homeoviscous adaptation. *Geochimica et Cosmochimica Acta*, *312*, 44–56. https://doi.org/10.1016/j.gca.2021.07.034 Oksanen, J., Blanchet, F. G., Friendly, M., Kindt, R., Legendre, P., McGlinn, D., et al. (2020). vegan: Community ecology package. Retrieved

from https://CRAN.R-project.org/package=vegan

Parish, M. C. (2022). A brGDGT-based reconstruction of terrestrial temperature from the Maritime Continent spanning the Last Glacial Maximum [Dataset]. PANGAEA. https://doi.org/10.1594/PANGAEA.948194

Pico, T., McGee, D., Russell, J., & Mitrovica, J. X. (2020). Recent constraints on MIS 3 sea level support role of continental shelf exposure as a control on Indo-Pacific hydroclimate. *Paleoceanography and Paleoclimatology*, *35*(8). https://doi.org/10.1029/2020PA003998

Powers, L., Werne, J. P., Vanderwoude, A. J., Sinninghe Damsté, J. S., Hopmans, E. C., & Schouten, S. (2010). Applicability and calibration of the TEX86 paleothermometer in lakes. *Organic Geochemistry*, *41*(4), 404–413. https://doi.org/10.1016/j.orggeochem.2009.11.009

Raberg, J. H., Harning, D. J., Crump, S. E., de Wet, G., Blumm, A., Kopf, S., et al. (2021). Revised fractional abundances and warm-season temperatures substantially improve brGDGT calibrations in lake sediments. *Biogeosciences Discussions*, 1–36. https://doi.org/10.5194/bg-2021-16 Reeves, J. M., Bostock, H. C., Ayliffe, L. K., Barrows, T. T., De Deckker, P., Devriendt, L. S., et al. (2013). Palaeoenvironmental change in trop-

ical Australasia over the last 30,000 years – A synthesis by the OZ-INTIMATE group. *Quaternary Science Reviews*, *74*, 97–114. https://doi.org/10.1016/j.quascirev.2012.11.027

Rosenthal, Y., Oppo, D. W., & Linsley, B. K. (2003). The amplitude and phasing of climate change during the last deglaciation in the Sulu Sea, Western equatorial Pacific: The amplitude and phasing of climate change. *Geophysical Research Letters*, *30*(8). https://doi.org/ 10.1029/2002GL016612

Ruddiman, W. F. (2003). The anthropogenic greenhouse era began thousands of years ago. *Climatic Change*, *61*(3), 261–293. https://doi. org/10.1023/B:CLIM.0000004577.17928.fa

Ruddiman, W. F., & Raymo, M. E. (2003). A methane-based time scale for Vostok ice. *Quaternary Science Review*s, *22*(2), 141–155. https:// doi.org/10.1016/S0277-3791(02)00082-3

Russell, J. M., Hopmans, E. C., Loomis, S. E., Liang, J., & Sinninghe Damsté, J. S. (2018). Distributions of 5- and 6-methyl branched glycerol dialkyl glycerol tetraethers (brGDGTs) in East African lake sediment: Effects of temperature, pH, and new lacustrine paleotemperature calibrations. *Organic Geochemistry*, *117*, 56–69. https://doi.org/10.1016/j.orggeochem.2017.12.003

Russell, J. M., Vogel, H., Bijaksana, S., Melles, M., Deino, A., Hafidz, A., et al. (2020). The late quaternary tectonic, biogeochemical, and environmental evolution of ferruginous Lake Towuti, Indonesia. *Palaeogeography, Palaeoclimatology, Palaeoecology*, *556*, 109905. https://doi. org/10.1016/j.palaeo.2020.109905

Russell, J. M., Vogel, H., Konecky, B. L., Bijaksana, S., Huang, Y., Melles, M., et al. (2014). Glacial forcing of central Indonesian hydroclimate since 60,000 y B.P. *Proceedings of the National Academy of Sciences*, *111*(14), 5100–5105. https://doi.org/10.1073/pnas.1402373111

Schilt, A., Baumgartner, M., Schwander, J., Buiron, D., Capron, E., Chappellaz, J., et al. (2010). Atmospheric nitrous oxide during the last 140,000years. *Earth and Planetary Science Letters*, *300*(1), 33–43. https://doi.org/10.1016/j.epsl.2010.09.027

Schouten, S., Hopmans, E. C., Schefuß, E., & Sinninghe Damsté, J. S. (2002). Distributional variations in marine crenarchaeotal membrane lipids: A new tool for reconstructing ancient sea water temperatures? *Earth and Planetary Science Letters*, *204*(1), 265–274. https://doi.org/10. 1016/S0012-821X(02)00979-2

Schröder, J. F., Kuhnt, W., Holbourn, A., Beil, S., Zhang, P., Hendrizan, M., & Xu, J. (2018). Deglacial warming and hydroclimate variability in the central Indonesian archipelago. *Paleoceanography and Paleoclimatology*, *33*(9), 974–993. https://doi.org/10.1029/2018PA003323

Setiawan, R. Y., Mohtadi, M., Southon, J., Groeneveld, J., Steinke, S., & Hebbeln, D. (2015). The consequences of opening the Sunda Strait on the hydrography of the eastern tropical Indian Ocean. *Paleoceanography*, *30*(10), 1358–1372. https://doi.org/10.1002/2015PA002802

Shakun, J. D., Clark, P. U., He, F., Marcott, S. A., Mix, A. C., Liu, Z., et al. (2012). Global warming preceded by increasing carbon dioxide concentrations during the last deglaciation. *Nature*, *484*(7392), 49–54. https://doi.org/10.1038/nature10915

Sinninghe Damsté, J. S., Ossebaar, J., Schouten, S., & Verschuren, D. (2012). Distribution of tetraether lipids in the 25-ka sedimentary record of Lake Challa: Extracting reliable TEX86 and MBT/CBT palaeotemperatures from an equatorial African lake. *Quaternary Science Reviews*, *50*, 43–54. https://doi.org/10.1016/j.quascirev.2012.07.001

Stefanescu, I. C., Shuman, B. N., & Tierney, J. E. (2021). Temperature and water depth effects on brGDGT distributions in sub-alpine lakes of mid-latitude North America. *Organic Geochemistry*, *152*, 104174. https://doi.org/10.1016/j.orggeochem.2020.104174

Steinke, S., Chiu, H.-Y., Yu, P.-S., Shen, C.-C., Erlenkeuser, H., Löwemark, L., & Chen, M.-T. (2006). On the influence of sea level and monsoon climate on the southern South China Sea freshwater budget over the last 22,000 years. *Quaternary Science Reviews*, *25*(13), 1475–1488. https://doi.org/10.1016/j.quascirev.2005.12.008

Stott, L., Timmermann, A., & Thunell, R. (2007). Southern hemisphere and deep-sea warming led deglacial atmospheric CO_2 rise and tropical warming. *Science*, *318*(5849), 435–438. https://doi.org/10.1126/science.1143791

Tierney, J. E., & Russell, J. M. (2009). Distributions of branched GDGTs in a tropical lake system: Implications for lacustrine application of the MBT/CBT paleoproxy. *Organic Geochemistry*, *40*(9), 1032–1036. https://doi.org/10.1016/j.orggeochem.2009.04.014

Tierney, J. E., Russell, J. M., Eggermont, H., Hopmans, E. C., Verschuren, D., & Sinninghe Damsté, J. S. (2010). Environmental controls on branched tetraether lipid distributions in tropical East African lake sediments. *Geochimica et Cosmochimica Acta*, *74*(17), 4902–4918. https://doi.org/ 10.1016/j.gca.2010.06.002

Tierney, J. E., Russell, J. M., Huang, Y., Damsté, J. S. S., Hopmans, E. C., & Cohen, A. S. (2008). Northern hemisphere controls on tropical southeast African climate during the past 60,000 years. *Science*, *322*(5899), 252–255. https://doi.org/10.1126/science.1160485

Tierney, J. E., Schouten, S., Pitcher, A., Hopmans, E. C., & Sinninghe Damsté, J. S. (2012). Core and intact polar glycerol dialkyl glycerol tetraethers (GDGTs) in Sand Pond, Warwick, Rhode Island (USA): Insights into the origin of lacustrine GDGTs. *Geochimica et Cosmochimica Acta*, *77*, 561–581. https://doi.org/10.1016/j.gca.2011.10.018

van Bree, L. G. J., Peterse, F., Baxter, A. J., De Crop, W., van Grinsven, S., Villanueva, L., et al. (2020). Seasonal variability and sources of in situ brGDGT production in a permanently stratified African crater lake. *Biogeosciences*, *17*(21), 5443–5463. https://doi.org/10.5194/ bg-17-5443-2020

Vuillemin, A., Friese, A., Alawi, M., Henny, C., Nomosatryo, S., Wagner, D., et al. (2016). Geomicrobiological features of ferruginous sediments from Lake Towuti, Indonesia. *Frontiers in Microbiology*, *7*. https://doi.org/10.3389/fmicb.2016.01007

Wang, X., Jian, Z., Lückge, A., Wang, Y., Dang, H., & Mohtadi, M. (2018). Precession-paced thermocline water temperature changes in response to upwelling conditions off southern Sumatra over the past 300,000 years. *Quaternary Science Reviews*, *192*, 123–134. https://doi. org/10.1016/j.quascirev.2018.05.035

Wei, T., Simko, V., Levy, M., Xie, Y., Jin, Y., Zemla, J., et al. (2021). corrplot: Visualization of a correlation matrix (version 0.92). Retrieved from https://CRAN.R-project.org/package=corrplot

Weijers, J. W. H., Schouten, S., van den Donker, J. C., Hopmans, E. C., & Sinninghe Damsté, J. S. (2007). Environmental controls on bacterial tetraether membrane lipid distribution in soils. *Geochimica et Cosmochimica Acta*, *71*(3), 703–713. https://doi.org/10.1016/j.gca.2006.10.003 Windler, G., Tierney, J. E., DiNezio, P. N., Gibson, K., & Thunell, R. (2019). Shelf exposure influence on Indo-Pacific Warm Pool climate for the last 450,000 years. *Earth and Planetary Science Letters*, *516*, 66–76. https://doi.org/10.1016/j.epsl.2019.03.038

Windler, G., Tierney, J. E., Zhu, J., & Poulsen, C. J. (2020). Unraveling glacial hydroclimate in the Indo-Pacific warm pool: Perspectives from water isotopes. *Paleoceanography and Paleoclimatology*, *35*(12), e2020PA003985. https://doi.org/10.1029/2020PA003985

Wu, J., Yang, H., Pancost, R. D., Naafs, B. D. A., Qian, S., Dang, X., et al. (2021). Variations in dissolved O_2 in a Chinese lake drive changes in microbial communities and impact sedimentary GDGT distributions. *Chemical Geology*, *579*, 120348. https://doi.org/10.1016/j.chemgeo. 2021.120348

Xu, J., Holbourn, A., Kuhnt, W., Jian, Z., & Kawamura, H. (2008). Changes in the thermocline structure of the Indonesian outflow during Termi nations I and II. *Earth and Planetary Science Letters*, *273*(1), 152–162. https://doi.org/10.1016/j.epsl.2008.06.029

Yao, Y., Zhao, J., Vachula, R. S., Werne, J. P., Wu, J., Song, X., & Huang, Y. (2020). Correlation between the ratio of 5-methyl hexamethylated to pentamethylated branched GDGTs (HP5) and water depth reflects redox variations in stratified lakes. *Organic Geochemistry*, *147*, 104076. https://doi.org/10.1016/j.orggeochem.2020.104076

Supporting information

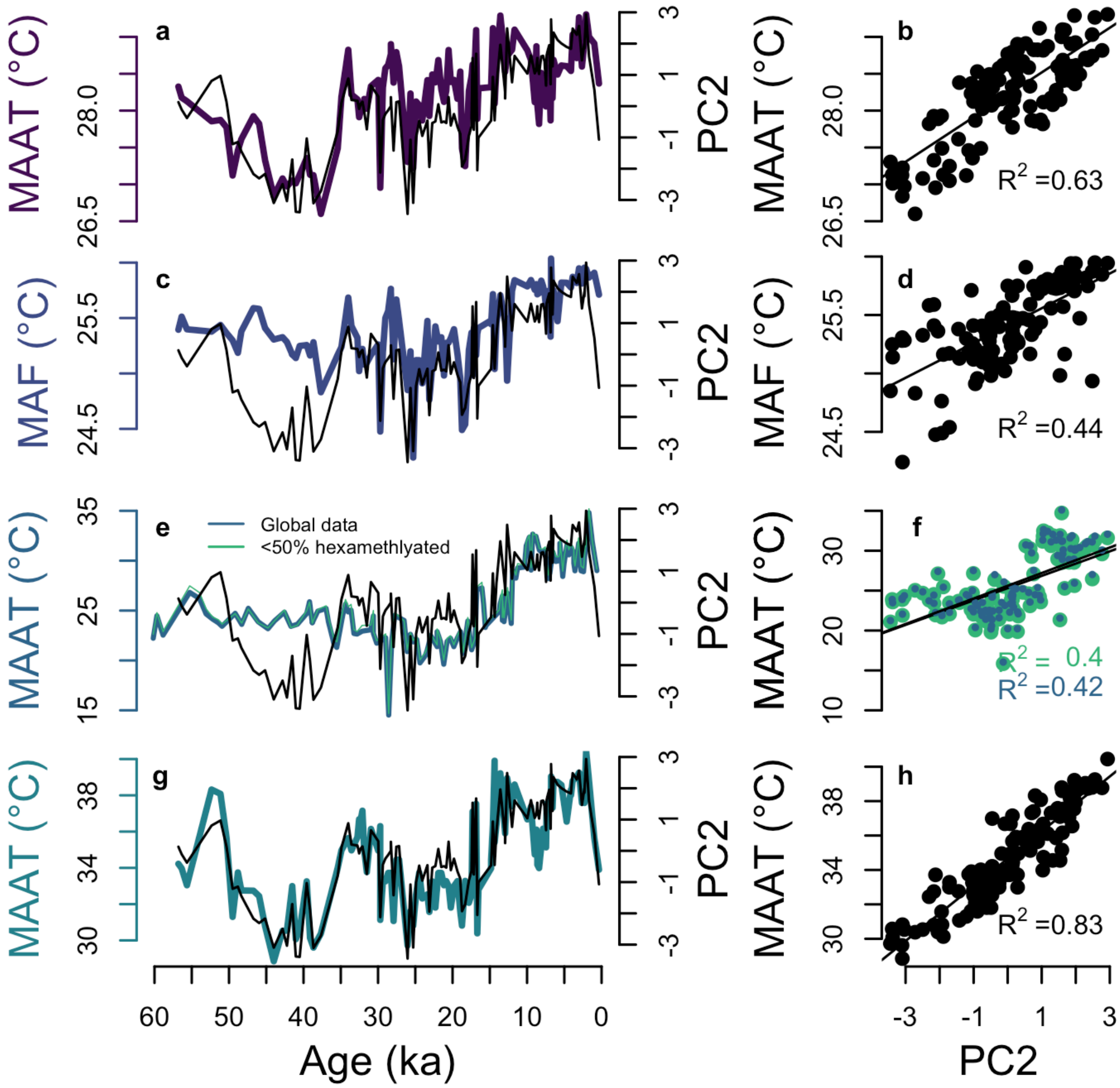

Figure S1. (a) Mean annual air temperature (MAAT) based on the MBT'$_{5me}$ calibration from Russell et al. (2018) (purple). (c) Mean temperature of the months above freezing (MAF) calculated using the calibration from Raberg et al. (2021) for use in samples with small abundances of IIIb (purple). (d) SFS/SBE MAAT based on all global lacustrine samples from Martinez-Sosa et al. (2021) (green) and SFS/SBE MAAT based only on surface samples with less than 50% hexmethylated brGDGTs (green). (g) SFS/SBE MAAT based on all samples from Russell et al. (2018) (blue). PC2 from the principal component is shown in black in all panels. (b, d, f, and h) Linear regressions between the index or reconstructed temperature and PC2.

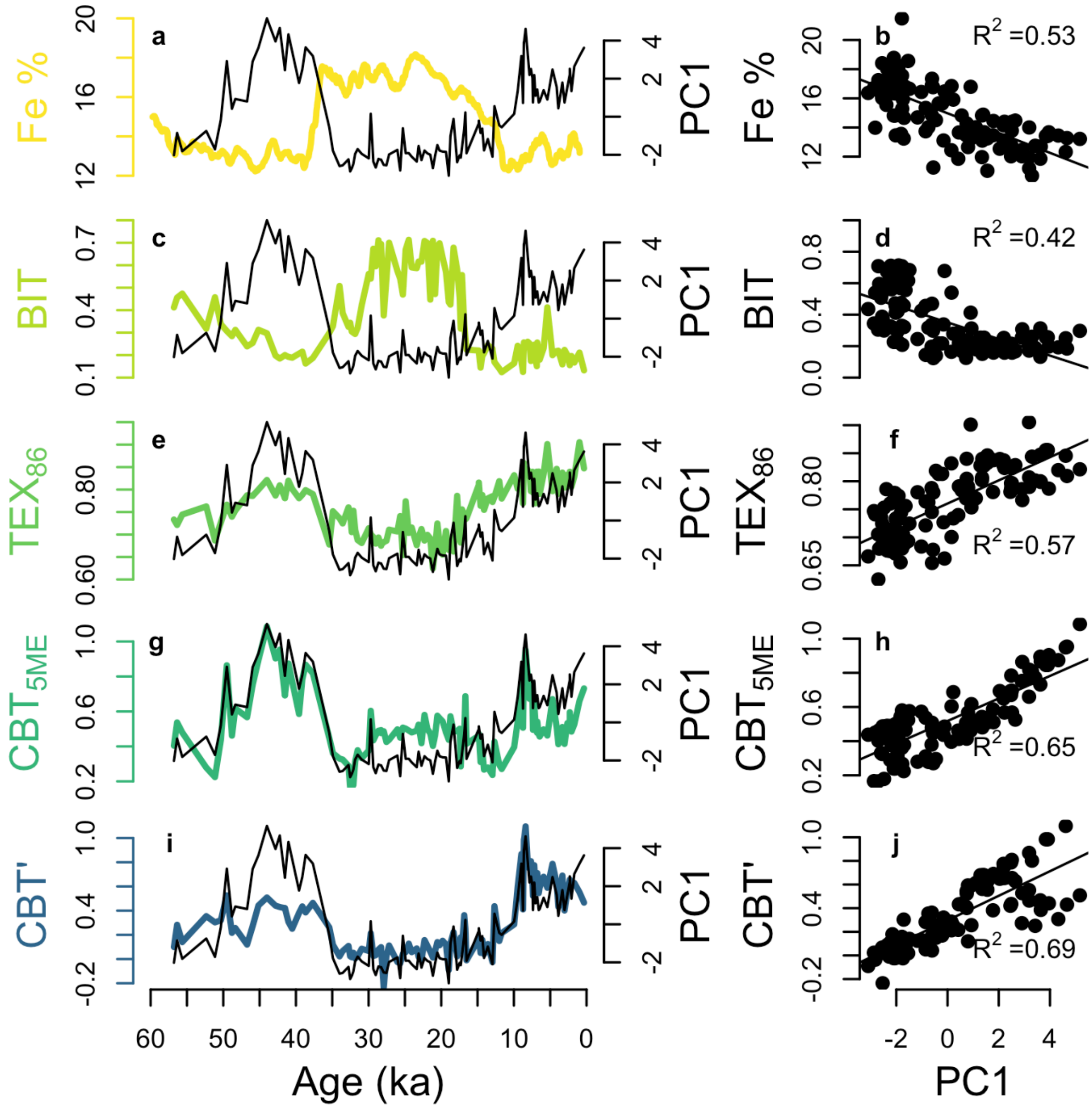

Figure S2. (a) Iron content from the Towuti lake sediment core (Costa et al., 2015). (c) Lake Towuti BIT index. (e) TEX_{86}. (g) The CBT index. (i) The CBT' index. Panels on the right (b, d, f, h, and j) show R^2 values from linear regressions between the variables on the left and PC1 from the principal component analysis shown in Figure 4 (black).

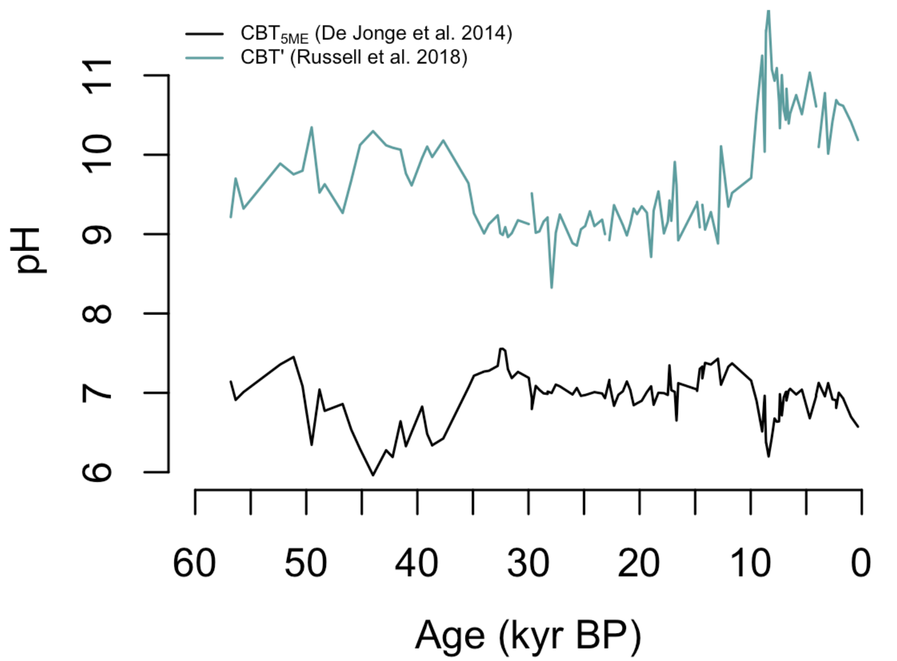

Figure S3. Reconstructions of pH using the CBT5ME-based calibration (black) and the CBT'-based calibration (teal).

$$CBT_{5ME} = -log((Ib + IIb)/(Ia + IIa))$$ De Jonge et al. (2014)

$$pH = 7.84 - 1.73 \times CBT_{5ME}$$ De Jonge et al. (2014)

$$CBT' = -log((Ic + IIa' + IIb' + IIc' + IIIa' + IIIb' + IIIc')/(Ia + IIa + IIIa))$$ De Jonge et al. (2014)

$$pH = 8.95 + 2.65 \times CBT'$$ Russell et al. (2018)

CHAPTER 3

Changes in Indo-Pacific Warm Pool hydroclimate and vegetation during the last deglaciation

Meredith Parish[1], James Russell[1], Bronwen Konecky[2], Xiaojing Du[3], Chengfei He[4], Satria Bijaksana[5], Hendrik Vogel[6]

[1]Department of Earth, Environmental, & Planetary Sciences, Brown University, Providence, RI, USA

[2]Department of Earth, Environmental, and Planetary Sciences, Washington University in St. Louis, St. Louis, MO, USA

[3]Atmospheric, Oceanic & Earth Sciences Department, George Mason University, Fairfax, VA, USA

[4]Rosenstiel School of Marine, Atmospheric, and Earth Science, University of Miami, Key Biscayne, FL, USA

[5]Global Geophysics Group, Faculty of Mining and Petroleum Engineering, Institut Teknologi Bandung, Bandung City, West Java, Indonesia

[6]Institute of Geological Sciences & Oeschger Centre for Climate Change Research, University of Bern, Bern, Switzerland

Published in 2024 in *Quaternary Science Reviews,* 336, 108755.

Abstract

Drying across much of the Indo-Pacific Warm Pool (IPWP) during the Last Glacial Maximum (LGM) has been widely recognized from interpretations of sedimentological, geochemical, and paleoecological records. Reconstructions of precipitation isotopic compositions have emerged as a powerful tool to reconstruct rainfall amount in many tropical regions, yet it has proven difficult to reconcile precipitation isotope records from the IPWP with records of widespread drying. To evaluate the signals preserved in precipitation isotope records, we produced new hydrogen and carbon isotope records from Lake Towuti and Lake Matano in Sulawesi, Indonesia using long-chain *n*-alkanes. We then compared these new records to existing n-alkanoic acid records from the same lakes and compiled available marine runoff, salinity, leaf wax hydrogen isotope (δ^2H_{wax}), and leaf wax carbon isotope ($\delta^{13}C_{wax}$) records in the IPWP. During the last deglaciation, marine runoff and salinity proxies reveal that precipitation amount began to increase dramatically at ~12.3 ka at the end of the Younger Dryas. A principal component analysis of precipitation isotope records indicates a shift from more ^2H-enriched to ^2H-depleted waxes at ~12.3 ka as sea level rise inundates most of the Sunda and Sahul shelves, coincident with runoff and salinity proxies, suggesting precipitation isotopes respond strongly to rainfall amount in this region. Over 70% of IPWP $\delta^{13}C_{wax}$ records show a transition from more to less ^{13}C-enriched waxes beginning about 19.9 ka, prior to the reconstructed increases in precipitation. We suggest that vegetation shifted in response to the changing seasonality of precipitation. The dramatic changes in the IPWP during the last deglaciation highlight the capacity for the region to experience dynamic changes in precipitation, vegetation, and atmospheric circulation.

1. Introduction

The Indo-Pacific Warm Pool (IPWP) is the largest area of ocean with sea surface temperatures over 28 °C year-round and plays a vital role in shaping global climate. IPWP climate variations are highly consequential to the diverse ecosystems in the region and to the livelihoods of millions of people living on the Maritime Continent. Despite the region's importance, global climate model projections of future precipitation change over the Maritime Continent diverge (Iturbide et al., 2020). Reconstructions of precipitation change over the past 30,000 year can provide valuable evidence to test the ability of global climate models to predict regional climate change, and to determine the dominant forcings of rainfall variations in the IPWP under the changing boundary conditions from the Last Glacial Maximum (LGM), at 22 ka, to present.

Sedimentological and palynological records have provided qualitative but critical insights into past rainfall changes over the Maritime Continent, indicating widespread aridity at the LGM (Costa et al., 2015; Hamilton et al., 2019; Hope, 2001; Reeves et al., 2013; Russell et al., 2014; van der Kaars et al., 2000, 2001, 2010; Vogel et al., 2015). Isotopic records have provided powerful additional constraints on past climate. Carbon isotopes measured in leaf waxes ($\delta^{13}C_{wax}$) generally show an expansion of C_3 plants during the last deglaciation, which has been attributed to extended and/or more arid dry seasons and/or reduced annual precipitation at the LGM relative to modern (Dubois et al., 2014; Ruan et al., 2019; Russell et al., 2014; Wicaksono et al., 2015, 2017; Windler et al., 2019; Wurster et al., 2019). Hydrogen isotope records from leaf waxes ($\delta^{2}H_{wax}$) and oxygen isotopes measured in speleothems ($\delta^{18}O_{speleo}$) show more heterogeneous changes (Ayliffe et al., 2013; Griffiths et al., 2009; Konecky et al., 2016; Krause et al., 2019; Niedermeyer et al., 2014; Partin et al., 2007; Ruan et al., 2019; Tierney et al., 2012; Wicaksono et al., 2017; Windler et al., 2019; Wurtzel et al., 2018; Yuan et al., 2023). Precipitation isotopes can be directly simulated by isotope-enabled climate models and therefore provide a more direct test of paleoclimate model simulations, yet the existing isotope records from the IPWP show diverse patterns and present discrepancies with simulated precipitation isotopes during the LGM (Du et al., 2021). It is uncertain whether the differences among precipitation isotope records indicate complications with the proxies, or whether they arise from actual regional heterogeneity in precipitation isotopes across the IPWP. For instance, *n*-alkanoic acids have been used to reconstruct precipitation isotope at several sites in the region but could derive from aquatic as well as terrestrial sources (van Bree et al., 2018). However, paleoclimate model simulations suggest precipitation isotopes may vary substantially within the Maritime Continent and may record processes other than precipitation amount, due in part to exposure of the Sunda and Sahul shelves during times with lower sea level than the present day (Du et al., 2021). Unraveling the signals embedded in precipitation isotope records in this region thus requires careful interrogation of the proxies themselves, as well as local and regional changes in atmospheric circulation during the LGM and the ensuing glacial termination.

This study assesses differences between leaf-wax isotope records based on *n*-alkanoic acids and *n*-alkanes preserved in sediments from Lakes Towuti and Matano, Indonesia, and evaluates the spatiotemporal patterns in precipitation isotope records, marine runoff and sea surface salinity records, and $\delta^{13}C_{wax}$ records across the Maritime Continent. We use runoff and salinity records to estimate the timing and patterns of precipitation change, and compare these to water isotope records to investigate the atmospheric circulation and water cycle changes recorded by these data. Additionally, $\delta^{13}C_{wax}$ records enable us to investigate changes in vegetation. The regional compilations of runoff, salinity, $\delta^{18}O_{speleo}$, $\delta^{2}H_{wax}$ and $\delta^{13}C_{wax}$ allow us to constrain the dominant drivers of hydroclimate and vegetation change in this region.

2. Regional Setting

Lake Towuti is a 560 km^2 lake located near the equator (2.75°S, 121.5°E) in central Sulawesi, Indonesia, a 174,600 km^2 island in the center of the IPWP (Figure 1). Lake Towuti is at 318 m elevation, receives ~2700 mm of precipitation per year, and has a ~1644 km^2 watershed (Konecky et al., 2016; Russell et al., 2020). The majority of precipitation falls from February to May during the Australian-Indonesian summer monsoon season, with over 200 mm of precipitation per month from the austral Asian monsoon sourced from the northwest (Konecky et al., 2016). Rainfall during the dry season (August to October), brought by winds from the southeast associated with the Asian summer monsoon, still averages over 50 mm of precipitation per month (Konecky et al., 2016). Lake Matano (2.5°S 121.3°E) is also located in Sulawesi, 10 km north of Lake Towuti. It is the deepest lake in Indonesia with a maximum depth of 590 m (Wicaksono et al., 2015). The catchment area has a mean altitude of 650 m and a lake-surface area of 276 km^2 (Wicaksono et al., 2015). HYSPLIT4 back-trajectory analysis indicates that air masses originate from the southeast during the June through October dry season and from the northwest in the November through May wet season, in addition to precipitation events sourced over local oceans (Konecky et al., 2016). Regionally, precipitation maxima migrate from northern Australia in December through January to southeast Asia in March through November (Figure A1). Precipitation minima migrate from southeast Asia in Boreal Winter to northern Australia in Austral Fall and Winter (Figure A1).

3. Methods

3.1 Modern precipitation isotopes

Konecky et al. (2016) presented monthly rain gauge and precipitation isotope measurements from 2013 to 2015. Here we present additional monthly modern isotope and rain gauge data, extending the study period from the beginning of the study in January 2013 into August of 2016. The rain gauge measurements and water samples were collected approximately ~8 km west of Lake Towuti in the village of Wawondula. Precipitation was collected as described by Konecky et al. (2016) and the amount was measured every day with a Stratus RG202 Professional rain gauge. The water samples were sealed, refrigerated, and analyzed on a Picarro L1102-I Isotopic Water Liquid Analyzer at Brown University. We averaged the monthly rainfall over the entire study period and calculated the average isotopic composition of the rainwater by weighting the isotopic composition by the precipitation amount.

3.2 LGM, Early Holocene, and Pre-Industrial climate simulations

iTRACE is performed with the isotope-enabled Community Earth System Model version 1.3 (iCESM) (Brady et al., 2019), which is composed of the Community Atmosphere Model version 1.3 (CAM5.3), the Community Land Model version 4 (CLM4), Parallel Ocean Program version 2 (POP2), and Los Alamos Sea Ice Model, version 4 (CICE4). Here we used simulated precipitation amount and isotopic precipitation at the LGM (20.0–19.9 ka), the Early Holocene (11.1–11.0 ka), and Pre-Industrial (PI; 1850 CE) from the isotope-enabled Transient Climate Evolution (iTRACE) experiment, as described in Du et al. (2021) and He et al. (2021), to compare with our proxy record and instrumental observations from Lake Towuti. The Lake Towuti and Matano region is defined as extending from 1°S to 4°S and 120°E−123°E, which includes two grids cells that we averaged.

3.3 Sample preparation and analysis

The samples from Lake Towuti were taken from a piston core (IDLE-TOW10-9B) recovered from the center of Towuti's northern basin (Russell et al., 2014, 2020). There are 23 radiocarbon dates in the top 43 kyr of sediment (Russell et al., 2014), which we calibrated to Intcal20 and used to develop an age-depth model with Bacon in R (Blaauw and Christen, 2011) as described in Parish et al. (2023). Samples from Lake Matano were collected from IDLE-MAT10-5A. There are 10 radiocarbon dates in the top 46-kyr of sediment (Wicaksono et al., 2015), which we calibrated to Intcal20 and used to develop an age-depth model with Bacon in R (Blaauw and Christen, 2011).

Previous work (Russell et al., 2014; Wicaksono et al., 2015) extracted lipids from these sediments using a DIONEX Accelerated Solvent Extractor using dichloromethane:methanol (9:1). The lipid extract was divided into neutral and acid fractions using dichloromethane:isopropanol (2:1) and ethyl ether:acetic acid (96:4) over an aminopropyl silica gel column. Whereas prior work (Russell et al., 2014; Wicaksono et al., 2015) analyzed the isotopic composition of *n*-alkanoic acids, we focused on analysis of *n*-alkanes. To do so, we used silica gel columns to separate lipids within the neutral fraction, using hexane to isolate *n*-alkanes. We used silver thiolate columns to remove unsaturated compounds (Garelick et al., 2021; Ruan et al., 2019). We quantified the abundance of C_{29}, C_{31}, C_{33} *n*-alkanes using a gas chromatography flame ionization detector (GC-FID), and measured δ^2H and $\delta^{13}C$ of C_{29}, C_{31}, and C_{33} *n*-alkanes using a gas chromatography isotope ratio mass spectrometer (GC-IRMS). δ^2H was measured in triplicate and $\delta^{13}C$ was measured in duplicate on an Agilent 6890 GC with an HP1-MS column (30 m × 0.25 mm × 0.25 μm), coupled to a Thermo Delta Plus XL IRMS with a reactor temperature of 1425 °C for hydrogen and 1000 °C for carbon. A mixture of *n*-alkane standards from Arndt Schimmelmann (Indiana University) was injected every six samples to test for instrument drift and was used to correct the measured values to Vienna Standard Mean Ocean Water (VSMOW). The H3 factor was ~2 and stable during the analyses, suggesting no or minimal fluctuation in IRMS performance. Measured isotopic values were accepted if the voltage was between 3 and 8 V. From Lake Towuti, we analyzed 55 samples, spanning the past 30,000 years for an average sampling resolution of 1 sample every 567 years, with a minimum sampling resolution of 121 years and maximum sample resolution of 2197 years. From Lake Matano, we measured 31 samples over the past 32 kyr, resulting in an average sampling resolution of one sample every 986 years. The minimum sampling resolution was 314 years and the maximum sampling resolution was 2172 years. We measured $\delta^{13}C_{wax}$ in both Towuti and Matano at about half the resolution of the δ^2H_{wax} data. From Lake Towuti we measured 31 samples and we measured 14 samples from Lake Matano.

3.4 Leaf wax isotope corrections and interpretations

The δ^2H of long-chain *n*-alkanes preserved in lake sediment generally reflects the isotopic composition of precipitation (Sachse et al., 2012). Longer chain length *n*-alkanes such as C_{31} alkanes are more likely to be derived from terrestrial leaf waxes than shorter chain length *n*-alkanes or *n*-alkanoic acids (Sachse et al., 2012; van Bree et al., 2018). Terrestrial plants take up meteoric water, derived from precipitation, to synthesize these epicuticular waxes, with an apparent fractionation between water and wax related primarily to evapotranspiration and biosynthetic fractionation. Because different plants have different apparent fractionation, it is common to correct the measured δ^2H_{wax} for changes in apparent fractionation to estimate the δ^2H of the precipitation (δ^2H_{precip}) (Konecky et al., 2016; Lupien et al., 2021). Changes in apparent fractionation are often estimated from $\delta^{13}C_{wax}$ values, which primarily record the relative abundances of plants that use the C_3 and C_4 photosynthetic pathways. Although this approach is common in the literature, we examined the apparent fractionation of C_{31} alkanes in plants using the C_3 and C_4 photosynthetic pathways from Sachse et al. (2012) taken within 30° of the equator and found no significant difference between C_3 and C_4 plants (Konecky et al., 2016; Figure A2). It is possible that a larger modern C_{31} alkane δ^2H dataset could document a larger apparent fraction in C_3 plants; however, the existing C_{31} alkane data indicates C_3 plants have a smaller (but not significantly different) mean apparent fractionation than C_4 plants (Hutchings and Konecky, 2020 , 2022). Because we are unable to determine the apparent fractionation from existing data, we therefore used the average apparent fractionation of both C_3 and C_4 plants, rather than using an endmember mixing model, to estimate δ^2H_{precip}. The average fractionation of all tropical C_3 and C_4 plants is −135‰ for C_{31} alkanes (Sachse et al., 2012). The Towuti C_{28} alkanoic acid δ^2H_{wax} record was corrected using a constant offset of −129‰, which is the average apparent fraction of all tropical C_3 and C_4 plants for C_{27} alkanes (Sachse et al., 2012).

To help visualize changes in δ^2H_{precip} attributable to rainfall amount and atmospheric circulation, we corrected the δ^2H_{precip} for changes in seawater δ^2H by interpolating the global benthic $\delta^{18}O$ stack (Lisiecki and Raymo, 2005) to the resolution of our measurements. To do so, we scaled the $\delta^{18}O$ stack values to account only for the change attributable to changing ice volume (Schrag et al., 1996), converted $\delta^{18}O$ to hydrogen space using the global meteoric water line, and subtracted the effect of the change in the isotopic composition of global seawater from the measured δ^2H_{precip}.

3.5 Proxy record synthesis

We compiled all regional runoff, $\delta^{18}O$ of sea water ($\delta^{18}O_{SW}$), $\delta^{18}O_{speleo}$, $\delta^{2}H_{wax}$, and $\delta^{13}C_{wax}$ records in the IPWP that span the last deglaciation. We only included records that had at least three age controls between 20 and 12 ka and that span 21 ka to 2 ka. $\delta^{18}O_{sw}$ records were produced using identical methods as Gibbons et al. (2014). Briefly, sea surface temperatures (SST) were used to convert the $\delta^{18}O_{calcite}$ records to $\delta^{18}O_{sw}$ using the following equation, where a = 16.5 ± 0.2 °C, b = −4.80 ± 0.16 °C, and T is the measured SST:

$$\delta^{18}O_{sw} = -T/b + a/b + \delta^{18}O_{calcite}$$

Then, a 0.27‰ adjustment was used to convert the records from VPDB to VSMOW, and isotopic changes in seawater driven by ice volume were removed. $\delta^{18}O_{speleo}$ measurements were converted to $\delta^{2}H$ values assuming $\delta^{18}O_{speleo}$ directly record precipitation isotopes, with no impact of changes in cave temperature, and scaling the $\delta^{18}O_{speleo}$ using the global meteoric water line. To detect the dominant modes of variability in the data, we performed both a principal component analysis (PCA) and stacking (averaging) of each set of proxy records after interpolating all records to a common timestep. The timestep was the mean resolution of all the records.

Using the $\delta^{13}C_{wax}$ we calculated the percentage of C_3 plants contributing to the sedimentary leaf wax pool using the mixing model described in Konecky et al. (2016). The median $\delta^{13}C$ composition of C_3 and C_4 plants calculated from the *n*-alkanes of tropical plants were used as the endmembers in the mixing model. In the tropics, C_3 plants have a median $\delta^{13}C$ of C_{31} *n*-alkanes of −35.9 ± 2.2‰ (median ± standard deviation, n = 20) and C_4 plants have $\delta^{13}C$ of C_{31} *n*-alkanes of −22.1 ± 2.6‰ (median ± standard deviation, n = 12; Figure A.2; Sachse et al., 2012).

3.6 Changepoint detection

We used the EnvCpt package in R to identify changepoints in the trend (slope) in all of the compiled hydroclimate records (Killick et al., 2021). The changepoints were determined by calculating stepwise linear functions that minimize the total residual error. We interpret the changepoint detected between 22 and 8 ka in each set of records as the timing of a deglacial changepoint, confirmed by visual inspection of the proxy data. We determined the uncertainty of the timing of each changepoint, using Bacon to recalibrate the published radiocarbon dates to IntCal20 and calculate the age uncertainty (Blaauw and Christen, 2011).

4. Results

4.1 Modern climatology and precipitation isotopes

From January 2013 to August 2016, the individual monthly isotopic composition of the collected precipitation is correlated, albeit weakly, with precipitation amount ($R^2 = 0.25$; $p<0.01$; Figure 2B). Precipitation amount and its isotopic composition are highly correlated when averaging the monthly values from the entire study ($R^2 = 0.79$; $p<0.01$; Figure 2C). The positive correlation between 2013-2015 rain gauge measurements from Lake Towuti and precipitation data from the region (Konecky et al., 2016) indicates that precipitation at Lake Towuti is representative of central Sulawesi precipitation, which itself is correlated to precipitation variations over a large region of central and southern Indonesia (Konecky et al., 2016).

4.2 Simulated LGM, Early Holocene, and PI climatology and precipitation isotopes

In the iTRACE simulation, the seasonal patterns of precipitation are somewhat similar to modern observations, though iTRACE simulates substantially less seasonality during the PI than we observe during the present-day. The model simulates wet conditions through much of the year, but with an ASO dry season, similar to the modern observations (Figure 3C). The monthly precipitation modeled by the PI iTRACE simulation is moderately correlated with δ^2H_{precip} ($R^2 = 0.31$; $p = 0.06$; Figure 3D). The monthly precipitation amount simulated with the PI iTRACE simulation is not strongly correlated with the modern 4-yr average ($R^2 = 0.27$; $p = 0.09$). The simulated δ^2H_{precip} is strongly correlated with the average from the modern 4-yr study ($R^2 = 0.69$; $p < 0.01$). Although the seasonality of precipitation is not simulated well in the area around Lake Towuti, the model's performance is satisfactory across the larger Asian monsoon region (He et al., 2021). During the LGM, the model simulates substantially less precipitation than in the modern, with a particularly large reduction in precipitation during the ASO dry season relative to preindustrial (Figure 3G). The isotopic composition of precipitation has a similar seasonality to the observations in the PI, Early Holocene, and LGM, and it is positively correlated with precipitation amount in the LGM simulation ($R^2 = 0.76$; $p < 0.01$; Figure 3H). The iTRACE-simulated Early Holocene precipitation shows precipitation maxima in June and December–January (Figure 3E). Precipitation amount is only moderately correlated with the isotopic composition of rainwater during the Early Holocene ($R^2 = 0.32$; $p < 0.01$; Figure 3F). Precipitation during the dry season greatly increased during the Early Holocene, compared to at the LGM (Figure 3). The transient iTRACE simulations shows that the percent of dry season (ASO) precipitation on Sulawesi increases from ∼15% at the LGM to ∼18% in the Early Holocene and ∼35% in the PI (Figure 3I).

4.3 Lake Towuti and Lake Matano leaf-wax isotope records

Variations in the relative abundance of different *n*-alkanes can provide information about the sources of these lipids. The carbon preference index (CPI) can be used to assess the state of preservation of the alkanes, wherein fresh vegetation can have a CPI of 6 or higher and a CPI of ~1 indicates that the hydrocarbons in a sample are highly degraded and potentially from oil (Bray and Evans, 1965). The average carbon preference index (CPI) value of the Towuti samples was 3.3, with a maximum of 4.8 and minimum of 2.6. The average CPI value from Matano was 4.0, with a maximum value of 5.8 and a minimum value of 2.6. Overall this indicates the *n*-alkanes were well-preserved. The average chain length (ACL) calculated for C25 to C33 from Towuti was 29.5, with a maximum of 30.0 and a minimum of 28.5. The average ACL from Matano was 29.7, with a maximum of 30.5 and a minimum of 27, indicating the *n*-alkanes are most likely derived from terrestrial plants.

The Towuti C_{29}, C_{31}, C_{33} δ^2H_{wax} records (not corrected for vegetation and ice volume) show ^{2}H-enrichment at the LGM relative to the ^{2}H-depletion in the Holocene (Figure 4A). All of the homologues show a similar structure and amplitude of change. C_{31} δ^2H_{wax} is positively correlated with C_{29} δ^2H_{wax} ($R^2 = 0.64$; $p<0.01$) and C_{33} δ^2H_{wax} ($R^2 = 0.30$; $p<0.01$). The greatest differences between homologues occurs between 30 and 26 ka, when C_{29} δ^2H_{wax} is more ^{2}H-depleted than C_{31} and C_{33} δ^2H_{wax} (Figure 4A). Like Towuti, the uncorrected C_{31} δ^2H_{wax} record from Lake Matano shows ^{2}H-enrichment at the LGM and ^{2}H-depletion during the Holocene, but the shift is smaller than observed at Lake Towuti (Figure 4C). The uncorrected Matano C_{29} δ^2H_{wax} record shows the greatest magnitude of change from the LGM to the Holocene. The C_{33} δ^2H_{wax} record has considerable ^{2}H-depletion at ~9.5 ka, which is not reflected in the other homologues. The shift to ^{2}H-depleted values in the Holocene in all of the homologues occurs about 12 ka, more than 5 kyr after the onset of deglacial warming on Sulawesi recorded from this same set of samples in Lake Towuti (Parish et al., 2023).

After correcting the δ^2H_{wax} values for ice volume and the isotopic fractionation by plants, the resulting δ^2H_{precip} indicates similar isotopic compositions during the LGM and Holocene with the most ^2H-enrichment occurring at 12 ka (Figure 5A). Using an end-member mixing model (Konecky et al., 2016), rather than our constant apparent fractionation, to estimate apparent fractionation and to correct the δ^2H_{wax} to $^2H_{precip}$ does not considerably impact the δ^2H_{precip} records (Figure A.7). The Towuti *n*-alkane-based δ^2H_{precip} record and the *n*-alkanoic acid based δ^2H_{precip} record (Konecky et al., 2016) share common trends (Figure 5A). Both records are slightly more ^2H-depleted during the LGM and during the Holocene and more ^2H-enriched between 17ka and 10 ka. The *n*-alkane and *n*-acid records are not strongly correlated when including all individual measurements (R^2=0.08; p>0.05). However, calculating the correlation between the 2,000-yr moving averages to smooth the data results in a stronger correlation (R^2=0.36; p=0.02).

The similarity between the alkane δ^2H_{precip} record from nearby Lake Matano and the Lake Towuti δ^2H_{precip} record supports the interpretation that the records reflect the isotopic composition of the rainwater received by terrestrial plants over the past 30 kyr. The different absolute values between the alkane and acid records at Lake Towuti may be due to aquatic contributions to C_{28} *n*-acid (van Bree et al., 2018). In principle, if the *n*-alkanoic acids were produced by aquatic plants that reflect the isotopic composition of the lake water, we might expect the *n*-alkanoic acids to be more ^2H-enriched than the terrestrial *n*-alkanes, particularly in samples from the LGM when the region experienced drying (Russell et al., 2014) and the lake level was ~30 meters lower than present (Vogel et al., 2015). However, we do not observe ^2H-enrichment of acids relative to alkanes during the LGM compared to the Holocene. Temperate sites have reported *n*-alkanes that are 30‰ more depleted than *n*-acids (Chikaraishi and Naraoka, 2007; Hou et al., 2008). However, in samples from the Amazon and Andes there is not a significant difference between C_{30} acids and

C_{29} alkanes (Feakins et al., 2016). The differences between the *n*-acid and *n*-alkane records may be due to differences in apparent fractionation for which we cannot account, particularly given the uncertainty in sources for C_{28} *n*-acid to tropical lake sediments (van Bree et al., 2018).

The C_{29}, C_{31}, C_{33} $\delta^{13}C$ records from Towuti show shifts from ^{13}C-enrichment at the LGM to ^{13}C-depletion during the Holocene. C_{29} $\delta^{13}C$ shows a ~6‰ shift from -27 to -33‰, C_{31} $\delta^{13}C$ shows a ~7‰ change from -26 to -33‰, and C_{33} $\delta^{13}C$ shows a ~8‰ change from -24 to -32‰ (Figure 4B). $\delta^{13}C$ *n*-alkane and *n*-acid records from Lake Towuti are similar throughout the past 30 kyr, though the *n*-acid record is more depleted during the Holocene than the alkane record (Figure 5B). At Lake Matano, the C_{31} $\delta^{13}C$ record shows a ~9‰ change, from -24‰ at the LGM to -35‰ in the Holocene, and the C_{29} $\delta^{13}C$ record shows a slightly smaller amplitude change (Figure 4D). The structure of LGM-to-Holocene change in the Matano C_{29} and C_{31} $\delta^{13}C$ records is similar to the C_{26} and C_{28} $\delta^{13}C$ records from Matano (Figure 5c; Wicaksono et al., 2015). However, the C_{26} and C_{28} *n*-acids from Matano are more ^{13}C-depleted for the last 20 kyr than at Towuti and show a smaller amplitude of change from the LGM to the Holocene. It is unclear why the *n*-acid amplitude of change in $\delta^{13}C$ is greater than *n*-alkanes at Towuti and less than *n*-alkanes at Matano (Figure 5B and 5C). The acid record may have non-terrestrial contributions (van Bree et al., 2018). Alternatively, different plants produce different relative abundances of alkanes and acids (Contreras et al., 2023).

5. Discussion

5.1 Surface runoff and precipitation during the deglaciation

Our syntheses of proxy reconstructions of rainfall, precipitation isotopes, and geochemical records of vegetation provide new insight into IPWP paleoclimate dynamics and the sensitivity of vegetation to rainfall. We rely on indicators of precipitation change other than precipitation isotopes and vegetation to help elucidate rainfall history and its influences on IPWP precipitation isotopes and ecosystems. Specifically, we synthesized four surface runoff records and 12 salinity records in the IPWP as recorders of precipitation amount. There are four marine and lacustrine geochemical runoff records in the IPWP with at least three age controls between 20 and 12 ka and that span 21 to 2 ka (Table 1; Costa et al., 2015; Fraser et al., 2014; Hollstein et al., 2018; Mohtadi et al., 2011). The two marine records of ln(Ti/Ca) (Hollstein et al., 2018; Mohtadi et al., 2011), one marine record of log(Fe/Ca) (Fraser et al., 2014), and one lacustrine Ti concentration record (Costa et al., 2015) included in our synthesis, assume that rainfall is the dominant control on erosion, which supplies Ti and Fe to sediments. Changepoint analysis of the four runoff records (Killick et al., 2021) shows that Ti began to increase at between 14.7 and 9.1 ka with an average of 12.4 ka (Table 1; Figure 10).

There are 12 $\delta^{18}O_{sw}$ records in the IPWP with at least three age controls between 20 and 12 ka and span 21 to 2 ka (Table 1; Fan et al., 2018; Gibbons et al., 2014; Levi et al., 2007; Mohtadi et al., 2010; Rosenthal et al., 2003; Sarnthein et al., 2011; Schröder et al., 2018; Stott et al., 2007, 2002; Visser et al., 2003; Xu et al., 2008). $\delta^{18}O_{sw}$ is a proxy for sea surface salinity and rainfall isotopic composition (Gibbons et al., 2014). Changepoint analysis indicates that shift to more isotopic depletion and likely decreased salinity begins at an average of 12.3 ka, with the earliest record shifting at 15.2 ka and the latest record shifting at 10.8 ka (Table 1; Figure 10).

The first principal component (PC1) and the mean of the 16 z-scored runoff and $\delta^{18}O_{sw}$ records indicate two pulses of decreased precipitation at ~16 and ~12.5 ka, followed by a shift to increased precipitation during the Holocene (Figure 6C). Although the LGM is characterized by depleted isotopic compositions and decreased runoff relative to Heinrich Stadial 1 (~19-15 ka) and the Younger Dryas (~12.9-11.7 ka), there is an overall shift to more depleted $\delta^{18}O_{sw}$ and increased runoff from the LGM to the Holocene that may be attributed to increased precipitation. These observations are supported by increasing mean grain size during the last deglaciation in a marine record from southern Java, which Mohtadi et al. (2011) interpreted to reflect increased river runoff in the region from the LGM to the Holocene, with even drier periods than the LGM at Heinrich Stadial 1 and the Younger Dryas.

There are potential confounding influences on runoff and salinity proxies. Ln(Ti/Ca) can be affected by changes in sea level and production and preservation of calcium carbonate, the main source of Ca to sediment. $\delta^{18}O_{sw}$ can reflect the isotopic composition of rainwater in addition to surface freshwater balance. For instance, Gibbons et al. (2014) suggest that the relatively salty (enriched) compositions observed during Heinrich Stadial 1 (~19-15 ka) and the Younger Dryas (~12.9-11.7 ka) were caused by a distinct isotopic composition of precipitation due to shifts in the position of the ITCZ, in addition to changes in precipitation amount. However, variations in the isotopic composition of precipitation are likely to be small relative to the isotopic difference between the ocean and rainfall, such that $\delta^{18}O_{sw}$ should primarily trace rainfall amount. The amplitude of shifts toward enriched $\delta^{18}O_{sw}$ during Heinrich Stadial 1 and the Younger Dryas are very large, and could mask the transition from the LGM to the Holocene. However, the $\delta^{18}O_{sw}$ records still indicate that the LGM is saltier (more enriched) than the Holocene.

5.2 Precipitation isotope records

$\delta^{18}O_{speleo}$ and $\delta^{2}H_{wax}$ records show heterogeneous precipitation isotope changes within the IPWP (Ayliffe et al., 2013; Griffiths et al., 2009; Konecky et al., 2016; Krause et al., 2019; Niedermeyer et al., 2014; Partin et al., 2007; Ruan et al., 2019; Wicaksono et al., 2017; Wurtzel et al., 2018; Yuan et al., 2023). This heterogeneity may indicate a complex suite of climatic processes that affect precipitation isotopes in the IPWP (Konecky et al., 2016, 2019). However, a PCA of all IPWP water isotope records (excluding the Towuti *n*-acid record to avoid overly-weighting Lake Towuti in the mean and PCA), with at least three age controls during the deglaciation, reveals that 65% of the variance in all δ^2H_{wax} and $\delta^{18}O_{speleo}$ records can be explained by the first principal component (PC1). The mean of the records is similar to PC1 and shows a clear shift from more ^2H-enriched to more ^2H-depleted precipitation centered at ~12.3 ka in most of the records, as detected by changepoint analysis (Figure 7C; Table 1). These findings are further supported by a shift in a Sumatran speleothem record at ~12.5 ka (Wurtzel et al., 2018), though the record was too short to include in the PCA. A PCA of only the δ^2H_{wax} records (excluding the $\delta^{18}O_{speleo}$ records) results in PC1 with a nearly identical structure as when the speleothem records are included (Figure A.5), though the first principal component only explains 48% of the variance in the δ^2H_{wax} records. Change point analysis of individual records also indicates an earlier shift around ~14.5 ka, during Heinrich Stadial 1, in four of the records in addition to the shift at ~12.3 ka (Figure 10).

The timing of the shift in precipitation isotope records, at 12.3 ka (Figure 7) coincides with the deglacial shift indicated in runoff and sea surface salinity proxies (Figure 10). The agreement between precipitation isotope records and other precipitation amount proxies may indicate that δ^2H_{wax} and speleothem $\delta^{18}O_{speleo}$ respond strongly to, and may be reliable proxies for, precipitation amount on orbital timescales in the IPWP. Additionally, the timing of the shift in precipitation isotope records coincides with flooding of the Sunda and Sahul shelves (Pico et al., 2020). Existing studies have observed the similar timing of shelf inundation and precipitation amount, as inferred from $\delta^{18}O_{speleo}$ records (Krause et al., 2019). However, δ^2H_{wax} and speleothem $\delta^{18}O_{speleo}$ records may also be affected by changes in moisture source, cloud type, convergence/divergence, and/or moisture transport, many of which also change with Sunda and Sahul shelf inundation (Du et al., 2021; Konecky et al., 2016, 2019).

5.3 Leaf wax isotope records of vegetation change

$\delta^{13}C_{wax}$ records from the IPWP share common trends (Dubois et al., 2014; Niedermeyer et al., 2014; Ruan et al., 2019; Russell et al., 2014; Wicaksono et al., 2017, 2015; Windler et al., 2019; Wurster et al., 2019). A PCA of all marine and lacustrine IPWP $\delta^{13}C_{wax}$ records with at least three age controls during the deglaciation (excluding the Towuti and Matano *n*-acid records to avoid overly weighting these sites) results in a PC1 that explains 96% of the variance in all records (Figure 8). All records show ^{13}C-enrichment during the LGM relative to ^{13}C-depletion during the Holocene, except for 91GGC from offshore eastern Borneo (Dubois et al., 2014) and SO189-144KL from offshore Sumatra (Niedermeyer et al., 2014). The ^{13}C-enrichment at the LGM ranges from 2 to 9‰ heavier than the mean $\delta^{13}C_{wax}$ between 10 and 8 ka in each record, excluding 91GGC and SO189-144KL (Table A.1; Figure 8B). Changepoint analysis reveals that the records begin to become more ^{13}C-depleted between 22.3 and 17.2 ka with an average of 19.9 ka (Table 1; Figure 10).

The amplitudes of change suggest variable changes in vegetation, with the largest amplitudes signaling substantial decreases in the abundance of plants using the C_4 photosynthetic pathway during the deglaciation. Averaging all $\delta^{13}C_{wax}$ records from the IPWP results in a ~4‰ shift, from -28 to -32‰, from the LGM to the Holocene (Figure 8C). The largest shifts in $\delta^{13}C_{wax}$ occurred at the sites with the highest modern mean annual precipitation (Figure 9B); however, modern mean annual precipitation is not significantly correlated with the magnitude of the LGM-Holocene shift in $\delta^{13}C_{wax}$ (R^2=0.19; $p>0.05$).

The $\delta^{13}C_{wax}$ shift in the records could be explained by changes in water stress and/or by changes in the ratio of C_3 to C_4 plants. Fractionation of carbon is dependent on plant moisture stress, with wetter conditions leading to more efficient leaf-gas exchange and more depleted $\delta^{13}C$ values (Diefendorf et al., 2010). A shift in $\delta^{13}C_{wax}$ can also be caused by a shift in the ratio of C_3 to C_4 plants because of their distinct isotopic compositions (Figure A.2). Many, if not most, of the records in the IPWP likely record both decreasing moisture stress and increasing C_3 plants during the deglaciation, given palynological evidence for decreasing grass abundance in many parts of the IPWP (Dubois et al., 2014; Hamilton et al., 2019; Hope, 2001; Ruan et al., 2019; van der Kaars et al., 2010).

The effects of water stress vs. changes in plant photosynthetic pathway can be difficult to discern, and we can only definitively diagnose increasing C_3 plants from $\delta^{13}C_{wax}$ when there is a large shift from values within the modern C_4 range to values within the C_3 range beyond that expected from water stress alone (Figure A.2). To assess the factors influencing $\delta^{13}C_{wax}$, we calculated the percent C_3 using a mixing model that does not take into account moisture stress (Konecky et al., 2016). The individual records show that the two sites with highest modern percent (> 78%) C_3 experienced the greatest change in fraction C_3 over the deglaciation (Figure 9). These sites – Lake Towuti and Lake Matano – shift from less than 30% C_3 plants at the LGM to over 70% C3 plants during the Holocene, suggesting a reduction in the extent of the closed-canopy rainforests during the LGM. GeoB10053-7 from offshore Java also shows a large magnitude shift from below 50% C_3 at the LGM to over 68% at modern. Of note, the three sites with highest modern fraction C_3 are also the three sites with records based on isotopic analyses of *n*-alkanes, rather than *n*-acids. However, the comparison between alkanes and acids at Lake Towuti and Lake Matano indicates that the use of *n*-acids can either amplify or dampen the magnitude of the shift in $\delta^{13}C$ compared to alkanes (Figure 5). The two sites with between 50 and 67% C_3 in the most modern samples (91GGC offshore Borneo and SO189-144KL from offshore Sumatra) do not show a trend from the LGM to the Holocene, hovering around 60% C_3 plants throughout the deglaciation. The lack of trend at the Borneo site is surprising, as a nearby bat guano $\delta^{13}C$ record from southern Borneo suggested savannah expansion during the LGM (Wurster et al., 2019). The modern reconstructed 66% C_3 plants at Borneo also does not reflect the tropical lowland and montane rainforest present today (Dubois et al., 2014), which may point to remote aeolian contributions of *n*-acids to these sediments. The two sites with less than 30% C_3 in their most modern measurements (SO18515 in Mandar Bay and GeoB10069-3 offshore Java) show a clear change to more negative values during the deglaciation, but the magnitude of change is much smaller than the sites that are rainforests today.

5.4 Forcings of precipitation change

Precipitation amount is challenging to reconstruct from proxy archives. Precipitation isotopes, vegetation change, clastic sediment fluxes, and a variety of other proxies have been used to estimate precipitation amounts in the past, but all of these proxies are influenced by multiple climatic, ecologic, and/or geologic processes. We rely on runoff records and $\delta^{18}O_{sw}$ records as more direct indicators of precipitation change, which point to increasing precipitation amount during the Younger Dryas in 8 records, although an initial moisture increase is detected during Heinrich Stadial 1 in three records (Figure 10). The spread in timing may reflect an increase in moisture during both Heinrich Stadial 1 and the Younger Dryas, potentially in different parts of the IPWP, but also highlights the continued difficulty in reconstructing precipitation amount.

PC1 of precipitation isotopes shifts at ~12.3 ka, which could be further evidence for increasing precipitation amount during the last deglaciation. However, there are many controls on the isotopic composition of precipitation in the IPWP. A comparison of precipitation amount and its isotopic composition during the LGM and the Early Holocene in the iTRACE simulations indicated variable relationships between precipitation amount and isotopic composition, including regions with both negative (as predicted by the amount effect) and positive (opposite the amount effect) correlations (Du et al., 2021). The latter occurred at some sites near exposed shelf areas, potentially due to shifts in moisture source. The iTRACE experiment simulated a SW-NE dipole pattern of δ^2H_{precip} anomalies over the IPWP, with the eastern Indian Ocean showing more ^{2}H-enrichment during the LGM relative to the Holocene, and ^{2}H-depletion at the LGM relative to the Holocene in Borneo, Sulawesi, and Papua (Du et al., 2021). The enrichment during the LGM was attributed to increased divergence and subsidence related to shelf exposure, which favor rain re-evaporation that removes lighter isotopes over the eastern Indian Ocean (Du et al., 2021). Although the δ^2H_{precip} anomaly showed a dipole structure, the first principal component of precipitation isotope records revealed more ubiquitous ^{2}H-enrichment during the LGM relative to the Holocene across the Maritime Continent (Du et al., 2021).

Despite the varied influences on runoff, salinity, and precipitation isotope proxies, when taken together, the synchrony of deglacial shifts in runoff, $\delta^{18}O_{sw}$, and precipitation isotope records provide support for increasing precipitation over the IPWP at ~12.3 ka. The shift from a drier LGM to a wetter Holocene is supported by a variety of other records, though not all agree with the timing of this change. A compilation of coral, marine sediment, lake sediment, speleothem, and charcoal was used to infer increasing precipitation in Indonesia starting at ~17 ka (Reeves et al., 2013). This timing was largely based on increasing lowland rainforest pollen detected in cores from Java and

Sumatra (Reeves et al., 2013); however, rainforest expansion may be influenced by a variety of factors including atmospheric CO_2 concentrations (Kimbrough et al., 2023) and precipitation seasonality (Dubois et al., 2014) rather than rainfall amount alone. On Sulawesi there is additional proxy evidence of increasing moisture during the deglaciation, including a lake level reconstruction from Lake Towuti (Vogel et al., 2015) and a charcoal record from Lake Lantoa (Hamilton et al., 2019). However, the timing of rising lake levels is difficult to determine, and fire frequency is influenced by a variety of climatic and ecological processes.

The timing of the shift in our syntheses, at ~12.3 ka, coincides with the timing of the flooding of the majority of the Sunda and Sahul shelves, when sea levels rose above 50 m below modern (Du et al., 2021; Lambeck et al., 2014) at ~12.5 ka (Hanebuth et al., 2000, 2011). Climate models suggest that the exposure of the continental shelves in the IPWP during the LGM induced anomalous southeasterlies off the coast of Java and Sumatra, which caused increased upwelling and cooling (DiNezio et al., 2018). Cooling in the eastern Indian Ocean decreased the zonal SST gradient and weakened Indian Ocean Walker Circulation, leading to atmospheric divergence and decreased precipitation over the Maritime Continent at the LGM compared to the Holocene (DiNezio et al., 2018, 2016; DiNezio and Tierney, 2013; Du et al., 2021). In the iTRACE simulation, the flooding of the Northwestern Australian Shelf, when sea level rose to 65 m below modern, caused large-scale precipitation change over the tropical Indian Ocean (Du et al., 2021). In iTRACE, the Northwestern Australian Shelf was inundated at 14 ka, which is the same time sea level was expected to be 65 m below modern in the Sunda core region (Hanebuth et al., 2011; Lambeck et al., 2014), but there are no estimates of the timing of this flooding from the Northwestern Australian Shelf itself (Lewis et al., 2013). The simulation also indicates increased precipitation over the Maritime Continent with the flooding of the majority of the Sunda and Sahul shelves at 12 ka, but the simulated increase in rainfall at this time does not cover as broad of a spatial scale as the shelf inundation at 14 ka (Du et al., 2021).

Our reconstructed timing of increased precipitation reflected in runoff, salinity, and precipitation isotope records at ~12.3 ka, suggests the flooding of the majority of the Sunda and Sahul shelves at 12.5 ka caused more significant precipitation increase over the Maritime Continent than the earlier flooding of the NW Australian shelf when sea level rose above 65 m below modern and caused the large-scale tropical Indian Ocean dipole. Seven records do indicate increasing precipitation during Heinrich Stadial 1 (Figure 10), when the NW Australian Shelf may have become inundated. Further work is needed to investigate interactions between flooding of different parts of the shelves and climate boundary conditions to unravel the causes of these rainfall changes.

5.5 Causes of vegetation change

Support for decreasing C_4 plants – most notably tropical grasses and sedges – during the deglaciation is apparent in many palynogical records from the IPWP. Decreasing *Cyperaceae*, which is mostly C_4 in the tropics (Bruhl and Wilson, 2007), and *Poaceae* was observed at Lake Lantoa and Wanda Swamp in Sulawesi, offshore Java, and offshore Sumatra (Dubois et al., 2014; Hamilton et al., 2019; Hope, 2001; Ruan et al., 2019; van der Kaars et al., 2010). Given the range in the $\delta^{13}C$ of C_3 and C_4 plants it is difficult to quantify the extent of C_4 expansion during the LGM. Overall the data are consistent with retraction of C_4 sedges and grasses during the deglaciation.

Despite this evidence, not all of the change in $\delta^{13}C_{wax}$ may be attributed to increasing C_3 plants during the deglaciation. A shift from more ^{13}C-enrichment at the LGM to more ^{13}C-depletion during the Holocene could be controlled by water-stress related to rainfall, humidity, or temperature, CO_2 concentration, or precipitation amount. Increased temperature would cause a shift to more ^{13}C-enriched values after the deglaciation (Pagani et al., 1999), suggesting temperature is not the primary control on the $\delta^{13}C_{wax}$ records in the IPWP. As plants are able to fractionate carbon isotopes more effectively at higher CO_2 concentrations, rising CO_2 could explain the direction of change during the deglaciation. In northwest Africa, for instance, the composition of savannah ecosystems is influenced by atmospheric CO_2 concentrations (Kuechler et al., 2013; O'Mara et al., 2022). However, changepoint analysis of our IPWP data indicates $\delta^{13}C_{wax}$ begins to increase at ~19.9 ka (Table 1), prior to the deglacial CO_2 increase (Marcott et al., 2014) at 17.5 ka. The earliest that any runoff or salinity record indicates increasing precipitation is 15.2 ka in SO189-2_039KL, and the largest changes appear to occur at about 12.3 ka, well after the shift in $\delta^{13}C_{wax}$. Although increasing precipitation likely contributes to the expansion of rainforests, the initial transition in $\delta^{13}C_{wax}$ cannot be explained by annual precipitation amount alone. Although the increasing CO_2 concentrations and increasing annual precipitation likely contributed to changes in $\delta^{13}C_{wax}$ through increasing carbon use efficiency and decreasing water stress, the initial shift in $\delta^{13}C_{wax}$ may be primarily related to other factors.

Dubois et al. (2014) showed, in the present day, $\delta^{13}C_{wax}$ is more strongly correlated to the severity of the dry season than to mean annual rainfall. Year-round high precipitation rates are required to maintain closed-canopy rainforest (Dubois et al., 2014), and a drier and/or longer dry season can reduce the extent of closed canopy forests and favor C_4 grass expansion (Dubois et al., 2014; Jiang et al., 2019). Although precipitation seasonality is very difficult to reconstruct, some regional records have inferred increased seasonality at the LGM compared to the Holocene in the Maritime Continent based on $\delta^{13}C_{wax}$, with longer, drier dry seasons and shorter, wetter wet seasons on Sumba and Palawan (Dubois et al., 2014; Ruan et al., 2019).

The iTRACE simulation indicates increasing dry season precipitation during the deglaciation (Figure 11). Although dry season rainfall in the simulation begins to increase at 17.2 ka, rather than 19.9 ka as indicated in the leaf wax records, the shift precedes the shelf-flooding events at 14 and 12 ka that lead to increased annual precipitation (Figure 11; Du et al., 2021). This suggests that controls on precipitation seasonality and mean annual amount may diverge, so if dry season precipitation increased during the deglaciation the change could favor C_3 plant expansion before substantial changes occurred in mean annual precipitation. An increase in JJA precipitation relative to DJF precipitation in the entire Sunda region (3° S–1° N, 100–104° E) was also observed in the TRACE simulation (Hällberg et al., 2022). The JJA/DJF ratio gradually begins to increase at the beginning of the simulation, at 20 ka, and rapidly increases at 14.7 ka at the beginning of the Bølling-Allerød (Hällberg et al., 2022).

Although we have no direct proxy evidence to support the simulated changes in precipitation seasonality, it is difficult to explain the early transitions in $\delta^{13}C_{wax}$ relative to changes in rainfall amount, temperature, and atmospheric CO_2 concentrations. We infer that the transition in $\delta^{13}C_{wax}$ may have been initiated by an increase in dry season precipitation. Continued increases in dry season precipitation, as well as mean annual precipitation and atmospheric CO_2, likely contributed to the subsequent expansion of closed-canopy rainforests and C3 plants later during the deglaciation.

6. Conclusions

As sea level rose during the last deglaciation, runoff and salinity proxies indicate increasing precipitation over the Maritime Continent as a result the flooding of large areas of the Sunda and Sahul shelves at ~12.3 ka. The inundation of the shelves led to a large-scale depletion in the isotopic composition of δ^2H_{wax} and $\delta^{18}O_{speleo}$ at ~12.3 ka in response to increasing precipitation amount and convergence. $\delta^{13}C_{wax}$ begins to decrease at ~19.9 ka, well before CO_2 and annual precipitation begin to increase, pointing to a change in the seasonality of the precipitation as the initiator of changing $\delta^{13}C_{wax}$ through a shift to more C_3 plants. The increase in CO_2 and annual precipitation continue to shift $\delta^{13}C_{wax}$ to more negative values throughout the deglaciation.

Declaration of competing interest

The authors declare that they have no known competing financial interests or personal relationships that could have appeared to influence the work reported in this paper.

Acknowledgements

We would like to thank Alexander Wilk for his careful and diligent lab assistance with processing some of the Lake Matano samples, and Ewerton Santos for his work maintaining the GC-FID and GC-IRMS. This material is based on work supported by National Science Foundation Grant EAR-2102856. The authors thank Gerald Tamuntuan, Satrio Wicaksono, Nigel Wattrus, and PT Vale Indonesia for field assistance. The authors acknowledge assistance and permission for this work from the Indonesian Ministry of Research and Technology (RISTEK).

Data availability

The Towuti and Matano leaf wax records are available at:

https://www.ncei.noaa.gov/access/paleo-search/study/39564

Table 1 – All IPWP records included in compilation. Deglacial changepoints as detected by detected using the "EnvCpt" package in R (Killick et al., 2021).

Paper	Proxy	Location	Core/Cave	Deglacial changepoint (ka)	Age uncertainty at changepoint (ka)
Mohtadi et al. (2011)	Ln(Ti/Ca)	South of East Java	GeoB10053-7	13.0	0.4
Hollstein et al. (2018)	Ln(Ti/Ca)	North of New Guinea	GeoB17419-1	9.1	0.9
Fraser et al. (2014)	Log(Fe/Ca)	Offshore Mindanao	MD06-3075	12.6	0.9
Costa et al. (2015)	Ti	Lake Towuti	TOW9B	14.7	0.9
Mohtadi et al. (2014)	$\delta^{18}O_{calcite}$	Offshore Sumatra	SO189-2_119KL	14.7	0.7
Mohtadi et al. (2014)	$\delta^{18}O_{calcite}$	Offshore Sumatra	SO189-2_039KL	15.2 and 11.5	0.2 and 0.2
Sarnthein et al. (2011) and Xu et al. (2008)	$\delta^{18}O_{calcite}$	Timor Sea	MD01-2378	Not detected	NA
Schröder et al. (2018)	$\delta^{18}O_{calcite}$	Makassar Strait	GIK18526-3	10.9	0.4
Schröder et al. (2018)	$\delta^{18}O_{calcite}$	Makassar Strait	GIK18519-2	Not detected	NA
Schröder et al. (2018)	$\delta^{18}O_{calcite}$	Makassar Strait	GIK18522-3	11.8	0.2
Fan et al. (2018)	$\delta^{18}O_{calcite}$	Makassar Strait	MD98-2178	11.4	0.3
Stott et al. (2007)	$\delta^{18}O_{calcite}$	Offshore West Papua	MD98-2176	Not detected	NA
Stott et al. (2002)	$\delta^{18}O_{calcite}$	Offshore Mindanao	MD98-2181	12.9	0.2
Gibbons et al. (2014)	$\delta^{18}O_{calcite}$	Savu Sea	GeoB10069-3	12.4	0.5
Levi et al. (2007)	$\delta^{18}O_{calcite}$	Offshore Flores	MD98-2165	12.7	0.4
Visser et al. (2003)	$\delta^{18}O_{calcite}$	Makassar Strait	MD98-2162	10.8	0.6
Ruan et al. (2019)	C_{31} *n*-alkane δ^2H	Offshore Java	GeoB10053-7	13.4	0.3
This study	C_{31} *n*-alkane δ^2H	Lake Towuti	TOW9B	9.5	0.6
Konecky et al. (2016)	C28 *n*-acid δ^2H	Lake Towuti	TOW9B	11.3	0.4

This study	C_{31} *n*-alkane δ^2H	Lake Matano	IDLE-MAT10-2B	12.0	2.2
Wicaksono et al. (2017)	C28 *n*-acid δ^2H	Mandar Bay	SO18515	10.8	0.4
Niedermeyer et al. (2014)	C30 *n*-acid δ^2H	Offshore Sumatra	SO189-144KL	Not detected	NA
Krause et al. (2019)	Speleothem $\delta^{18}O$	Sulawesi	Gempa Bumi Cave	14.4 and 12.4	0.1and 0.2
Partin et al. (2007)	Speleothem $\delta^{18}O$	Borneo	Snail Shell and Bukit Assam caves	14.6 and 12.3	0.1 and 0.1
Ayliffe et al. (2013)	Speleothem $\delta^{18}O$	Flores	Liang Luar Cave	11.5	0.1
Yuan et al. (2023)	Speleothem $\delta^{18}O$	Sulawesi	Southwest Sulawesi caves	14.7 and 10.5	0.2 and 0.2
Dubois et al. (2014)	C30 *n*-acid $\delta^{13}C$	Offshore Borneo	91GGC	Not detected	NA
Niedermeyer et al. (2014)	C30 *n*-acid $\delta^{13}C$	Offshore Sumatra	SO189-144KL	Not detected	NA
Dubois et al. (2014)	C30 *n*-acid $\delta^{13}C$	Offshore Java	GeoB10069-3	19.8	0.7
Wicaksono et al. (2017)	C28 *n*-acid $\delta^{13}C$	Mandar Bay	SO18515	19.8	0.5
Ruan et al. (2019)	C_{31} *n*-alkane $\delta^{13}C$	Offshore Java	GeoB10053-7	19.5	0.5
This study	C_{31} *n*-alkane $\delta^{13}C$	Lake Towuti	TOW9B	22.3	0.8
Konecky et al. (2016)	C28 *n*-acid $\delta^{13}C$	Lake Towuti	TOW9B	17.2	0.6
This study	C_{31} *n*-alkane $\delta^{13}C$	Lake Matano	IDLE-MAT10-2B	20.8	1.4
Wicaksono et al. (2015)	C28 *n*-acid $\delta^{13}C$	Lake Matano	IDLE-MAT10-2B	Not detected	NA

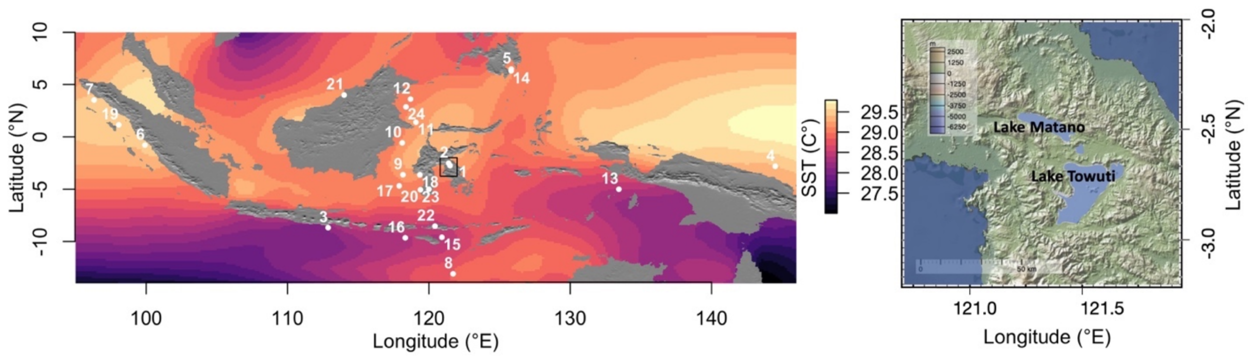

Figure 1 – Lake Towuti and Lake Matano are located on the island of Sulawesi near the middle of the Indo-Pacific Warm Pool. The map on the left shows nearby hydroclimate records that span the last deglaciation, numbered as follows: 1. Lake Towuti (this study; Konecky et al., 2016; Russell et al., 2014), 2. Lake Matano (this study; Wicaksono et al., 2015), 3. GeoB10053-7 (Mohtadi et al., 2011; Ruan et al., 2019), 4. GeoB17419-1 (Hollstein et al., 2018), 5. MD06-3075 (Fraser et al., 2014), 6. SO189-2_039KL (Mohtadi et al., 2014), 7. SO189-2_119KL (Mohtadi et al., 2014), 8. MD01-2378 (Sarnthein et al., 2011; Xu et al., 2008), 9. GIK18526-3 (Schröder et al., 2018)**, 10. GIK18519-2** (Schröder et al., 2018)**, 11. GIK18522-3** (Schröder et al., 2018)**, 12. MD98-2178 (Fan et al., 2018), 13. MD98-2176 (Stott et al., 2007), 14. MD98-2181 (Stott et al., 2002), 15. GeoB10069-3 (Dubois et al., 2014; Gibbons et al., 2014), 16. MD98-2165 (Levi et al., 2007), 17. MD98-2162 (Visser et al., 2003), 18. SO18515 (Wicaksono et al., 2017), 19. SO189-144KL (Niedermeyer et al., 2014), 20. Gempa Bumi Cave (Krause et al., 2019), 21. Snail Shell and Bukit Assam caves (Partin et al., 2007), 22. Liang Luar Cave (Ayliffe et al., 2013), 23. SW Sulawesi caves (Yuan et al., 2023), and 24. 91GGC (Dubois et al., 2014). Mean annual sea surface temperatures (SST) from 1991-2021 from reanalysis data (Kalnay et al., 1996). SST and the digital elevation models are plotted using the "raster" package in R (Hijmans et al., 2022).**

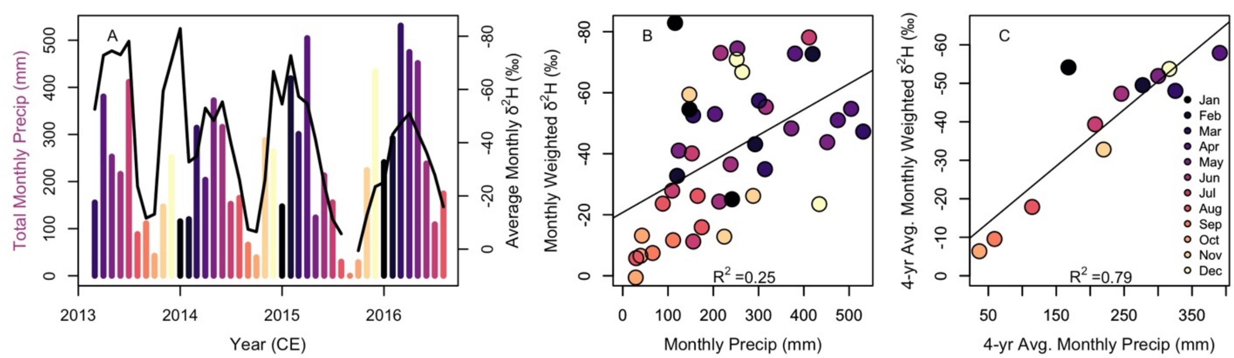

Figure 2 – A) Monthly rain gauge and precipitation isotope data from Lake Towuti from 2013-2016. B) Linear regression of the monthly precipitation amount and δ^2H. C) Linear regression of the average monthly precipitation amount and weighted δ^2H from 2013-2015 measurements from the rain gauge.

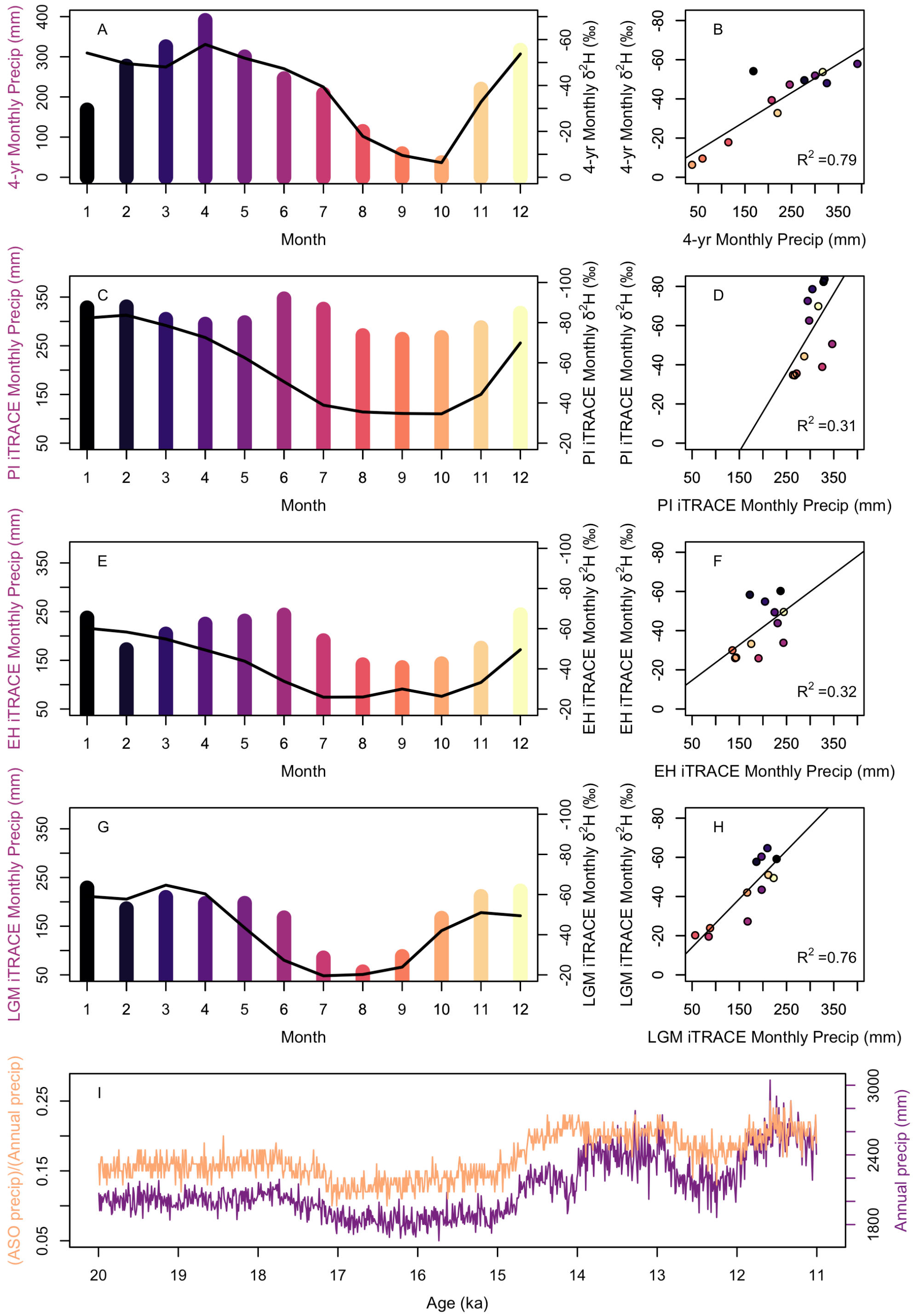

Figure 3 – A) Monthly average precipitation and isotopic composition from the 2013-2015 study period and B) the associated linear regression. C) Monthly iTRACE-simulated difference between precipitation amount and precipitation isotopic composition at the Pre-Industrial (PI, 1850 CE) and D) the linear correlation, E) Last Glacial Maximum (LGM, 20-19.9 ka) and F) the linear correlation, and G) the Early Holocene (EH, 11.1-11.0 ka) and H) the linear correlation. I) The transient evolution of the ASO fraction of annual precipitation and annual precipitation.

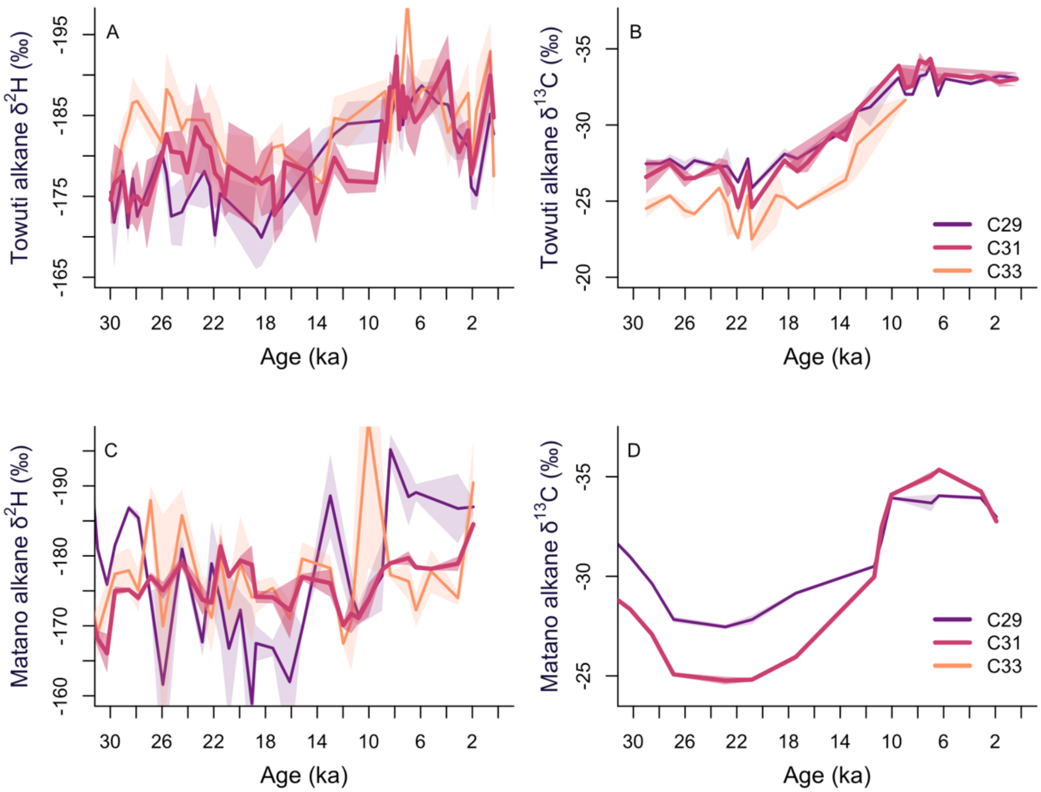

Figure 4 – A) Uncorrected δ^2H_{wax} of C_{29}, C_{31}, and C_{33} alkanes measured from Lake Towuti. B) $\delta^{13}C_{wax}$ of C_{29}, C_{31}, and C_{33} alkanes measured from Lake Towuti. C) Uncorrected δ^2H_{wax} of C_{29}, C_{31}, and C_{33} alkanes measured from Lake Matano. D) $\delta^{13}C_{wax}$ of C_{29} and C_{31} alkanes measured from Lake Matano.

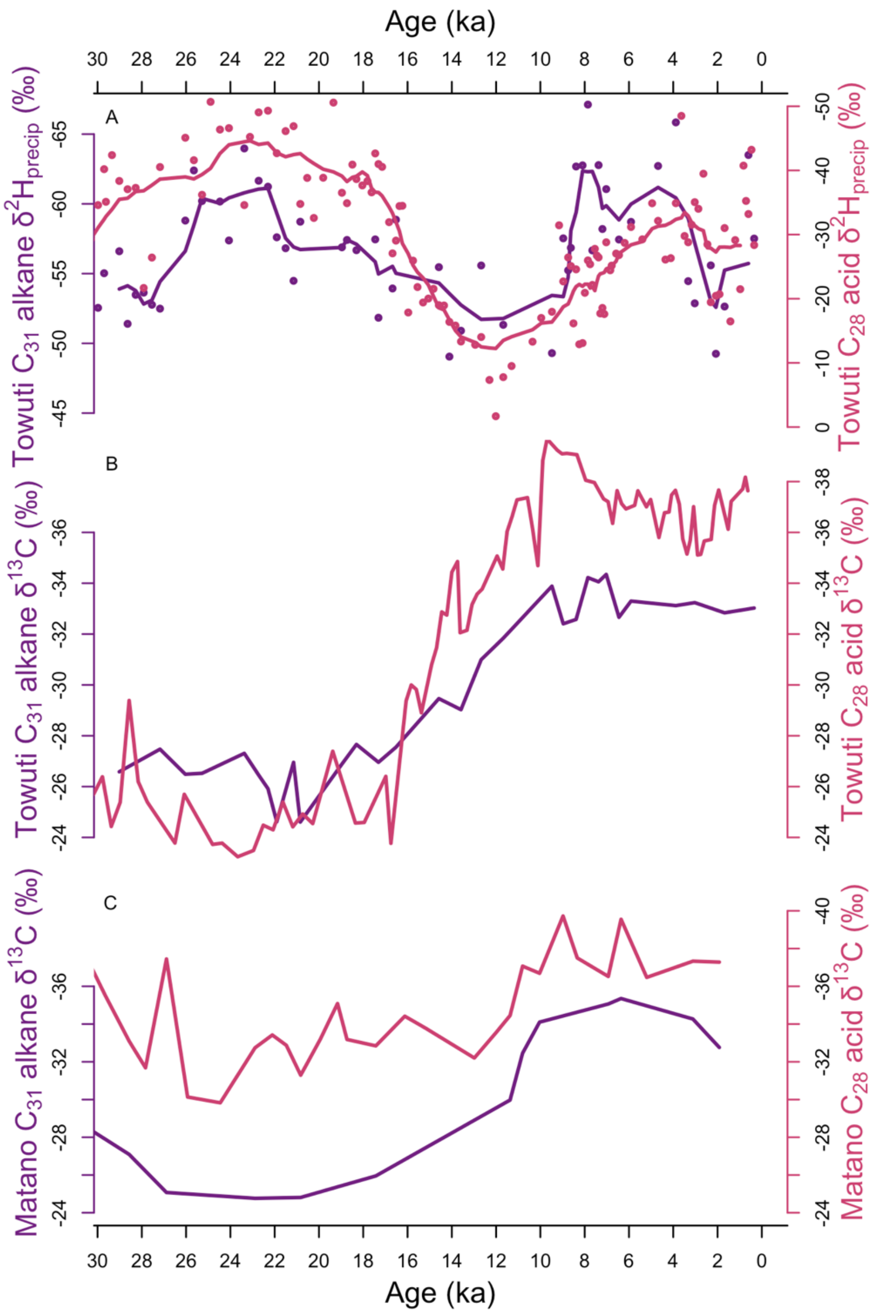

Figure 5 – A) Lake Towuti δ^2H_{precip} of C_{31} *n*-alkanes (purple) and δ^2H_{precip} of C_{28} *n*-acids (pink) corrected for changes in ice volume and vegetation. The solid line is a 2,000-yr moving average. B) Lake Towuti $\delta^{13}C$ of C_{31} *n*-alkanes (purple) and C_{28} *n*-alkanoic acids (pink). C) Lake Matano $\delta^{13}C$ of C_{31} *n*-alkanes (purple) and C_{28} *n*-alkanoic acids (pink).

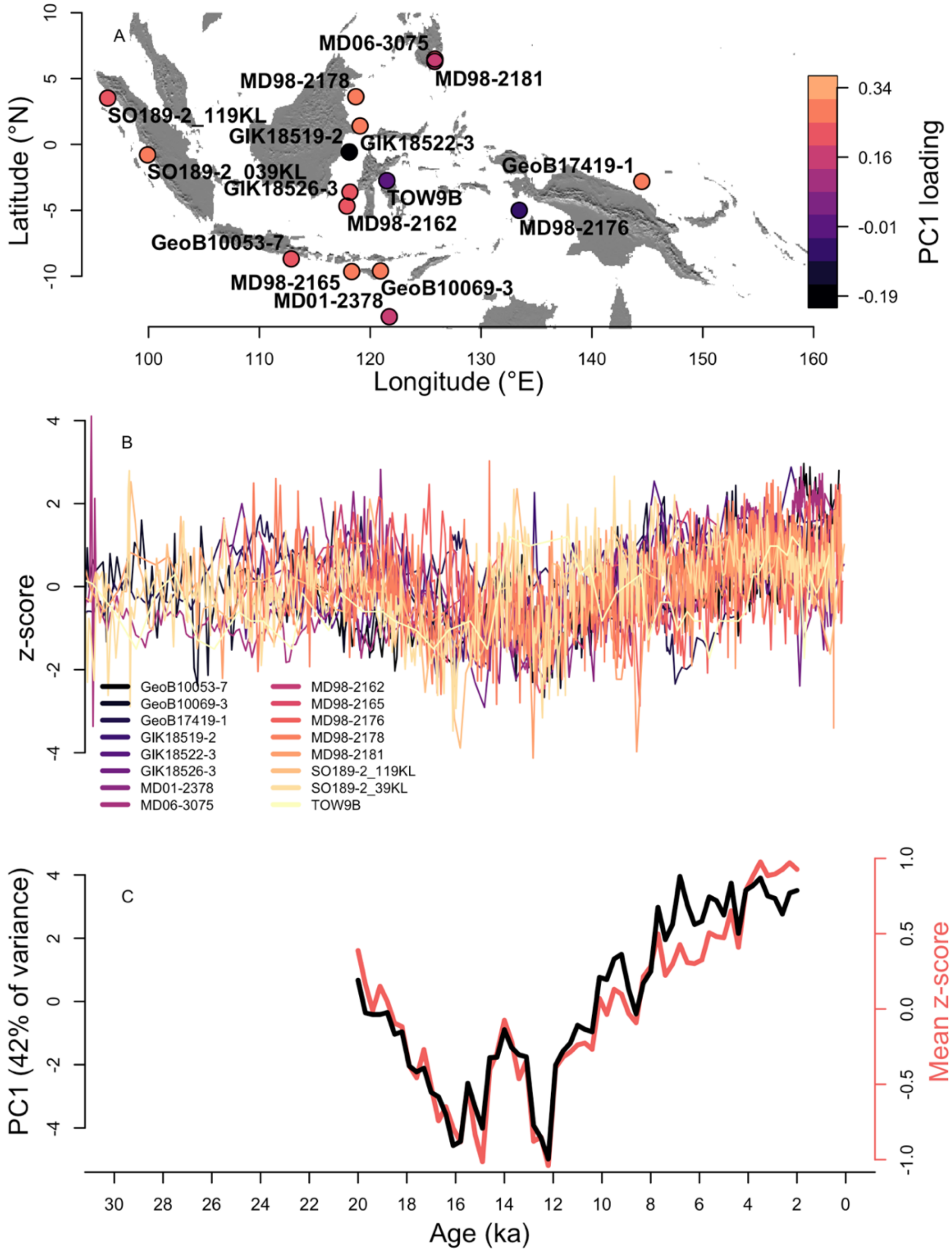

Figure 6 – (A) Map of the location of all the sites included in the synthesis of IPWP $\delta^{18}O_{sw}$ and runoff records with at least three age controls between 20 and 12 ka (Costa et al., 2015; Fan et al., 2018; Fraser et al., 2014; Gibbons et al., 2014; Hollstein et al., 2018; Levi et al., 2007; Mohtadi et al., 2014, 2011; Rosenthal et al., 2003; Sarnthein et al., 2011; Schröder et al., 2018; Stott et al., 2007, 2002; Visser et al., 2003; Xu et al., 2008), colored by their loading on PC1. (B) Z-scores of all the $\delta^{18}O_{sw}$ and runoff records. (C) The mean z-score (orange) and PC1 (black) of the records.

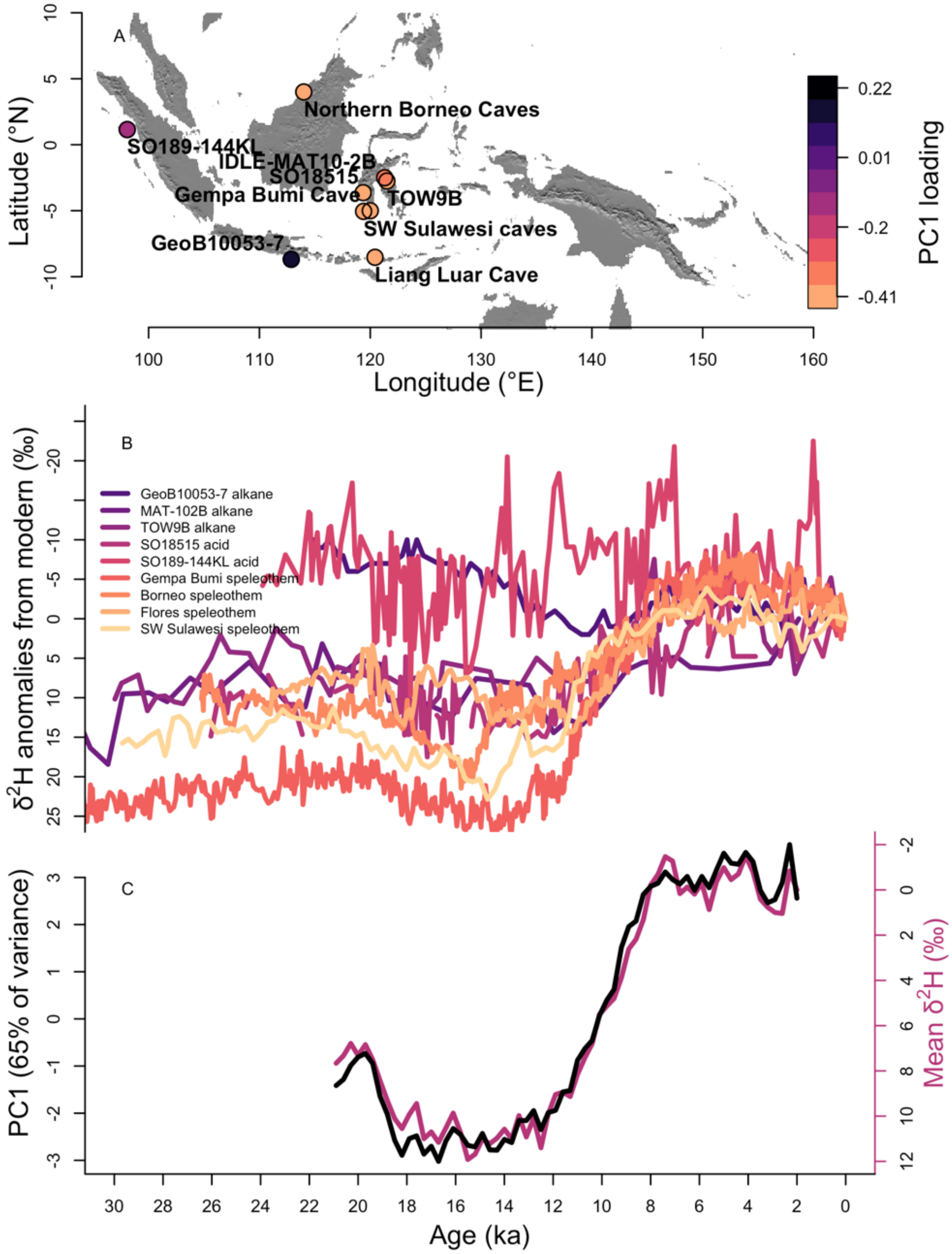

Figure 7 – (A) Map of the location of all the sites included in the synthesis of IPWP δ^2H_{wax} and $\delta^{18}O_{speleo}$ (converted to δ^2H-space using the global meteoric water line) records with at least three age controls between 20 and 12 ka (Ayliffe et al., 2013; Griffiths et al., 2009; Konecky et al., 2016; Krause et al., 2019; Niedermeyer et al., 2014; Partin et al., 2007; Ruan et al., 2019; Wicaksono et al., 2017; Yuan et al., 2023), colored by their loading on PC1. The Towuti acid record is excluded to avoid overly-weighting Lake Towuti in the mean and PCA. (B) The δ^2H anomalies from modern. (C) The mean δ^2H anomaly from modern (pink) and PC1 (black) of the records.

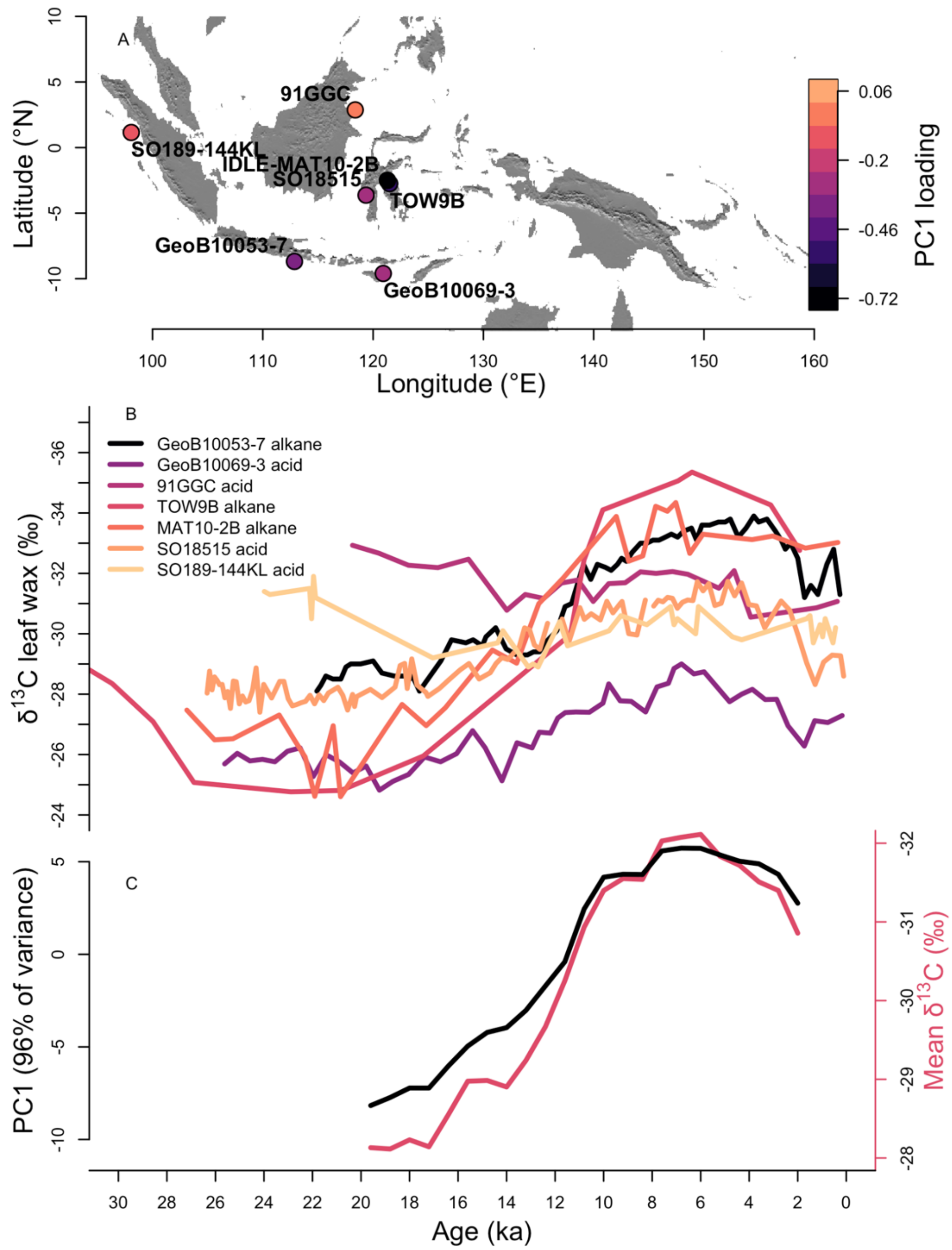

Figure 8 – (A) Map of the location of all the sites included in the synthesis of IPWP $\delta^{13}C_{wax}$ records with at least three age controls between 20 and 12 ka (Dubois et al., 2014; Niedermeyer et al., 2014; Ruan et al., 2019; Wicaksono et al., 2017), colored by their loading on PC1. The Towuti and Matano acid records are excluded to avoid overly-weighting Lake Towuti and Lake Matano in the mean and PCA. (B) The measured $\delta^{13}C_{wax}$ of all the records. (C) The mean $\delta^{13}C_{wax}$ (pink) and PC1 (black) of the records.

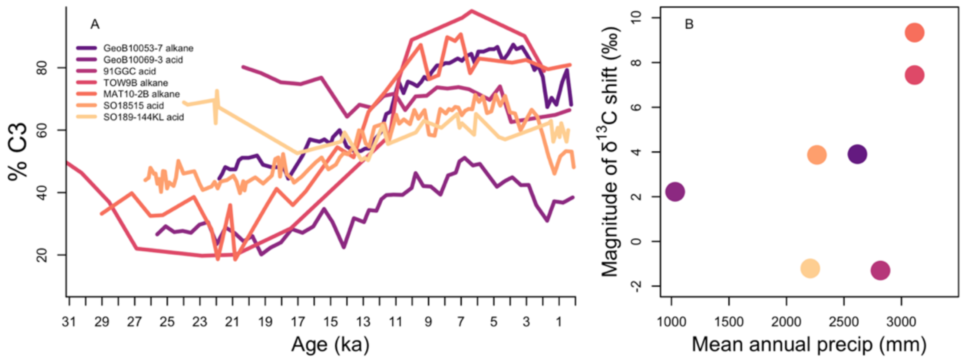

Figure 9 – A) Percent C_3 estimated from an end-member mixing model based on all leaf wax $\delta^{13}C_{wax}$ records from the IPWP (excluding the Towuti and Matano acid records). B) Mean annual precipitation from 1992-2022 from GPCP data with 1° resolution (Adler et al., 2018) and the magnitude of deglacial shift in $\delta^{13}C_{wax}$ calculated by subtracting the mean between 10 and 8 ka from the mean between 22 and 20 ka.

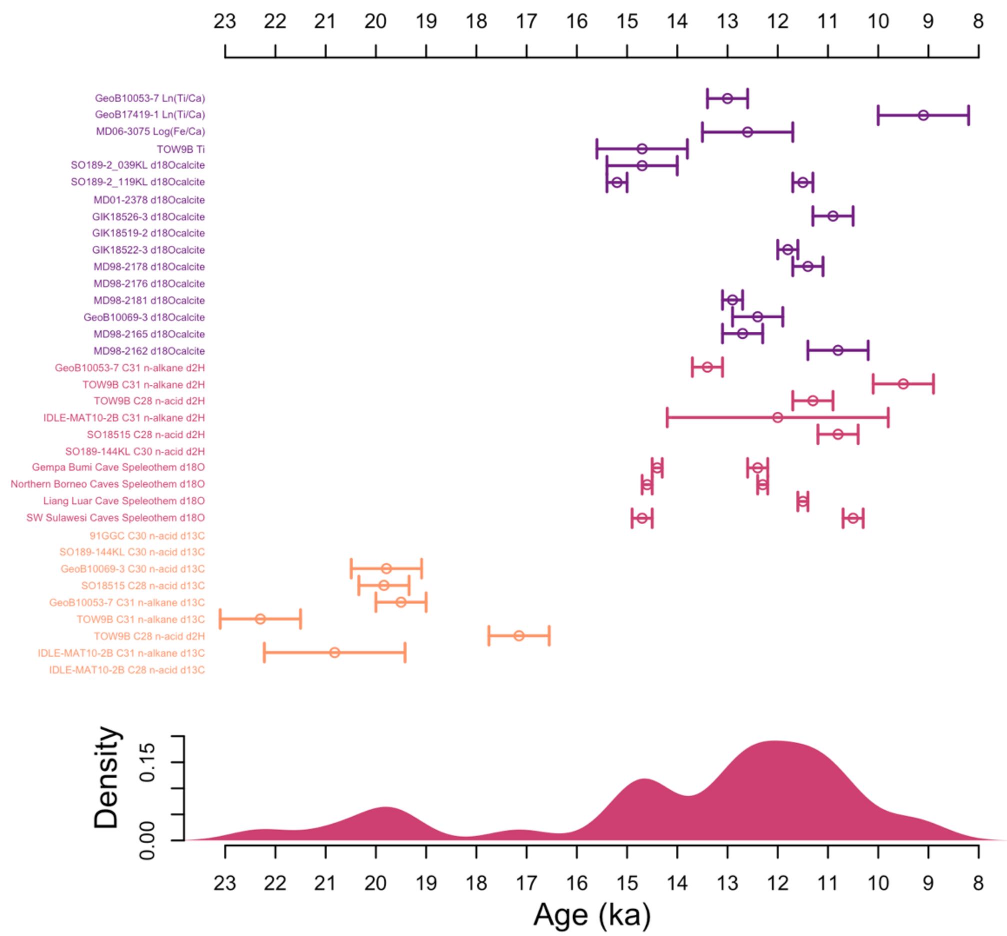

Figure 10 – Deglacial changepoints detected using the "EnvCpt" package in R (Killick et al., 2021), also shown in Table 1. The 1-sigma uncertainty was determined by recalibrating the radiocarbon dates to IntCal20 and determining the uncertainty of the age-models using Bacon (Blaauw and Christen, 2011). A probability density function of the changepoints from all of the hydroclimate and vegetation proxies is shown in the bottom panel.

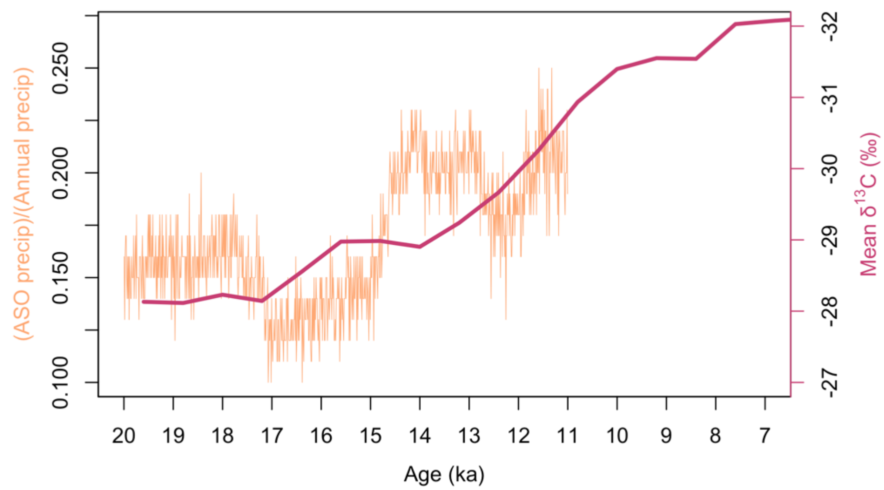

Figure 11 – The transient evolution of the ASO fraction of annual precipitation from iTRACE (orange) and the mean $\delta^{13}C_{wax}$ of all IPWP records (pink).

References

Adler, R.F., Sapiano, M.R.P., Huffman, G.J., Wang, J.-J., Gu, G., Bolvin, D., Chiu, L., Schneider, U., Becker, A., Nelkin, E., Xie, P., Ferraro, R., Shin, D.-B., 2018. The Global Precipitation Climatology Project (GPCP) Monthly Analysis (New Version 2.3) and a Review of 2017 Global Precipitation. Atmosphere 9, 138. https://doi.org/10.3390/atmos9040138

Ayliffe, L.K., Gagan, M.K., Zhao, J., Drysdale, R.N., Hellstrom, J.C., Hantoro, W.S., Griffiths, M.L., Scott-Gagan, H., Pierre, E.S., Cowley, J.A., Suwargadi, B.W., 2013. Rapid interhemispheric climate links via the Australasian monsoon during the last deglaciation. Nature Communications 4, 2908. https://doi.org/10.1038/ncomms3908

Blaauw, M., Christen, J.A., 2011. Flexible paleoclimate age-depth models using an autoregressive gamma process. Bayesian Analysis 6, 457–474. https://doi.org/10.1214/11-BA618

Brady, E., Stevenson, S., Bailey, D., Liu, Z., Noone, D., Nusbaumer, J., Otto-Bliesner, B.L., Tabor, C., Tomas, R., Wong, T., Zhang, J., Zhu, J., 2019. The Connected Isotopic Water Cycle in the Community Earth System Model Version 1. Journal of Advances in Modeling Earth Systems 11, 2547–2566. https://doi.org/10.1029/2019MS001663

Bray, E.E., Evans, E.D., 1965. Hydrocarbons in Non-Reservoir-Rock Source Beds1. AAPG Bulletin 49, 248–257. https://doi.org/10.1306/A663352E-16C0-11D7-8645000102C1865D

Bruhl, J., Wilson, K., 2007. Towards a Comprehensive Survey of C3 and C4 Photosynthetic Pathways in Cyperaceae. Aliso: A Journal of Systematic and Floristic Botany 23, 99–148. https://doi.org/10.5642/aliso.20072301.11

Chikaraishi, Y., Naraoka, H., 2007. δ13C and δD relationships among three n-alkyl compound classes (n-alkanoic acid, n-alkane and n-alkanol) of terrestrial higher plants. Organic Geochemistry 38, 198–215. https://doi.org/10.1016/j.orggeochem.2006.10.003

Contreras, S., Werne, J.P., Araneda, A., Tejos, E., Moscoso, J., 2023. Abundance and distribution of plant derived leaf waxes (long chain *n*-alkanes & fatty acids) from lake surface sediments along the west coast of southern South America: Implications for environmental and climate reconstructions. Science of The Total Environment 895, 165065. https://doi.org/10.1016/j.scitotenv.2023.165065

Costa, K.M., Russell, J.M., Vogel, H., Bijaksana, S., 2015. Hydrological connectivity and mixing of Lake Towuti, Indonesia in response to paleoclimatic changes over the last 60,000years. Palaeogeography, Palaeoclimatology, Palaeoecology 417, 467–475. https://doi.org/10.1016/j.palaeo.2014.10.009

Diefendorf, A.F., Mueller, K.E., Wing, Scott.L., Koch, P.L., Freeman, K.H., 2010. Global patterns in leaf 13C discrimination and implications for studies of past and future climate. Proceedings of the National Academy of Sciences 107, 5738–5743. https://doi.org/10.1073/pnas.0910513107

DiNezio, P.N., Tierney, J.E., 2013. The effect of sea level on glacial Indo-Pacific climate. Nature Geosci 6, 485–491. https://doi.org/10.1038/ngeo1823

DiNezio, P.N., Tierney, J.E., Otto-Bliesner, B.L., Timmermann, A., Bhattacharya, T., Rosenbloom, N., Brady, E., 2018. Glacial changes in tropical climate amplified by the Indian Ocean. Science Advances 4, eaat9658. https://doi.org/10.1126/sciadv.aat9658

DiNezio, P.N., Timmermann, A., Tierney, J.E., Jin, F.-F., Otto-Bliesner, B., Rosenbloom, N., Mapes, B., Neale, R., Ivanovic, R.F., Montenegro, A., 2016. The climate response of the

Indo-Pacific warm pool to glacial sea level. Paleoceanography 31, 866–894. https://doi.org/10.1002/2015PA002890

Du, X., Russell, J.M., Liu, Z., Otto-Bliesner, B.L., Gao, Y., Zhu, C., Oppo, D.W., Mohtadi, M., Yan, Y., Galy, V.V., He, C., 2021. Deglacial trends in Indo-Pacific warm pool hydroclimate in an isotope-enabled Earth system model and implications for isotope-based paleoclimate reconstructions. Quaternary Science Reviews 270, 107188. https://doi.org/10.1016/j.quascirev.2021.107188

Dubois, N., Oppo, D.W., Galy, V.V., Mohtadi, M., van der Kaars, S., Tierney, J.E., Rosenthal, Y., Eglinton, T.I., Lückge, A., Linsley, B.K., 2014. Indonesian vegetation response to changes in rainfall seasonality over the past 25,000 years. Nature Geoscience 7, 513–517. https://doi.org/10.1038/ngeo2182

Fan, W., Jian, Z., Chu, Z., Dang, H., Wang, Y., Bassinot, F., Han, X., Bian, Y., 2018. Variability of the Indonesian Throughflow in the Makassar Strait over the Last 30 ka. Sci Rep 8, 5678. https://doi.org/10.1038/s41598-018-24055-1

Feakins, S.J., Bentley, L.P., Salinas, N., Shenkin, A., Blonder, B., Goldsmith, G.R., Ponton, C., Arvin, L.J., Wu, M.S., Peters, T., West, A.J., Martin, R.E., Enquist, B.J., Asner, G.P., Malhi, Y., 2016. Plant leaf wax biomarkers capture gradients in hydrogen isotopes of precipitation from the Andes and Amazon. Geochimica et Cosmochimica Acta 182, 155–172. https://doi.org/10.1016/j.gca.2016.03.018

Fraser, N., Kuhnt, W., Holbourn, A., Bolliet, T., Andersen, N., Blanz, T., Beaufort, L., 2014. Precipitation variability within the West Pacific Warm Pool over the past 120 ka: Evidence from the Davao Gulf, southern Philippines. Paleoceanography 29, 1094–1110. https://doi.org/10.1002/2013PA002599

Garelick, S., Russell, J.M., Dee, S., Verschuren, D., Olago, D.O., 2021. Atmospheric controls on precipitation isotopes and hydroclimate in high-elevation regions in Eastern Africa since the Last Glacial Maximum. Earth and Planetary Science Letters 567, 116984. https://doi.org/10.1016/j.epsl.2021.116984

Gibbons, F.T., Oppo, D.W., Mohtadi, M., Rosenthal, Y., Cheng, J., Liu, Z., Linsley, B.K., 2014. Deglacial δ18O and hydrologic variability in the tropical Pacific and Indian Oceans. Earth and Planetary Science Letters 387, 240–251. https://doi.org/10.1016/j.epsl.2013.11.032

Griffiths, M.L., Drysdale, R.N., Gagan, M.K., Zhao, J. -x, Ayliffe, L.K., Hellstrom, J.C., Hantoro, W.S., Frisia, S., Feng, Y. -x, Cartwright, I., Pierre, E.S., Fischer, M.J., Suwargadi, B.W., 2009. Increasing Australian–Indonesian monsoon rainfall linked to early Holocene sea-level rise. Nature Geoscience 2, 636–639. https://doi.org/10.1038/ngeo605

Hällberg, P.L., Schenk, F., Yamoah, K.A., Kuang, X., Smittenberg, R.H., 2022. Seasonal aridity in the Indo-Pacific Warm Pool during the Late Glacial driven by El Niño-like conditions. Climate of the Past 18, 1655–1674. https://doi.org/10.5194/cp-18-1655-2022

Hamilton, R., Stevenson, J., Li, B., Bijaksana, S., 2019. A 16,000-year record of climate, vegetation and fire from Wallacean lowland tropical forests. Quaternary Science Reviews 224, 105929. https://doi.org/10.1016/j.quascirev.2019.105929

Hanebuth, T., Stattegger, K., Grootes, P.M., 2000. Rapid Flooding of the Sunda Shelf: A Late-Glacial Sea-Level Record. Science 288, 1033–1035. https://doi.org/10.1126/science.288.5468.1033

Hanebuth, T.J.J., Voris, H.K., Yokoyama, Y., Saito, Y., Okuno, J., 2011. Formation and fate of sedimentary depocentres on Southeast Asia's Sunda Shelf over the past sea-level cycle and biogeographic implications. Earth-Science Reviews 104, 92–110. https://doi.org/10.1016/j.earscirev.2010.09.006

He, C., Liu, Z., Otto-Bliesner, B.L., Brady, E.C., Zhu, C., Tomas, R., Clark, P.U., Zhu, J., Jahn, A., Gu, S., Zhang, J., Nusbaumer, J., Noone, D., Cheng, H., Wang, Y., Yan, M., Bao, Y., 2021. Hydroclimate footprint of pan-Asian monsoon water isotope during the last deglaciation. Science Advances 7, eabe2611. https://doi.org/10.1126/sciadv.abe2611

Hijmans, R.J., Etten, J. van, Sumner, M., Cheng, J., Baston, D., Bevan, A., Bivand, R., Busetto, L., Canty, M., Fasoli, B., Forrest, D., Ghosh, A., Golicher, D., Gray, J., Greenberg, J.A., Hiemstra, P., Hingee, K., Ilich, A., Geosciences, I. for M.A., Karney, C., Mattiuzzi, M., Mosher, S., Naimi, B., Nowosad, J., Pebesma, E., Lamigueiro, O.P., Racine, E.B., Rowlingson, B., Shortridge, A., Venables, B., Wueest, R., 2022. raster: Geographic Data Analysis and Modeling.

Hollstein, M., Mohtadi, M., Rosenthal, Y., Prange, M., Oppo, D.W., Martínez Méndez, G., Tachikawa, K., Moffa Sanchez, P., Steinke, S., Hebbeln, D., 2018. Variations in Western Pacific Warm Pool surface and thermocline conditions over the past 110,000 years: Forcing mechanisms and implications for the glacial Walker circulation. Quaternary Science Reviews 201, 429–445. https://doi.org/10.1016/j.quascirev.2018.10.030

Hope, G., 2001. Environmental change in the Late Pleistocene and later Holocene at Wanda site, Soroako, South Sulawesi, Indonesia. Palaeogeography, Palaeoclimatology, Palaeoecology, Quaternary Environmental Change in the Indonesian Region 171, 129–145. https://doi.org/10.1016/S0031-0182(01)00243-7

Hou, J., D'Andrea, W.J., Huang, Y., 2008. Can sedimentary leaf waxes record D/H ratios of continental precipitation? Field, model, and experimental assessments. Geochimica et Cosmochimica Acta 72, 3503–3517. https://doi.org/10.1016/j.gca.2008.04.030

Hutchings, J., Konecky, B.L., 2022. Improved Forward Models of Leaf Wax Hydrogen Isotope Ratios from a Synthesis of 3,500+ Measurements in Modern Plants 2022, PP32D-0972.

Hutchings, J., Konecky, B.L., 2020. Phylogenetic, Adaptational, and Environmental Controls on Hydrogen Isotope Apparent Fractionation in Leaf Waxes from a Synthesis of 3,000+ Plant Specimens 2020, PP006-01.

Iturbide, M., Gutiérrez, J.M., Alves, L.M., Bedia, J., Cerezo-Mota, R., Cimadevilla, E., Cofiño, A.S., Di Luca, A., Faria, S.H., Gorodetskaya, I.V., Hauser, M., Herrera, S., Hennessy, K., Hewitt, H.T., Jones, R.G., Krakovska, S., Manzanas, R., Martínez-Castro, D., Narisma, G.T., Nurhati, I.S., Pinto, I., Seneviratne, S.I., van den Hurk, B., Vera, C.S., 2020. An update of IPCC climate reference regions for subcontinental analysis of climate model data: definition and aggregated datasets. Earth System Science Data 12, 2959–2970. https://doi.org/10.5194/essd-12-2959-2020

Jiang, Y., Zhou, L., Tucker, C.J., Raghavendra, A., Hua, W., Liu, Y.Y., Joiner, J., 2019. Widespread increase of boreal summer dry season length over the Congo rainforest. Nat. Clim. Chang. 9, 617–622. https://doi.org/10.1038/s41558-019-0512-y

Kalnay, E., Kanamitsu, M., Kistler, R., Collins, W., Deaven, D., Gandin, L., Iredell, M., Saha, S., White, G., Woollen, J., Zhu, Y., Chelliah, M., Ebisuzaki, W., Higgins, W., Janowiak, J., Mo, K.C., Ropelewski, C., Wang, J., Leetmaa, A., Reynolds, R., Jenne, R., Joseph, D., 1996. The NCEP/NCAR 40-Year Reanalysis Project. Bulletin of the American

Meteorological Society 77, 437–472. https://doi.org/10.1175/1520-0477(1996)077<0437:TNYRP>2.0.CO;2

Killick, R., Beaulieu, C., Taylor, S., Hullait, H., 2021. EnvCpt: Detection of Structural Changes in Climate and Environment Time Series.

Kimbrough, A.K., Gagan, M.K., Dunbar, G.B., Hantoro, W.S., Shen, C.-C., Hu, H.-M., Cheng, H., Edwards, R.L., Rifai, H., Suwargadi, B.W., 2023. Multi-proxy validation of glacial-interglacial rainfall variations in southwest Sulawesi. Commun Earth Environ 4, 1–13. https://doi.org/10.1038/s43247-023-00873-8

Konecky, B., Russell, J., Bijaksana, S., 2016. Glacial aridity in central Indonesia coeval with intensified monsoon circulation. Earth and Planetary Science Letters 437, 15–24. https://doi.org/10.1016/j.epsl.2015.12.037

Konecky, B.L., Noone, D.C., Cobb, K.M., 2019. The Influence of Competing Hydroclimate Processes on Stable Isotope Ratios in Tropical Rainfall. Geophysical Research Letters 46, 1622–1633. https://doi.org/10.1029/2018GL080188

Krause, C.E., Gagan, M.K., Dunbar, G.B., Hantoro, W.S., Hellstrom, J.C., Cheng, H., Edwards, R.L., Suwargadi, B.W., Abram, N.J., Rifai, H., 2019. Spatio-temporal evolution of Australasian monsoon hydroclimate over the last 40,000 years. Earth and Planetary Science Letters 513, 103–112. https://doi.org/10.1016/j.epsl.2019.01.045

Kuechler, R.R., Schefuß, E., Beckmann, B., Dupont, L., Wefer, G., 2013. NW African hydrology and vegetation during the Last Glacial cycle reflected in plant-wax-specific hydrogen and carbon isotopes. Quaternary Science Reviews 82, 56–67. https://doi.org/10.1016/j.quascirev.2013.10.013

Lambeck, K., Rouby, H., Purcell, A., Sun, Y., Sambridge, M., 2014. Sea level and global ice volumes from the Last Glacial Maximum to the Holocene. Proceedings of the National Academy of Sciences 111, 15296–15303. https://doi.org/10.1073/pnas.1411762111

Levi, C., Labeyrie, L., Bassinot, F., Guichard, F., Cortijo, E., Waelbroeck, C., Caillon, N., Duprat, J., de Garidel-Thoron, T., Elderfield, H., 2007. Low-latitude hydrological cycle and rapid climate changes during the last deglaciation. Geochemistry, Geophysics, Geosystems 8. https://doi.org/10.1029/2006GC001514

Lewis, S.E., Sloss, C.R., Murray-Wallace, C.V., Woodroffe, C.D., Smithers, S.G., 2013. Post-glacial sea-level changes around the Australian margin: a review. Quaternary Science Reviews, Linking Southern Hemisphere records and past circulation patterns: the AUS-INTIMATE project 74, 115–138. https://doi.org/10.1016/j.quascirev.2012.09.006

Lisiecki, L.E., Raymo, M.E., 2005. A Pliocene-Pleistocene stack of 57 globally distributed benthic δ^{18}O records: PLIOCENE-PLEISTOCENE BENTHIC STACK. Paleoceanography 20, n/a-n/a. https://doi.org/10.1029/2004PA001071

Lupien, R.L., Russell, J.M., Subramanian, A., Kinyanjui, R., Beverly, E.J., Uno, K.T., de Menocal, P., Dommain, R., Potts, R., 2021. Eastern African environmental variation and its role in the evolution and cultural change of Homo over the last 1 million years. Journal of Human Evolution 157, 103028. https://doi.org/10.1016/j.jhevol.2021.103028

Marcott, S.A., Bauska, T.K., Buizert, C., Steig, E.J., Rosen, J.L., Cuffey, K.M., Fudge, T.J., Severinghaus, J.P., Ahn, J., Kalk, M.L., McConnell, J.R., Sowers, T., Taylor, K.C., White, J.W.C., Brook, E.J., 2014. Centennial-scale changes in the global carbon cycle during the last deglaciation. Nature 514, 616–619. https://doi.org/10.1038/nature13799

Mohtadi, M., Oppo, D.W., Steinke, S., Stuut, J.-B.W., De Pol-Holz, R., Hebbeln, D., Lückge, A., 2011. Glacial to Holocene swings of the Australian–Indonesian monsoon. Nature Geosci 4, 540–544. https://doi.org/10.1038/ngeo1209

Mohtadi, M., Prange, M., Oppo, D.W., De Pol-Holz, R., Merkel, U., Zhang, X., Steinke, S., Lückge, A., 2014. North Atlantic forcing of tropical Indian Ocean climate. Nature 509, 76–80. https://doi.org/10.1038/nature13196

Mohtadi, M., Steinke, S., Lückge, A., Groeneveld, J., Hathorne, E.C., 2010. Glacial to Holocene surface hydrography of the tropical eastern Indian Ocean. Earth and Planetary Science Letters 292, 89–97. https://doi.org/10.1016/j.epsl.2010.01.024

Niedermeyer, E.M., Sessions, A.L., Feakins, S.J., Mohtadi, M., 2014. Hydroclimate of the western Indo-Pacific Warm Pool during the past 24,000 years. PNAS 111, 9402–9406. https://doi.org/10.1073/pnas.1323585111

O'Mara, N.A., Skonieczny, C., McGee, D., Winckler, G., Bory, A.J.-M., Bradtmiller, L.I., Malaizé, B., Polissar, P.J., 2022. Pleistocene drivers of Northwest African hydroclimate and vegetation. Nat Commun 13, 3552. https://doi.org/10.1038/s41467-022-31120-x

Pagani, M., Freeman, K.H., Arthur, M.A., 1999. Late Miocene Atmospheric CO2 Concentrations and the Expansion of C4 Grasses. Science 285, 876–879. https://doi.org/10.1126/science.285.5429.876

Parish, M.C., Du, X., Bijaksana, S., Russell, J.M., 2023. A brGDGT-Based Reconstruction of Terrestrial Temperature From the Maritime Continent Spanning the Last Glacial Maximum. Paleoceanography and Paleoclimatology 38, e2022PA004501. https://doi.org/10.1029/2022PA004501

Partin, J.W., Cobb, K.M., Adkins, J.F., Clark, B., Fernandez, D.P., 2007. Millennial-scale trends in west Pacific warm pool hydrology since the Last Glacial Maximum. Nature 449, 452–455. https://doi.org/10.1038/nature06164

Pico, T., McGee, D., Russell, J., Mitrovica, J.X., 2020. Recent Constraints on MIS 3 Sea Level Support Role of Continental Shelf Exposure as a Control on Indo-Pacific Hydroclimate. Paleoceanography and Paleoclimatology 35. https://doi.org/10.1029/2020PA003998

Reeves, J.M., Bostock, H.C., Ayliffe, L.K., Barrows, T.T., De Deckker, P., Devriendt, L.S., Dunbar, G.B., Drysdale, R.N., Fitzsimmons, K.E., Gagan, M.K., Griffiths, M.L., Haberle, S.G., Jansen, J.D., Krause, C., Lewis, S., McGregor, H.V., Mooney, S.D., Moss, P., Nanson, G.C., Purcell, A., van der Kaars, S., 2013. Palaeoenvironmental change in tropical Australasia over the last 30,000 years – a synthesis by the OZ-INTIMATE group. Quaternary Science Reviews, Linking Southern Hemisphere records and past circulation patterns: the AUS-INTIMATE project 74, 97–114. https://doi.org/10.1016/j.quascirev.2012.11.027

Rosenthal, Y., Oppo, D.W., Linsley, B.K., 2003. The amplitude and phasing of climate change during the last deglaciation in the Sulu Sea, western equatorial Pacific: the amplitude and phasing of climate change. Geophys. Res. Lett. 30. https://doi.org/10.1029/2002GL016612

Ruan, Y., Mohtadi, M., van der Kaars, S., Dupont, L.M., Hebbeln, D., Schefuß, E., 2019. Differential hydro-climatic evolution of East Javanese ecosystems over the past 22,000 years. Quaternary Science Reviews 218, 49–60. https://doi.org/10.1016/j.quascirev.2019.06.015

Russell, J.M., Vogel, H., Bijaksana, S., Melles, M., Deino, A., Hafidz, A., Haffner, D., Hasberg, A.K.M., Morlock, M., von Rintelen, T., Sheppard, R., Stelbrink, B., Stevenson, J., 2020. The late quaternary tectonic, biogeochemical, and environmental evolution of ferruginous Lake Towuti, Indonesia. Palaeogeography, Palaeoclimatology, Palaeoecology 556, 109905. https://doi.org/10.1016/j.palaeo.2020.109905

Russell, J.M., Vogel, H., Konecky, B.L., Bijaksana, S., Huang, Y., Melles, M., Wattrus, N., Costa, K., King, J.W., 2014. Glacial forcing of central Indonesian hydroclimate since 60,000 y B.P. PNAS 111, 5100–5105. https://doi.org/10.1073/pnas.1402373111

Sachse, D., Billault, I., Bowen, G.J., Chikaraishi, Y., Dawson, T.E., Feakins, S.J., Freeman, K.H., Magill, C.R., McInerney, F.A., Van Der Meer, M.T.J., Polissar, P., Robins, R.J., Sachs, J.P., Schmidt, H.L., Sessions, A.L., White, J.W.C., West, J.B., Kahmen, A., 2012. Molecular paleohydrology: Interpreting the hydrogen-isotopic composition of lipid biomarkers from photosynthesizing organisms. Annual Review of Earth and Planetary Sciences 40, 221–249. https://doi.org/10.1146/annurev-earth-042711-105535

Sarnthein, M., Grootes, P.M., Holbourn, A., Kuhnt, W., Kühn, H., 2011. Tropical warming in the Timor Sea led deglacial Antarctic warming and atmospheric CO2 rise by more than 500yr. Earth and Planetary Science Letters 302, 337–348. https://doi.org/10.1016/j.epsl.2010.12.021

Schrag, D.P., Hampt, G., Murray, D.W., 1996. Pore Fluid Constraints on the Temperature and Oxygen Isotopic Composition of the Glacial Ocean. Science 272, 1930–1932. https://doi.org/10.1126/science.272.5270.1930

Schröder, J.F., Kuhnt, W., Holbourn, A., Beil, S., Zhang, P., Hendrizan, M., Xu, J., 2018. Deglacial Warming and Hydroclimate Variability in the Central Indonesian Archipelago.

Paleoceanography and Paleoclimatology 33, 974–993. https://doi.org/10.1029/2018PA003323

Stott, L., Poulsen, C., Lund, S., Thunell, R., 2002. Super ENSO and global climate oscillations at millennial time scales. Science 297, 222–226. https://doi.org/10.1126/science.1071627

Stott, L., Timmermann, A., Thunell, R., 2007. Southern Hemisphere and Deep-Sea Warming Led Deglacial Atmospheric CO2 Rise and Tropical Warming. Science 318, 435–438. https://doi.org/10.1126/science.1143791

Tierney, J.E., Oppo, D.W., LeGrande, A.N., Huang, Y., Rosenthal, Y., Linsley, B.K., 2012. The influence of Indian Ocean atmospheric circulation on Warm Pool hydroclimate during the Holocene epoch. Journal of Geophysical Research: Atmospheres 117. https://doi.org/10.1029/2012JD018060

van Bree, L.G.J., Peterse, F., van der Meer, M.T.J., Middelburg, J.J., Negash, A.M.D., De Crop, W., Cocquyt, C., Wieringa, J.J., Verschuren, D., Sinninghe Damsté, J.S., 2018. Seasonal variability in the abundance and stable carbon-isotopic composition of lipid biomarkers in suspended particulate matter from a stratified equatorial lake (Lake Chala, Kenya/Tanzania): Implications for the sedimentary record. Quaternary Science Reviews 192, 208–224. https://doi.org/10.1016/j.quascirev.2018.05.023

van der Kaars, S., Bassinot, F., De Deckker, P., Guichard, F., 2010. Changes in monsoon and ocean circulation and the vegetation cover of southwest Sumatra through the last 83,000years: The record from marine core BAR94-42. Palaeogeography, Palaeoclimatology, Palaeoecology 296, 52–78. https://doi.org/10.1016/j.palaeo.2010.06.015

van der Kaars, S., Penny, D., Tibby, J., Fluin, J., Dam, R.A.C., Suparan, P., 2001. Late Quaternary palaeoecology, palynology and palaeolimnology of a tropical lowland swamp: Rawa Danau, West-Java, Indonesia. Palaeogeography, Palaeoclimatology, Palaeoecology, Quaternary Environmental Change in the Indonesian Region 171, 185–212. https://doi.org/10.1016/S0031-0182(01)00245-0

van der Kaars, S., Wang, X., Kershaw, P., Guichard, F., Setiabudi, D.A., 2000. A Late Quaternary palaeoecological record from the Banda Sea, Indonesia: patterns of vegetation, climate and biomass burning in Indonesia and northern Australia. Palaeogeography, Palaeoclimatology, Palaeoecology 155, 135–153. https://doi.org/10.1016/S0031-0182(99)00098-X

Visser, K., Thunell, R., Stott, L., 2003. Magnitude and timing of temperature change in the Indo-Pacific warm pool during deglaciation. Nature 421, 152–155. https://doi.org/10.1038/nature01297

Vogel, H., Russell, J.M., Cahyarini, S.Y., Bijaksana, S., Wattrus, N., Rethemeyer, J., Melles, M., 2015. Depositional modes and lake-level variability at Lake Towuti, Indonesia, during the past ~29 kyr BP. J Paleolimnol 54, 359–377. https://doi.org/10.1007/s10933-015-9857-z

Wicaksono, S.A., Russell, J.M., Bijaksana, S., 2015. Compound-specific carbon isotope records of vegetation and hydrologic change in central Sulawesi, Indonesia, since 53,000 yr BP. Palaeogeography, Palaeoclimatology, Palaeoecology 430, 47–56. https://doi.org/10.1016/j.palaeo.2015.04.016

Wicaksono, S.A., Russell, J.M., Holbourn, A., Kuhnt, W., 2017. Hydrological and vegetation shifts in the Wallacean region of central Indonesia since the Last Glacial Maximum.

Quaternary Science Reviews 157, 152–163. https://doi.org/10.1016/j.quascirev.2016.12.006

Windler, G., Tierney, J.E., DiNezio, P.N., Gibson, K., Thunell, R., 2019. Shelf exposure influence on Indo-Pacific Warm Pool climate for the last 450,000 years. Earth and Planetary Science Letters 516, 66–76. https://doi.org/10.1016/j.epsl.2019.03.038

Wurster, C.M., Rifai, H., Zhou, B., Haig, J., Bird, M.I., 2019. Savanna in equatorial Borneo during the late Pleistocene. Sci Rep 9, 6392. https://doi.org/10.1038/s41598-019-42670-4

Wurtzel, J.B., Abram, N.J., Lewis, S.C., Bajo, P., Hellstrom, J.C., Troitzsch, U., Heslop, D., 2018. Tropical Indo-Pacific hydroclimate response to North Atlantic forcing during the last deglaciation as recorded by a speleothem from Sumatra, Indonesia. Earth and Planetary Science Letters 492, 264–278. https://doi.org/10.1016/j.epsl.2018.04.001

Xu, J., Holbourn, A., Kuhnt, W., Jian, Z., Kawamura, H., 2008. Changes in the thermocline structure of the Indonesian outflow during Terminations I and II. Earth and Planetary Science Letters 273, 152–162. https://doi.org/10.1016/j.epsl.2008.06.029

Yuan, S., Chiang, H.-W., Liu, G., Bijaksana, S., He, S., Jiang, X., Imran, A.M., Wicaksono, S.A., Wang, X., 2023. The strength, position, and width changes of the intertropical convergence zone since the Last Glacial Maximum. Proceedings of the National Academy of Sciences 120, e2217064120. https://doi.org/10.1073/pnas.2217064120

Appendix

Table A.1 – $\delta^{13}C_{wax}$ records included in compilation. Mean annual precipitation from 1992-2022 from GPCP data with 1° resolution (Adler et al., 2018). Magnitude of deglacial shift in $\delta^{13}C_{wax}$ calculated by subtracting the mean between 10 and 8 ka from the mean between 22 and 20 ka.

Paper	Proxy	Location	Core	Mean annual precipitation (mm)	Magnitude of shift (‰)
Dubois et al. (2014)	C30 *n*-acid	Offshore Borneo	91GGC	2817	-1.3
Niedermeyer et al. (2014)	C30 *n*-acid	Offshore Sumatra	SO189-144KL	2207	-1.21
Dubois et al. (2014)	C30 *n*-acid	Offshore Java	GeoB10069-3	1032	2.22
Wicaksono et al. (2017)	C28 *n*-acid	Mandar Bay	SO18515	2265	3.87
Ruan et al. (2019)	C_{31} *n*-alkane	Offshore Java	GeoB10053-7	2617	3.9
This study	C_{31} *n*-alkane	Lake Towuti	TOW9B	3114	7.44
This study	C_{31} *n*-alkane	Lake Matano	IDLE-MAT10-2B	3114	9.34

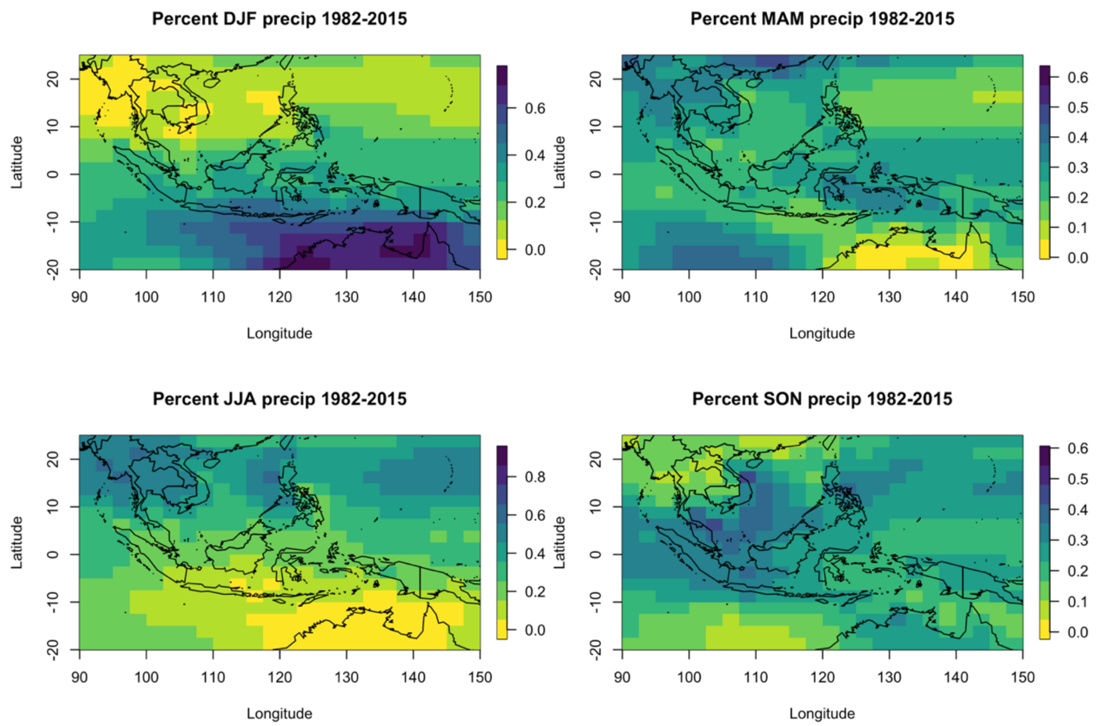

Figure A.1 – Fraction rainfall in every season across the IPWP using GPCP data (Adler et al., 2018).

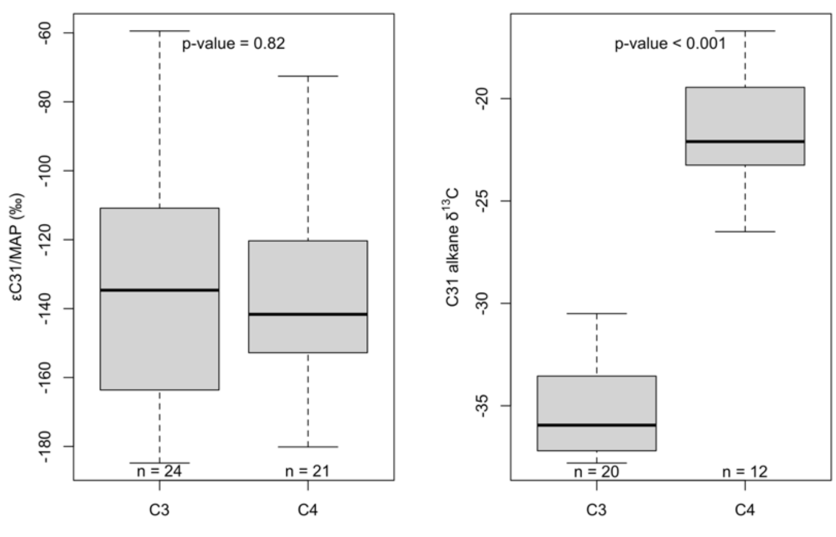

Figure A.2 – Boxplots of the apparent fractionation of δ^2H and $\delta^{13}C$ of C_{31} *n*-alkanes by all C3 and C4 plants included in the Sachse et al. (2012) compilation from between 30°S to 30°N. A t-test reveals that the mean apparent fractionation $^2H/H$ of C3 and C4 plants is not significantly different (p-value = 0.82), and mean $\delta^{13}C$ is significantly different ($p < 0.001$).

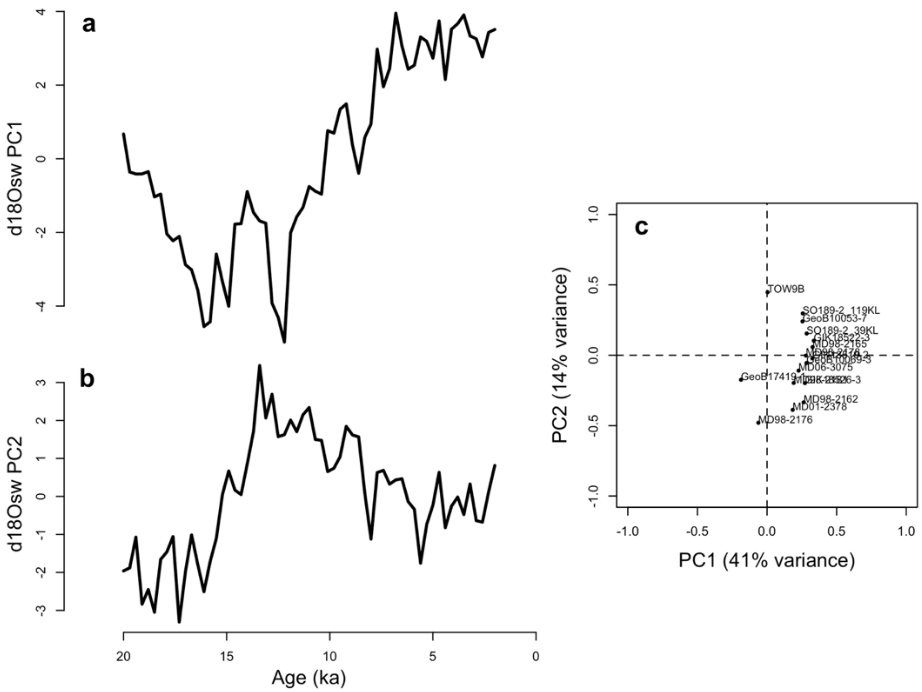

Figure A.3– PCA of all runoff and $\delta^{18}O_{sw}$ records from the IPWP with three age controls between 20 and 12 ka. The mean resolution of all the records is 0.3 ka, which was used as the common timestep.

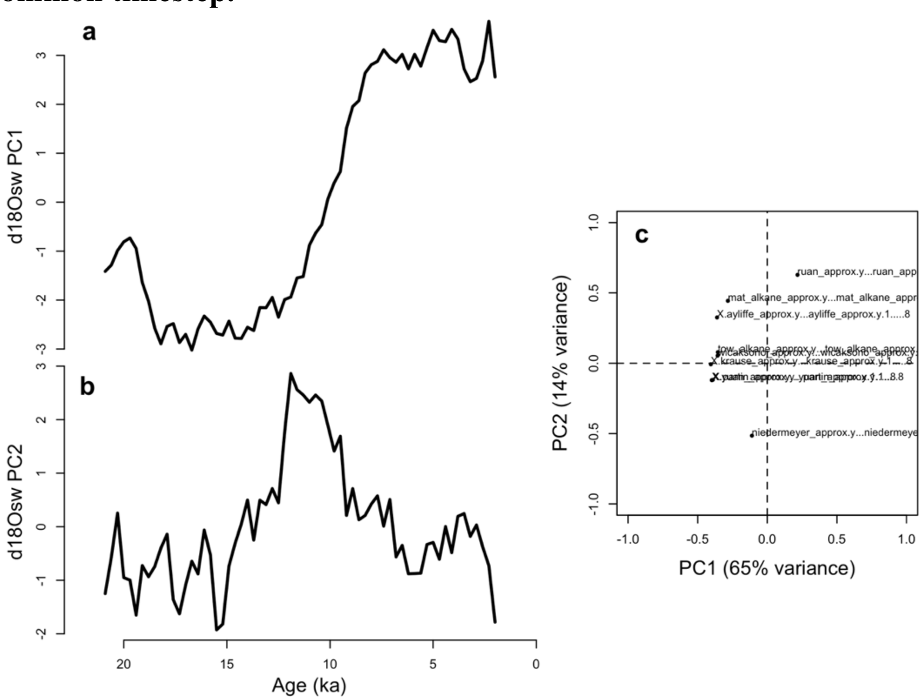

Figure A.4 – PCA of all δ^2H_{wax} and $\delta^{18}O_{speleo}$ (converted to δ^2H-space using the local meteoric water line) records from the IPWP that have at least three age controls during the last deglaciation (excluding the Towuti acid record to avoid overly-weighting Lake Towuti in the mean and PCA). The mean resolution of all the records is 0.3 ka, which was used as the common timestep.

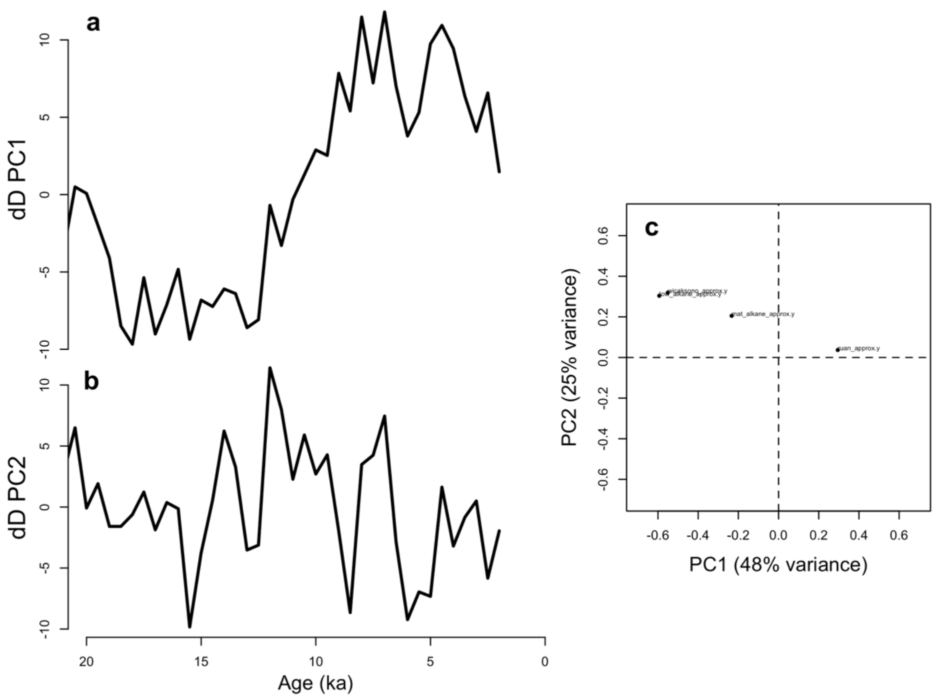

Figure A.5 – PCA of all δ^2H_{wax} records from the IPWP that have at least three age controls during the last deglaciation (excluding the Towuti acid record to avoid overly-weighting Lake Towuti in the mean and PCA).

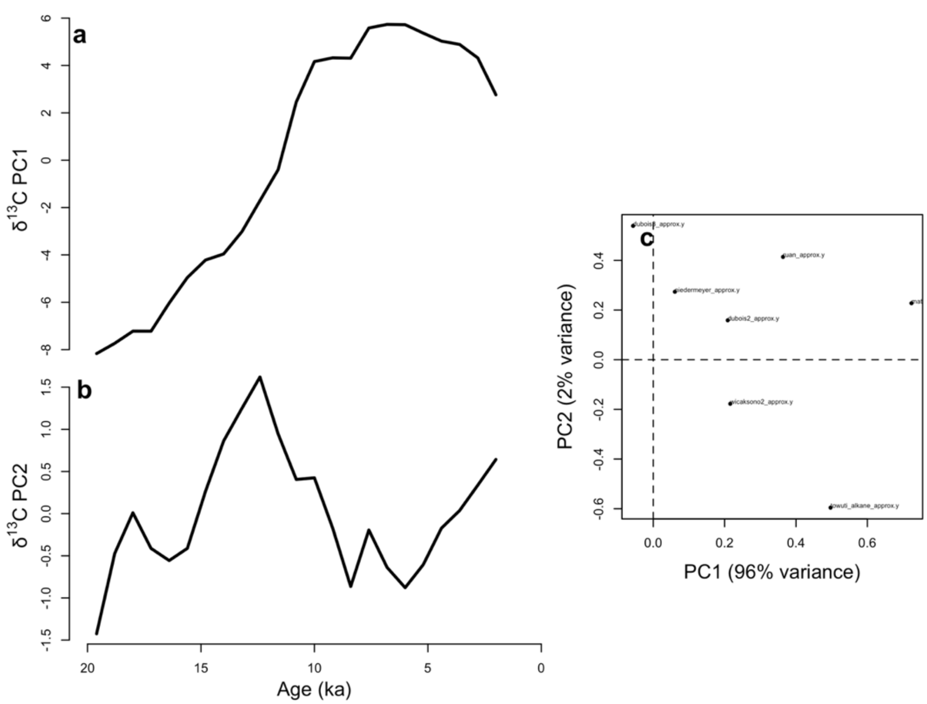

Figure A.6 – PCA of all $\delta^{13}C_{wax}$ records from the IPWP (excluding the Matano acid record to avoid overly weighting Lake Matano in the mean and PCA). The mean resolution of all the records is 0.8 ka, which was used as the common timestep.

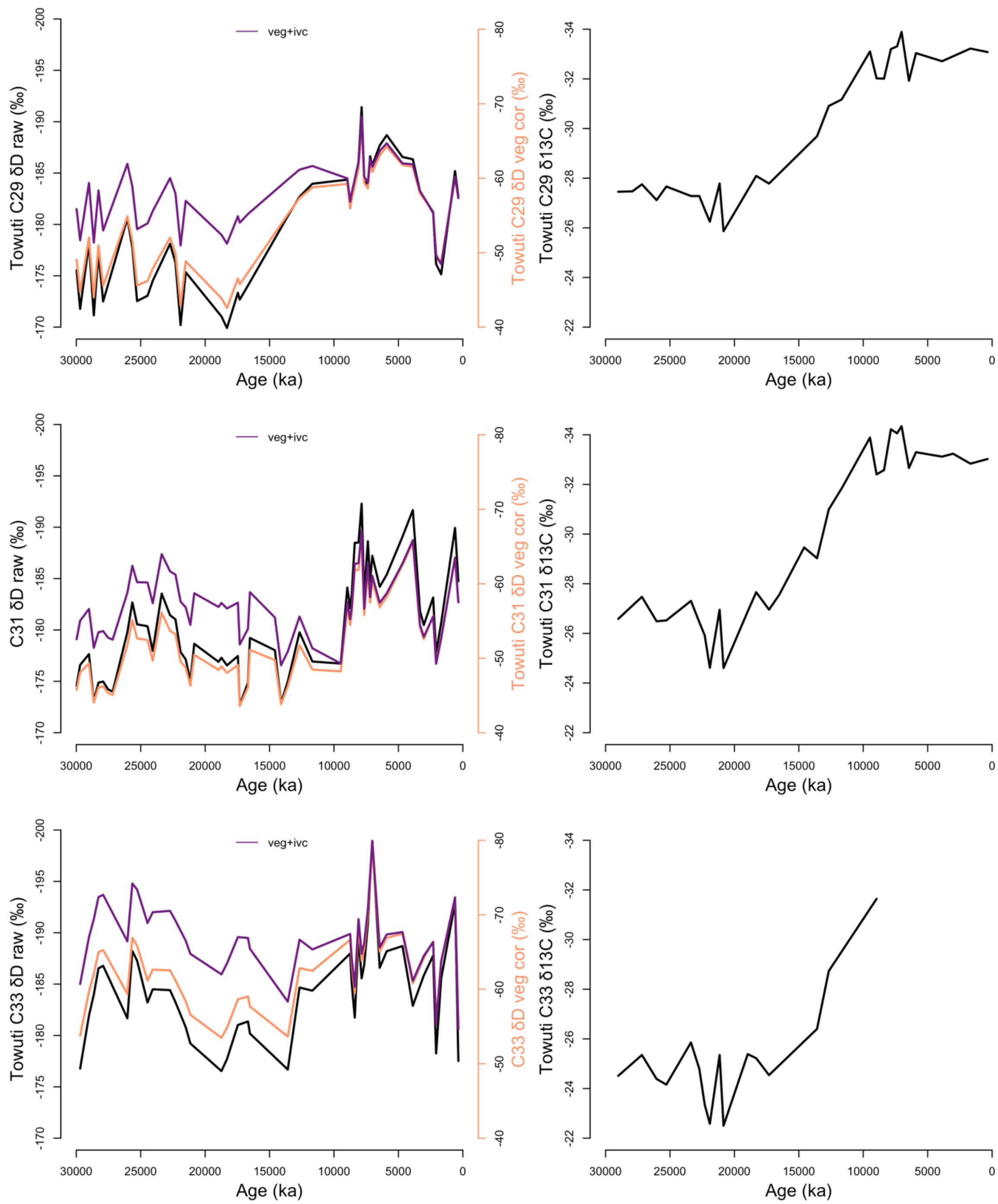

Figure A.7 – Raw δ^2H_{wax} of C_{29}, C_{31}, and C_{33} alkanes measured from Lake Towuti (black), vegetation corrected using an end-member mixing model described in Konecky et al. (2016) (orange), and vegetation and ice volume corrected (purple). $\delta^{13}C_{wax}$ of C_{29}, C_{31}, and C_{33} alkanes measured from Lake Towuti.

CHAPTER 4

A 1-million year record of terrestrial temperature from the Maritime Continent

M. C. Parish[1], J. M. Russell[1], J. W. King[2], A. L. Deino[3], C. J. Harpel[4], H. Vogel[5], S. Bijaksana[6], A. Wilk[1,7], and G. Traietti[1]

[1]Department of Earth, Environmental, & Planetary Sciences, Brown University, Providence, RI, USA.

[2]Graduate School of Oceanography, University of Rhode Island, Narragansett, RI, USA.

[3]Berkeley Geochronology Center, Berkeley, CA, USA.

[4]Casacades Volcano Observatory, Volcano Disaster Assistance Program, US Geological Survey, Vancouver, WA, USA.

[5]Institute of Geological Sciences & Oeschger Centre for Climate Change Research, University of Bern, Bern, Switzlerand.

[6]Global Geophysics Group, Faculty of Mining and Petroleum Engineering, Institut Teknologi Bandung, Bandung, Indonesia.

[7]Department of Earth, Geographic, and Climate Sciences University of Massachusetts Amherst, Amherst, MA, USA.

Abstract

The Mid-Pleistocene Transition (MPT, ~950 ka) was a fundamental change in Earth's climate, when 100-kyr glacial cycles began to dominate the high latitudes. Though the MPT is considered a global climate transition, there are few records from the Indo-Pacific Warm Pool (IPWP) and none from the Maritime Continent (MC). We produced an organic geochemical record of temperature from Lake Towuti, Indonesia that spans the past one million years to document regional patterns and to constrain the forcings and amplitude of terrestrial temperature in the region. Temperatures cool after the MPT, consistent with global patterns, and the appearance of 100-kyr cycles and increasing amplitude of glacial-interglacial cycles point to CO_2 as the dominant forcing of temperature. Significant 41-kyr cycles during the past ~430 kyr point to an additional role of global ice volume in determining MC temperature through ice sheet topography and/or sea level effects. Over the past 700 kyr we observe 1.45 times as much warming during deglaciations as SSTs, consistent with existing estimates from other regions in the tropics during the last deglaciation.

Plain Language Summary

Over the past one million years the earth has cycled between glacial periods – when all of Canada, the northern United States, and northern Europe were covered by massive ice sheets – and interglacial periods like today. These cycles have a global impact in large part because atmospheric greenhouse gas concentrations cycle with large changes in ice volume, with more greenhouse gases in the atmosphere during interglacial periods and less greenhouse gases in the atmosphere during glacial periods. We used these cycles to test the impact of changing greenhouse gases on climate in Southeast Asia. Ultimately, we hope this will tell us how sensitive this region, which has one of the highest populations on Earth, will be to anthropogenic increases in greenhouse gases. For now, we determined that Indonesia will likely experience 1.5 times as much warming as is predicted for ocean temperatures, which is similar to other regions in the tropics.

1. Introduction

The Mid-Pleistocene Transition (MPT) at ~950 ka is the most recent major reorganization of the Earth's climate, when 100-kyr glacial cycles became the dominant mode of variability (Herbert, 2023). SST records show that in many regions cooling accompanied the transition to 100-kyr cycles after the MPT. The Indo-Pacific Warm Pool (IPWP) plays a critical role in shaping global climate through the export of heat to higher latitudes (Zhou et al., 2019), yet records from this region suggest the IPWP did not cool at the MPT (Clark et al., 2024). However, this observation is based on very few SST records in the IPWP region (Clark et al., 2024). The Maritime Continent (MC) lies in the heart of the IPWP, where deep atmospheric convection delivers heavy rainfall to the islands of Indonesia and exports heat to the high latitudes, yet we have no temperature records from the MC and very few from other tropical continents that span the MPT. Thus, we lack adequate data to fully constrain the MC's role and response to this recent reorganization of Earth's carbon cycle.

Existing records indicate that glacial-interglacial cycles in global δ^{18}O covary with tropical SSTs during the past 3.5 million years, suggesting a dominant role for radiative forcing of greenhouse gas concentrations (GHGs) on tropical temperature (Herbert et al. 2010). Far less is known about long-term changes in tropical land surface temperatures. Existing terrestrial records are sparse and controversial; a 3-Myr record from the Chinese loess plateau (Lu et al.,

2022) and a 1.3 Myr record from Lake Malawi in East Africa (Johnson et al., 2016) show warming across the MPT, opposite SST records. Comparisons between SST and terrestrial records can be used to constrain the degree of terrestrial amplification in response to increasing GHG concentrations, which is vital for accurate projections of future terrestrial warming (Seltzer et al., 2023). Existing proxy estimates of terrestrial amplification from the last deglaciation suggest 1.4 times more terrestrial warming than marine warming, consistent with global climate models and historical estimates (Lambert & Chiang, 2007; Seltzer et al., 2021, 2023). However, this analysis only spans the last deglaciation and the estimates of terrestrial amplification are only from nine records of dissolved noble gases in groundwater (Seltzer et al., 2021), which show considerably larger changes in temperature than other proxies (Loomis et al., 2017; Powers et al., 2005; Tierney et al., 2008). Estimates of terrestrial amplification from multiple deglaciations allows for a more robust quantification of the magnitude of terrestrial warming relative to marine warming during periods of increasing GHG concentrations.

Here, we present an orbitally-resolved million-year record of terrestrial temperature from a continuous sediment record from Lake Towuti, Indonesia based on the abundances of branched Glycerol Dialkyl Glycerol Tetraethers (brGDGTs). The degree of methylation of these microbial membrane lipids (Schouten et al., 2013) varies with temperature, enabling paleotemperature calibrations and reconstructions (Zhao et al., 2023). Our new record helps to reconcile outstanding questions about the pattern of IPWP temperature changes during the mid- to late Pleistocene and helps to constrain the degree of terrestrial amplification in the MC, with critical implications for future climate change.

2. Materials and Methods

Lake Towuti is a 560 km^2 lake located in a ~1644 km^2 watershed near the equator (2.75°S, 121.5°E, 318 m above sea level) on Sulawesi, Indonesia in the center of the IPWP (Figure 1; Konecky et al., 2016; Russell et al., 2020). The temperature of the modern lake surface ranges from 30.5°C to 28.5° (Costa et al., 2015). We sampled a composite sediment stratigraphy developed from drill cores recovered from Site 1 in the central basin of Lake Towuti by the Towuti Drilling Project (Russell et al., 2020). We sampled at a mean resolution of 2.3 kyr, with a minimum of 0.5 kyr and a maximum of 9 kyr. The most recent 60 kyr of samples are from IDLE10-TOW9B with a mean sampling resolution of 0.5 ka (Parish et al., 2023).

To develop the temperature record, we quantified the fractional abundances of brGDGTs in each sample. See Supporting Information for detailed methods. We calculated MAAT with the multiple linear regression calibration (Equation 1) developed using 187 tropical lakes (Zhao et al., 2023), including lakes on Sulawesi.

$$MAAT = -4.11 + 31.63\ f(Ia) + 64.50\ f(Ib) + 32.28\ f(IIa') \quad (1)$$

The brGDGT-based temperature reconstruction from the most recent 60 kyr that was previously published in Parish et al. (2023), which used the Russell et al. (2018) East African calibration, and was updated here to the Zhao et al. (2023) tropical calibration. We also evaluated the isomerization, cyclization, and microbial community composition to assess possible confounding changes in microbial community (Figure S2).

The age model for the composite Towuti drill core uses a combination of radiocarbon dates, magnetic reversals, tephras, and stratigraphic tie points of the temperature record to a IPWP SST stack (Figure 2; Clark et al., 2024). We used *rbacon* in R to calibrate the radiocarbon dates to 'IntCal20' and produce the age model for the Towuti drill core (Blaauw & Christen, 2011). More information about the age control points can be found in the Supporting Information (Table S1 and Figure S1).

We analyzed the spectral frequencies in the temperature reconstruction using the *Astrochron* package in R. We used the ‘eha’ function to perform an evolutive harmonic analysis to see how the record evolved spectrally over time, the ‘mtm’ function to use the multi-taper method to determine the significant cycles for the entire record, and ‘bandpass’ to isolated 41-kyr cyclicity. To test the magnitude of warming during deglaciations over the past 1 million years, we calculated the difference between the mean of three measured temperatures at the highest temperature within 20 kyr of the peak of the interglacial detected in the IPWP SST stack and the mean of three measured temperatures at the lowest temperature within 20 kyr of the glacial period detected in the IPWP SST stack (Clark et al., 2024).

3. Results

3.1 Chronology

A tephra at 72.93 mcd in the composite record was dated using $^{40}Ar/^{39}Ar$ to 797.3 ± 1.7 ka (Russell et al., 2020). Tephrochemistry indicated that the tephra at 53.17 mcd was the Makalisung Tuff (471 ± 6 ka), and the tephra at 25.46 mcd was equivalent to the Tondano area ignimbrite we are calling the Manado Tuff (Unit G, main ignimbrite, (173.5 ± 4.0 ka, 1-sigma error). Two magnetic reversals were detected in the composite record: the oldest at 90.31 mcd and the youngest at 72.2 mcd (Figure S1). The stratigraphic position of the reversal at 72.20 mcd close to the Oldest Toba Tuff is consistent with the Brunhes-Matuyama reversal at 778.0 ± 5.0 ka (Mark et al., 2017). The reversal at 90.31 mcd likely corresponds to the Matuyama-Jaramillo reversal at 990 ± 4 ka (Channell et al., 2020).

We used the 23 radiocarbon, three tephra ages, and two magnetic reversal ages to produce a preliminary model using *rbacon* (Figure 2a; Table S1). Applying this preliminary model to the brGDGT data, the reconstructed temperature has a significant (95% CL) 41-kyr peak and two significant peaks straddling the 100-kyr band (Figure 2c) and orbital-scale variations in the data align well with an IPWP SST stack, particularly after ~800 ka (Figure 2b; Clark et al., 2024). In light of this relationship, we identified 32 tie points between the Towuti temperature reconstruction and the IPWP SST reconstruction (Clark et al., 2024) and produced a final age model for the 1-Myr Towuti record, which includes the tie points, radiocarbon, tephra, and magnetic reversals (Figure 2d). None of the tie points shift the age model outside the uncertainty from the original age model (Figure 2a). The average age uncertainty in the age model is 10.9 ka and a maximum age uncertainty of 36.4 ka (at the base of the succession at 97 mcd). The final age model applied to the temperature data aligns the most obvious glacial-interglacial features (Figure 2e). Spectral analysis shows significant (95% CL) 100- and 41-kyr cycles (Figure 2f).

3.2 Temperature reconstruction

Changes in brGDGT isomerization, cyclization, and abundances do not show obvious relationships with reconstructed temperatures, and changes in temperature do not appear coincident with major changes in the lithology of the TDP-1 composite succession. Thus, there is little evidence for changes in the microbial community structure or brGDGT source that raise questions about the reliability of the temperature reconstruction (Figure S2).

Between the base of the record at ~1.1 Mya and 800 ka, temperatures averaged ~29 ºC. Glacial-interglacial variations are muted (~1°C) and their structure is less clear than in younger sediment (Figure 3). IPWP SST variability is also lower during this time period (~1°C), but the structure of the cycles are more distinct than in the Towuti record (Clark et al., 2024). A 100-kyr cyclicity emerges at ~750 ka in the Towuti temperature record, when glacial periods became much colder. A 41-kyr cycle emerges after 430 ka (Figure 4a), when the amplitude of glacial-interglacial variations increases further. The magnitude of the temperature changes in the past 700-kyr are greater in our record (~3.2°C) than in the most recent tropical SST stack (~2.2°C; Clark et al., 2024) and a prior alkenone-based tropical SST stack (~2.3°C; Herbert et al., 2010; Figure 4).

Interglacial temperatures are warmer after the Mid-Brunhes Transition (MBT; ~430 ka), when the magnitude of glacial-interglacial cycles increased. The "Super Interglacial" at MIS11 (Melles et al., 2012), which is prominent in the IPWP SST stack (Clark et al., 2024), is not considerably warmer than other interglacials in the Towuti record. MIS5e (~127 ka), which is a particularly warm interglacial globally (Pages, 2016), is warmer than MIS7, MIS9, MIS11, MIS13, and MIS15, and the current interglacial is relatively warm as well. Glacial temperatures are approximately equivalent during MIS8, MIS10, and the Last Glacial Maximum. Prior to ~750 ka both glacial and interglacial temperatures are consistently warmer and less variable than after the MPT (Figure 3).

4. Discussion

Our 1-Myr temperature record from Lake Towuti is the first reconstruction of terrestrial temperature from Southeast Asia that extends beyond the last ice age, and one of only a handful of terrestrial temperature records from the tropics. The record provides new insights into the response of MC temperatures to global climate transitions during the mid- to late-Pleistocene, but also documents puzzling phenomena that do not align with trends in global or tropical SSTs.

In particular, our record suggests that Maritime Continental temperature underwent a fundamental transition during the MPT, from an interval of sustained warmth with very limited glacial-interglacial variability to a period with striking 100-kyr cycles in temperature and strong cooling during glacials. There is no obvious global forcing for this transition, suggesting it could stem from regional processes such as tectonically-driven changes in land-sea exposure. Below we discuss forcings and possible forcings and responses to explain this novel record of terrestrial temperature.

4.1 The Mid-Pleistocene and Mid-Brunhes transitions in tropical temperature

SSTs across most the oceans cool during the MPT (Clark et al., 2024). This near-global cooling suggests that gradually declining CO_2 is the dominant forcing of ocean temperature during the Pleistocene, and through the impacts of cooling on ice sheet extent, is partially responsible for the establishment of 100-kyr glacial cycles (Clark et al., 2024). In contrast, records from the IPWP show no mean cooling (Clark et al., 2024). The absence of cooling during the MPT in IPWP SST records is curious, and could indicate local forcings or feedbacks that mitigate the impacts of GHGs on regional temperature (Clark et al., 2024), and could suggest the region may be relatively insensitive to GHG forcing in the coming century.

Unlike IPWP SST records, the Lake Towuti temperature record shows a mean cooling during the MPT, coincident with a shift to larger variability and distinct glacial-interglacial cycles (Figure 3). Although we cannot fully explain the divergence between our temperature record and IPWP SSTs, we note that the cooling in our data is consistent with cooling in most parts of the oceans outside of the IPWP. The IPWP SST stack may not show cooling due to saturation of the alkenone paleothermometer above 28 ºC (Gray & Evans, 2019), as our record suggests a mean of 27°C with interglacial temperatures warmer than 28° C; however, SST records from the IPWP based on Mg/Ca also do not cool. Although we cannot explain the SST patterns, our data suggest the MC responded to and, though its role in latent heat export, participated in global cooling during the MPT.

Climate models suggest that tropical temperatures are influenced by local insolation, ice sheet topography, sea level effects of the MC, and the radiative forcing of GHGs (DiNezio et al., 2018; Otto-Bliesner et al., 2014). SST records are additionally sensitive to heat advection associated with changes in ocean circulation (Martínez-Garcia et al., 2010). Terrestrial temperatures estimated from lake records are not directly sensitive to changes in ocean circulation, providing a powerful proxy to uncover the forcings of temperature in the MC.

Many records suggest radiative forcing by GHGs is the dominant control on tropical SSTs (Dyez et al., 2016; Herbert et al., 2010; Medina-Elizalde & Lea, 2005). This is indicated by covariation of the global benthic $\delta^{18}O$ stack and tropical SSTs over the past 3.5 Myr (Herbert et al., 2010), the in-phase relationship between CO_2 and SSTs in the tropical Pacific during the past 800 kyr (Dyez et al., 2016), and the broad similarity of tropical SST changes in different regions (Herbert et al., 2010). These relationships are most apparent in the 100-kyr band; in the 41-kyr band, SSTs in the eastern equatorial Pacific (EEP) are also coherent with high-latitude insolation and ice volume, but sites in the western equatorial Pacific do not show these relationships (Dyez et al., 2016). In the 19-23-kyr band, local insolation is directly correlated with EEP SST (Dyez et al., 2016).

The Towuti temperature record has a significant 100-kyr cycle from ~ 750 ka to present and a significant 41-kyr cycle from ~500 ka to present (Figure 4a). In contrast, the tropical SST stacks have significant 41-kyr and 100-kyr cycles over the past 1 million years (Figure S3). For instance, the tropical SST stack (Clark et al., 2024) shows a 100-kyr cycle and a 41-kyr cycle prior to 800 ka which largely disappears from 800 ka to present (Figure 4d). As noted above, our record indicates 100-kyr temperature cycles emerged later in the MC than in the surrounding oceans, suggesting the impact of forcings that amplified glacial-interglacial changes in GHGs. The 41-kyr cycle also emerges relatively late in the Towuti temperature record, and may be caused by ice volume or high latitude forcing, similar to the EEP, and/or to sea level effects and land shelf exposure that impact regional temperatures in the MC. Indeed, the combined response of ice sheet albedo and sea level impacts on land exposure over the MC showed the strongest proxy-model agreement in a study comparing the Community Earth System Model version 1.2 (CESM1) to SST and hydroclimate proxies at the LGM (DiNezio et al., 2018). If so, the 41-kyr cycle may emerge in the Towuti temperature because gradual uplift of the Sunda Shelf established cycles of exposure and submersion during glacial-interglacial cycles after ~500 ka (McGrath et al., 2023; Sarr et al., 2019). However, the estimated timing of the first submersion of the Sunda Shelf is uncertain and depends on the estimated subsidence rate of the Sunda Shelf (McGrath et al., 2023; Sarr et al., 2019).

The 100-kyr cycle emerged at ~750 ka in the Towuti temperature record, a timing similar to but slightly lagging the establishment of 100-kyr glacial-interglacial periods during the MPT. The timing of the emergence of the 100-kyr cycle in the Towuti record lags the estimated timing of the MPT by 50 kyr (von der Heydt et al., 2021), though others do place the timing at 750 ka (Herbert, 2023). The 100-kyr cycle is evident in the tropical SST stacks and ice volume for the entirety of the past 1 million years even before the MPT (Figure S3). The absence of this cycle could reflect the lack of age constraints in the oldest sediments at Lake Towuti. However, the emergence of this cycle could also reflect a response of MC temperatures to high-latitude forcing such as that observed during the last deglaciation (e.g. di Nezio et al., 2018), again implicating changes in land-sea configuration earlier than predicted by current tectonic models (Sarr et al., 2019).

Over the past 700 kyr the magnitude of warming in the Towuti record during deglaciations significantly increases (R = 0.84, P = 0.02; Figure 5), with much of the increase due to warmer interglacials after the MBT. This transition also occurs in the tropical SST stack (R = 0.80, P = 0.03; Clark et al., 2024), but is not significant in the alkenone-based SST stack (R = 0.55, P = 0.20; (Herbert et al., 2010). The benthic oxygen isotope stack (Lisiecki & Raymo, 2005) does not exhibit a statistically significant increase in the magnitude of glacial-interglacial cycles during the past 700 kyr (R = 0.40, P = 0.38), but CO_2 does show a significant increase in the magnitude of glacial-interglacial cycles (R = 0.76, P = 0.05; Bereiter et al., 2015). The increasing magnitude of glacial-interglacial cycles in the Towuti record thus suggests a dependence of MC temperature on atmospheric pCO_2 during the last ~750 kyr.

4.2 Forcings of MC terrestrial temperature

A high-resolution record of temperature from Lake Towuti showed that temperature change during the last deglaciation is likely forced by CO_2, inferred by the synchronous onset of warming and the deglacial increase in CO_2 (Marcott et al., 2014; Parish et al., 2023). The increasing magnitude of interglacial temperatures after the MBE in Lake Towuti adds further support for CO_2 as the dominant forcing of MC temperature, as does the gradual cooling across the MPT. However, the absence of clear glacial-interglacial cycles prior to 750 ka, when tropical SST records showed clear 100- and 41-kyr cycles, suggests MC temperature was relatively insensitive to GHG forcing during that time. The temperatures during this time sometimes exceed 28 ºC, near the upper end of the brGDGT calibration range (Zhao et al., 2023), and it is possible that our proxy is missing large interglacial warmings. It is also possible that consistently warm, wet (Parish, Chapter 5) conditions and high humidity suppressed the impacts of GHG forcing, which were likely weaker prior to the MPT. A third alternative, noted above, is that temperature fluctuations in the MC locked to the beat of glacial-interglacial cycles after the MPT when the combined effects of multiple forcings, including GHGs, ice volume, and potentially continental shelf exposure became large enough to impact regional temperature.

The prominent 41-kyr cycle detected in the Towuti record may also point to ice volume, albedo, and/or sea level effects on shelf exposure as additional forcings of MC temperature. 41-kyr bandpass-filtering of the Towuti temperature record shows that the amplitude of 41-kyr cycles increases at ~430 ka, during the MBT (Figure 4c). The 41-kyr bandpass-filtered CO_2 record (Bereiter et al., 2015) does not show an increased amplitude until ~350 ka (Figure 4f), but the global benthic $\delta^{18}O$ stack (Lisiecki & Raymo, 2005) does show a simultaneous increase in the amplitude of 41-kyr cyclicity at ~430 ka with the Towuti temperature record (Figure 4c). This increase at ~430 ka strongly implicates ice volume forcing, through either topography or sea level, as a forcing of MC temperature. The appearance of the 41-kyr cycle at ~430 ka could reflect a threshold in the sensitivity of Maritime temperature to ice volume, where the cycles have a great enough magnitude to impact MC temperature after the MBT.

4.3 Terrestrial amplification

Existing estimates of glacial-interglacial temperature change from noble gas data indicate temperatures warmed by 5.8°C during the most recent deglaciation between 45°S and 35°N (Seltzer et al., 2021). A tropical (30°S-30°N) warming of only 3.9°C during the last deglaciation is estimated based on data assimilation and climate reanalysis using SST records (Tierney et al., 2020). The Towuti temperature change during the last deglaciation has a 6.1°C difference between the mean glacial and interglacial temperatures, closer to the noble gas-based estimate than the data assimilation estimate.

The Towuti record provides the opportunity to evaluate amplification over multiple glacial-interglacial cycles and with varying boundary conditions (CO_2, insolation, ice volume). The median G-IG temperature change in the Towuti temperature record is 1.45 times greater than the tropical SST stack and 1.39 times greater than the alkenone-based tropical SST stack (Figure 3b). In historical observations, deglacial proxy records, and general circulation models, this ratio is 1.4:1 to 1.5:1, with terrestrial temperatures experiencing greater change (Lambert & Chiang, 2007; Seltzer et al., 2023). The terrestrial amplification indicated in the Towuti record is 1.45:1, which is consistent with existing estimates from the last deglaciation. Consistent terrestrial amplification despite large-scale adjustments such as the MBT, suggests consistent CO_2 forcing as interglacial pCO_2 increases during the past 430 kyr. In projections of future warming, the MC exhibits muted terrestrial amplification compared to other tropical regions (Iturbide et al., 2020). Similar terrestrial amplification in the MC to other tropical regions could indicate climate models have difficulty predicting temperature in such a geographically complicated region and the MC may warm more than currently anticipated.

5. Conclusions

Our new record from Sulawesi, Indonesia documents long-term trends and glacial-interglacial variations in temperature during the past 1.1 Ma. We observe cooling during the MPT, the emergence of strong 100-kyr cycles in temperature at 750 ka, and an increasing magnitude in glacial-interglacial temperature change during the past 700 kyr. These changes are similar to records of tropical sea-surface temperatures and ice-core records of atmospheric pCO_2, and are thus consistent with a dominant influence of radiative forcing from atmospheric GHGs on tropical terrestrial temperatures. Our record further suggests similar terrestrial amplification in response to variations in CO_2 concentrations as observed in other parts of the tropics, suggesting that despite the complex geography of the MC that the land will likely warm as much as other regions in the tropics.

Acknowledgements

We would like to thank Marcelo Da Rosa Alexandre for analytical assistance and the Continental Scientific Drilling Facility for sampling. This material is based on work supported by National Science Foundation Grant EAR-2102856, a Continental Scientific Drilling Division Geological Society of America Research Grant, and the Institute at Brown for Environment and Society Graduate Research, Training, and Travel Award. The authors thank members of the Towuti Drilling Project and PT Vale Indonesia for field assistance. The authors acknowledge assistance and permission for this work from the Indonesian Ministry of Research and Technology (RISTEK).

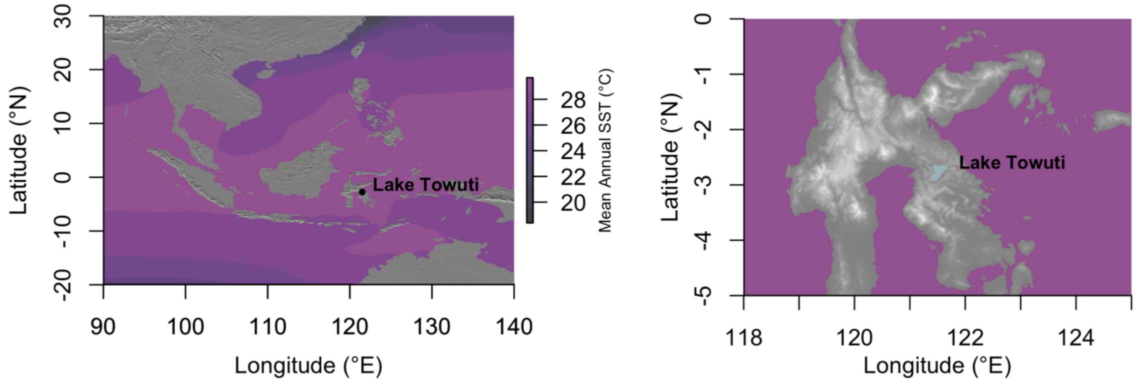

Figure 1 – Lake Towuti is located on the island of Sulawesi, Indonesia. Mean annual sea surface temperatures (SST) from 1991-2021 from reanalysis data (Kalnay et al., 1996). SST and the digital elevation models are plotted using the "raster" package in R (Hijmans et al., 2022).

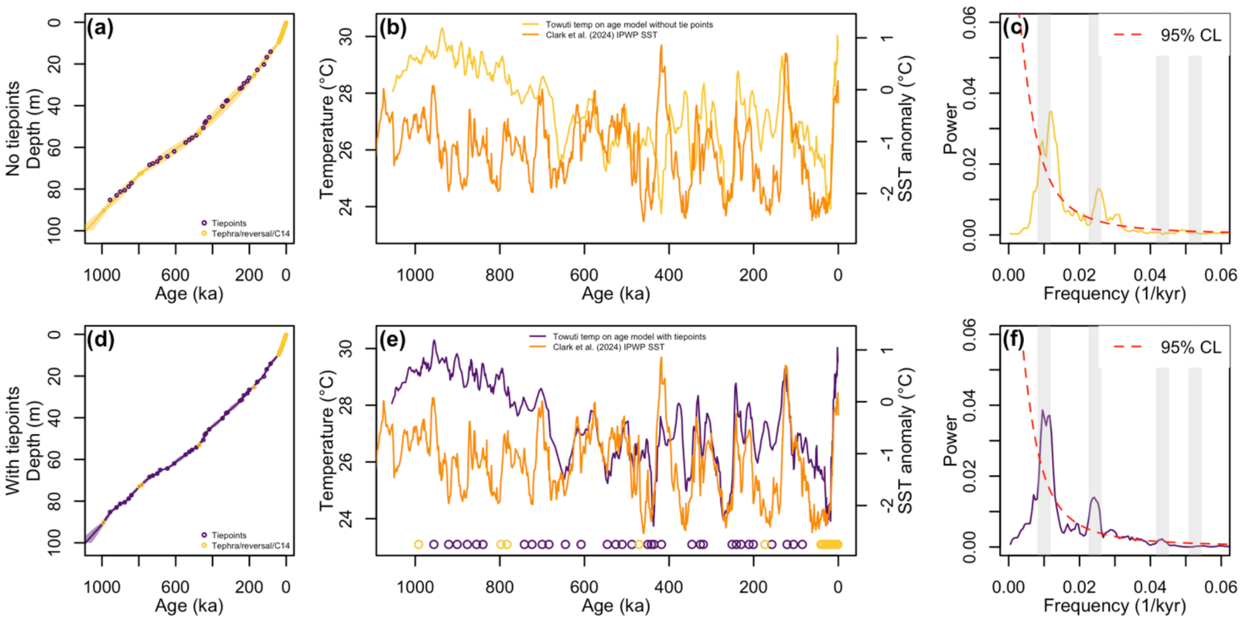

Figure 2 – Comparison of the age model with and without tie points. (a) The yellow ribbon shows the age model based on radiocarbon, tephras, and magnetic reversals (yellow circles). The tie points that are not included in this age model are shown as purple circles. (b) The Towuti temperature record on the age model without tie points (yellow) and the IPWP SST stack (orange, Clark et al., 2024). (c) Multi-taper method spectral power of 100-kyr, 41-kyr, 23-kyr and 19-kyr cycles (gray bars). (d) The purple ribbon shows the age model based on radiocarbon, tephras, magnetic reversals, and tie points. (e) The Towuti temperature record on the age model with tie points (purple) and the IPWP SST stack (orange, Clark et al., 2024). The radiocarbon, tephras, and magnetic reversals are shown in yellow and the tie points are show in purple circles. (c) Multi-taper method spectral power of 100-kyr, 41-kyr, 23-kyr and 19-kyr cycles (gray bars).

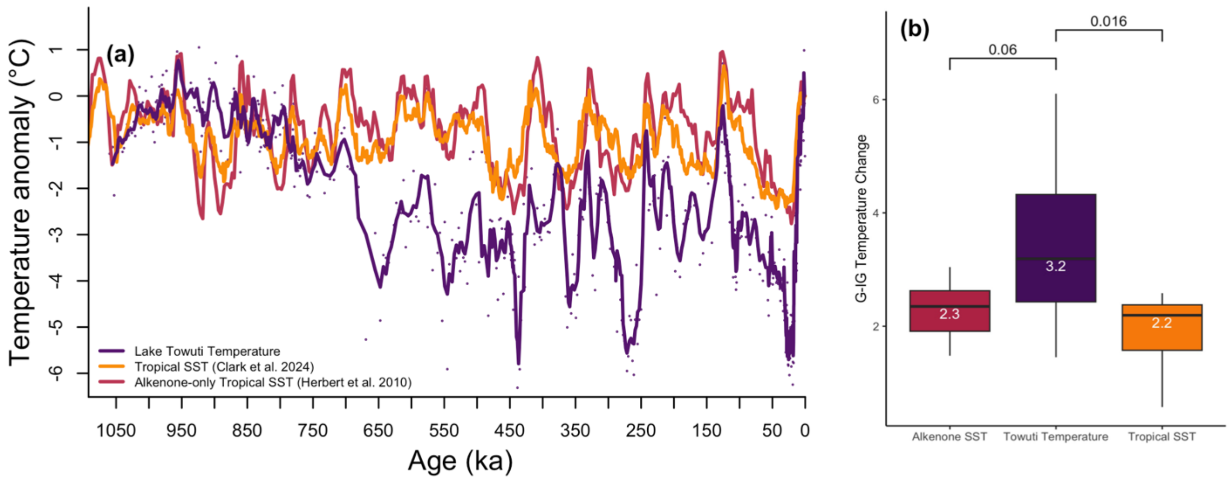

Figure 3 – (a) Temperature anomalies from modern from the Towuti temperature reconstruction (purple), the tropical SST stack (orange; Clark et al., 2024), and the alkenone-based tropical SST stack (red; Herbert et al., 2010). (b) The Glacial-Interglacial temperature change reconstructed at Lake Towuti compared to the temperature change reconstructed in the tropical SST stack (Clark et al., 2024) during the past 700 kyr. A paired t-test between the GI-IG temperature changes recorded at Lake Towuti and the tropical SST stack reveal significant (p=0.016) differences during the past 700 kyr. The G-IG temperature change is not significantly different between the Towuti record and the alkenone-based tropical stack (p=0.06). The median G-IG temperature change in the Towuti temperature record is 1.45 times greater than the tropical SST stack and 1.39 times greater than the alkenone-based tropical SST stack.

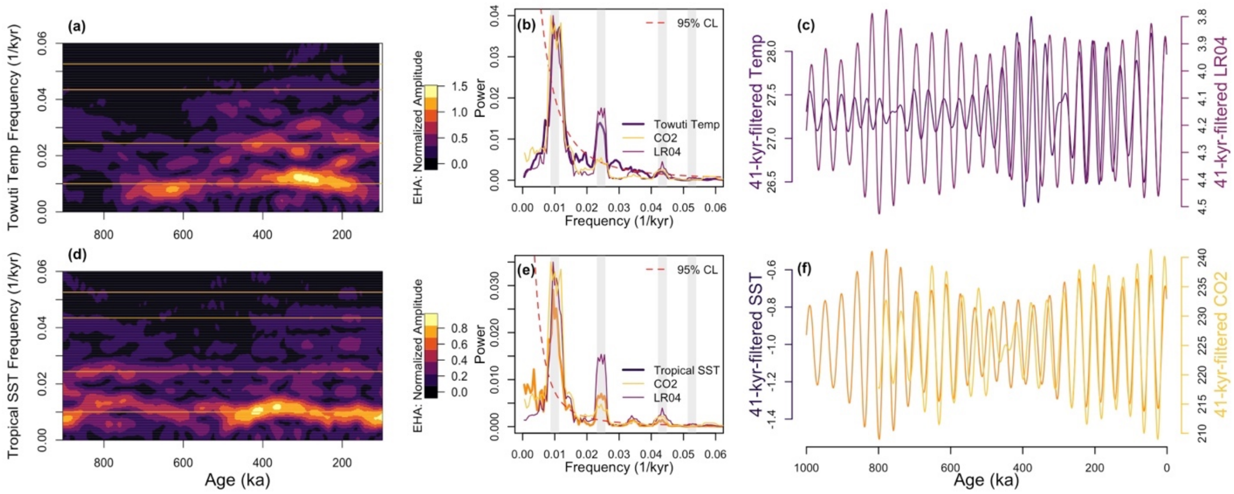

Figure 4 – (a) Evolutive harmonic analysis and (b) multi-taper method spectral analysis of the Towuti temperature record. (c) 41-kyr bandpass-filtered Towuti temperature record and global benthic $\delta^{18}O$ stack (Lisiecki & Raymo, 2005). (d) Evolutive harmonic analysis and (e) multi-taper method spectral analysis of the tropical SST stack (Clark et al., 2024). (f) 41-kyr bandpass-filtered tropical SST (Clark et al., 2024) and the Antarctic CO_2 composite (Bereiter et al., 2015).

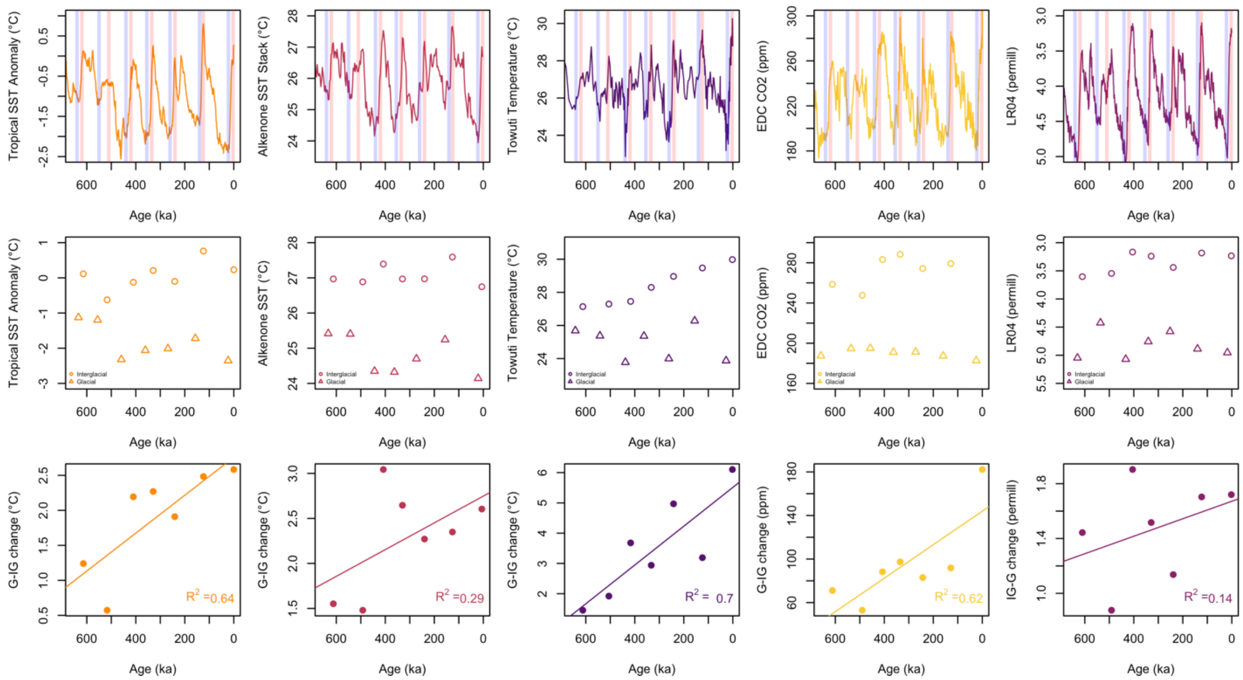

Figure 5 – Comparison of the minimum and maximum values of glacial and interglacial periods from a tropical, SST stack (orange; Clark et al., 2024), an alkenone-based tropical SST stack (red; Herbert et al., 2010), the Towuti temperature record (purple), the Antarctic composite CO_2 record (yellow, Bereiter et al., 2015), and the benthic stack (maroon; Lisiecki & Raymo, 2005). The middle row shows temperatures during interglacials and glacials, and the bottom row shows the difference between glacial and interglacial temperatures during the past 700 kyr.

References

Bereiter, B., Eggleston, S., Schmitt, J., Nehrbass-Ahles, C., Stocker, T. F., Fischer, H., et al. (2015). Revision of the EPICA Dome C CO2 record from 800 to 600 kyr before present. *Geophysical Research Letters*, *42*(2), 542–549. https://doi.org/10.1002/2014GL061957

Blaauw, M., & Christen, J. A. (2011). Flexible paleoclimate age-depth models using an autoregressive gamma process. *Bayesian Analysis*, *6*(3), 457–474. https://doi.org/10.1214/11-BA618

Channell, J. E. T., Singer, B. S., & Jicha, B. R. (2020). Timing of Quaternary geomagnetic reversals and excursions in volcanic and sedimentary archives. *Quaternary Science Reviews*, *228*, 106114. https://doi.org/10.1016/j.quascirev.2019.106114

Clark, P. U., Shakun, J. D., Rosenthal, Y., Köhler, P., & Bartlein, P. J. (2024). Global and regional temperature change over the past 4.5 million years. *Science*, *383*(6685), 884–890. https://doi.org/10.1126/science.adi1908

Costa, K. M., Russell, J. M., Vogel, H., & Bijaksana, S. (2015). Hydrological connectivity and mixing of Lake Towuti, Indonesia in response to paleoclimatic changes over the last 60,000years. *Palaeogeography, Palaeoclimatology, Palaeoecology*, *417*, 467–475. https://doi.org/10.1016/j.palaeo.2014.10.009

DiNezio, P. N., Tierney, J. E., Otto-Bliesner, B. L., Timmermann, A., Bhattacharya, T., Rosenbloom, N., & Brady, E. (2018). Glacial changes in tropical climate amplified by the Indian Ocean. *Science Advances*, *4*(12), eaat9658. https://doi.org/10.1126/sciadv.aat9658

Dyez, K. A., Ravelo, A. C., & Mix, A. C. (2016). Evaluating drivers of Pleistocene eastern tropical Pacific sea surface temperature. *Paleoceanography*, *31*(8), 1054–1069. https://doi.org/10.1002/2015PA002873

Gray, W. R., & Evans, D. (2019). Nonthermal Influences on Mg/Ca in Planktonic Foraminifera: A Review of Culture Studies and Application to the Last Glacial Maximum. *Paleoceanography and Paleoclimatology*, *34*(3), 306–315. https://doi.org/10.1029/2018PA003517

Herbert, T. D. (2023). The Mid-Pleistocene Climate Transition. *Annual Review of Earth and Planetary Sciences*, *51*(1), 389–418. https://doi.org/10.1146/annurev-earth-032320-104209

Herbert, T. D., Peterson, L. C., Lawrence, K. T., & Liu, Z. (2010). Tropical Ocean Temperatures Over the Past 3.5 Million Years. *Science*, *328*(5985), 1530–1534. https://doi.org/10.1126/science.1185435

von der Heydt, A. S., Ashwin, P., Camp, C. D., Crucifix, M., Dijkstra, H. A., Ditlevsen, P., & Lenton, T. M. (2021). Quantification and interpretation of the climate variability record. *Global and Planetary Change*, *197*, 103399. https://doi.org/10.1016/j.gloplacha.2020.103399

Hijmans, R. J., Etten, J. van, Sumner, M., Cheng, J., Baston, D., Bevan, A., et al. (2022, January 22). raster: Geographic Data Analysis and Modeling (Version 3.5-15). Retrieved from https://CRAN.R-project.org/package=raster

Hopmans, E. C., Schouten, S., & Sinninghe Damsté, J. S. (2016). The effect of improved chromatography on GDGT-based palaeoproxies. *Organic Geochemistry*, *93*, 1–6. https://doi.org/10.1016/j.orggeochem.2015.12.006

Iturbide, M., Gutiérrez, J. M., Alves, L. M., Bedia, J., Cerezo-Mota, R., Cimadevilla, E., et al. (2020). An update of IPCC climate reference regions for subcontinental analysis of climate model data: definition and aggregated datasets. *Earth System Science Data*, *12*(4), 2959–2970. https://doi.org/10.5194/essd-12-2959-2020

Johnson, T. C., Werne, J. P., Brown, E. T., Abbott, A., Berke, M., Steinman, B. A., et al. (2016). A progressively wetter climate in southern East Africa over the past 1.3 million years. *Nature*, *537*(7619), 220–224. https://doi.org/10.1038/nature19065

Kalnay, E., Kanamitsu, M., Kistler, R., Collins, W., Deaven, D., Gandin, L., et al. (1996). The NCEP/NCAR 40-Year Reanalysis Project. *Bulletin of the American Meteorological Society*, *77*(3), 437–472. https://doi.org/10.1175/1520-0477(1996)077<0437:TNYRP>2.0.CO;2

Kirana, K. H., Bijaksana, S., King, J., Tamuntuan, G. H., Russell, J., Ngkoimani, L. O., et al. (2018). A high-resolution, 60 kyr record of the relative geomagnetic field intensity from Lake Towuti, Indonesia. *Physics of the Earth and Planetary Interiors*, *275*, 9–18. https://doi.org/10.1016/j.pepi.2017.12.007

Konecky, B., Russell, J., & Bijaksana, S. (2016). Glacial aridity in central Indonesia coeval with intensified monsoon circulation. *Earth and Planetary Science Letters*, *437*, 15–24. https://doi.org/10.1016/j.epsl.2015.12.037

Lambert, F. H., & Chiang, J. C. H. (2007). Control of land-ocean temperature contrast by ocean heat uptake. *Geophysical Research Letters*, *34*(13). https://doi.org/10.1029/2007GL029755

Lisiecki, L. E., & Raymo, M. E. (2005). A Pliocene-Pleistocene stack of 57 globally distributed benthic δ18O records. *Paleoceanography*, *20*(1). https://doi.org/10.1029/2004PA001071

Loomis, S. E., Russell, J. M., Verschuren, D., Morrill, C., De Cort, G., Sinninghe Damsté, J. S., et al. (2017). The tropical lapse rate steepened during the Last Glacial Maximum. *Science Advances*, *3*(1), e1600815. https://doi.org/10.1126/sciadv.1600815

Marcott, S. A., Bauska, T. K., Buizert, C., Steig, E. J., Rosen, J. L., Cuffey, K. M., et al. (2014). Centennial-scale changes in the global carbon cycle during the last deglaciation. *Nature*, *514*(7524), 616–619. https://doi.org/10.1038/nature13799

Mark, D. F., Renne, P. R., Dymock, R. C., Smith, V. C., Simon, J. I., Morgan, L. E., et al. (2017). High-precision 40Ar/39Ar dating of pleistocene tuffs and temporal anchoring of the Matuyama-Brunhes boundary. *Quaternary Geochronology*, *39*, 1–23. https://doi.org/10.1016/j.quageo.2017.01.002

Martínez-Garcia, A., Rosell-Melé, A., McClymont, E. L., Gersonde, R., & Haug, G. H. (2010). Subpolar Link to the Emergence of the Modern Equatorial Pacific Cold Tongue. *Science*, *328*(5985), 1550–1553. https://doi.org/10.1126/science.1184480

McGrath, S. M., Clemens, S. C., & Huang, Y. (2023). Pleistocene Sunda Shelf submersion-exposure cycles initiate vegetation Walker Circulation feedback. *Geology*. https://doi.org/10.1130/G51412.1

Medina-Elizalde, M., & Lea, D. W. (2005). The Mid-Pleistocene Transition in the Tropical Pacific. *Science*, *310*(5750), 1009–1012. https://doi.org/10.1126/science.1115933

Melles, M., Brigham-Grette, J., Minyuk, P. S., Nowaczyk, N. R., Wennrich, V., DeConto, R. M., et al. (2012). 2.8 Million Years of Arctic Climate Change from Lake El'gygytgyn, NE Russia. *Science*, *337*(6092), 315–320. https://doi.org/10.1126/science.1222135

Niespolo, E. M., Rutte, D., Deino, A. L., & Renne, P. R. (2017). Intercalibration and age of the Alder Creek sanidine 40Ar/39Ar standard. *Quaternary Geochronology*, *39*, 205–213. https://doi.org/10.1016/j.quageo.2016.09.004

Otto-Bliesner, B. L., Russell, J. M., Clark, P. U., Liu, Z., Overpeck, J. T., Konecky, B., et al. (2014). Coherent changes of southeastern equatorial and northern African rainfall during the last deglaciation. *Science*, *346*(6214), 1223–1227. https://doi.org/10.1126/science.1259531

Pages, P. I. W. G. of. (2016). Interglacials of the last 800,000 years. *Reviews of Geophysics*, *54*(1), 162–219. https://doi.org/10.1002/2015RG000482

Parish, M. C., Du, X., Bijaksana, S., & Russell, J. M. (2023). A brGDGT-Based Reconstruction of Terrestrial Temperature From the Maritime Continent Spanning the Last Glacial Maximum. *Paleoceanography and Paleoclimatology*, *38*(3), e2022PA004501. https://doi.org/10.1029/2022PA004501

Powers, L. A., Johnson, T. C., Werne, J. P., Castañeda, I. S., Hopmans, E. C., Damsté, J. S. S., & Schouten, S. (2005). Large temperature variability in the southern African tropics since the Last Glacial Maximum. *Geophysical Research Letters*, *32*(8). https://doi.org/10.1029/2004GL022014

Russell, J. M., Vogel, H., Bijaksana, S., Melles, M., Deino, A., Hafidz, A., et al. (2020). The late quaternary tectonic, biogeochemical, and environmental evolution of ferruginous Lake Towuti, Indonesia. *Palaeogeography, Palaeoclimatology, Palaeoecology*, *556*, 109905. https://doi.org/10.1016/j.palaeo.2020.109905

Sarr, A.-C., Husson, L., Sepulchre, P., Pastier, A.-M., Pedoja, K., Elliot, M., et al. (2019). Subsiding Sundaland. *Geology*, *47*(2), 119–122. https://doi.org/10.1130/G45629.1

Schouten, S., Hopmans, E. C., & Sinninghe Damsté, J. S. (2013). The organic geochemistry of glycerol dialkyl glycerol tetraether lipids: A review. *Organic Geochemistry*, *54*, 19–61. https://doi.org/10.1016/j.orggeochem.2012.09.006

Seltzer, A. M., Ng, J., Aeschbach, W., Kipfer, R., Kulongoski, J. T., Severinghaus, J. P., & Stute, M. (2021). Widespread six degrees Celsius cooling on land during the Last Glacial Maximum. *Nature*, *593*(7858), 228–232. https://doi.org/10.1038/s41586-021-03467-6

Seltzer, A. M., Blard, P.-H., Sherwood, S. C., & Kageyama, M. (2023). Terrestrial amplification of past, present, and future climate change. *Science Advances*, *9*(6), eadf8119. https://doi.org/10.1126/sciadv.adf8119

Tierney, J. E., Russell, J. M., Huang, Y., Damsté, J. S. S., Hopmans, E. C., & Cohen, A. S. (2008). Northern Hemisphere Controls on Tropical Southeast African Climate During the Past 60,000 Years. *Science*, *322*(5899), 252–255. https://doi.org/10.1126/science.1160485

Tierney, J. E., Zhu, J., King, J., Malevich, S. B., Hakim, G. J., & Poulsen, C. J. (2020). Glacial cooling and climate sensitivity revisited. *Nature*, *584*(7822), 569–573. https://doi.org/10.1038/s41586-020-2617-x

Vuillemin, A., Mayr, C., Schuessler, J. A., Friese, A., Bauer, K. W., Lücke, A., et al. (2022). A one-million-year isotope record from siderites formed in modern ferruginous sediments. *GSA Bulletin*, *135*(1–2), 504–522. https://doi.org/10.1130/B36211.1

Zhao, B., Russell, J. M., Tsai, V. C., Blaus, A., Parish, M. C., Liang, J., et al. (2023). Evaluating global temperature calibrations for lacustrine branched GDGTs: Seasonal variability, paleoclimate implications, and future directions. *Quaternary Science Reviews*, *310*, 108124. https://doi.org/10.1016/j.quascirev.2023.108124

Zhou, X., Chen, Q., Xie, F., Li, J., Li, M., Ding, R., et al. (2019). Nonlinear response of Northern Hemisphere stratospheric polar vortex to the Indo–Pacific warm pool (IPWP) Niño. *Scientific Reports*, *9*(1), 13719. https://doi.org/10.1038/s41598-019-49449-7

Supporting Information

Drill core details

The temperature of the modern lake surface of Lake Towuti ranges from 30.5°C in March-May to 28.5° in August-October (Costa et al., 2015), when the upper 100 m of the water column undergo isothermal mixing (Costa et al., 2015). Site 1 was cored four times to capture a near-continuous sediment record back to ~1.1 million years ago (Ma), when accelerated tectonic subsidence created a permanent lake basin (Russell et al., 2020). The lithology has been described in detail in Russell et al. (2020), which characterizes the top ~100 mcd (mean composite depth) of the core as continuous lake sedimentation. The sediment primarily alternates between red and green clays, with a couple diatomaceous oozes at 32 and 45 mcd (Russell et al., 2020; Vuillemin et al., 2022). The pH of Lake Towuti is ~7.8 and the lake is ultraoligotrophic.

brGDGTs

To develop the temperature record, lipids were extracted using a DIONEX Accelerated Solvent Extractor and the polar fraction was isolated using silica and alumina gel chromatography. The brGDGT fraction was filtered through 0.45 μm PTFE filter in hexane: isopropanol (99:1) prior to analysis by atmospheric pressure chemical ionization/high-performance liquid chromatography mass spectrometry (APCI/HPLC-MS) based on methods in (Hopmans et al., 2016).

Radiocarbon

23 radiocarbon dates in the top 45-kyr of sediment were correlated from TOW-9 as described in Russell et al. (2020). The radiocarbon dates were calibrated to IntCal20 using Bacon (Blaauw & Christen, 2011).

Tephrochronology

There are three tephra that were dated directly or chemo-stratigraphically correlated to tephras of known age derived from the Tondano Caldera complex in North Sulawesi. The $^{40}Ar/^{39}Ar$ dating method was used to directly date sanidine crystals within the tephra at 72.95 mcd. Two samples were taken from this depth. The methods were described in detail Russell et al. (2020). In brief, ~100–250 μm crystals were hand-picked out of the 60 μm-sieved samples. The mineral concentrates were irradiated for one hour in the Oregon State University TRIGA reactor. The neutron fluence monitor was sanidine phenocrysts from the Alder Creek Rhyolite of California with an age of 1.1848 ± 0.0006 Ma (Niespolo et al., 2017). The crystals were analyzed using single-grain total fusion (SCTF) and single-grain incremental heating (SCIH), with a CO_2 laser as the heating instrument. At the Berkeley Geochronology Center, argon gas measurements were performed on a 5-collector Nu Instruments Noblesse noble-gas mass spectrometer operating in simultaneous ion-counting mode. The $^{40}Ar/^{39}Ar$ dating method resulted in an age of 797.3 ± 1.7 ka, corresponding to the Old Toba Tuff (Russell et al., 2020). Additional dates for Site 1 was provided by tephrachemistry for the tephras at 25.46 and 53.17 mcd.

Magnetic reversals

To add additional age constraints, we identified magnetic reversals in the Site 1 composite record. To identify the magnetic reversals, we looked for 180° reversals in the measured declination that occur during magnetic intensity lows. Magnetic intensity lows were identified by measuring natural remanent magnetization (NRM) and anhysteretic remanent magnetization (ARM) in u-channels from the Site 1 cores. Following the methods used for IDLE-TOW10-9B by Kirana et al. (2018) we used the ratio of NRM to ARM after alternating field demagnetization to a peak field of 20 mT (NRM20mT/ARM20mT) because it best reflects the strength of the geomagnetic field. We looked for the reversals in declination with a demagnetization to a peak field of 20 mT (Dec20mT) to identify the 180° reversals. We looked for the reversals in Dec20mT in multiple holes (Hole E and Hole F) to avoid problems associated with core breaks (Figure S1). We only used cores recovered with the hydraulic drill, not an alien corer, to avoid possible rotations within a core section.

Two magnetic reversals were detected in the composite record: the oldest at 90.31 mcd, where Dec20mT goes from 100 to 360° in core F and 345 to 59° in core E (Figure S1), and the youngest at 72.2 mcd, where Dec20mT goes from 341 to 176° in core 1F (Figure S1). The reversal at 72.2 mcd is also detected in core 1E, where Dec20mT goes from 260 to 86°. The reversal at 72.20 mcd is stratigraphically close to the Oldest Toba Tuff at 72.93 mcd, which was dated directly using $^{40}Ar/^{39}Ar$ (Russell et al., 2020). The proximity of this reversal to the Oldest Toba Tuff is consistent with as the Brunhes-Matuyama reversal at 778.0 ± 5.0 ka (Mark et al., 2017). The reversal at 90.31 mcd likely corresponds to the Matuyama-Jaramillo reversal at 990 ± 4 ka (Channell et al., 2020).

Tie points

After generating a preliminary age model for the Site 1 composite using the radiocarbon ages, magnetic reversals, and tephras, we found a strong 100-kyr cycle in the brGDGT-inferred temperatures. Based on this finding, we added tie points between the Towuti temperature reconstruction and a IPWP SST stack (Clark et al., 2024), using the radiocarbon, tephra, and magnetic reversal ages as guides. We selected 32 tie points between only the most obvious peaks and troughs, and assigned a 3-kyr uncertainty given the uncertainty of the IPWP SST stack (Table S1).

Table S1 – Ages used in the age model.

labID	age	error	depth
TOW91	930	25	19
TOW92	2150	25	45
TOW93	3460	30	86
TOW94	5730	35	124
TOW95	6700	35	175
TOW96	7980	40	221
TOW97	9180	50	250
TOW98	11460	45	274
TOW99	13490	65	326
TOW100	14500	70	369
TOW101	16760	90	412
TOW102	17600	70	447
TOW103	19440	80	490
TOW104	20740	150	521
TOW105	22730	220	566
TOW106	24920	240	616
TOW107	28300	230	692
TOW108	27400	180	731
TOW109	30400	140	772
TOW110	35580	420	806
TOW111	36580	620	850
TOW112	38370	360	936

TOW113	41060	1000	969
Tie1	85000	3000	1407.5
Tie2	106000	3000	1679
Tie3	121000	3000	2025
Tie4	157000	3000	2282
Tephra correlation	173500	4000	2546
Tie5	201000	3000	2661.5
Tie6	211000	3000	2825.75
Tie7	230000	3000	2927.25
Tie8	241000	3000	3134.5
Tie9	251000	3000	3185.5
Tie10	319000	3000	3746
Tie11	326000	3000	3776.83
Tie12	346000	3000	4025.83
Tie13	418000	3000	4557.17
Tie14	436000	3000	4749.5
Tie15	442000	3000	4821
Tie16	450000	3000	5062.5
Tephra correlation	471000	6000	5317
Tie17	488000	3000	5423.5
Tie18	511000	3000	5542.83
Tie19	526000	3000	5635.5
Tie20	546000	3000	5767.25
Tie21	608000	3000	6192.75
Tie22	645000	3000	6434.25
Tie23	684000	3000	6505.5
Tie24	700000	3000	6678.5
Tie25	724000	3000	6773
Tie26	742000	3000	6837.67
Brunhes-Matuyama Reversal	783400	5000	7220
$^{40}Ar/^{39}Ar$	797300	1700	7293
Tie27	840000	3000	7714.5
Tie28	855000	3000	7880.17
Tie29	877000	3000	8056.2
Tie30	901000	3000	8127
Tie31	921000	3000	8301.67
Tie32	956000	3000	8521
Matuyama-Jaramillo Reversal	990000	4000	9031

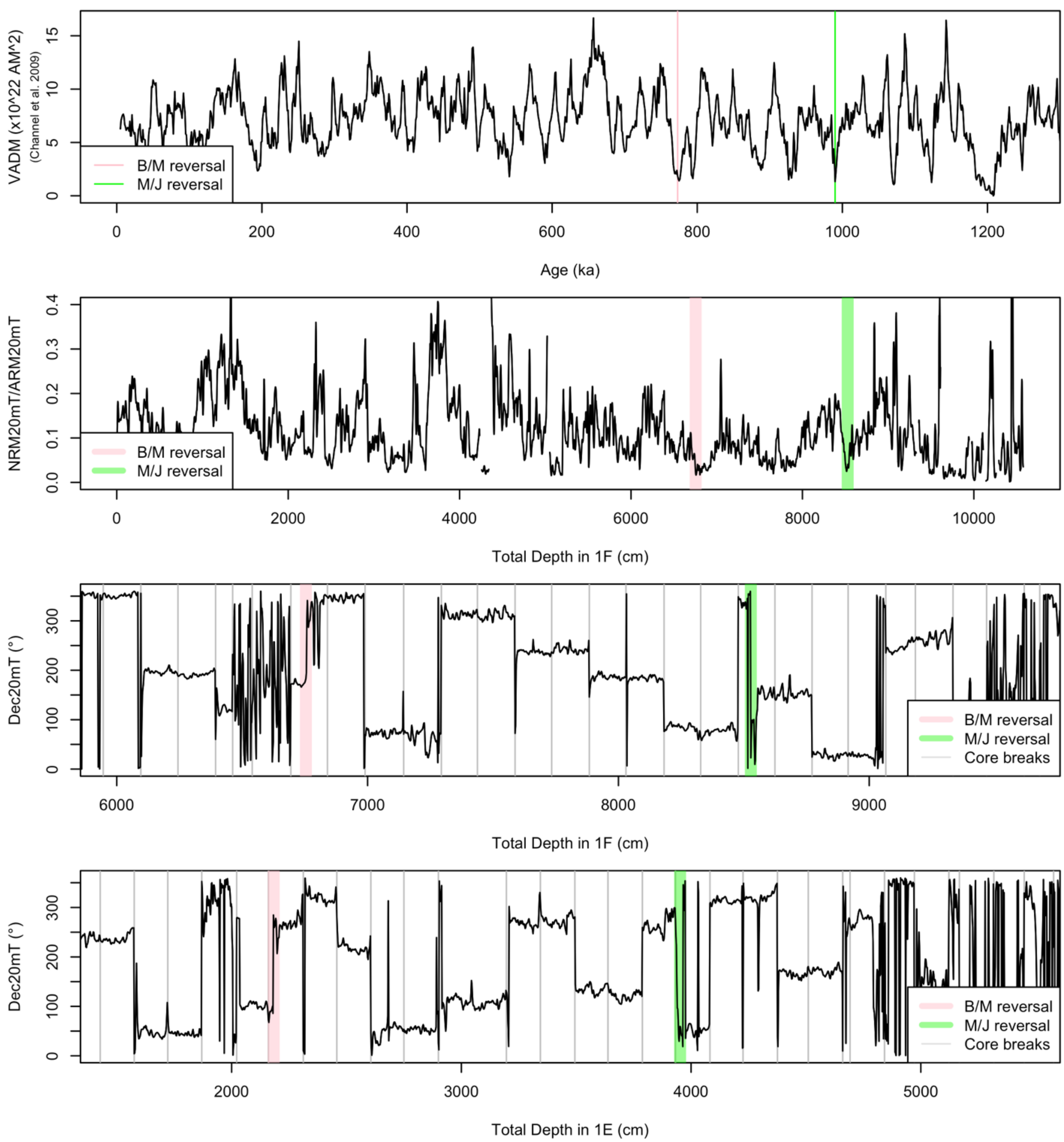

Figure S1 – The top panel shows a global stack of relative paleointensity expressed as virtual axial dipole moment (VADM). The second from the top panel shows NRM20mT divided by ARM20mT in core F and the location of the Brunhes-Matuyama and the Matuyama-Jaramillo reversals. The bottom panels show Dec20mT in cores F and E and the locations of the reversals and core breaks.

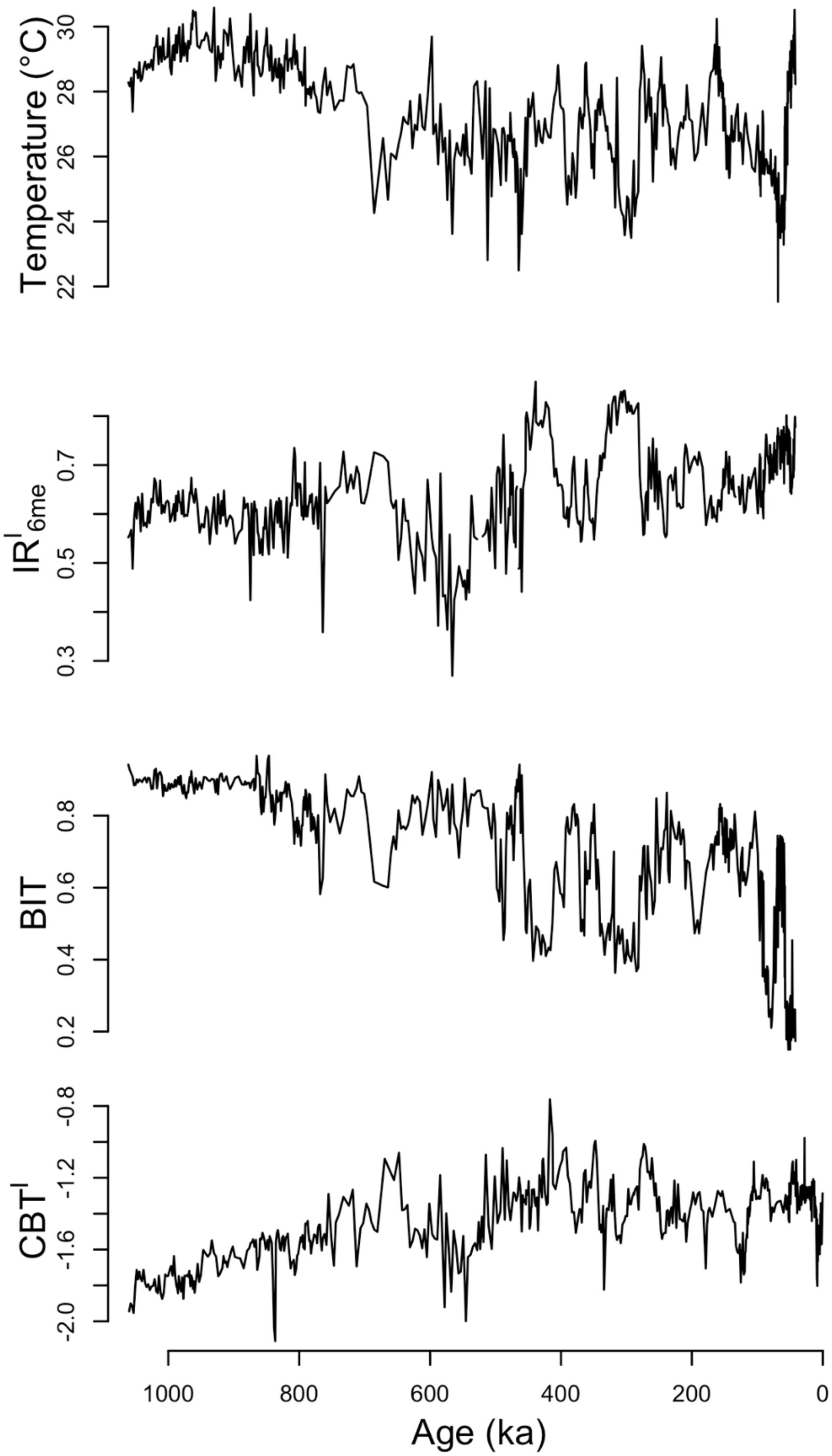

Figure S2 – Lake Towuti temperature, IR'$_{5me}$, BIT, and CBT'.

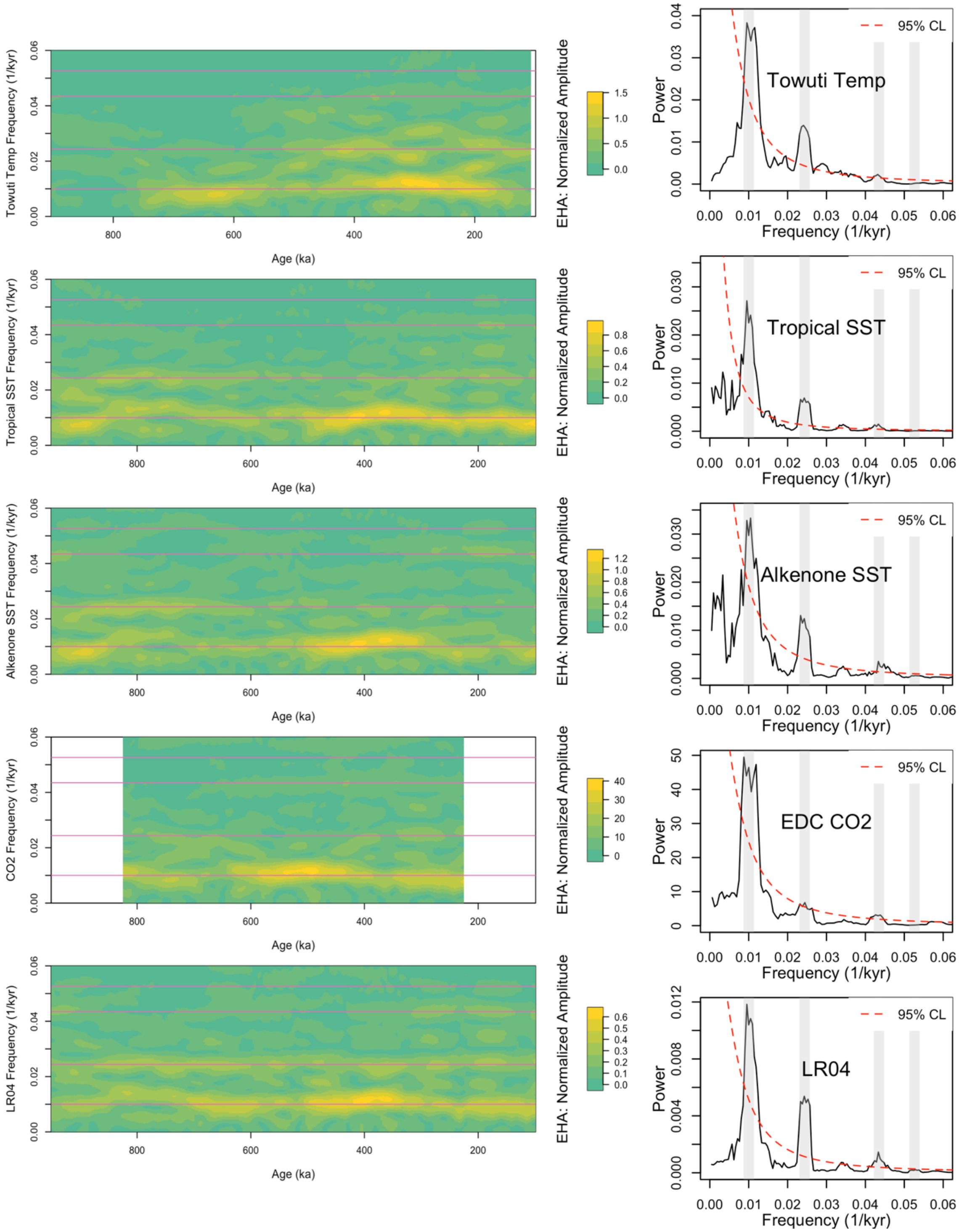

Figure S2 – EHA and mtm of the Towuti temperature reconstruction, the tropical SST stack (Clark et al., 2024), the alkenone-based tropical SST stack (Herbert et al., 2010), Antarctic CO2 (Bereiter et al., 2015) and LR04 (Lisiecki and Raymo, 2005).

CHAPTER 5

A 1-Myr record of Maritime Continent hydroclimate

M. C. Parish[1], J. M. Russell[1], H. Vogel[2], S. Bijaksana[3], A. Wilk[1,4], and G. Traietti[1]

[1]Department of Earth, Environmental, & Planetary Sciences, Brown University, Providence, RI, USA.

[2]Institute of Geological Sciences & Oeschger Centre for Climate Change Research, University of Bern, Bern, Switzerland.

[3]Global Geophysics Group, Faculty of Mining and Petroleum Engineering, Institut Teknologi Bandung, Bandung, Indonesia.

[4]Department of Earth, Geographic, and Climate Sciences University of Massachusetts Amherst, Amherst, MA, USA.

Abstract

The past one million years encompasses major changes in the Earth's glacial-interglacial cycles, with a shift from 41- to 100-kyr cycles in ice volume and temperature during the Mid-Pleistocene Transition (MPT). This was followed by an increase in temperature and CO_2 during interglacial periods across the Mid-Brunhes Transition (MBT). These reorganizations of the Earth's climate and carbon cycle provide natural experiments to test the impacts of CO_2 on tropical rainfall and water resources, yet their impacts on tropical hydroclimate are largely unknown. We produced long, orbitally-resolved hydroclimate and vegetation reconstructions to uncover the evolution of hydroclimate and its primary climate forcing mechanisms in the Maritime Continent (MC), a region with global importance through transport of heat to higher latitudes. We show that the MC experienced hydroclimatic stability during a period of stable, warm temperature prior to the MBT, followed by increasing orbital-scale instability as interglacial CO_2 concentrations rose after the MBT, suggesting strong sensitivity to climate warming. We observe prominent 41-kyr cycles in rainfall, suggesting an important role for ice volume and/or greenhouse gas concentrations in controlling precipitation in the MC. Insolation has long been presumed as the dominant forcing of hydroclimate in the tropics, yet our data point to temperature and glacial-interglacial cycles as the primary forcing of MC hydroclimate.

1. Introduction

The energy export associated with intense convection in the Indo-Pacific Warm Pool (IPWP) gives the region its title of Earth's Heat Engine (De Deckker, 2016). Despite the region's global significance, consensus on the long-term controls on IPWP hydroclimate has not been reached. Existing studies have largely focused on changing terrestrial precipitation during the last deglaciation, when CO_2 increased from 195 ppm at the Last Glacial Maximum (LGM) to 275 ppm during the Holocene (Marcott et al., 2014), yet the primary patterns of rainfall and their associated forcings are disputed even over this short and relatively well-characterized interval. This uncertainty limits our understanding of the role of IPWP convection in global climate change, and our ability to test the results of paleoclimate models to inform our understanding of Maritime Continent (MC) future climates.

Most terrestrial hydroclimate records in the MC indicate the LGM was drier than modern (Parish et al., 2024), including speleothems (Ayliffe et al., 2013; Carolin et al., 2016; M. L. Griffiths et al., 2009; Michael L. Griffiths et al., 2013; Krause et al., 2019; Partin et al., 2007), leaf wax carbon isotopes (Dubois et al., 2014; Y. Ruan et al., 2020; Ruan et al., 2019; Russell et al., 2014; Wicaksono et al., 2015; Windler et al., 2021), pollen (van der Kaars et al., 2001, 2010), lake level (Vogel et al., 2015), and other geochemical records (Costa et al., 2015; Russell et al., 2014). Multiple climate model simulations of LGM climate also show drier conditions than during the Holocene (DiNezio et al., 2016, 2018; DiNezio & Tierney, 2013; Du et al., 2021). Many different mechanisms are hypothesized to have caused this relative drying compared to the Holocene, including local seasonal insolation (Carolin et al., 2016), Sunda and Sahul shelf exposure (DiNezio et al., 2016, 2018; DiNezio & Tierney, 2013; Krause et al., 2019; Windler et al., 2020, 2021), Northern Hemisphere ice sheet expansion (Russell et al., 2014), and greenhouse gas (GHG) concentrations (Mohtadi et al., 2017; Russell et al., 2014), but disentangling these forcings over a single glacial termination has proven difficult. There are few hydroclimate proxy records from the MC that span multiple glacial-interglacial cycles, and they also suggest conflicting dominant hydroclimate controls. A Sumatra δ^2H_{wax} record indicates sensitivity to shelf exposure (Windler et al., 2020), whereas Borneo $\delta^{18}O$ speleothem records appear responsive to local insolation (Carolin et al., 2016). Neither record captures glacial cycles before the Mid-Pleistocene Transition (MPT), when glacial-interglacial cycles transitioned from symmetrical, 41-kyr cycles to sawtooth-shaped, 100-kyr cycles at ~950 ka (Herbert, 2023), and only the Borneo speleothem record spans the Mid-Brunhes Transition (MBT) at ~430 ka, which marks the beginning of higher amplitude glacial-interglacial changes in CO_2 (Barth et al., 2018). Both the MPT and the MBT provide experiments to test how the MC responds to major reorganizations of glacial-interglacial cycles, while orbital forcings continuously oscillate.

To determine the dominant forcing mechanisms controlling MC hydroclimate on glacial-interglacial timescales, we produced leaf wax δ^2H (δ^2H_{wax}) and $\delta^{13}C$ ($\delta^{13}C_{wax}$) records, as proxies for hydroclimate and vegetation (Chikaraishi & Naraoka, 2003; Dansgaard, 1964), using long-chain n-alkanes preserved in a sediment drill-core from Lake Towuti, Sulawesi, Indonesia. The Lake Towuti sediment record continuously spans the past 1.1 Myr and has high-enough sedimentation rates to produce a ~3-kyr sampling resolution to capture orbital-scale hydroclimatic variability (Parish et al., in prep.; Russell et al., 2020). Lake Towuti's precipitation is regionally representative of MC precipitation (Konecky et al., 2016; Figure 1), allowing us to determine the controls on MC hydroclimate on orbital timescales based on the 1 Myr records of δ^2H_{wax} and $\delta^{13}C_{wax}$ from Lake Towuti.

2. Study site

Lake Towuti is a 560 km^2 lake located near the equator (2.75°S, 121.5°E) in central Sulawesi, Indonesia, a 174,600 km^2 island in the center of the IPWP. Lake Towuti receives ~2700 mm of precipitation per year, and has a ~1644 km^2 watershed (Konecky et al., 2016; Russell et al., 2020). The majority of precipitation falls from November to May during the Australian-Indonesian summer monsoon season with over 180 mm of precipitation per month and a northeast moisture source (Konecky et al., 2016). The dry season from August to October has a southeast moisture source (Konecky et al., 2016; Parish et al., 2024). The composite record from Lake Towuti consists of drill cores recovered from Site 1 in the central basin of Lake Towuti during the Towuti Drilling Project in 2015. Cores from four holes were recovered from Site 1 to capture a near-continuous sediment record back to 1.1 Ma (Russell et al., 2020). The age model for the Site 1 composite record includes 23 radiocarbon dates in the top 45-kyr of sediment, two magnetic reversals, three tephras, and 32 tie points between the Towuti temperature reconstruction and tropical SST (Parish et al., in prep). The age model is described in detail in Parish et al. (in prep).

3. Methods

We sampled at a mean resolution of 2.7 kyr, with a minimum of 0.1 kyr and a maximum of 10.5 kyr. The most recent 30 kyr of samples are from IDLE10-TOW9B with a mean sampling resolution of 0.5 ka, and the δ^2H_{wax} and $\delta^{13}C_{wax}$ records were previously published in Parish et al. (2024). In the MC, δ^2H_{wax} reflects precipitation amount, moisture transport and source, and convergence/divergence (Konecky et al., 2016, 2019). The combination of these processes creates ^{2}H-depletion in wetter climates on orbital timescales (Parish et al., 2024). MC δ^2H_{wax} records from the last deglaciation show a widespread shift to ^{2}H-depleted waxes as precipitation increased over the MC during the last deglaciation (Parish et al., 2024), suggesting δ^2H_{wax} is sensitive to the amount effect on the MC like observed in other tropical regions (Dansgaard, 1964). $\delta^{13}C_{wax}$ records reflect the ratio of C_3 to C_4 plants and the leaf-gas exchange efficiency related to moisture stress (Diefendorf et al., 2010; Sachse et al., 2012). Increased dry season precipitation can cause a shift to more C_3 plants, which are more ^{13}C-depleted than C_4 plants

(Chikaraishi & Naraoka, 2007). Increased precipitation also leads to greater fractionation of carbon isotopes as water use efficiency decreases (Diefendorf et al., 2010). Taken together, ^{13}C-depletion indicates increased precipitation. During the last deglaciation, $\delta^{13}C_{wax}$ records from the MC largely reflect a decrease in C_4 plants in response to a wetter dry season that can support C_3 plant (Dubois et al., 2014), and subsequent increases in precipitation and CO_2, which continued to cause ^{13}C-depletion (Parish et al., 2024).

Lipids were extracted from sediments using a DIONEX Accelerated Solvent Extractor using dichloromethane:methanol (9:1). The lipid extract was divided into neutral and acid fractions using dichloromethane:isopropanol (2:1) and ethyl ether:acetic acid (96:4) over an aminopropyl silica gel column. To isolate *n*-alkanes, we used silica gel columns to separate lipids within the neutral fraction, using hexane to isolate *n*-alkanes. We used silver nitrate-impregnated silica gel columns to remove unsaturated compounds (Garelick et al., 2021; Ruan et al., 2019). We quantified the abundance of C_{29}, C_{31}, C_{33} *n*-alkanes using a gas chromatography flame ionization detector (GC-FID), and measured δ^2H and $\delta^{13}C$ of C_{29}, C_{31}, and C_{33} *n*-alkanes using a gas chromatography isotope ratio mass spectrometer (GC-IRMS). δ^2H was measured in triplicate and $\delta^{13}C$ was measured in duplicate on an Agilent 6890 GC with an HP1-MS column (30 m × 0.25 mm × 0.25 μm), coupled to a Thermo Delta Plus XL IRMS with a reactor temperature of 1425 °C for hydrogen and 1000°C for carbon. A mixture of *n*-alkane standards from Arndt Schimmelmann (Indiana University) was injected every six samples to test for instrument drift and was used to correct the measured values to Vienna Standard Mean Ocean Water (VSMOW). The H3 factor was ~2 and stable during the analyses, suggesting no or minimal fluctuation in IRMS performance. Measured isotopic values were accepted if the voltage was between 3 and 8 V. δ^2H is corrected for ice volume's impact on the isotopic composition of seawater, by scaling the global benthic stack (Lisiecki & Raymo, 2005) to a 1‰ change during the LGM (Schrag et al., 1996).

To determine the controls on MC hydroclimate, we analyzed the dominant spectral frequencies of the entire 1.1 Myr δ^2H_{wax} and $\delta^{13}C_{wax}$ records. Using these methods does not allow us to differentiate between ice volume and GHG forcing because the dominant spectral frequencies of ice volume and GHG concentrations are similar, and the structure of the full-length records are similar as well (Bereiter et al., 2015; Lisiecki & Raymo, 2005; McGrath et al., 2021).

4. Results

The mean CPI_{27-31} of all samples is 3.4, with a maximum of 17.4 and minimum of 1.1 (Figure S1). Since samples with a CPI of 1 may indicate oil, we tested the impact of removing samples with a CPI_{27-31} less than 2, and determined that the structure of the records is not significantly impacted by the inclusion of samples with low CPI_{27-31} values (Figure S2). Additionally, neither CPI nor average chain length are strongly correlated with δ^2H_{wax} (R = -0.28, and R = -0.16, respectively) or $\delta^{13}C_{wax}$ (R = -0.25, and R = -0.12, respectively). We therefore conclude that δ^2H_{wax} and $\delta^{13}C_{wax}$ are relatively unaffected by wax source. We focus are analysis on C_{31} alkanes because they were the most abundant in most samples, but C_{29} alkanes were also analyzed and have nearly identical values (Figure S3).

The Lake Towuti δ^2H_{wax} record indicates low variability from 1.05 Ma until ~430 ka (Figure 2a). The largest fluctuations occur from ~430 ka to ~300 ka, when there are large shifts to ^2H-enrichment during glacial periods (MIS10 and MIS12). Multi-taper spectral analysis reveals significant peaks at 41- and 100-kyr (Figure 2b). Evolutive harmonic analysis shows that the 41-kyr peak emerges at ~430 ka, when the variability in the record increases (Figure 2c), and dissipates around 300 ka. The 100-kyr peak intensifies around ~430 ka in the δ^2H_{wax} record (Figure 2c). The emergence of the 41-kyr periodicity coincides with the emergence of the 41-kyr periodicity in the Lake Towuti temperature reconstruction (Figure 2i; Parish et al., in prep), whereas the emergence of the 100-kyr periodicity in δ^2H_{wax} lags the emergence of 100-kyr temperature cycles by ~300 kyr. There are not significant 19- or 21-kyr cycles in the record.

Like the Lake Towuti δ^2H_{wax} record, $\delta^{13}C_{wax}$ from Lake Towuti is relatively stable prior to ~430 ka and less stable after, but the variability continues to increase towards present (Figure 2d). The record has significant 23- and 41-kyr peaks, but the 100-kyr peak is not significant (Figure 2e). However, in evolutive harmonic analysis, a 100-kyr peak is evident for almost the entire record (Figure 2f). The 41-kyr peak does not emerge until ~250 ka and persists until present. Towuti $\delta^{13}C_{wax}$ shows a slight trend to more ^{13}C-enriched over the past 1-Myr (Figure 4). This trend is even more apparent in the $\delta^{13}C_{wax}$ records from offshore Sumatra and the Andaman Sea (Figure 4; McGrath et al., 2023; Windler et al., 2019). This gradual shift towards more ^{13}C-enirched likely reflects gradual drying in the greater MC region.

5. Discussion

5.1 Long-term trends in MC hydroclimate

The MPT (950 ka) and the MBT (430 ka) represent major reorganizations of the Earth's glacial-interglacial cycles. Analysis of the dominant spectral frequencies of the Lake Towuti δ^2H_{wax} and $\delta^{13}C_{wax}$ records across these transitions allow tests of the forcings of MC hydroclimate and their dependence on the changing state of glacial cycles. Our data suggest that climate has gradually dried over the last 1 Ma, as global and regional climate cooled (Clark et al., 2024; Parish et al., in prep). The Towuti $\delta^{13}C_{wax}$ record shows a 100-kyr cycle for most of the past 1 million years with increased variability after ~250 ka, and the δ^2H_{wax} record documents strong orbital variability after ~430 ka. We see little change across the MPT, and the stability early in the Towuti record is unlike speleothem and some loess records from Asia, which indicate wet/dry cycles throughout the past ~650 kyr (Cheng et al., 2016) and 1 million years, respectively (Sun et al., 2019). The increased variability suggests MC hydroclimate is sensitive to the increasing amplitude of glacial-interglacial changes in CO_2 during the past 1-Myr.

5.2 Insolation

Insolation is often invoked as the dominant driver of tropical precipitation (Cheng et al., 2012), and has been invoked to explain precipitation variations in Borneo (Carolin et al., 2016). The lack of precession cycles in the Towuti δ^2H_{wax} record suggests local insolation, which is dominated by orbital precession, is not a dominant driver of MC precipitation. A δ^2H_{wax} record from offshore Sumatra also does not have dominant precession cycles (Windler et al., 2021), supporting the inference that insolation is not a primary forcing of hydroclimate in the MC. The lack of precession cycles also suggests a limited impact of the east Asian Monsoon, as speleothem records of the east Asian Monsoon are dominated by precession cycles (Cheng et al., 2016). It should be noted, runoff records from east China do not exhibit the 19-23-kyr cycles of insolation, raising concerns about the speleothem records as monsoon recorders (Clemens et al., 2018). Overall, our data challenge the theory that precession dominates MC precipitation, as observed in higher-latitude monsoon records (Cheng et al., 2012).

A speleothem record from northern Borneo indicates that local precipitation tracks local September-November insolation, potentially by modulating the strength of Walker Circulation over the tropical Pacific (Carolin et al., 2016). Precipitation in central Sulawesi is also highly sensitive to changes in the strength of the Walker Circulation, and the absence of this signal suggests that the impacts of insolation on precipitation in Northern Borneo are modulated by other processes. Indeed, northern Borneo has a different precipitation regime than most of the MC (Aldrian & Dwi Susanto, 2003) and is sensitive to different climate forcings. Monthly precipitation measured at Lake Towuti from 2013-2016 is positively correlated with monthly precipitation in the majority of the MC, but Lake Towuti is not correlated with northern Borneo monthly precipitation (Figure 1). That said, there are weak, but significant, 21- and 23-kyr cycles detected in the Lake Towuti $\delta^{13}C_{wax}$ record (Figure 2e), which may indicate vegetation is sensitive to insolation through its impact on the seasonality of precipitation. Wetter dry seasons can increase the percentage of C_3 plants, leading to ^{13}C-depletion (Dubois et al., 2014; Parish et al., 2024). The precession cycles in $\delta^{13}C_{wax}$ may suggest insolation plays a role in determining the seasonality of precipitation on the MC, without playing a dominant role determining annual precipitation as was observed during the last deglaciation (Parish et al., 2024).

5.3 Shelf exposure

The exposure of the Sunda, Sahul, and Australian continental shelves during the LGM is thought to have weakened the Indian Ocean Walker circulation and caused decreased precipitation over the MC, impacting regions as far afield as tropical Africa (DiNezio et al., 2016, 2018; DiNezio & Tierney, 2013; Du et al., 2021). Model agreement with hydroclimate proxy records indicating drying at the LGM also provide support for shelf exposure controlling MC hydroclimate on glacial-interglacial timescales (DiNezio et al., 2018). Lake Towuti $\delta^{2}H_{wax}$ shows slight ^{2}H-enrichment during some glacial periods (Figure 3b), and isotopic enrichment during glacial periods in an offshore Sumatra $\delta^{2}H_{wax}$ and northern Borneo speleothem $\delta^{18}O$ record suggests decreased precipitation as a possible response to shelf exposure (Carolin et al., 2016; Windler et al., 2021). However, the water isotope records in the MC show isotopic enrichment during glacial periods prior to the first submersion of the continental shelves (Carolin et al., 2016; Windler et al., 2019) which occurred between 400 and 250 ka (Sarr et al., 2019). Assuming this timing is correct, other glacial-interglacial forcings must impact hydroclimate in the MC prior to the exposure/inundation cycles.

The Towuti $\delta^{13}C_{wax}$ record shows a clear shift to ^{13}C-enrichment, indicating more C_4 plants, during the last two glacial periods (MIS 2 and MIS 6). There are also smaller amplitude shifts toward ^{13}C-enrichment during preceding glacial periods, which could reflect more C_4 plants or increased leaf-gas exchange efficiency related to decreased moisture and/or CO_2 (Diefendorf et al., 2010; O'Mara et al., 2022; Parish et al., 2024). The high amplitude shifts to increased C_4 plants during glacial periods may indicate dry seasons became dry enough to give C_4 plants an advantage during the last two glacial periods (Dubois et al., 2014; Parish et al., 2024; Windler et al., 2019). These C_4 expansions could suggest that shelf exposure impacted the strength of the dry season enough to allow grassland expansion, as the timing of the high-amplitude ^{13}C-enrichments postdates the onset of shelf emergence-submergence cycles. $\delta^{13}C_{wax}$ records from offshore Sumatra and from the Andaman Sea also show substantial grassland expansion during the two most recent glacial periods, interpreted to reflect shelf exposure (McGrath et al., 2023; Windler et al., 2019). However, the shelf was exposed for a prolonged interval prior to MIS 7. McGrath et al. (2023) suggested that grasses were sourced from shelf area exposed by lowered sea level during glacial periods, and only the most recent two glacial periods show definitive evidence of grassland expansion because the continental shelves first submerged around ~250 ka (McGrath et al., 2023; Sarr et al., 2019). Lake Towuti receives leaf waxes from its hydrological basin and does not receive leaf waxes from exposed shelf area. Therefore, Lake Towuti likely only shows C_4 expansion when dry season precipitation is low enough to favor C_4 plants in the lake's watershed.

Although the Lake Towuti $\delta^{13}C_{wax}$ record shows the most extreme ^{13}C-enrichment during the two most recent glacial periods, similar to the offshore Sumatra and Andaman Sea $\delta^{13}C_{wax}$ records, the duration of the isotopic excursions in the Towuti record are shorter than in the other records. The shorter duration of the excursion at Towuti could be an artefact of our age model, but could also reflect different leaf wax source areas, with Towuti only receiving leaf waxes from its watershed and not the continental shelf. Alternatively, the short duration of the extreme ^{13}C-enrichment could indicate changes in precipitation at different times at each site. Indeed, a transient model simulation of the last deglaciation indicates widespread drying over the MC when sea level falls more than 80 meters, suggesting widespread drought only during the coldest intervals of recent glacial cycles.

However, shelf exposure cannot explain the gradual trend towards ^{13}C-enrichment during the past 1-Myr observed in Towuti $\delta^{13}C_{wax}$ nor can it explain the presence of 100-kyr cycles prior to the first shelf inundation. A gradual hydrologic shift caused by shelf exposure is difficult to explain given that Sunda Shelf was likely permanently exposed prior to 400 ka, which should have caused persistent drying and ^{13}C-enrichment prior to the first inundation. The Towuti $\delta^{13}C_{wax}$ record is more ^{13}C-depleted prior to 400 ka (Figure 4) and the $\delta^{13}C_{wax}$ records from offshore Sumatra and the Andaman Sea also show a gradual shift to ^{13}C-enrichment across the entirety of the records, 650 and 450 kyr, respectively (Figure 4; McGrath et al., 2023; Windler et al., 2019). Decreasing temperature since 1 Ma, and its impacts on the strength of convection and MC rainfall, could potentially cause the long-term trend towards ^{13}C-enrichment indicated in the records (Figure 2; Liu and An, 2020). Shelf exposure during the last two glacial periods may have amplified ^{13}C-enrichment, but long-term trends and 100-kyr cycles prior to the submersion of the continental shelves point to global ice volume and GHG concentrations as important forcings of MC hydroclimate.

5.4 Global ice volume and GHG concentrations

Remote forcing by the large Northern Hemisphere ice sheets and radiative forcing by GHGs, which vary on ~41- and ~100-kyr cycles, are additional proposed forcings of MC hydroclimate. The 41-kyr cycle is statistically significant in the Towuti δ^2H_{wax} and $\delta^{13}C_{wax}$ records (Figure 2). The cycle emerges at ~430 ka in the δ^2H_{wax} record and ~250 ka in the $\delta^{13}C_{wax}$ record (Figure 2), and its presence in our records suggests that ice volume and/or GHG concentrations play an important role controlling MC precipitation. After the MBT (~430 ka), interglacial CO_2 gradually increases (Barth et al., 2018). In the evolutive harmonic analysis of the δ^2H_{wax} and $\delta^{13}C_{wax}$ records, 41- and 100-kyr cycles emerge around ~430 ka, providing further support for CO_2 as a primary driver of MC hydroclimate. 41- and 100-kyr cycles are significant in the Towuti temperature record (Parish et al., in prep) in addition to being significant in the Towuti δ^2H_{wax} and $\delta^{13}C_{wax}$ records (Figure 2). Cross-wavelet spectral analysis indicates that the Towuti δ^2H_{wax} and $\delta^{13}C_{wax}$ are highly coherent with Towuti Temperature in the 41-kyr and 100-kyr bands, with 100-kyr coherence between $\delta^{13}C_{wax}$ and temperature emerging at the end of the MPT and the 41-kyr coherence appearing during the MBT for both δ^2H_{wax} and $\delta^{13}C_{wax}$ (Figure 5). The high coherence between Towuti temperature and δ^2H_{wax} and $\delta^{13}C_{wax}$, may suggest that terrestrial temperature, hydroclimate, and vegetation are all strongly impacted by the same forcing(s), and that terrestrial temperature is likely an important driver of terrestrial hydroclimate and vegetation. During the last deglaciation, analysis of a temperature reconstruction from Lake Towuti indicated that temperature change is driven by varying CO_2 concentrations (Parish et al., 2023). This, combined with the spectral coherence of temperature and our wax records, supports the hypothesis that GHG concentrations strongly influence hydroclimate and vegetation on the MC. The Lake Towuti hydroclimate records add evidence to support precipitation in the MC being predominantly controlled by GHG concentrations.

6. Conclusions

Hydroclimate and vegetation are relatively stable in the Lake Towuti records prior to the MBT, suggesting that the MC did not experience the consistent instability with frequent periods of aridity like observed in other areas of the tropics. The minimal precession forcing indicated in the MC suggests hydroclimate is not dominantly controlled by local insolation, but rather suggests precipitation is sensitive to the forcings of ice volume and/or GHG concentrations. The onset of shelf exposure cycles may have influenced the large shifts in vegetation, but the long-term trends in hydroclimate do not match the climate changes predicted by shelf inundation. Strengthened δ^2H_{wax} and $\delta^{13}C_{wax}$ variability during the MBT and the coherence of δ^2H_{wax} and $\delta^{13}C_{wax}$ with temperature at Lake Towuti both point to CO_2 as a primary forcing of hydroclimate and vegetation during the past 1 Myr.

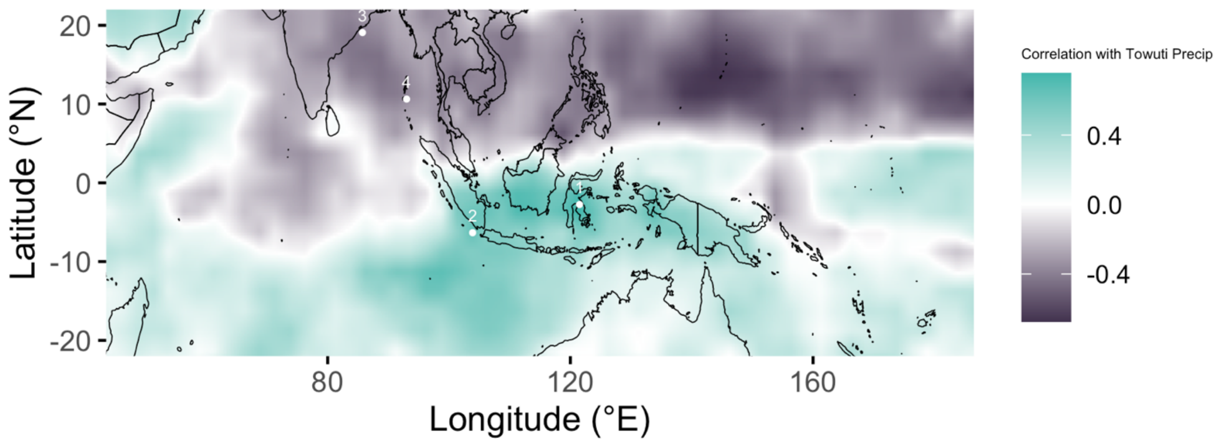

Figure 1 – Locations of (1) Lake Towuti, (2), MD98-2152 (Windler et al., 2019), (3) U1446 (McGrath et al., 2021), and (4) U1448 (McGrath et al., 2023). Field correlation of the monthly precipitation measured at Lake Towuti from March 2013-August 2016 with monthly precipitation from The Global Precipitation Climatology Project (GPCP) monthly precipitation (Adler et al., 2018). Precipitation and the digital elevation models are plotted using the "raster" package in R (Hijmans et al., 2022).

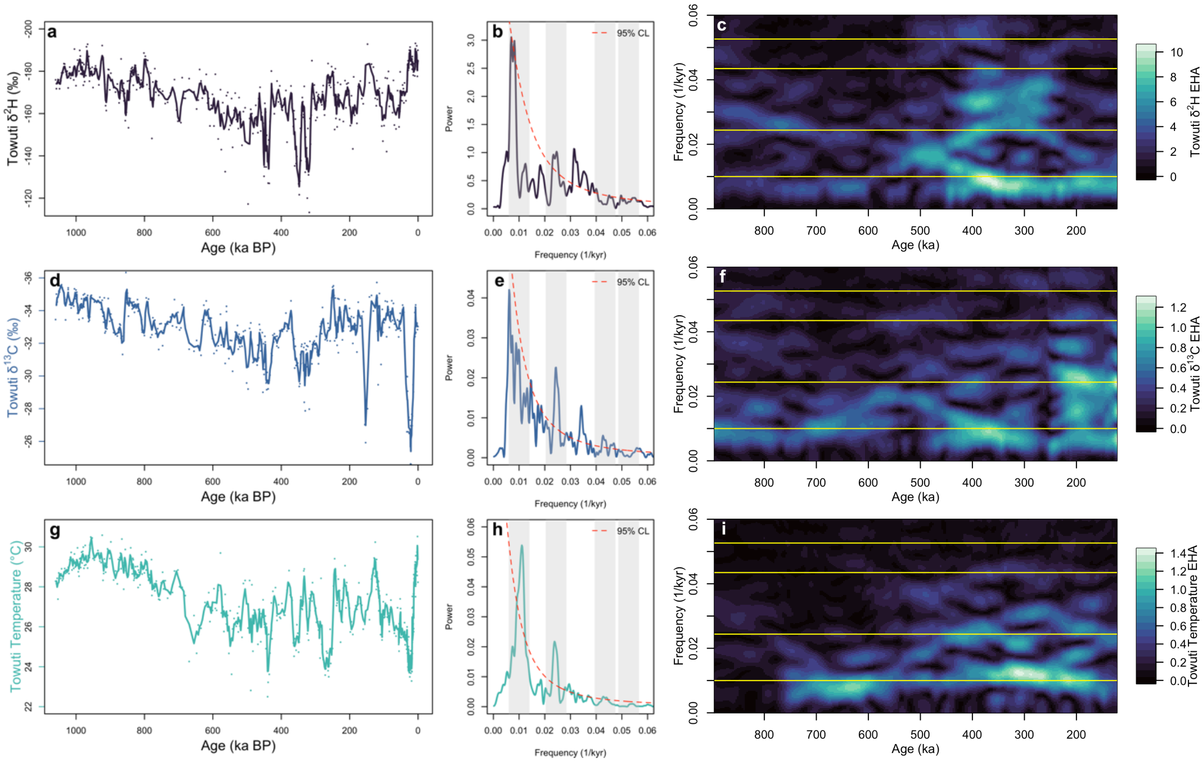

Figure 2 – (a) Lake Towuti δ^{2}H$_{wax}$, (b) multi-taper spectral analysis, and (c) evolutive harmonic analysis (EHA). (d) Lake Towuti δ^{13}C$_{wax}$, (e) multi-taper spectral analysis, and (f) EHA. (g) Lake Towuti temperature, (h) multi-taper spectral analysis, and (i) EHA.

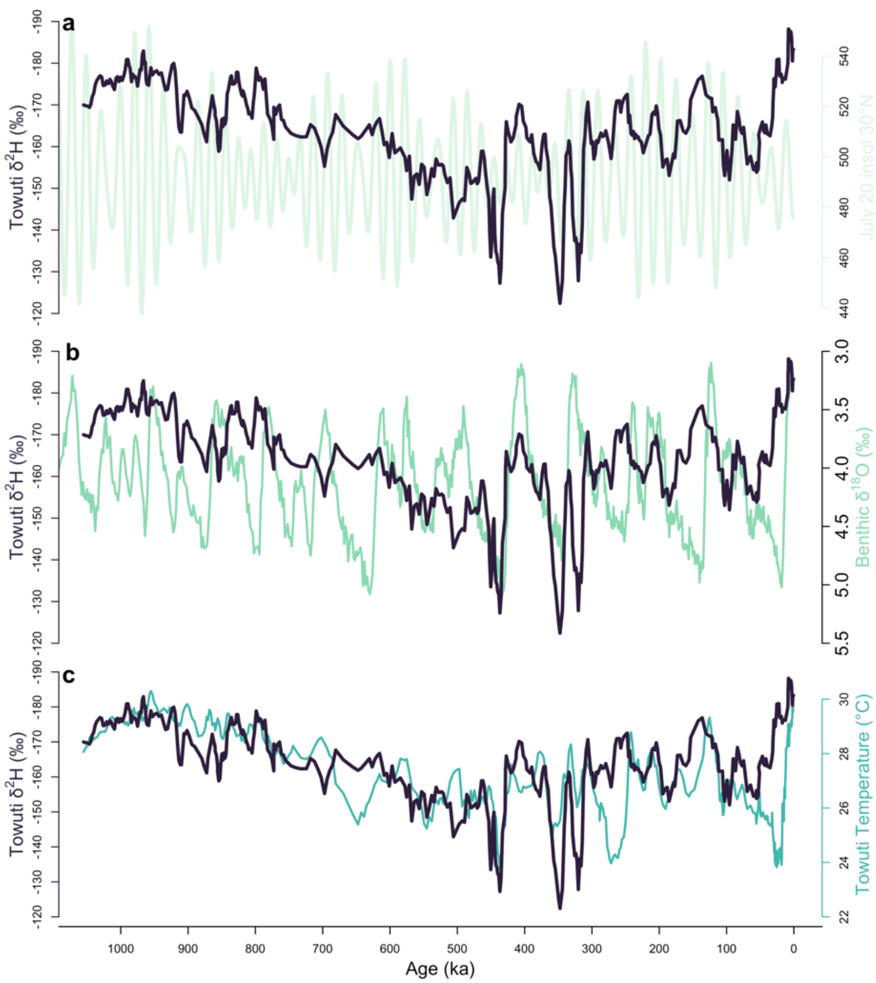

Figure 3 – (a) Towuti δ^2H_{wax} (black) and July 20 insolation from 30°N (light green). (b) Towuti δ^2H_{wax} (black) and the global benthic $\delta^{18}O$ stack (green; (Lisiecki & Raymo, 2005). (C) Towuti δ^2H_{wax} (black) and the Towuti temperature (turquoise; Parish et al., in prep).

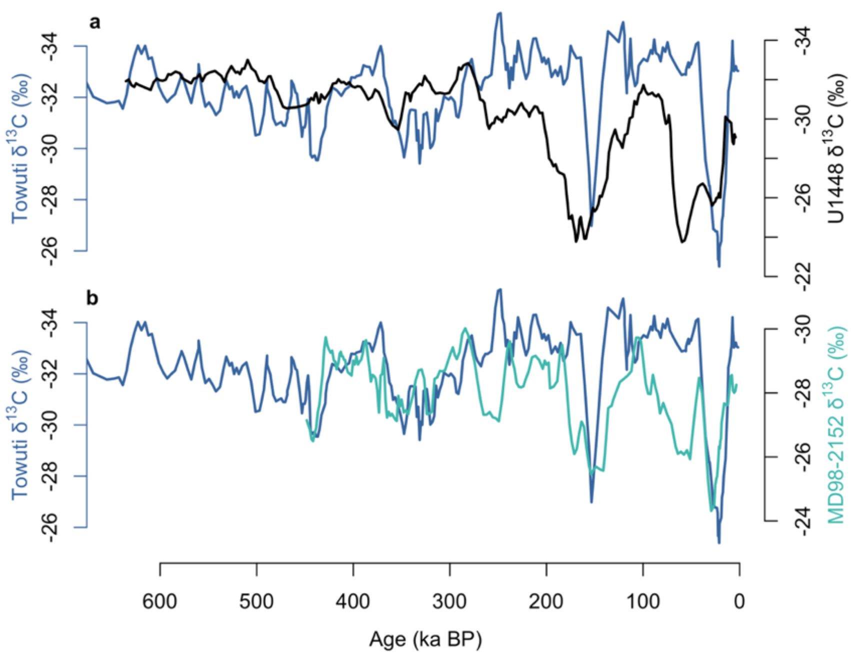

Figure 4 – (a) Towuti $\delta^{13}C_{wax}$ (blue) and U1448 $^{13}C_{wax}$ (black; McGrath et al., 2023). (b) Towuti $\delta^{13}C_{wax}$ (blue) and MD98-2152 $\delta^{13}C_{wax}$ (turquoise; Windler et al., 2019).

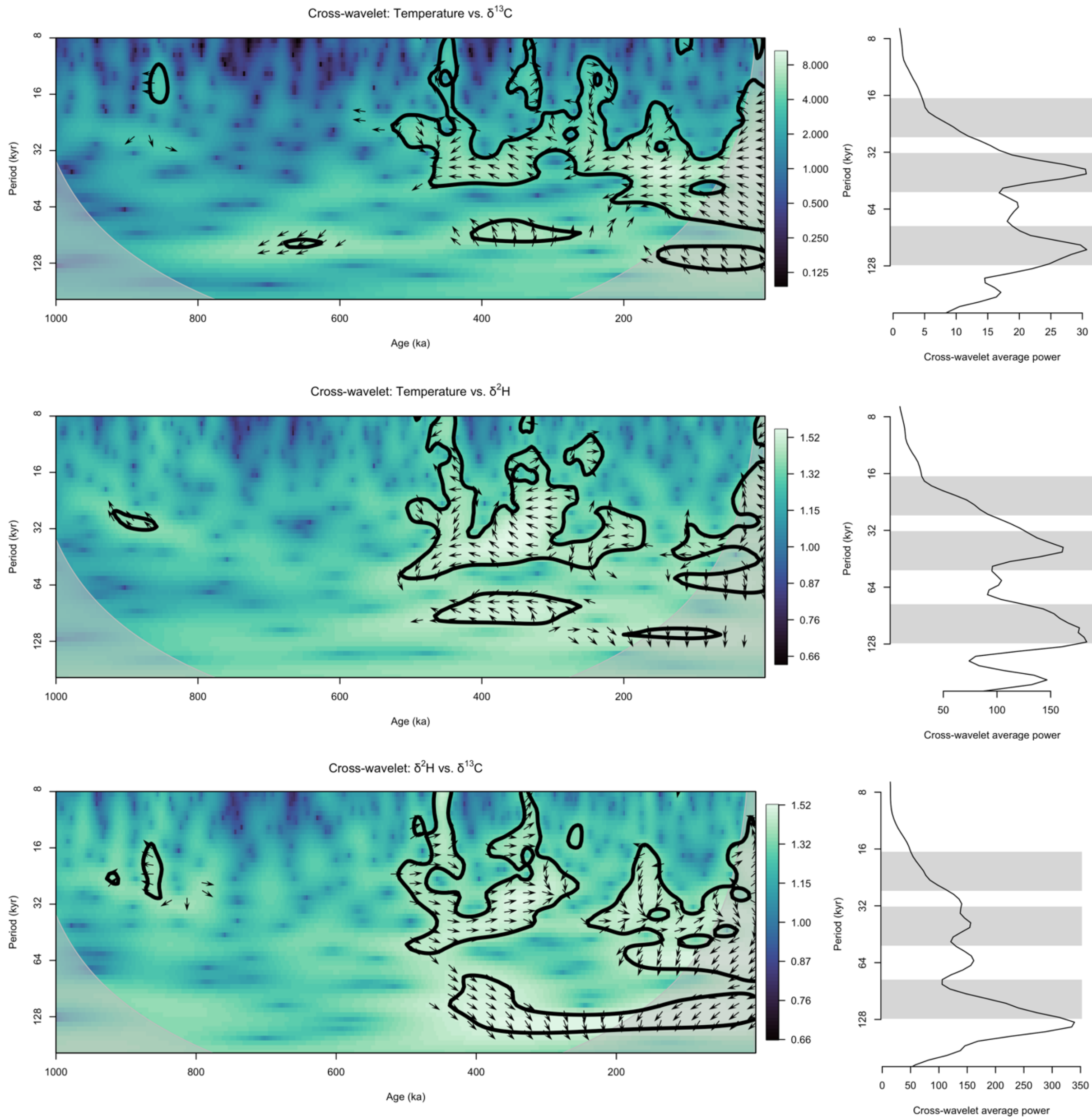

Figure 5 - Cross-wavelet analysis of Towuti temperature, δ^2H_{wax}, and $\delta^{13}C_{wax}$ records. Arrows pointing to the left indication 0° phase lead/lag. Right panel shows the average cross-wavelet power. Grey bars indicate 19-, 23-, 41-, and 100-kyr cycles.

References

Adler, R. F., Sapiano, M. R. P., Huffman, G. J., Wang, J.-J., Gu, G., Bolvin, D., et al. (2018). The Global Precipitation Climatology Project (GPCP) Monthly Analysis (New Version 2.3) and a Review of 2017 Global Precipitation. *Atmosphere*, *9*(4), 138. https://doi.org/10.3390/atmos9040138

Aldrian, E., & Dwi Susanto, R. (2003). Identification of three dominant rainfall regions within Indonesia and their relationship to sea surface temperature. *International Journal of Climatology*, *23*(12), 1435–1452. https://doi.org/10.1002/joc.950

Ayliffe, L. K., Gagan, M. K., Zhao, J., Drysdale, R. N., Hellstrom, J. C., Hantoro, W. S., et al. (2013). Rapid interhemispheric climate links via the Australasian monsoon during the last deglaciation. *Nature Communications*, *4*(1), 2908. https://doi.org/10.1038/ncomms3908

Barth, A. M., Clark, P. U., Bill, N. S., He, F., & Pisias, N. G. (2018). Climate evolution across the Mid-Brunhes Transition. *Climate of the Past*, *14*(12), 2071–2087. https://doi.org/10.5194/cp-14-2071-2018

Bates, S. L., Siddall, M., & Waelbroeck, C. (2014). Hydrographic variations in deep ocean temperature over the mid-Pleistocene transition. *Quaternary Science Reviews*, *88*, 147–158. https://doi.org/10.1016/j.quascirev.2014.01.020

Bereiter, B., Eggleston, S., Schmitt, J., Nehrbass-Ahles, C., Stocker, T. F., Fischer, H., et al. (2015). Revision of the EPICA Dome C CO2 record from 800 to 600 kyr before present. *Geophysical Research Letters*, *42*(2), 542–549. https://doi.org/10.1002/2014GL061957

Carolin, S. A., Cobb, K. M., Lynch-Stieglitz, J., Moerman, J. W., Partin, J. W., Lejau, S., et al. (2016). Northern Borneo stalagmite records reveal West Pacific hydroclimate across MIS

5 and 6. *Earth and Planetary Science Letters*, *439*, 182–193. https://doi.org/10.1016/j.epsl.2016.01.028

Cheng, H., Sinha, A., Wang, X., Cruz, F. W., & Edwards, R. L. (2012). The Global Paleomonsoon as seen through speleothem records from Asia and the Americas. *Climate Dynamics*, *39*(5), 1045–1062. https://doi.org/10.1007/s00382-012-1363-7

Cheng, H., Edwards, R. L., Sinha, A., Spötl, C., Yi, L., Chen, S., et al. (2016). The Asian monsoon over the past 640,000 years and ice age terminations. *Nature*, *534*(7609), 640–646. https://doi.org/10.1038/nature18591

Chikaraishi, Y., & Naraoka, H. (2003). Compound-specific δD-13C analyses of n-alkanes extracted from terrestrial and aquatic plants. *Phytochemistry*, *63*(3), 361–371. https://doi.org/10.1016/S0031-9422(02)00749-5

Chikaraishi, Y., & Naraoka, H. (2007). δ13C and δD relationships among three n-alkyl compound classes (n-alkanoic acid, n-alkane and n-alkanol) of terrestrial higher plants. *Organic Geochemistry*, *38*(2), 198–215. https://doi.org/10.1016/j.orggeochem.2006.10.003

Clemens, S. C., Holbourn, A., Kubota, Y., Lee, K. E., Liu, Z., Chen, G., et al. (2018). Precession-band variance missing from East Asian monsoon runoff. *Nature Communications*, *9*(1), 3364. https://doi.org/10.1038/s41467-018-05814-0

Costa, K. M., Russell, J. M., Vogel, H., & Bijaksana, S. (2015). Hydrological connectivity and mixing of Lake Towuti, Indonesia in response to paleoclimatic changes over the last 60,000years. *Palaeogeography, Palaeoclimatology, Palaeoecology*, *417*, 467–475. https://doi.org/10.1016/j.palaeo.2014.10.009

Dansgaard, W. (1964). Stable isotopes in precipitation. *Tellus*, *16*(4), 436–468. https://doi.org/10.3402/tellusa.v16i4.8993

De Deckker, P. (2016). The Indo-Pacific Warm Pool: critical to world oceanography and world climate. *Geoscience Letters*, *3*(1), 20. https://doi.org/10.1186/s40562-016-0054-3

Diefendorf, A. F., Mueller, K. E., Wing, Scott. L., Koch, P. L., & Freeman, K. H. (2010). Global patterns in leaf 13C discrimination and implications for studies of past and future climate. *Proceedings of the National Academy of Sciences*, *107*(13), 5738–5743. https://doi.org/10.1073/pnas.0910513107

DiNezio, P. N., & Tierney, J. E. (2013). The effect of sea level on glacial Indo-Pacific climate. *Nature Geoscience*, *6*(6), 485–491. https://doi.org/10.1038/ngeo1823

DiNezio, P. N., Timmermann, A., Tierney, J. E., Jin, F.-F., Otto-Bliesner, B., Rosenbloom, N., et al. (2016). The climate response of the Indo-Pacific warm pool to glacial sea level. *Paleoceanography*, *31*(6), 866–894. https://doi.org/10.1002/2015PA002890

DiNezio, P. N., Tierney, J. E., Otto-Bliesner, B. L., Timmermann, A., Bhattacharya, T., Rosenbloom, N., & Brady, E. (2018). Glacial changes in tropical climate amplified by the Indian Ocean. *Science Advances*, *4*(12), eaat9658. https://doi.org/10.1126/sciadv.aat9658

Du, X., Russell, J. M., Liu, Z., Otto-Bliesner, B. L., Gao, Y., Zhu, C., et al. (2021). Deglacial trends in Indo-Pacific warm pool hydroclimate in an isotope-enabled Earth system model and implications for isotope-based paleoclimate reconstructions. *Quaternary Science Reviews*, *270*, 107188. https://doi.org/10.1016/j.quascirev.2021.107188

Dubois, N., Oppo, D. W., Galy, V. V., Mohtadi, M., van der Kaars, S., Tierney, J. E., et al. (2014). Indonesian vegetation response to changes in rainfall seasonality over the past 25,000 years. *Nature Geoscience*, *7*(7), 513–517. https://doi.org/10.1038/ngeo2182

Garelick, S., Russell, Js. M., Dee, S., Verschuren, D., & Olago, D. O. (2021). Atmospheric controls on precipitation isotopes and hydroclimate in high-elevation regions in Eastern Africa since the Last Glacial Maximum. *Earth and Planetary Science Letters*, *567*, 116984. https://doi.org/10.1016/j.epsl.2021.116984

Griffiths, M. L., Drysdale, R. N., Gagan, M. K., Zhao, J. -x, Ayliffe, L. K., Hellstrom, J. C., et al. (2009). Increasing Australian–Indonesian monsoon rainfall linked to early Holocene sea-level rise. *Nature Geoscience*, *2*(9), 636–639. https://doi.org/10.1038/ngeo605

Griffiths, Michael L., Drysdale, R. N., Gagan, M. K., Zhao, J., Hellstrom, J. C., Ayliffe, L. K., & Hantoro, W. S. (2013). Abrupt increase in east Indonesian rainfall from flooding of the Sunda Shelf ~9500 years ago. *Quaternary Science Reviews*, *74*, 273–279. https://doi.org/10.1016/j.quascirev.2012.07.006

Herbert, T. D. (2023). The Mid-Pleistocene Climate Transition. *Annual Review of Earth and Planetary Sciences*, *51*(1), 389–418. https://doi.org/10.1146/annurev-earth-032320-104209

van der Kaars, S., Penny, D., Tibby, J., Fluin, J., Dam, R. A. C., & Suparan, P. (2001). Late Quaternary palaeoecology, palynology and palaeolimnology of a tropical lowland swamp: Rawa Danau, West-Java, Indonesia. *Palaeogeography, Palaeoclimatology, Palaeoecology*, *171*(3), 185–212. https://doi.org/10.1016/S0031-0182(01)00245-0

van der Kaars, S., Bassinot, F., De Deckker, P., & Guichard, F. (2010). Changes in monsoon and ocean circulation and the vegetation cover of southwest Sumatra through the last 83,000years: The record from marine core BAR94-42. *Palaeogeography, Palaeoclimatology, Palaeoecology*, *296*(1), 52–78. https://doi.org/10.1016/j.palaeo.2010.06.015

Konecky, B., Russell, J., & Bijaksana, S. (2016). Glacial aridity in central Indonesia coeval with intensified monsoon circulation. *Earth and Planetary Science Letters*, *437*, 15–24. https://doi.org/10.1016/j.epsl.2015.12.037

Konecky, B. L., Noone, D. C., & Cobb, K. M. (2019). The Influence of Competing Hydroclimate Processes on Stable Isotope Ratios in Tropical Rainfall. *Geophysical Research Letters*, *46*(3), 1622–1633. https://doi.org/10.1029/2018GL080188

Krause, C. E., Gagan, M. K., Dunbar, G. B., Hantoro, W. S., Hellstrom, J. C., Cheng, H., et al. (2019). Spatio-temporal evolution of Australasian monsoon hydroclimate over the last 40,000 years. *Earth and Planetary Science Letters*, *513*, 103–112. https://doi.org/10.1016/j.epsl.2019.01.045

Lisiecki, L. E., & Raymo, M. E. (2005). A Pliocene-Pleistocene stack of 57 globally distributed benthic $\delta^{18}O$ records: PLIOCENE-PLEISTOCENE BENTHIC STACK. *Paleoceanography*, *20*(1), n/a-n/a. https://doi.org/10.1029/2004PA001071

Liu, J., & An, Z. (2020). Leaf wax *n*-alkane carbon isotope values vary among major terrestrial plant groups: Different responses to precipitation amount and temperature, and implications for paleoenvironmental reconstruction. *Earth-Science Reviews*, *202*, 103081. https://doi.org/10.1016/j.earscirev.2020.103081

Marcott, S. A., Bauska, T. K., Buizert, C., Steig, E. J., Rosen, J. L., Cuffey, K. M., et al. (2014). Centennial-scale changes in the global carbon cycle during the last deglaciation. *Nature*, *514*(7524), 616–619. https://doi.org/10.1038/nature13799

McGrath, S. M., Clemens, S. C., Huang, Y., & Yamamoto, M. (2021). Greenhouse Gas and Ice Volume Drive Pleistocene Indian Summer Monsoon Precipitation Isotope Variability.

Geophysical Research Letters, *48*(4), e2020GL092249. https://doi.org/10.1029/2020GL092249

McGrath, S. M., Clemens, S. C., & Huang, Y. (2023). Pleistocene Sunda Shelf submersion-exposure cycles initiate vegetation Walker Circulation feedback. *Geology*. https://doi.org/10.1130/G51412.1

Mohtadi, M., Prange, M., Schefuß, E., & Jennerjahn, T. C. (2017). Late Holocene slowdown of the Indian Ocean Walker circulation. *Nature Communications*, *8*(1), 1015. https://doi.org/10.1038/s41467-017-00855-3

O'Mara, N. A., Skonieczny, C., McGee, D., Winckler, G., Bory, A. J.-M., Bradtmiller, L. I., et al. (2022). Pleistocene drivers of Northwest African hydroclimate and vegetation. *Nature Communications*, *13*(1), 3552. https://doi.org/10.1038/s41467-022-31120-x

Parish, M., Russell, J., Konecky, B., Du, X., He, C., Bijaksana, S., & Vogel, H. (2024). Changes in Indo-Pacific Warm Pool hydroclimate and vegetation during the last deglaciation. *Quaternary Science Reviews*, *336*, 108755. https://doi.org/10.1016/j.quascirev.2024.108755

Parish, M., Russell, J., King, J., Deino, A., Harpel, C., Vogel, H., et al. (in prep.). A 1-million year record of terrestrial temperature from the Indo-Pacific Warm Pool.

Parish, M. C., Du, X., Bijaksana, S., & Russell, J. M. (2023). A brGDGT-Based Reconstruction of Terrestrial Temperature From the Maritime Continent Spanning the Last Glacial Maximum. *Paleoceanography and Paleoclimatology*, *38*(3), e2022PA004501. https://doi.org/10.1029/2022PA004501

Partin, J. W., Cobb, K. M., Adkins, J. F., Clark, B., & Fernandez, D. P. (2007). Millennial-scale trends in west Pacific warm pool hydrology since the Last Glacial Maximum. *Nature*, *449*(7161), 452–455. https://doi.org/10.1038/nature06164

Ruan, Y., Mohtadi, M., Dupont, L. M., Hebbeln, D., Kaars, S. van der, Hopmans, E. C., et al. (2020). Interaction of Fire, Vegetation, and Climate in Tropical Ecosystems: A Multiproxy Study Over the Past 22,000 Years. *Global Biogeochemical Cycles*, *34*(11), e2020GB006677. https://doi.org/10.1029/2020GB006677

Ruan, Yanming, Mohtadi, M., van der Kaars, S., Dupont, L. M., Hebbeln, D., & Schefuß, E. (2019). Differential hydro-climatic evolution of East Javanese ecosystems over the past 22,000 years. *Quaternary Science Reviews*, *218*, 49–60. https://doi.org/10.1016/j.quascirev.2019.06.015

Russell, J. M., Vogel, H., Konecky, B. L., Bijaksana, S., Huang, Y., Melles, M., et al. (2014). Glacial forcing of central Indonesian hydroclimate since 60,000 y B.P. *Proceedings of the National Academy of Sciences*, *111*(14), 5100–5105. https://doi.org/10.1073/pnas.1402373111

Russell, J. M., Vogel, H., Bijaksana, S., Melles, M., Deino, A., Hafidz, A., et al. (2020). The late quaternary tectonic, biogeochemical, and environmental evolution of ferruginous Lake Towuti, Indonesia. *Palaeogeography, Palaeoclimatology, Palaeoecology*, *556*, 109905. https://doi.org/10.1016/j.palaeo.2020.109905

Sachse, D., Billault, I., Bowen, G. J., Chikaraishi, Y., Dawson, T. E., Feakins, S. J., et al. (2012). Molecular paleohydrology: Interpreting the hydrogen-isotopic composition of lipid biomarkers from photosynthesizing organisms. *Annual Review of Earth and Planetary Sciences*, *40*, 221–249. https://doi.org/10.1146/annurev-earth-042711-105535

Sarr, A.-C., Husson, L., Sepulchre, P., Pastier, A.-M., Pedoja, K., Elliot, M., et al. (2019). Subsiding Sundaland. *Geology*, *47*(2), 119–122. https://doi.org/10.1130/G45629.1

Schrag, D. P., Hampt, G., & Murray, D. W. (1996). Pore Fluid Constraints on the Temperature and Oxygen Isotopic Composition of the Glacial Ocean. *Science*, *272*(5270), 1930–1932. https://doi.org/10.1126/science.272.5270.1930

Sun, Y., Yin, Q., Crucifix, M., Clemens, S. C., Araya-Melo, P., Liu, W., et al. (2019). Diverse manifestations of the mid-Pleistocene climate transition. *Nature Communications*, *10*(1), 352. https://doi.org/10.1038/s41467-018-08257-9

Vogel, H., Russell, J. M., Cahyarini, S. Y., Bijaksana, S., Wattrus, N., Rethemeyer, J., & Melles, M. (2015). Depositional modes and lake-level variability at Lake Towuti, Indonesia, during the past ~29 kyr BP. *Journal of Paleolimnology*, *54*(4), 359–377. https://doi.org/10.1007/s10933-015-9857-z

Wicaksono, S. A., Russell, J. M., & Bijaksana, S. (2015). Compound-specific carbon isotope records of vegetation and hydrologic change in central Sulawesi, Indonesia, since 53,000 yr BP. *Palaeogeography, Palaeoclimatology, Palaeoecology*, *430*, 47–56. https://doi.org/10.1016/j.palaeo.2015.04.016

Windler, G., Tierney, J. E., DiNezio, P. N., Gibson, K., & Thunell, R. (2019). Shelf exposure influence on Indo-Pacific Warm Pool climate for the last 450,000 years. *Earth and Planetary Science Letters*, *516*, 66–76. https://doi.org/10.1016/j.epsl.2019.03.038

Windler, G., Tierney, J. E., Zhu, J., & Poulsen, C. J. (2020). Unraveling Glacial Hydroclimate in the Indo-Pacific Warm Pool: Perspectives From Water Isotopes. *Paleoceanography and Paleoclimatology*, *35*(12), e2020PA003985. https://doi.org/10.1029/2020PA003985

Windler, G., Tierney, J. E., & Anchukaitis, K. J. (2021). Glacial-Interglacial Shifts Dominate Tropical Indo-Pacific Hydroclimate During the Late Pleistocene. *Geophysical Research Letters*, *48*(15), e2021GL093339. https://doi.org/10.1029/2021GL093339

Supplement

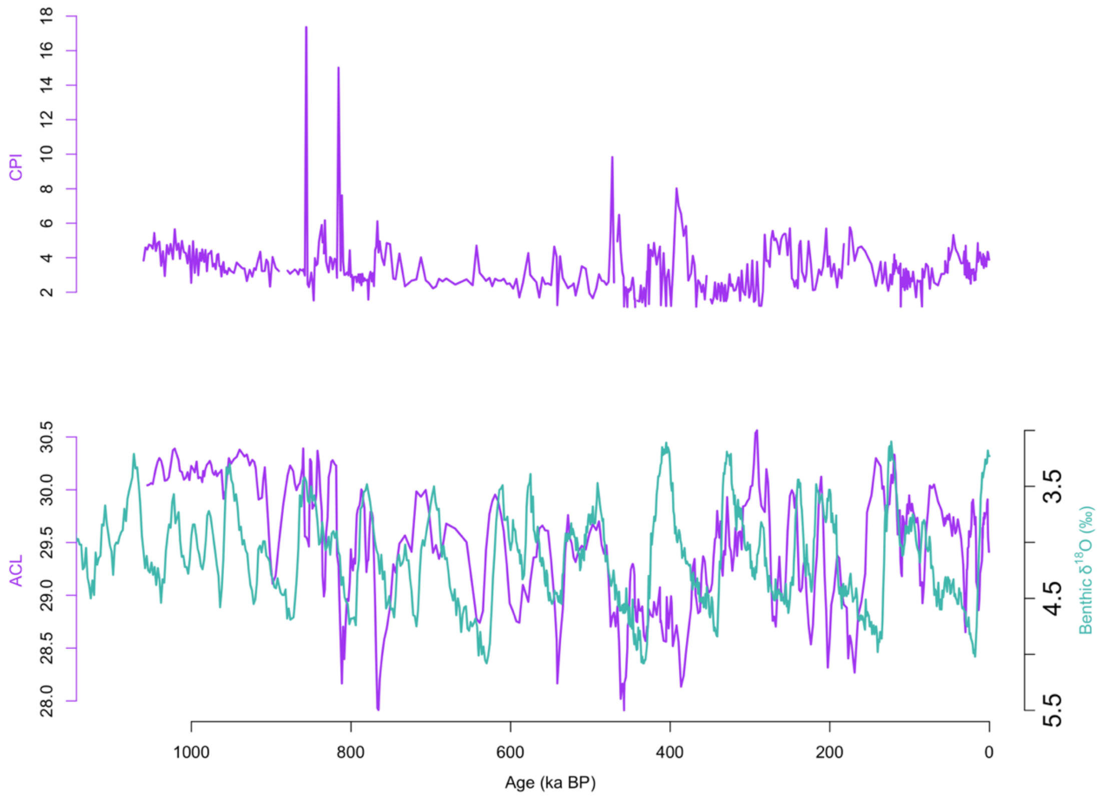

Figure S1 – $CPI_{27\text{-}31}$ and $ACL_{25\text{-}33}$ from Lake Towuti.

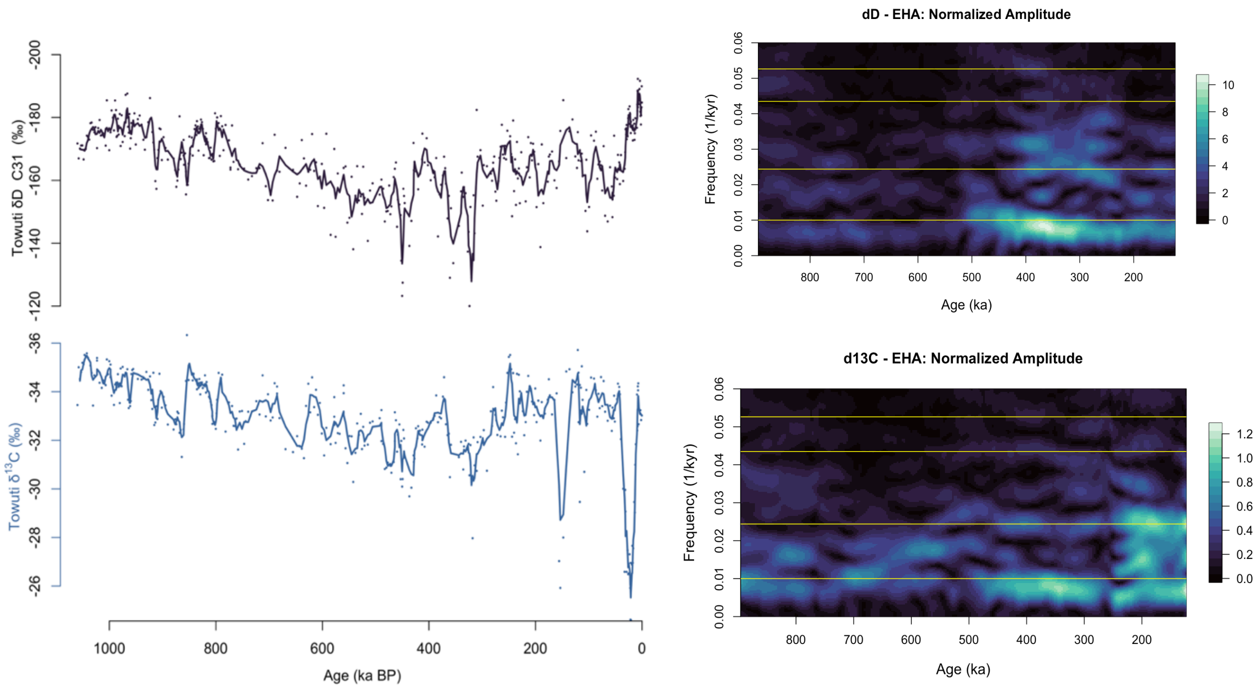

Figure S2 – Towuti δ^2H_{wax} and $\delta^{13}C_{wax}$, excluding samples with a $CPI_{27\text{-}31}$ less than 2.

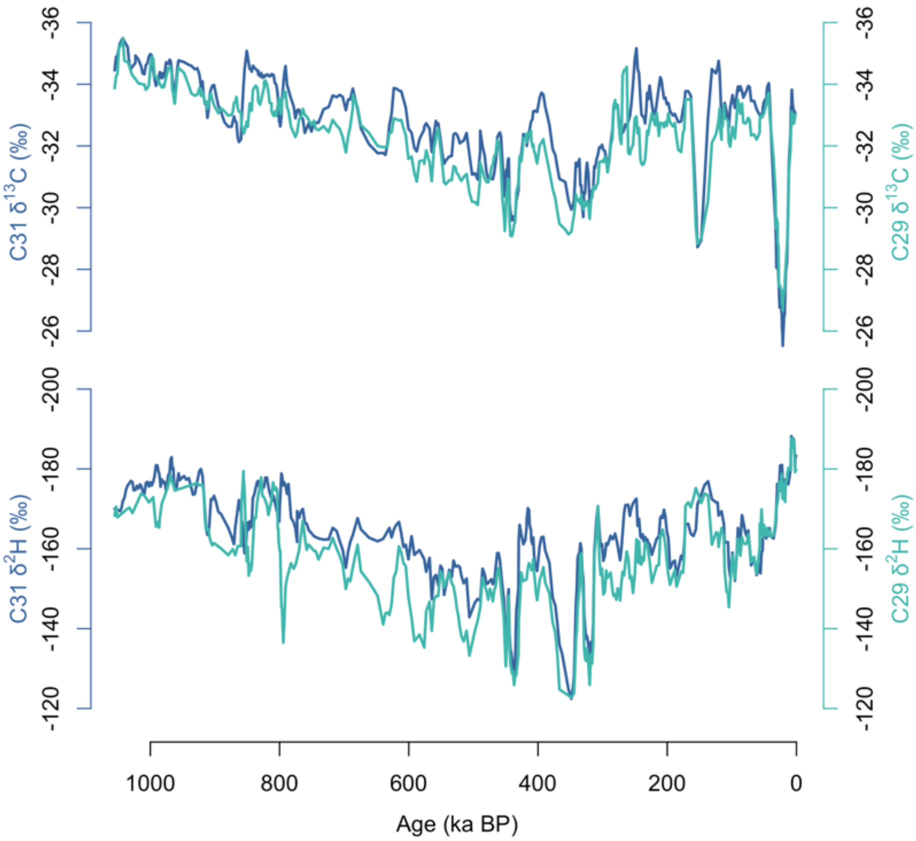

Figure S3 – $\delta^{13}C_{wax}$ and $\delta^{2}H_{wax}$ of C_{30} and C_{29} alkanes.